Ruthenium hydride complexes bearing the ligand 1,3-bis(2,4,6-trimethylphenyl)imidazol-2-ylidene

Chatwin, Sarah Louise

Award date:
2007

Awarding institution:
University of Bath

Ruthenium hydride complexes bearing the ligand 1,3-bis(2,4,6-trimethylphenyl)imidazol-2-ylidene

Sarah Louise Chatwin

A thesis submitted in partial fulfilment of the requirements for the degree of

Doctor of Philosophy

UNIVERSITY OF
BATH

University of Bath
Department of Chemistry

May 2007

ProQuest LLC
789 East Eisenhower Parkway
P.O. Box 1346
Ann Arbor, MI 48106-1346

Acknowledgements

Firstly, I would like to thank Dr Mike Whittlesey for his help and guidance throughout my time at the University of Bath. I am incredibly grateful for the opportunity I have been given to work on this project with such an enthusiastic and supportive supervisor.

I thank Dr Mary Mahon for solving my crystal structures, Dr Stuart Macgregor and his group for computational work and Dr John Lowe for his help with NMR queries. I am indebted to all of those who have endured my never-ending questions, in particular to John and his lovely wife Claire for their insights into borohydride systems. Thanks to Dr Andrew Weller for his belief in me and his support throughout my time as an undergraduate.

It has been a privilege to work with such a great group of people in the last three years and I have made some very good friends in the process. Special thanks go to Dr Suzanne Burling for her support as the best post-doc ever and to Drs Susie Douglas and Belinda Paine, and (soon-to-be) Drs Steve Reade and Olly Saker for all being so much more than lab-mates. I would also like to acknowledge Dr Rodolphe Jazzar for giving up his time to help me get started as a very scared MChem project student all those years ago, and to mention some of the brilliant Whittlesey MChem students since, including Vicky Brown, Minty, Charlie, Tom and especially Vicky Chantler. Thanks to Gemma and Gan for the fun we have had together and for their huge amounts of encouragement when things didn't look so good: you were the best housemates I could have had. Extended thanks also go to Susie and Graham for putting me up and indeed putting up with me in the final throes of writing up – thank you!

Most of all I express my thanks to my family for their unfaltering belief in me and all of their support, I am very lucky to have you all. Last but certainly not least, I would like to thank Rob for his understanding, patience and love.

Funding: I would like to acknowledge DTA funding for my PhD; Roberts' grant for sending me to the IOMC 2006 and the loan of $RuCl_3.nH_2O$ from Johnson Matthey Plc.

Abstract

This thesis expands on previous work carried out on ruthenium hydride complexes bearing two of the N-heterocyclic carbene ligands, 1,3-bis(2,4,6-trimethylphenyl)imidazol-2-ylidene (IMes). The complexes $Ru(IMes)_2(CO)(XH)H_2$ (X = OH, OEt, SH, S^{n}Pr, F, Cl) have been reformulated as the 16-electron mono hydride complexes $Ru(IMes)_2(CO)(X)H$, based on computational insights from the Macgregor group and new spectroscopic details. As coordinatively unsaturated complexes, these systems have been used as catalysts for the hydrogenation of ketones, showing moderate activity. In addition, $Ru(IMes)_2(CO)(X)H$ reacted readily with CO to afford the 18-electron dicarbonyl complexes $Ru(IMes)_2(CO)_2(X)H$.

A series of acetylide complexes have been prepared from the reaction of $Ru(IMes)_2(CO)(OH)H$ (**2**) with acetylenes. **2** reacted with stoichiometric amounts of HC≡CPh to yield the mono phenylacetylide complex $Ru(IMes)_2(CO)(C{\equiv}CPh)H$ (**13**), whereas excess HC≡CPh resulted in the bis species $Ru(IMes)_2(CO)(C{\equiv}CPh)_2$ (**14**). The reaction between **13** and **14** is reversible upon addition of H_2 and possible mechanisms have been proposed. In comparison to **2**, the reaction of $Ru(IMes)_2(CO)(Cl)H$ (**7**) with HC≡CPh produced the vinyl complex $Ru(IMes)_2(CO)(Cl)(HC{=}CHPh)$ (**15**). Progressing to the bulkier substrate $HC{\equiv}CSiMe_3$, the analogous reaction with **2** afforded only the mono acetylide complex $Ru(IMes)_2(CO)(C{\equiv}CSiMe_3)H$ (**16**), without formation of a bis species. All of these complexes have been structurally characterised.

Attempted formation of the dihydride complex $RuL_2(CO)H_2$ {L_2 = $(IMes)_2$; $(PPh_3)(IMes)$} by reduction of $RuL_2(CO)(Cl)H$ with $NaBH_4$ was unsuccessful, affording instead the borohydride complexes $RuL_2(CO)(\eta^2\text{-}BH_4)H$, which have been probed by NMR studies and deuterium labelling reactions. Low temperature reactions with CO made it possible to observe the $\eta^1\text{-}BH_4^-$ intermediate $RuL_2(CO)_2(\eta^1\text{-}BH_4)H$ on the pathway to formation of $RuL_2(CO)_2H_2$ and subsequently $RuL_2(CO)_3$. Investigation into the stability of the borohydride complexes and their reactivity with PMe_2Ph and 4-Mepy revealed that $Ru(IMes)_2(CO)(\eta^2\text{-}BH_4)H$ (**19**) is significantly less reactive than $Ru(IMes)_2(CO)(\eta^2\text{-}BH_4)H$ (**26**).

Abbreviations

BDE	bond dissociation energy
DFT	density functional theory
ROMP	ring opening metathesis polymerisation
TOF	turn over frequency
TON	turn over number
DH	direct hydrogenation
TH	transfer hydrogenation

Spectroscopy

IR	infrared
υ_L	IR shift of L
NMR	nuclear magnetic resonance
δ	NMR chemical shift
J_{XY}	coupling constant of X to Y
COSY	correlation spectroscopy
EXSY	exchange spectroscopy
HMBC	heteronuclear multiple bond correlation
HMQC	heteronuclear multiple quantum coherence
MS	mass spectrometry
NOESY	nuclear Overhauser effect spectroscopy
RCM	ring closing metathesis
ROESY	rotating frame over enhancement spectroscopy
VT	variable temperature
s	singlet
d	doublet
t	triplet
q	quartet
m	multiplet
br	broad

Units

cm^{-1}	wavenumber
ee	enantiomeric excess
h	hours
Hz	Hertz
K	Kelvin
kJ	kilojoule
min	minutes
ppm	parts per million

Chemical

arphos	$Ph_2PCH_2CH_2AsPh_2$
bq	benzoquinoline
Cy	cyclohexyl
dmpe	$Me_2PCH_2CH_2PMe_2$
dppe	$Ph_2PCH_2CH_2PPh_2$
Hal	halide
L	generic ligand
μ-L	bridging ligand
M	generic metal
PCP	1,3-(^{t}Bu$_2$PCH$_2$)C$_6$H$_4$
^{i}Pr	isopropyl
py	pyridine
R	alkyl or aryl
THF	tetrahydrofuran
tripod	$MeC(CH_2PPh_2)_3$
X	halide or other heteroatom
i	*ipso*
o	*ortho*
m	*meta*
p	*para*

NHC	N-heterocyclic carbene
I*	1,3-bis((*S*)1-phenylethyl)imidazol-2-ylidene
IAd	1,3-diadamantylimidazol-2-ylidene
I^{n}Bu	1,3-bis(*normal*-butyl)-imidazol-2-ylidene
I^{t}Bu	1,3-diisobutylimidazol-2-ylidene
ICy	1,3-bis(cyclohexyl)-imidazol-2-ylidene
IEt$_2$Me$_2$	1,3-diethyl-4,5-dimethylimidazol-2-ylidene
IH	1,3-imidazol-2-ylidene
IMe	1,3-dimethylimidazol-2-ylidene
IMe$_4$	1,3,4,5-tetramethylimidazol-2-ylidene
IMes	1,3-bis(2,4,6-trimethylphenyl)imidazol-2-ylidene
IMes'	C-H activated IMes
IMes''	C-C activated IMes
SIMes	1,3-bis(2,4,6-trimethylphenyl)imidazolin-2-ylidene
IPh	1,3-bisphenylimidazolin-2-ylidene
I^{n}Pr	1,3-bis(*normal*-propyl)-imidazol-2-ylidene
I^{i}Pr	1,3-diisopropylimidazol-2-ylidene
I^{i}Pr$_2$Me$_2$	1,3-diisopropyl-4,5-dimethylimidazol-2-ylidene
IPr	1,3-bis(2,6-diisopropylphenyl)imidazol-2-ylidene
SIPr	1,3-bis(2,6-diisopropylphenyl)imidazolin-2-ylidene
IXyl	1,3-bis(2,6-dimethylphenyl)imidazol-2-ylidene

Contents

Chapter 1

Chapter 2

Chapter 3

Chapter 5

Appendices

Chapter 1

1. Introduction

1.1 N-heterocyclic carbenes

N-heterocyclic carbenes (NHCs) have been widely investigated for their use in organometallic chemistry, especially for applications in homogeneous catalysis. NHCs are neutral ligands containing a carbenic carbon incorporated into a heterocyclic ring with vicinal nitrogen atoms, such as the structures shown in **Figure 1.1**. R_A groups can be either alkyl or aryl moieties, and are generally identical (chelating groups such as phosphines can be incorporated to create a tethered system).[1,2] Imidazol-2-ylidenes contain an unsaturated backbone, which contains the groups R_B; generally both are either hydrogen atoms or methyl groups, although backbone chloride atoms are known.[3] Unsaturated NHCs are referred to as '$IR_A(R_B)$' where R_B is only used when the backbone moities are not hydrogen atoms; saturated NHCs or imidazolidin-2-ylidenes, are known as '$SIR_A(R_B)$' to denote a saturated imidazol ring (see **Figure 1.1** for examples).

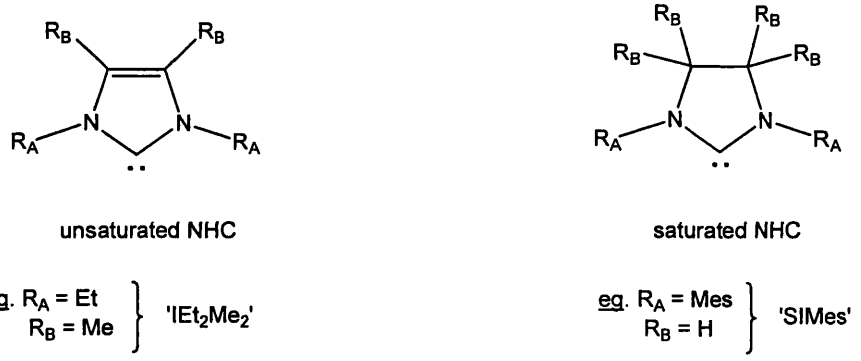

Figure 1.1 Unsaturated and saturated examples of NHCs.

The nitrogen atoms in NHCs create a 'pull–push' system as shown in **Figure 1.2**, which helps to stabilise the non-bonding electrons on the carbenic carbon (C_{NHC}) due to their σ-electron withdrawing and π-electron donating nature. π-electrons are donated into the empty p-orbital of the C_{NHC}, and σ-electron density removed from C_{NHC} *via* a negative inductive effect. Thus, the electrophilicity and reactivity of the carbene is reduced, so much so that in some cases a free carbene can be stabilised.

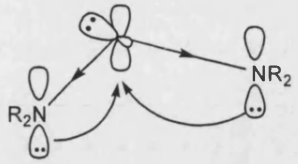

Figure 1.2 'Pull–push' system in NHCs.

The non-bonding electrons on C_{NHC} are paired in the non-bonding sp^2 hybridised orbital leaving an empty *p* orbital corresponding with singlet state multiplicity. A relatively large separation in the energy levels (at least 2 eV) results in the electrons pairing up in the lower energy orbital to afford a singlet state carbene, whereas if there is only a small energy separation (below 1.5 eV), the triplet state multiplicity is favoured (**Figure 1.3**).[4-6]

The energy gap between the orbitals is affected by the groups directly bound to C_{NHC}, with electron rich substituents such as N giving rise to singlet state multiplicity. Vicinal groups with π-lone pairs can interact with the empty *p* orbital on C_{NHC} (**Figure 1.2** above) and produce a lower energy orbital for both non-bonding electrons to reside in. Furthermore, Harrison *et al.* found that the singlet state is stabilised when R_B is a σ-electron withdrawing group.[7, 8]

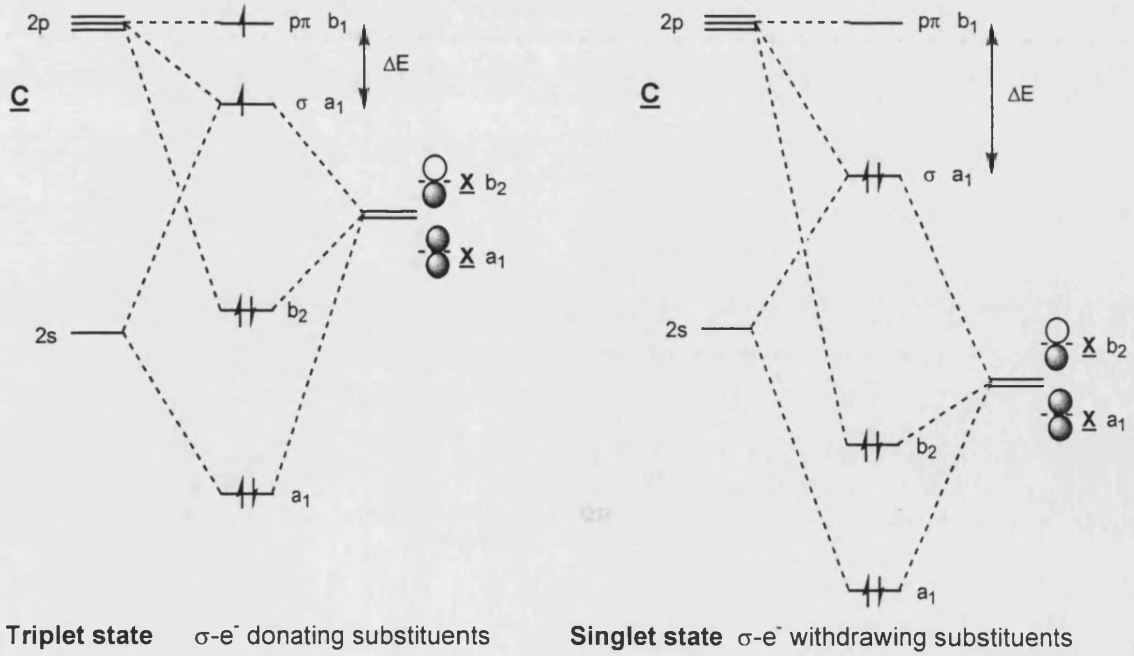

Figure 1.3 MO diagrams showing the stabilising effect of σ–donating substituents by orbital perturbation. The singlet state occurs when the σ-p_π energy gap is large (>2 eV).[4-6]

1.2 Synthesis of NHCs

The first NHC complexes $[Hg(IPh)_2]^{2+}$ and $Cr(IMe)(CO)_5$ were prepared by Wanzlick and Öfele in the late 1960s,[9, 10] but it was not until 1991 that an uncomplexed carbene in the form of 1,3-diadamantylimidazol-2-ylidene (IAd) was isolated by Arduengo *et al.*[11] As the field of NHCs has developed there have been more reliable synthetic routes reported for NHCs, some of which are displayed in **Scheme 1.1**. Kuhn's preparation involving thiones can only afford unsaturated NHCs, whereby methyl groups are always present on the backbone due to limitations of the preceding step.[12]

Successful preparations such as those in **Scheme 1.1** (overleaf), rely on elimination of a stable molecule to form the free NHC and make the overall process favourable, including loss of chloride salts (eg. AgCl),[13] KS,[12] and a variety of phenyl substituents containing electron withdrawing groups.[14] The first commercially available NHC was prepared by elimination of MeOH.[15] In fact, Wanzlick was the first to attempt isolation of a free NHC by the elimination of $CHCl_3$ from $SIPhCCl_3$, however a dimeric compound, an enetetramine was formed instead (**Scheme 1.2**).[16] It was suggested that the dimer was in equilibrium with the free NHC, but the hypothesis was not upheld.[17] Ultimately, Wanzlick was unfortunate in his choice of NHC as stable NHCs do not dimerise;[18] Arduengo attributed Wanzlick's failure to isolate free NHC to 'inconvenient physical properties of the carbene and possible problems with respect to purity.'[19]

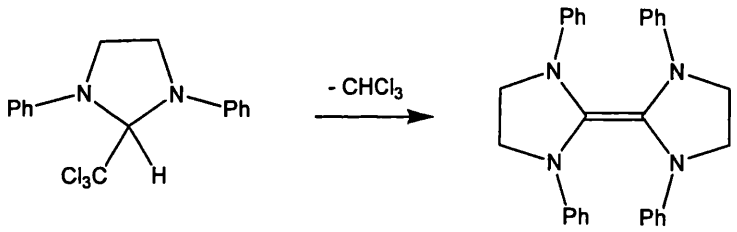

Scheme 1.2. First attempted, but unsuccessful preparation of a free NHC.[16]

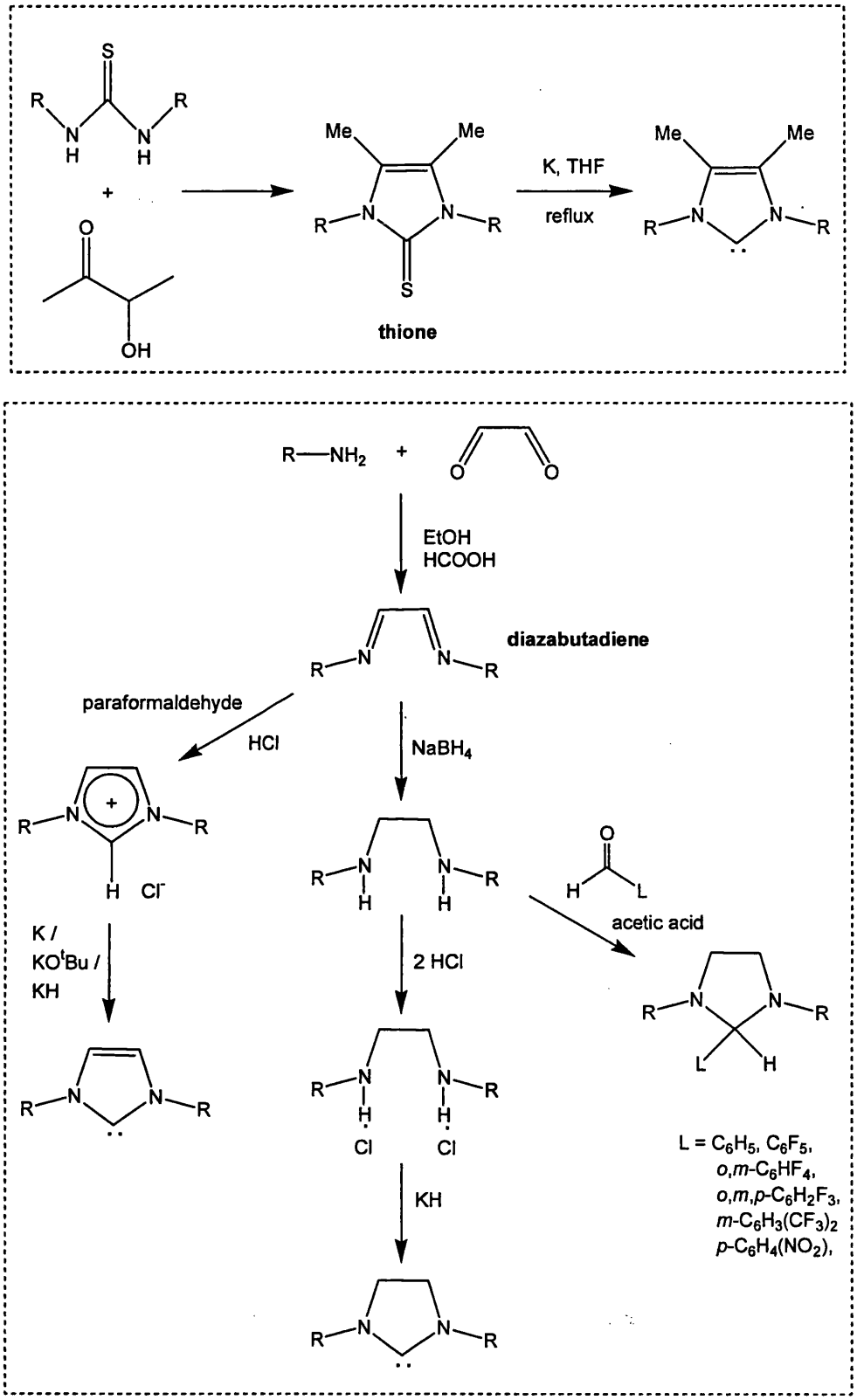

Scheme 1.1. General synthetic routes for preparation of NHCs.

1.3 NHC bonding to metals

NHC ligands bind to metals *via* the 2 free electrons on the C2 position. This bond is best represented by a single bond as the M-C_{NHC} distance measured in X-ray crystal structures (>2.1 Å) is longer than a double bond (<2.0 Å). This is due to the negligible π-acceptor characteristics of the carbene. Green *et al.* have studied the molecular orbitals involved in the bonding in M(I^tBu)$_2$ (M = Pd, Pt) with photoelectron (PE) spectroscopy. PE bands attributed to π MOs do not shift or split in comparison to the free NHC, suggesting that there is little or no interaction between the π MOs of the ligand and the metal.[20] Furthermore, a Be-NHC complex has been successfully prepared in the absence of any π-electrons to back donate to the metal, as Be is one of the hardest Lewis acids.[21]

Abnormal NHC bonding can also occur when the NHC is bound to the metal centre *via* C4/C5 as opposed to C2. Crabtree was the first to report an abnormal NHC complex in 2001 (**Figure 1.4**),[22] and since then a variety of abnormal NHC complexes have been prepared, [23-26] including a complex containing both a normally **and** abnormally bound NHCs.[27] Recently the Whittlesey group have produced the first abnormally NHC-bound complex of Ru.[28]

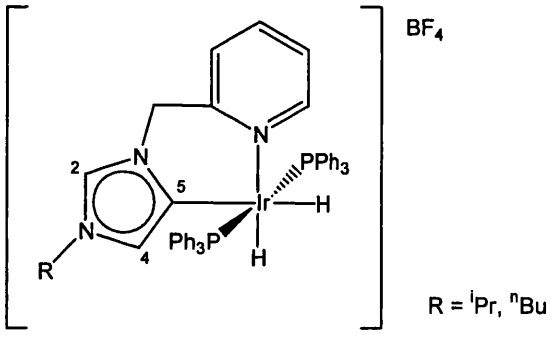

Figure 1.4. An abnormally bound NHC complex.

The manner in which NHCs bond to metals is in some ways analogous to phosphine-metal bonding. Phosphines (PR_3) are commonly used as ligands in transition metal complexes because they are excellent soft-donor ligands and so bond favourably to late transition metals that are also soft, such as Ru (II). In fact, since NHCs have been known they have been widely thought of as an alternative to

phosphines. However a lot of work has been carried out to show that NHCs cannot be defined in such a simplistic manner and should be thought of as a class of their own.

> "NHCs are not just phosphine mimics, there is increasing experimental evidence that NHC metal catalysts surpass their phosphine-based counterparts in both ability and scope of application."
>
> Herrmann, 2002.[29]

1.4 Differences between NHC and phosphine ligands

1.4.1 Electronic considerations

NHC ligands have been established as better σ-donors than their phosphine counterparts. The former bind more strongly to the metal centre and there are markedly less examples of NHCs dissociating from metals than phosphines,[30, 31] which are used for their lability in many catalytic reactions.

The ability to donate σ-electrons to the metal centre can be quantified by basicity (pK_a values), bond dissociation energies and the extent of metal back-bonding to carbonyl ligands (ν_{CO}) (**Table 1.1**).[32-34]

Although there is no pK_a data for IMes, Cavell and Yates did report theoretical values for similar free NHCs, namely IPh and IXyl with respective pK_a values of 27.4 and 28.2.[32] These aryl NHCs only differ slightly from each other in basicity, which suggests that the methyl arms on IXyl do not have a significant effect. It is therefore expected that the pK_a value for IMes is also just below 30, making it significantly more basic than any of the phosphines shown.
Stronger σ-donor ligands are associated with stronger binding to the metal centre and furthermore, pK_a values are indicative of the electron density that is available for bonding. Consequently increasing pK_a values in **Table 1.1** correspond with increasing bond dissociation energies (BDEs) of the ligand (L) in both $Ni(CO)_3(L)$ and $Ni(CO)_2(L)$. The trend observed in the BDE values here is exemplary of other metal systems too as shown by a separate study on $Ru(\eta^5\text{-}C_5Me_5)(L)(Cl)$ (L = P^iPr_3, PCy_3 and NHCs including IMes).[35]

Ligand (L)	pK_a (H_2O) [32]	BDE of L (kJ mol^{-1}) [33, 34]		ν_{CO} (cm^{-1}) $Ni(CO)_3(L)$ [33]	
		$Ni(CO)_3(L)$	$Ni(CO)_2(L)$	A_1	E
PH_3	-	94.9	107.4	-	-
PMe_3	8.65	-	-	2064.1	-
PEt_3	8.69	-	-	2061.7	-
P^iPr_3	-	-	-	2059.2	-
P^tBu_3	11.40	117.0	143.4	2056.1	1971
PCy_3	9.70	-	-	2056.4	1973
PPh_3	2.73	111.6	125.4	2068.9	1990
IMes	-	171.8	194.4	2050.7	1969.8
SIMes	-	168.0	197.3	2051.5	1970.6
IPr	-	160.9	189.8	2051.5	1970.0
SIPr	-	158.8	192.7	2052.2	1971.3
ICy	-	165.5	193.5	2049.6	1964.6

Table 1.1 Some theoretical and experimental values to illustrate the difference between a range of phosphines and NHCs; PPh_3 and IMes entries are highlighted as they feature largely in this thesis (- = not reported).

To ensure that the examples given are not oversimplified by only accounting for mono NHC or mono PR_3 systems we can look at work carried out by Herrmann (**Table 1.2**).[36] Calculation of BDE values were extended to mixed NHC/phosphine complexes and show that even in mixed species, NHCs bind much more strongly to the metal than phosphines, supporting the trends observed in **Table 1.1** above.

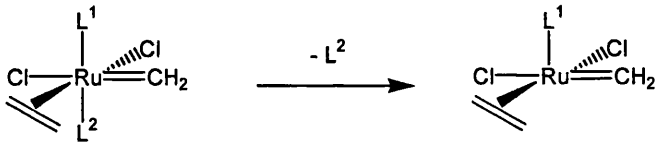

Ligands (L^1 and L^2)	BDE of PH_3 (kJ mol^{-1})	BDE of PMe_3 (kJ mol^{-1})	BDE of NHC (kJ mol^{-1})
$L^1 = L^2 = PH_3$	76.1	-	-
$L^1 = L^2 = PMe_3$	-	112.9	-
$L^1 = L^2 = NHC$	-	-	188.1
$L^1 = PH_3$, $L^2 = NHC$	78.2	-	196.0
$L^1 = PMe_3$ $L^2 = NHC$	-	108.7	175.6

Table 1.2 Calculated bond dissociation energies (BDEs) for phosphine and NHC ligands in the model complex $Ru(\eta^2\text{-}C_2H_4)(CH_2)(Cl)_2(L^1)(L^2)$ shown above (- = N/A).[36]

Infrared carbonyl stretches are also a good indication of σ-donor ability. In fact Tolman pioneered an electronic parameter for phosphines based on A_1 ν_{CO} values of $Ni(CO)_3(L)$ like those in **Table 1.1**.[34] Increased electron density on the metal centre causes more back-bonding into the available carbonyl ligands, weakening the C≡O bond and lowering the CO stretching frequency. So, decreased ν_{CO} values signify that L is a better σ-donor.

All of the measurements conclude that there is a substantial electronic difference between alkyl and aryl phosphine ligands with the former having more donor ability and therefore forming stronger M-P bonds. However, it is apparent that NHCs bind more strongly than any of the phosphine examples.

1.4.2 Steric considerations

Tolman's cone angle (θ) was introduced in the 1970s as a measurement to quantify the steric bulk of phosphines.[34] However, the fence-like structure of NHCs excluded them from description by θ as the Tolman model only accounted for more 3-dimensional spherical structures. Nolan has recently overcome this problem with a

method that can be used for both phosphines and NHCs, called percentage volume buried ($\%V_{Bur}$).[35] (**Figure 1.5**).

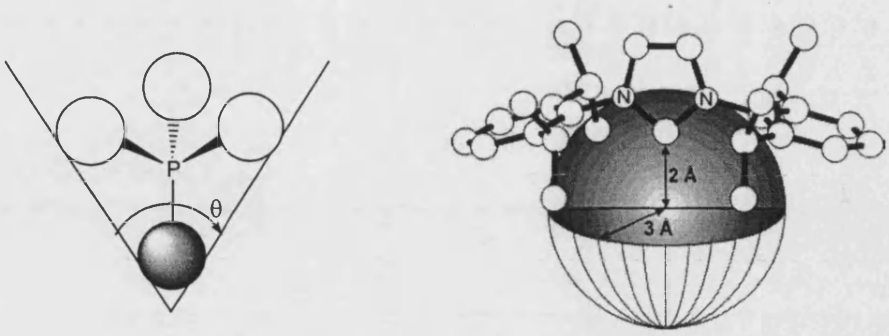

Figure 1.5 Pictorial representations to show how Tolman cone angle (θ) and $\%V_{Bur}$ values are obtained.

Percentage volume buried is calculated by imposing a sphere of 3 Å radius around the metal centre and looking at the volume of the sphere that the ligand occupies. Some values are given in **Table 1.3** along with corresponding cone angle values for phosphine ligands.

Ligand	$\%V_{Bur}$ [35, 37]	Cone angle (θ) [34]
PH_3	17	-
P^iPr_3	32	160
P^tBu_3	30	182
PCy_3	26*	170
PPh_3	22	145
IMes	26	
SIMes	27	
IPr	29	
SIPr	30	
ICy	23	

Table 1.3 $\%V_{Bur}$ and cone angles values for a range of phosphine ligands and IMes.

* $\%V_{Bur}$ for PCy_3 is also quoted as 32 elsewhere.[35] However, Nolan notes that $\%V_{Bur}$ for IMes is similar to that for PCy_3[33] and it is on this basis that 26 is the value used in **Table 1.3**.

Nolan has commented that BDEs are essentially controlled by steric requirements of the ligand in question, which would explain why the BDE values for P^tBu_3 and PPh_3 are not wildly different whereas the other comparative data in **Table 1.1** are. The relationship between BDE and steric influence was confirmed by plotting experimental BDEs for $Ru(C_5Me_5)(L)(Cl)$ against $\%V_{Bur}$, exhibiting their linear relationship.[35]

1.5 NHC complexes

Grubbs' second generation metathesis catalyst $Ru(PCy_3)(SIMes)(=CHPh)Cl_2$ (**B** in **Figure 1.6**) is a prominent example of the attributes of NHC use in catalysis over full phosphine systems, providing better activity and enhanced stability over the original first generation catalyst $Ru(PCy_3)_2(=CHPh)Cl_2$ (**A** in **Figure 1.6**).[38-40] Substitution of both phosphine groups for NHC ligands does not improve the catalytic activity as the system relies on dissociation of a labile ligand, such as PR_3 to form the electron-deficient active catalyst $RuL(=CHPh)Cl_2$.[41-43] The use of NHCs in Ru-alkylidene catalysis has 'closed the gap' between the previous Ru and Mo based systems, which suffered from either decreased reactivity or low tolerance of different organic functional groups, respectively.[44] In fact a culmination of Grubbs and Hoveyda's work has led to the preparation of the very stable, phosphine-free and highly selective cross metathesis (CM) and ring-closing metathesis (RCM) catalyst **C** (**Figure 1.6**).[45]

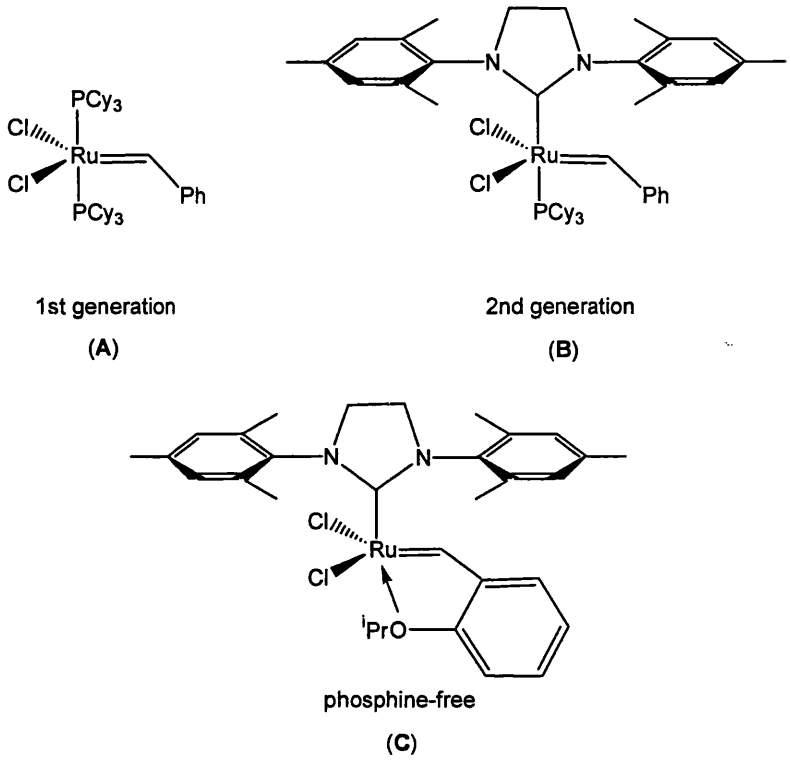

Figure 1.6 Important metathesis catalysts.

This class of complex can be 'tuned' by varying the substituents of the imidazol ring, such as the use of unsymmetrical backbone moieties to afford chiral metathesis catalysts.[46-49] Sterically and electronically different complexes have been prepared by employing different groups on the N atoms or even by changing the size of the heterocyclic ring itself.[50-53] Complexes containing the more bulky NHCs generally favour dissociation of the labile ligand, necessary for initiation, whereas a sterically congested metal centre results in disfavoured alkene coordination. Both of these effects can be observed by changing the NHC in $Ru(PCy_3)(NHC)(=CPh)Cl_2$ from SIMes to SIPr; when the more sterically demanding ligand SIPr is used there is a corresponding increase in the self-metathesis of terminal alkenes (6 times higher TON), but decreased activity for internal alkenes (> 100 times lower TON), which require better access to the metal centre (**Scheme 1.3**).[54]

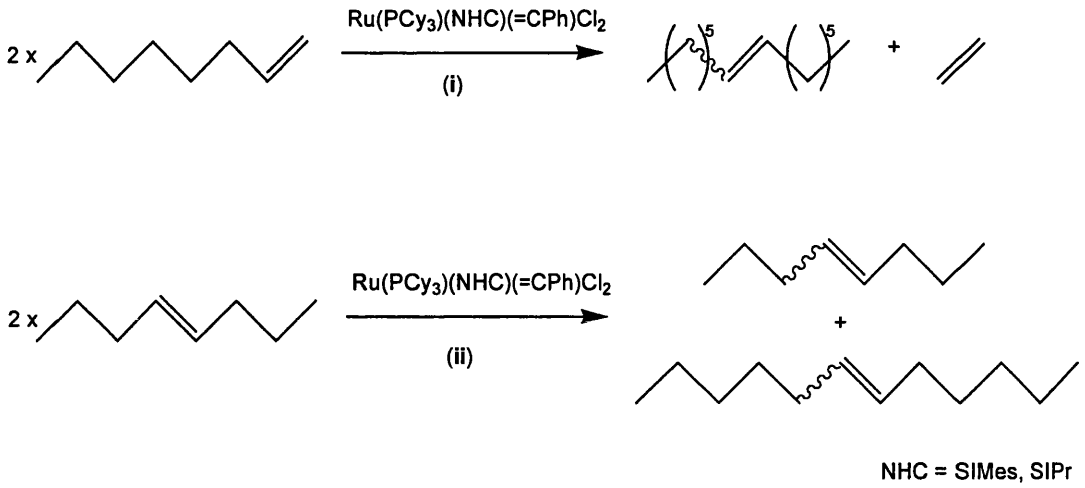

Scheme 1.3 Self-metathesis of terminal and internal alkenes 1-octene and *trans*-4-decene, **i** and **ii** respectively.

NHCs have also been incorporated into Ru-vinylidene RCM catalysts (**D**), with mixed PR_3/NHC complexes displaying substantially higher activity over their bis PR_3 counterparts (**Figure 1.7**).[55] This is also the case for the related, more thermally stable Ru-indenylidene complexes (**E**); substitution of a phosphine ligand (PPh_3, PCy_3) for an NHC (IMes, IPr) further enhances both stability and activity.[56]

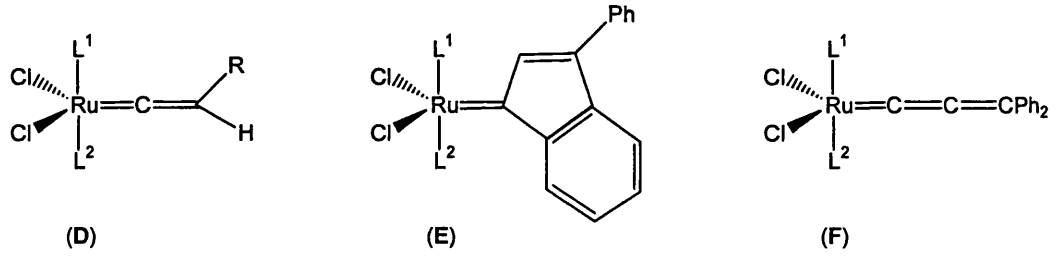

$L^1 = L^2 = PCy_3$;	R = Ph	$L^1 = L^2 = PCy_3$	$L^1 = L^2 = PCy_3$
$L^1 = L^2 = PCy_3$;	R = ^{t}Bu	$L^1 = L^2 = PPh_3$	L^1 = IMes; $L^2 = PCy_3$
$L^1 = L^2 = {}^i PrMe_2$;	R = Ph	L^1 = IMes; $L^2 = PPh_3$	
L^1 = IMes; $L^2 = PCy_3$;	R = ^{t}Bu	L^1 = IMes; $L^2 = PCy_3$	
		L^1 = IPr; $L^2 = PPh_3$	
		L^1 = IPr; $L^2 = PCy_3$	

Figure 1.7 Ru-vinylidene, Ru-indenylidene and Ru-allenylidene complexes with varying ligands.[55, 56]

In contrast, the bis phosphine allenylidene analogue **F** is a more active RCM catalyst than the related mono IMes species (although neither are particularly active), however, the inclusion of IMes in the latter does increase thermal stability. More details on NHC-use in metathesis reactions are covered particularly well in several reviews by Nolan, Glorius and Dragutan.[57-59]

As well as their pivotal role in metathesis chemistry, Grubbs' first and second generation catalysts (**A** and **B**) are also reported to catalyse other reactions as well as metathesis.[60] For example, PCy_3 analogues of **A**, **B** (L^1 = IMes, SIMes) and the indenylidene complex **E** (L^1 = IMes) have all been shown to be active in the hydrosilylation of terminal alkynes.[61] **Scheme 1.4** shows the reaction of phenylacetylene with triethylsilane to produce vinylsilane (exclusively the *cis* addition isomer *Z*-vinylsilane), some α-addition product and significant amounts of the phenylacetylene dimer. This work followed on from Herrmann's initial use of NHCs in hydrosilylation catalysts such as Rh(NHC)(cod)Cl.[62]

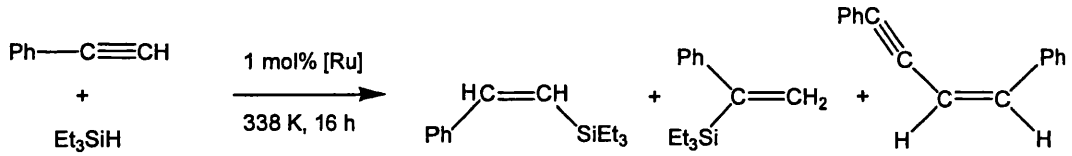

Scheme 1.4 Hydrosilylation of styrene.

Mol *et al* have studied the degradation of **A**, **B** and the related species $Ru(PCy_3)(SIPr)(=CHPh)Cl_2$, by treatment with primary alcohols in the presence of base (NEt_3) to investigate whether these complexes also act as precatalysts. The degradation reactions of **A**, **B** and the analogous species $Ru(PCy_3)(SIPr)(=CHPh)Cl_2$ gave rise to the hydride chloride complexes $RuL_2(CO)(Cl)H$ {L_2 = $(PCy_3)_2$; $(PCy_3)(SIMes)$; $(PCy_3)(SIPr)$} (**G**) formed *via* a non-catalytic alcohol dehydrogenation pathway (**Scheme 1.5**).[63-65] Importantly, the bis phosphine complex $Ru(PCy_3)_2(CO)(Cl)H$ is reported to be highly active in alkene hydrogenation reactions,[66] and similar 5-coordinate systems based on Os are also active hydrogenation catalysts.[67-70]

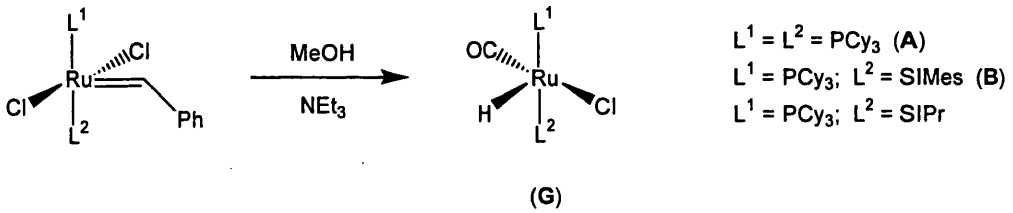

Scheme 1.5 Formation of hydride chloride complexes from Grubbs'-type catalysts.

Mixed PR_3/NHC complexes $RuL_2(CO)(Cl)H$ (**G**) can be prepared by simple PR_3/NHC ligand exchange in $Ru(PR_3)_n(CO)(Cl)H$ (n = 2, 3). This method has been used by Nolan to form $Ru(PCy_3)(IMes)(CO)(Cl)H$ and $Ru(PPh_3)(IMes)(CO)(Cl)H$, both active hydrogenation catalysts.[71, 72] Within the Whittlesey group bis NHC versions of $RuL_2(CO)(Cl)H$ (**G**) are the subject of investigation, including complexes where L = IMes, IPr, SIPr.[73, 74] In addition, the hydride fluoride systems $Ru(PPh_3)(L)(CO)(F)H$ (L = IMes, SIMes, IPr, SIPr) are being studied with a view towards catalysis.[75]

1.6 Bond activation in Ru-NHC complexes

A substantial contribution to this area has come from within the Whittlesey group. Reaction of IMes with $Ru(PPh_3)_3(CO)H_2$ at 353 K produces both mono and bis IMes complexes $Ru(PPh_3)_2(IMes)(CO)H_2$ and $Ru(PPh_3)(IMes)_2(CO)H_2$. The former undergoes C-H activation when treated with trimethylvinylsilane ($Me_3SiCH{=}CH_2$) or other alkenes at room temperature to yield $Ru(PPh_3)_2(IMes')(CO)H$. Furthermore, the reaction between excess IMes and $Ru(PPh_3)_3(CO)H_2$ at 383 K results in the formation of the C-C activated complex $Ru(PPh_3)_2(IMes'')(CO)H$.[76] (**Scheme 1.6**).

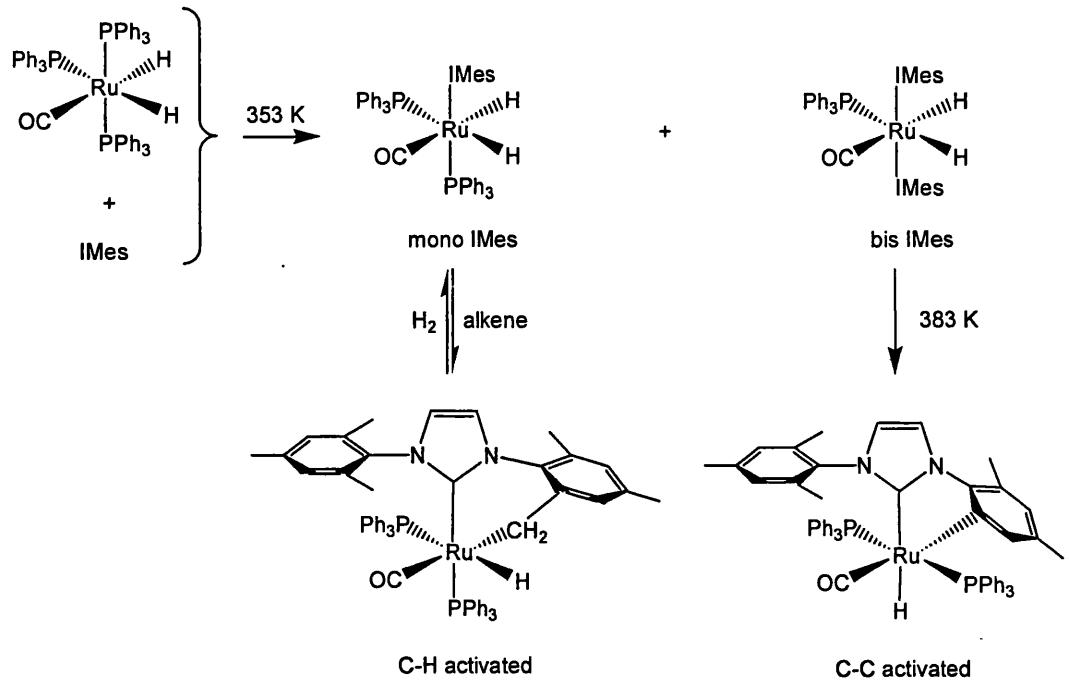

Scheme 1.6 Formation of mono, bis, C-H and C-C activated Ru-IMes complexes.[76]

A variety of other NHC ligands have been prepared and reacted with $Ru(PPh_3)_3(CO)H_2$ to achieve mono substituted NHC complexes, $Ru(PPh_3)_2(NHC)(CO)H_2$ as displayed in **Scheme 1.7** overleaf. Substitution of PPh_3 for an IMes ligand in $Ru(PPh_3)_3(CO)H_2$ resulted in IMes lying in the axial position as shown above, whereas the other NHCs are located equatorially due to steric factors. The reaction with I^{i}Pr gave rise to a C-H activated product immediately, whereas the other complexes underwent C-H activation upon addition of $Me_3SiCH{=}CH_2$. In the case of IMe_4 and ICy, C-H activation of the NHC was not observed.[77] The C-H activation process was reversible with H_2 or ROH; a process that has been exploited for catalysis, such as indirect Wittig reactions on alcohols.[77, 78]

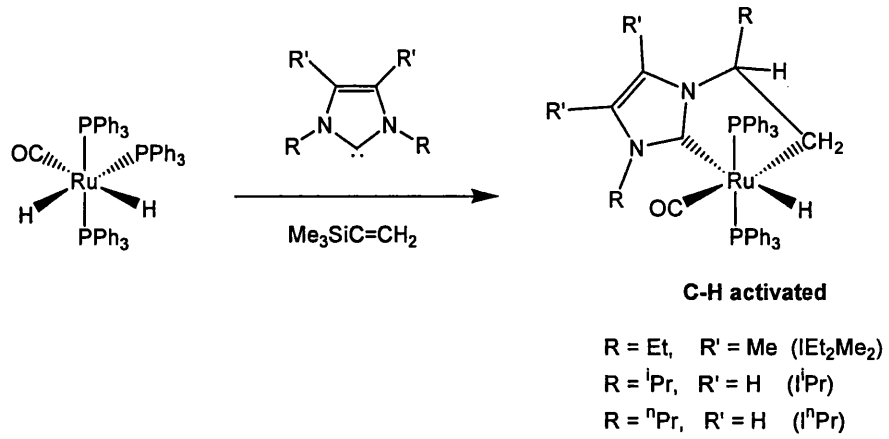

Scheme 1.7 The reaction of $Ru(PPh_3)_3(CO)H_2$ with a variety of NHCs.

Clearly the choice of NHC has an effect on the propensity for C-H activation, while the ancillary ligands on the ruthenium starting complex are also a contributing factor. The related chelating phosphine complexes Ru(dppp)(IMes)(CO)H and Ru(arphos)(IMes)(CO)H require much higher temperatures to achieve C-H activation with alkene (373 and 348 K respectively). The reverse reaction with H_2 back to non-activated products is slow (12 h) and involves similar temperatures.[79]

Other groups have reported C-H activation of NHC ligands with ruthenium precursors. For example, Morris reacted $Ru(PPh_3)_3(Cl)H$ with IMes and SIMes to form mono NHC C-H activated complexes $Ru(PPh_3)_2(IMes')H$ and $Ru(PPh_3)_2(SIMes')H$ with elimination of the corresponding imidazolium chlorides. Bis NHC complexes were not formed, which has been attributed to steric factors. The reaction of $Ru(PPh_3)_3(Cl)H$ with I^{t}Bu in THF did not lead to the C-H activated complex but a highly reactive species assigned as '$Ru(PPh_3)_2(I^tBu)$', which when treated with H_2, gave isomers of $Ru(PPh_3)_2(I^tBu)H_2$ stabilised by an agostic Ru···H interaction (**Scheme 1.8**).[80]

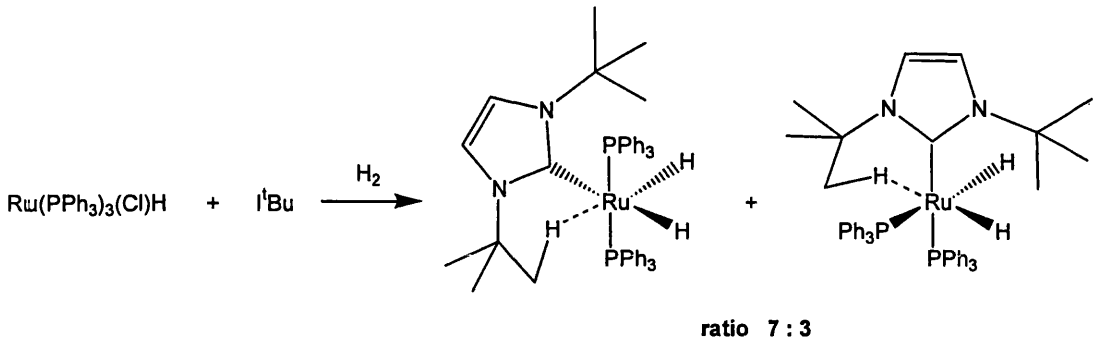

Scheme 1.8 The reaction of $Ru(PPh_3)_3(Cl)H$ with I^tBu to form two isomers with agostic interactions.[80]

Agostic interactions are a potential indication of whether C-H activation could occur in a system, based on the distance between the metal centre and the potential activation centre. The Whittlesey group have expanded on the work of Morris by reacting $Ru(PPh_3)_3(Cl)H$ with ICy and $I^iPr_2Me_2$ in CH_2Cl_2. The reaction with ICy yielded $Ru(PPh_3)_2(ICy)(Cl)H$ with an agostic bond from the α-CH_2 of the cyclohexyl group, similar to Morris' reports. However, the reaction between $Ru(PPh_3)_3(Cl)H$ and $I^iPr_2Me_2$ formed both a C-H activated complex and a product with agostic interactions shown in **Figure 1.8**.

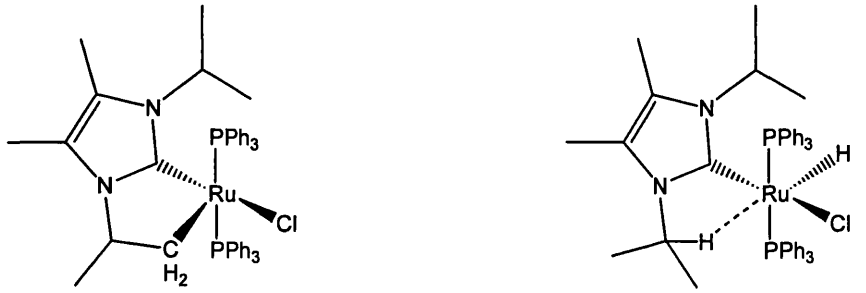

Figure 1.8 Formation of C-H activated and agostic complexes of Ru- $I^iPr_2Me_2$.

In contrast, the monocarbonyl starting complex $Ru(PPh_3)_3(CO)(Cl)H$ reacted with $I^iPr_2Me_2$ in THF to afford not only the C-H activated product $Ru(PPh_3)_2(I^iPr_2Me_2')(CO)(Cl)$ but also unique examples of C- and N- bound tautomers $Ru(PPh_3)_2(C\text{-}I^iPrHMe_2)(CO)(Cl)H$ and

$Ru(PPh_3)_2(N\text{-}I^iPrHMe_2)(CO)(Cl)H$, with loss of propene from the system (**Figure 1.9**).[81] The analogous reaction with IEt_2Me_2 produced the simple substitution product $Ru(PPh_3)_2(IEt_2Me_2)(CO)(Cl)H$, in line with the higher reactivity consistently observed for Ru-$I^iPr_2Me_2$ complexes.[77]

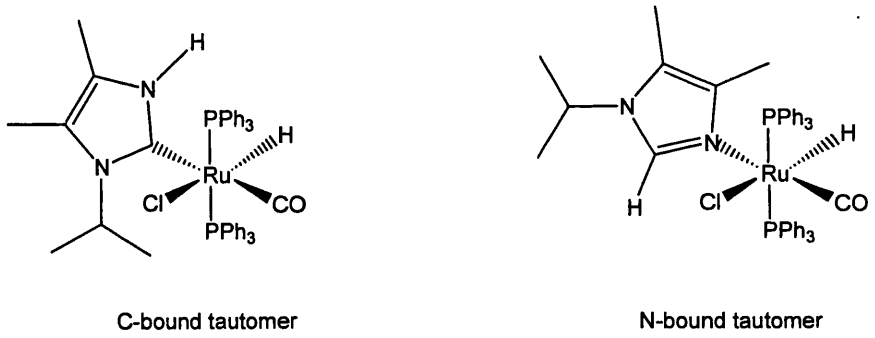

Figure 1.9 C- and N- bound tautomers from the reaction of $Ru(PPh_3)_3(CO)(Cl)H$ with $I^iPr_2Me_2$.[81]

1.7 Metal-hydride NHC complexes

Metal-hydride complexes have been used extensively in catalysis, whether directly or formed *in situ* from more stable pre-catalysts (eg. Noyori's DH and TH systems).[82-84] Hydride ligands serve various purposes depending on the system. They can help to stabilise complexes, provide a *trans* effect to labilise *trans* ligands such as phosphine ligands, hold substrates in the correct stereochemistry for catalysis *via* H-bonding and act as a source of hydrogen for transformations.

Dihydride complexes are very sought after, not only because of the fundamentally interesting non-classical η^2-H_2 bonding,[85] but also because they are considered to be precursors to active dihydride species upon loss of molecular hydrogen.[86] **Scheme 1.9** shows their potential for use as DH catalysts.

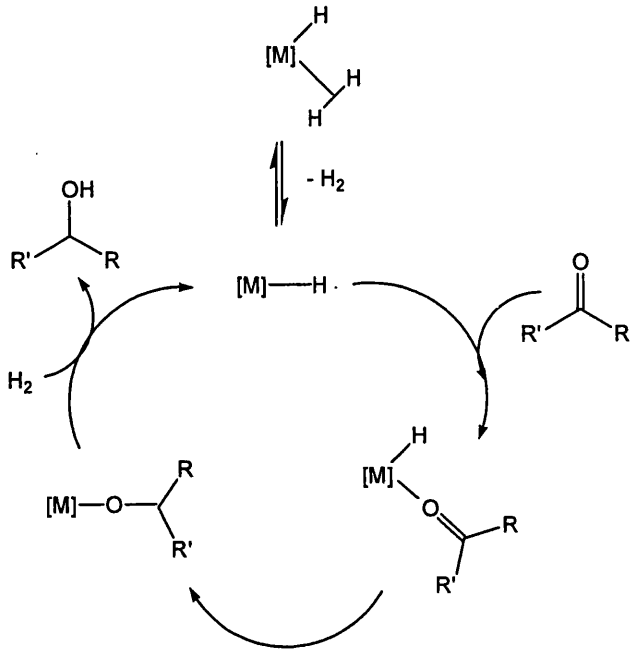

Scheme 1.9 Use of dihydrogen catalysts in DH systems.

Although extensive studies have recently been carried out on the effect of exchanging phosphine ligands with NHCs, there are still relatively few Ru-hydride NHC complexes.

1.8 Thesis Synopsis

This thesis describes the use IMes to stabilise Ru heteroatom containing species, including coordinatively unsaturated systems. **Chapter 2** provides details on previously prepared bis IMes heteroatom complexes and explains the recharacterisation of this class of complex in light of new information. Novel, related complexes are described, which support the reformulation of the species as mono hydridic, 16-electron systems. Furthermore, their potential for use as catalysts in hydrogenation of ketones is probed.

Chapter 3 describes the synthesis and characterisation of an array of Ru-bis IMes acetylide complexes. The work highlights reversible processes and investigates the possible mechanisms involved.

The reduction of hydride chloride Ru-IMes complexes is explored in **Chapter 4** in an attempt to synthesise 16-electron dihydride complexes. However,

reaction with $NaBH_4$ gave instead borohydride systems. A brief introduction to borohydride complexes is provided at the start of this chapter, and the synthesis, characterisation and reactivity of novel borohydride species are reported. This chapter also depicts other attempts to sythesise coordinatively unsaturated dihydride complexes.

Experimental details for all of the complexes described in this thesis are given in **Chapter 5**.

1.9 References

1. McGuinness, D.S.; Cavell, K.J., *Organometallics*, **2000**, *19*, 741.
2. Nielsen, D.J.; Cavell, K.J.; Skelton, B.W.; White, A.H., *Inorg. Chim. Acta*, **2002**, *327*, 116.
3. Arduengo, A.J.; Davidson, F.; Dias, H.V.R.; Goerlich, J.R.; Marshall, W.J.; Khasnis, D.; Prakasha, T.K., *J. Am. Chem. Soc.*, **1997**, *119*, 12742.
4. Stoll, M.E.; Lovelace, S.R.; Geiger, W.E.; Schimanke, H.; Hyla-Kryspin, I.; Gleiter, R., *J. Am. Chem. Soc.*, **1999**, *121*, 9343.
5. Hoffmann, R., *J. Am. Chem. Soc.*, **1968**, *90*, 1475.
6. Hoffmann, R.; Zeiss, G.D.; van Dine, G.W., *J. Am. Chem. Soc.*, **1968**, *90*, 1485.
7. Harrison, J.F., *J. Am. Chem. Soc.*, **1971**, *93*, 4112.
8. Harrison, J.F.; Liedke, C.R.; Liebman, J.F., *J. Am. Chem. Soc.*, **1979**, *101*, 7162.
9. Wanzlick, H.W.; Schönherr, H.J., *Angew. Chem.-Int. Ed.*, **1968**, *7*, 141.
10. Öfele, K., *J. Organomet. Chem.*, **1968**, *12*, P42.
11. Arduengo, A.J.; Harlow, R.L.; Kline, M., *J. Am. Chem. Soc.*, **1991**, *113*, 361.
12. Kuhn, V.; Kratz, T., *Synthesis*, **1993**, *6*, 561.
13. Bonnet, L.G.; Douthwaite, R.E.; Kariuki, B.M., *Organometallics*, **2003**, *22*, 4187.
14. Nyce, G.W.; Csihony, S.; Waymouth, R.M.; Hedrick, J.L., *Chem.-Eur. J.*, **2004**, *10*, 4073.

15. Enders, D.; Breuer, K.; Kallfass, U.; Balensiefer, T., *Synthesis*, **2003**, *8*, 1292.
16. Wanzlick, H.W.; Kleiner, H.J., *Angew. Chem.*, **1961**, *73*, 493.
17. Lemal, D.M.; A., L.R.; Kawano, K.I., *J. Am. Chem. Soc.*, **1964**, *86*, 2518.
18. Nyulászi, L.; Veszprérni, T.; Forró, A., *Phys. Chem. Chem. Phys.*, **2000**, *2*, 3127.
19. Arduengo, A.J.; Goerlich, J.R.; Krafczyk, R.; Marshall, W.J., *Angew. Chem. -Int. Ed.*, **1998**, *37*, 1963.
20. Green, J.C.; Scurr, R.G.; Arnold, P.L.; Cloke, F.G.N., *Chem. Commun.*, **1997**, 1963.
21. Herrmann, W.A.; Runte, O.; Artus, G., *J. Organomet. Chem.*, **1995**, *501*, C1.
22. Grundemann, S.; Kovacevic, A.; Albrecht, M.; Faller, J.W.; Crabtree, R.H., *Chem. Commun.*, **2001**, 2274.
23. Kovacevic, A.; Grundemann, S.; Miecznikowski, J.R.; Clot, E.; Eisenstein, O.; Crabtree, R.H., *Chem. Commun.*, **2002**, 2580.
24. Lebel, H.; Janes, M.K.; Charette, A.B.; Nolan, S.P., *J. Am. Chem. Soc.*, **2004**, *126*, 5046.
25. Crabtree, R.H., *Dalton Trans.*, **2003**, 3985.
26. Grundemann, S.; Kovacevic, A.; Albrecht, M.; Faller, J.W.; Crabtree, R.H., *J. Am. Chem. Soc.*, **2002**, *124*, 10473.
27. Danopoulos, A.A.; Tsoureas, N.; Wright, J.A.; Light, M.E., *Organometallics*, **2004**, *23*, 166.
28. Ellul, C.; Mahon, M.F.; Saker, O.; Whittlesey, M.K., *unpublished results*, **2007**.
29. Herrmann, W.A., *Angew. Chem.-Int. Ed.*, **2002**, *41*, 1290.
30. Simms, R.W.; Drewitt, M.J.; Baird, M.C., *Organometallics*, **2002**, *21*, 2958.
31. Titcomb, L.r.; Caddick, S.; Cloke, F.G.N.; Wilson, D.J.; McKerrecher, D., *Chem. Commun.*, **2001**, 1388.
32. Magill, A.M.; Cavell, K.J.; Yates, B.F., *J. Am. Chem. Soc.*, **2004**, *126*, 8717.
33. Nolan, S.P.; Dorta, R.; Stevens, E.D.; Scott, N.M.; Costabile, C.; Cavallo, L.; Hoff, C.D., *J. Am. Chem. Soc.*, **2005**, *127*, 2485.
34. Tolman, C.A., *Chem. Rev.*, **1977**, *77*, 313.
35. Hillier, A.C.; Sommer, W.J.; Yong, B.S.; Petersen, J.L.; Cavallo, L.; Nolan, S.P., *Organometallics*, **2003**, *22*, 4322.

36. Weskamp, T.; Kohl, F.J.; Hieringer, W.; Gleich, D.; Herrmann, W.A., *Angew. Chem.-Int. Ed.*, **1999**, *38*, 2416.
37. Scott, N.M.; Nolan, S.P., *Eur. J. Chem.*, **2005**, *10*, 1815.
38. Trnka, T.M.; Grubbs, R.H., *Acc. Chem. Res.*, **2001**, *34*, 18.
39. Grubbs, R.H.; Chang, S., *Tetrahedron*, **1998**, *54*, 4413.
40. Herrmann, W.A.(Ed), *Applied Homogenous Catalysis with Organometallic Compounds; VHC, Weinheim*, **1996**, 712.
41. Dias, E.L.; Nguyen, S.T.; Grubbs, R.H., *J. Am. Chem. Soc.*, **1997**, *119*, 3887.
42. Weskamp, T.; Schattenmann, W.C.; Spiegler, M.; Herrmann, W.A., *Angew. Chem.-Int. Ed.*, **1998**, *37*, 2490.
43. Ackermann, L.; Furstner, A.; Weskamp, T.; Kohl, F.J.; Herrmann, W.A., *Tetrahedron Lett.*, **1999**, *40*, 4787.
44. Love, J.A.; Sanford, M.S.; Day, M.W.; Grubbs, R.H., *J. Am. Chem. Soc.*, **2003**, *125*, 10103.
45. Garber, S.B.; Kingsbury, J.S.; Gray, B.L.; Hoveyda, A.H., *J. Am. Chem. Soc.*, **2000**, *122*, 8168.
46. Seiders, T.J.; Ward, D.W.; Grubbs, R.H., *Org. Lett.*, **2001**, *3*, 3225.
47. Van Veldhuizen, J.J.; Gillingham, D.G.; Garber, S.B.; Kataoka, O.; Hoveyda, A.H., *J. Am. Chem. Soc.*, **2003**, *125*, 12502.
48. Van Veldhuizen, J.J.; Garber, S.B.; Kingsbury, J.S.; Hoveyda, A.H., *J. Am. Chem. Soc.*, **2002**, *124*, 4954.
49. Herrmann, W.A.; Goossen, L.J.; Artus, G.R.J.; Kocher, C., *Organometallics*, **1997**, *16*, 2472.
50. Yun, J.; Marinez, E.R.; Grubbs, R.H., *Organometallics*, **2004**, *23*, 4172.
51. Yang, L.R.; Mayr, M.; Wurst, K.; Buchmeister, M.R., *Chem. -Eur. J.*, **2004**, *10*, 5761.
52. Despagnet-Ayoub, E.; Grubbs, R.H., *J. Am. Chem. Soc.*, **2004**, *126*, 10198.
53. Despagnet-Ayoub, E.; Grubbs, R.H., *Organometallics*, **2005**, *24*, 338.
54. Dinger, M.B.; Mol, J.C., *Adv. Synth. Catal.*, **2002**, *344*, 671.
55. Louie, J.; Grubbs, R.H., *Angew. Chem. -Int. Ed.*, **2001**, *40*, 247.
56. Jafarpour, L.; Schanz, H.J.; Stevens, E.D.; Nolan, S.P., *Organometallics*, **1999**, *18*, 5416.
57. Nolan, S.P.(Ed), *N-Heterocyclic Carbenes in Synthesis; Wiley-VCH*, **2006**.

58. Glorius, F.(Ed), *Topics in Organometallic Chemistry: N-Heterocyclic Carbenes in Transition Metal Catalysis; Springer*, **2007**, *21*.
59. Dragutan, I.; Dragutan, V.; Filip, P., *Arkivoc*, **2005**, *10*, 105.
60. Alcaide, B.; Almendros, P., *Chem.-Eur. J.*, **2003**, *9*, 1258.
61. Maifield, S.V.; Tran, M.N.; Lee, D., *Tetrahedron Lett.*, **2005**, *46*, 105.
62. Herrmann, W.A.; Goossen, L.J.; Kocher, C.; Artus, G.R.J., *Angew. Chem. Int. Ed.*, **1996**, *35*, 2805.
63. Dinger, M.B.; Mol, J.C., *Organometallics*, **2003**, *22*, 1089.
64. Dinger, M.B.; Mol, J.C., *Eur. J. Chem.*, **2003**, 2827.
65. Banti, D.; Mol, J.C., *J. Organomet. Chem.*, **2004**, *689*, 3113.
66. Yi, C.S.; Lee, D.W., *Organometallics*, **1999**, *18*, 5152.
67. Esteruelas, M.A.; Sola, E.; Oro, L.A.; Werner, H.; Meyer, U., *J. Mol. Cat.*, **1988**, *45*, 1.
68. Esteruelas, M.A.; Sola, E.; Oro, L.A.; Meyer, U.; Werner, H., *Angew. Chem.-Int. Ed.*, **1988**, *27*, 1563.
69. Esteruelas, M.A.; Valero, C.; Oro, L.A.; Meyer, U.; Werner, H., *Inorg. Chem.*, **1991**, *30*, 1159.
70. Esteruelas, M.A.; Oro, L.A.; Valero, C., *Organometallics*, **1992**, *11*, 3362.
71. Lee, H.M.; Smith, J., D. C.; He, Z.; Stevens, E.D.; Yi, C.S.; Nolan, S.P., *Organometallics*, **2001**, *20*, 794.
72. Nolan, S.P.; Fogg, D.E.; dos Santos, E.N.; Foucault, H.M.; Dharmasena, U.L., *Organometallics*, **2005**, *24*, 1056.
73. Jazzar, R.F.R., *PhD Thesis, University of Bath*, **2003**.
74. Saker, O., *unpublished results*, **2007**.
75. Reade, S.P., *unpublished results*, **2007**.
76. Jazzar, R.F.R.; Macgregor, S.A.; Mahon, M.F.; Richards, S.P.; Whittlesey, M.K., *J. Am. Chem. Soc.*, **2002**, *124*, 4944.
77. Burling, S.; Paine, B.M.; Nama, D.; Brown, V.S.; Mahon, M.F.; Prior, T.J.; Pregosin, P.S.; Whittlesey, M.K.; Williams, J.M.J., *J. Am. Chem. Soc.*, **2007**, *129*, 1987.
78. Edwards, M.G.; Jazzar, R.F.R.; Paine, B.M.; Shermer, D.J.; Whittlesey, M.K.; Williams, J.M.J.; Edney, D.D., *Chem. Commun.*, **2004**, 90.
79. Chilvers, M.J.; Jazzar, R.F.R.; Mahon, M.F.; Whittlesey, M.K., *Adv. Synth. Catal.*, **2003**, *345*, 1111.

80. Abdur-Rashid, K.; Fedorkiw, T.; Lough, A.J.; Morris, R.H., *Organometallics*, **2004**, *23*, 86.

81. Burling, S.; Mahon, M.F.; Powell, R.E.; Whittlesey, M.K.; Williams, J.M.J., *J. Am. Chem. Soc.*, **2006**, *128*, 13702.

82. Haack, K.J.; Hashiguchi, S.; Fujii, A.; Ikariya, T.; Noyori, R., *Angew. Chem. Int. Ed.*, **1997**, *36*, 285.

83. Chowdhury, R.L.; Backvall, J.E., *J. Chem. Soc., Chem. Commun.*, **1991**, 1063.

84. Aranyos, A.; Csjernyik, G.; Szabó, K.J.; Backväll, J.E., *Chem. Commun.*, **1999**, 351.

85. Kubas, G.J.; Ryan, R.R.; Swanson, B.I.; Vergamini, P.J.; Wasserman, H.J., *J. Am. Chem. Soc.*, **1984**, *106*, 451.

86. Peruzzini, M.; (Ed); Poli, R.; (Ed), *Recent Advances in Hydride Chemistry; Elsevier, Amsterdam*, **2001**.

Chapter 2

2. Ruthenium-IMes heteroatom containing complexes

2.1 Preamble

This chapter is split into four parts, starting with an introduction into the use of IMes in the Whittlesey group and the history behind this project. We deal with the reformulation of the bis IMes, 18-electron, *trans* dihydride complexes $Ru(IMes)_2(CO)(XH)H_2$ as in fact 16-electron mono hydride species $Ru(IMes)_2(CO)(X)H$, using insights gained from computational studies performed in collaboration with Dr Stuart Macgregor at Heriot-Watt University. There is some discussion on the difficulty of correctly assigning our products and description of the additional techniques utilised to secure their characterisation as $Ru(IMes)_2(CO)(X)H$, including the preparation of analogous complexes. Comparisons to complexes reported in the literature are provided throughout the sections and a summary of our 16-electron complexes appears towards the end of the first section. Secondly we report attempts to observe the non-classically bound H_2 complex $Ru(IMes)_2(CO)(X)(\eta^2\text{-}H_2)H$, a proposed intermediate in the formation of $Ru(IMes)_2(CO)(X)H$. In the third section $Ru(IMes)_2(CO)(X)H$ complexes are investigated as potential hydrogenation catalysts. Finally, there are descriptions of efforts to trap the 16-electron complexes by small molecules including CO and NH_3.

2.2 Previous work

Jazzar reacted the complex $Ru(PPh_3)_3(CO)H_2$ with IMes in order to form the mixed phosphine/NHC species $Ru(PPh_3)_2(IMes)(CO)H_2$ by simple ligand exchange. $Ru(PPh_3)_2(IMes)(CO)H_2$ was used a starting material for both C-C and C-H activated complexes.[1] However, the preparation of $Ru(PPh_3)_2(IMes)(CO)H_2$ required relatively high temperatures and prolonged reaction times (353 K, 14 days♥).[1] We proposed that using 'softer' arsine ligands in $Ru(AsPh_3)_3(CO)H_2$ might lead to milder reaction conditions.

However the reaction between $Ru(AsPh_3)_3(CO)H_2$ and IMes is not analogous to the reaction described above. In fact there is no evidence of the analogous product $Ru(AsPh_3)_2(IMes)(CO)H_2$ in the reaction mixture at any point as displayed in **Scheme 2.1**. After 3 days at 343 K it is possible to observe the bis NHC complex $Ru(AsPh_3)(IMes)_2(CO)H_2$ (**1**) by ^1H NMR spectroscopy but not possible to isolate this very reactive species.[2]

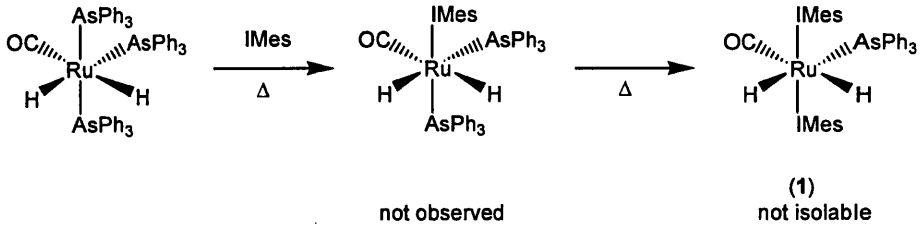

Scheme 2.1 The reaction of $Ru(AsPh_3)_3(CO)H_2$ with IMes.

1 is so reactive that any attempts to isolate the species led to the production of other complexes. When recrystallisation of **1** from C_6H_6 layered with hexane was attempted, reaction with adventitious water gave instead $Ru(IMes)_2(CO)(OH)H$ (**2**). Even the use of vigorously dried solvents resulted in the formation of **2**, but in lower yields. Ultimately H_2O was added to samples of **1** to maximise production of other $Ru(IMes)_2(CO)(OH)H$ (**2**). In the same manner, **1** was treated with a variety of HX substrates (X = OEt, SH, S^{n}Pr) to give the coordinatively unsaturated complexes, $Ru(IMes)_2(CO)(X)H$.[2, 3] Details and further reactions are discussed in the next section.

2.3 Coordinatively unsaturated NHC complexes with hydride ligands

Initially it was believed that reaction of $Ru(AsPh_3)(IMes)_2(CO)H_2$ (**1**) with HX gave a series of 18-electron dihydride complexes of formula $Ru(IMes)_2(CO)(XH)H_2$.[2, 3]

* Since published,[1] the reaction has been optimised by Paine and $Ru(PPh_3)_2(IMes)(CO)H_2$ can now be produced after just 4 days in toluene at 353 K.

These complexes were proposed to have *trans*-hydride structures based on the extreme upfield hydride shifts (*ca.* -25 ppm) in the ^{1}H NMR spectra and X-ray crystal structure determinations. However, further work suggested that this class of species is unstable with respect to the hydrogen-transfer (referred to as H-transfer from now on) complexes $Ru(IMes)_2(CO)(X)(\eta^2\text{-}H_2)H$. Hydrogen loss from $Ru(IMes)_2(CO)(X)(\eta^2\text{-}H_2)H$ results in the isolated complexes, correctly formulated as $Ru(IMes)_2(CO)(X)H$ as shown in **Scheme 2.2**.[4]

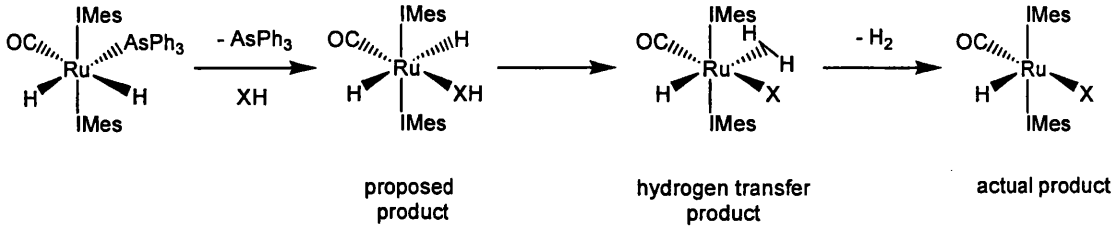

Scheme 2.2 Pathway for the reaction of $Ru(AsPh_3)(IMes)_2(CO)H_2$ with HX to produce $Ru(IMes)_2(CO)(X)H$.

Scheme 2.2 shows the pathway investigated computationally by Macgregor *et al* to find the relative stabilities of $Ru(IMes)_2(CO)(XH)H_2$ with respect to the H-transfer complexes $Ru(IMes)_2(CO)(X)(\eta^2\text{-}H_2)H$. Initial studies considered the energetics of $Ru(IH)_2(CO)(SH_2)H_2$ and $Ru(IH)_2(CO)(SH)(\eta^2\text{-}H_2)H$ with IH (imidazol-2-ylidene) as a model ligand to simplify the studies rather than the real IMes group. These calculations revealed that H-transfer from $Ru(IH)_2(CO)(SH_2)H_2$ has an activation energy of only 15.0 kJ mol^{-1},[4] suggesting that the transformation to $Ru(IH)_2(CO)(SH)(\eta^2\text{-}H_2)H$ should take place readily. In addition, $Ru(IH)_2(CO)(SH)(\eta^2\text{-}H_2)H$ was found to be 116.2 kJ mol^{-1} more stable than $Ru(IH)_2(CO)(SH_2)H_2$ indicating that the *trans*-dihydride hydrogen sulfide complex could not be an isolable species.[4] The H-transfer process itself takes place with lengthening of the Ru-S distance from 2.46 to 2.64 Å so that the SH_2 ligand is orientated to present one hydrogen toward the accepting hydride. It is important to note that H-transfer also affects the orientation of IH ligands from lying parallel to H-Ru-H, to lying close enough to SH_2 to form H-bonding interactions

(N-H···S = 2.35 Å). It is clear that these interactions are solely a result of using IH in the computational study rather than IMes.

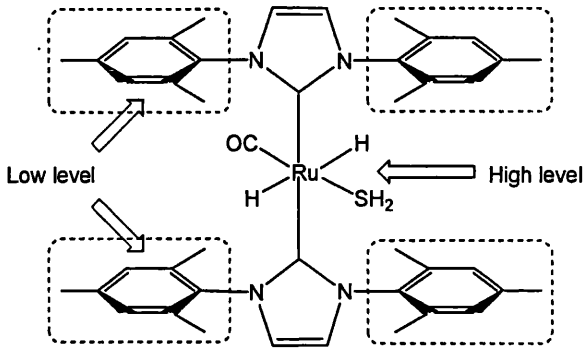

Figure 2.1 QM/MM description used to model $Ru(IMes)_2(CO)(SH_2)H_2$.

Hybrid QM/MM models of $Ru(IMes)_2(CO)(SH_2)H_2$ were used so that the mesityl arms of IMes groups could be described at a molecular mechanics level, whereas the rest of the complex was studied in more depth by density functional calculations as depicted in **Figure 2.1**. These new calculations showed that H-transfer has an activation barrier of almost the same magnitude (18.8 kJ mol^{-1}), although the formation of $Ru(IMes)_2(CO)(SH)(\eta^2\text{-}H_2)H$ is still exothermic although by 54.3 kJ mol^{-1} rather than 116.2 kJ mol^{-1}.[3] The process of H-transfer occurs similarly in $Ru(IMes)_2(CO)(SH)(\eta^2\text{-}H_2)H$ with elongation of the Ru-S bond etc. Any differences from calculations with IH can be attributed to the inclusion of the bulky mesityl groups in the calculation. This includes lengthening of Ru-C_{NHC} bonds by *ca.* 0.04 Å as well as the arrangement of the IMes ligands, which are staggered slightly with respect to each other but remain over the H-Ru-H axis. Deviation of IMes ligands from coplanarity remains in the range 35-48° throughout the process as significantly there are no hydrogen atoms available to undergo H-bonding and to cause possible NHC ligand rotation as found in $Ru(IH)_2(CO)(SH)(\eta^2\text{-}H_2)H$ (**Figure 2.2**). The orientation of the IMes ligands away from Ru-S also allows the S-H bond to lie out of the equatorial plane in $Ru(IMes)_2(CO)(SH)(\eta^2\text{-}H_2)H$. From the above information it is clear that inclusion of the mesityl groups has an impact on the overall energy change by decreasing the

stability of $Ru(IMes)_2(CO)(SH)(\eta^2\text{-}H_2)H$, possibly due to the absence of H-bonding and/or the steric effects of IMes.

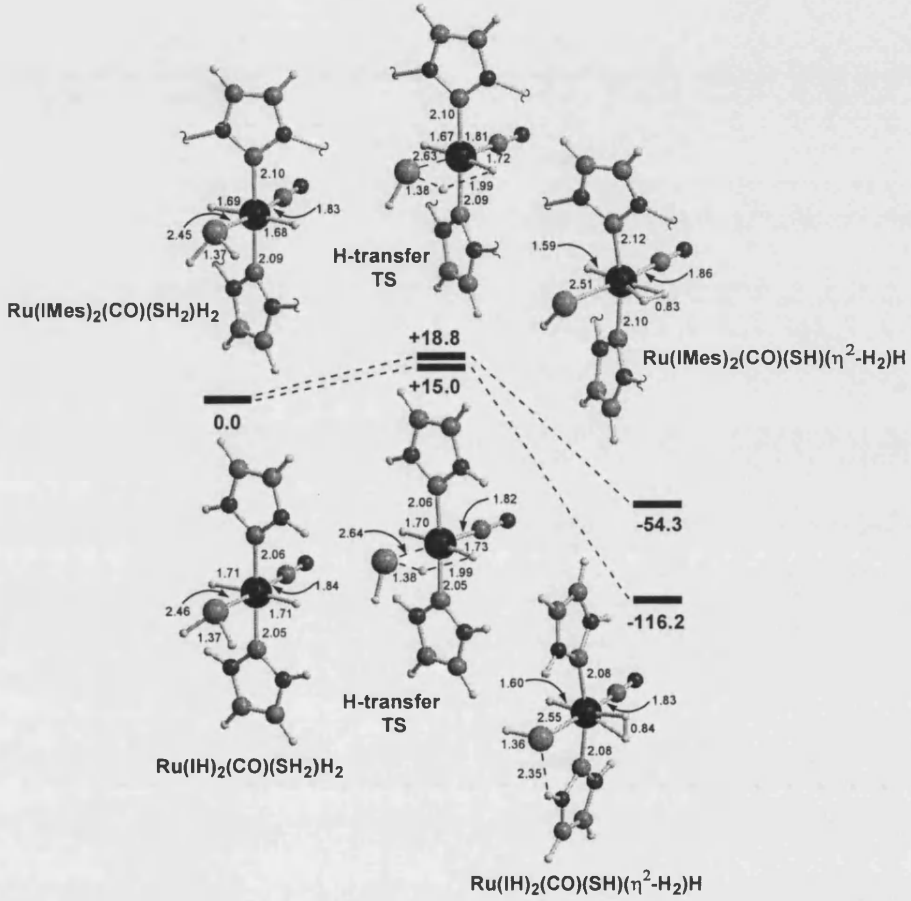

Figure 2.2 Computed reaction profiles (kJ mol^{-1}) for H-transfer in *trans*-$Ru(IR)_2(CO)(SH_2)H_2$ (R = H, Mes). Key distances are given in Å and structures for the IMes model are truncated at the N-Mes bonds for clarity.

Overall, the calculations carried out on both computational models show that H-transfer is favourable and suggest that $Ru(IMes)_2(CO)(X)(\eta^2\text{-}H_2)H$ should be observed in preference to $Ru(IMes)_2(CO)(XH)H_2$. With this in mind it was possible to reconsider the reaction of **1** with HX without necessarily having to account for all-*trans*-$Ru(IMes)_2(CO)(XH)H_2$, questioning the formulation of the isolated products as *trans*

dihydride complexes. Consequently the importance of the reaction pathway shown above in **Scheme 2.2** was reassessed. The first step in **Scheme 2.2** is loss of $AsPh_3$ and isomerisation to justify a geometry change to give *trans* hydride ligands. The *trans* effect makes it unlikely that isomerisation would occur to produce a *trans* hydride arrangement, especially as a vacant site is available. Accordingly the mechanism has been revised to provide a more favourable pathway without *trans* hydride ligands, as displayed below in **Scheme 2.3**. **1** loses $AsPh_3$ to create a vacant site, into which XH can bind to the metal centre. Subsequent H-transfer occurs and H_2 is lost to yield the product $Ru(IMes)_2(CO)(X)H$.

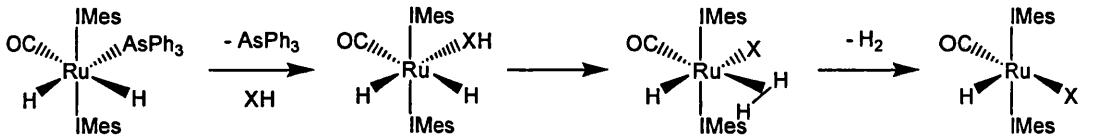

Scheme 2.3 Proposed reaction mechanism for the reaction of $Ru(AsPh_3)(IMes)_2(CO)H_2$ with HX to yield $Ru(IMes)_2(CO)(X)H$.

2.3.1 Characterisation difficulties associated with this class of complex

Although $Ru(IMes)_2(CO)(OH)H$ (**2**), $Ru(IMes)_2(CO)(OEt)H$ (**3**) and $Ru(IMes)_2(CO)(SH)H$ (**4**) were all characterised by X-ray crystallography there are a few factors that hindered correct assignment of the structures as $Ru(IMes)_2(CO)(X)H$. Firstly, the Ru-X bond lengths were not reliable in **3** and **4** due to disorder over X and CO positions, a well known problem seen in related *trans*-phosphine complexes.[5] Consequently the bond lengths could not be reliably assigned by comparison with Ru-XH in the literature. However, it was noted[6] that Ru-O distances in both **2** {2.023(2) Å} and **3** {1.881(10) Å} appeared significantly shorter than in other related aqua[7, 8] and ethanol[9-11] complexes (see **Table 2.1** and **2.2**).

There are very few monomeric ruthenium hydroxide complexes that have been structurally characterised to compare with **2**.[2, 5, 12-15] **Table 2.1** displays a number of Ru-OH_2 and Ru-OH distances including $Ru(IMes)_2(CO)_2(OH)H$, the 18-electron

dicarbonyl analogue of **2**. The Ru-O distance in **2** is more in line with the majority of the hydroxide species (*ca.* 2.0 Å)[2, 5, 14, 15] than aqua complexes (*ca.* 2.2 Å). However, it is worth noting that some reported hydroxide complexes such as $Ru(PMe_3)_4(OH)(Ph)$[13] and $[Ru(dmpe)_2(\mathbf{OH})H(\mu\text{-}OH_2)]_2$[16] contain Ru-O distances similar to aqua complexes (2.168(3) and 2.230(2) Å respectively). Many hydroxide complex structures are complicated by hydrogen bonding interactions with solvent in the unit cells, however this does not explain the longer Ru-O bond length in $Ru(PMe_3)_4(OH)(Ph)$ as the species is free from hydrogen bound water.[13]

Complex	Ru-O (Å)
2 [2]	2.023(2)
$Ru(dppb)(OH_2)Cl_3$ [7]	2.216(5)
$[Ru(dppe)(CO)(OH_2)_3]^{2+}$ [8]	2.180(2) 2.170(2) 2.157(2)
$Ru(dppe)(CO)(OH_2)(OTf)_2$ [8]	2.198(5)
$Ru(Tp^{iPr_2})(dppe)(OH)$ [15]	2.067(4)
$[Ru(\eta^6\text{-}C_5Me_4CH_2)(Me_2NCH_2CH_2NMe_2)(OH)]^+$ [14]	1.990(3)
$Ru(IMes)_2(CO)_2(OH)H$ [2]	2.058(3)

Table 2.1 Ru-O bond lengths (Å) for aqua and hydroxide complexes for comparion with **2**.

It is clear from **Table 2.2** that the Ru-O bond length in **3** is more comparable to values found for ethoxide species (bottom three entries *ca.* 1.9 Å) as opposed to ethanol complexes (*ca.* 2.1 – 2.2 Å).

Complex	M-O (Å)
3 [2]	1.881(10)
$Ru(PPh_3)(nMePPh)(HOEt)Cl$ [9]	2.224(9)
[*mer*-RuOTf(CO)(**NN'N**)(HOEt)]$^+$ [10]	2.159(2)
$[(OEP)Os(NO)(HOEt)]^+$ [11]	2.075(3)
(OEP)Os(NO)(OEt) [11]	1.89(2)
$Ru(C_6H_{16}N_2)(NO)(NO_2)_2(OEt)$ [17]	1.898(7)
$[Ru(anti\text{-}Me_8[16]aneS_4)(OEt)_2]^+$ [18]	1.983(4)

Table 2.2 M-O bond lengths (Å) for ethanol and ethoxy complexes for comparion with **3**.

Comparison of **4** with the directly related complexes $Ru(IMes)_2(CO)_2(SH)H$, $Ru(IMes)_2(CO)(SH)_2$ and $Ru(IMes)_2(CO)_2(SH)_2$ shows that the Ru-S bond lengths are similar (*ca.* 2.4 Å) consistent with the reassignment of **4** as $Ru(IMes)_2(CO)(SH)H$, containing a SH group rather than bound SH_2 (**Table 2.3**).

Complex	Ru-S (Å)
4 [3]	2.402(2)
$Ru(IMes)_2(CO)_2(SH)H$ [6]	2.4352(15)
$Ru(IMes)_2(CO)(SH)_2$ [3]	2.3764(5), 2.3693(5)
$Ru(IMes)_2(CO)_2(SH)_2$ [6]	2.4440(5), 2.4478(5)

Table 2.3 Ruthenium-sulfur bond lengths (Å) to show the similarity between **4** and well established examples containing bound SH.

Correct geometry assignment of **2**, **3** and **4** by their respective X-ray crystal structures was also hindered by the inability to reliably locate the hydrogen atoms in EtO-*H*, O-H_2 and HS-*H*. This was originally attributed to the inherent difficulties in finding the small electron density for hydrogen atoms rather than the fact that hydrogen atoms were not present. Analytical characterisation did not sufficiently highlight the

difference between $Ru(IMes)_2(CO)(XH)H_2$ and $Ru(IMes)_2(CO)(X)H$ because of their small difference in mass (only 2H).

By ^1H NMR spectroscopy, the chemical shifts for the ligand XH are generally broad and difficult to assign with certainty. Integration of the hydride resonance with respect to the IMes methyl protons was typically 1.5:36 and taken to be 2:36, consistent with the dihydride formulation $Ru(IMes)_2(CO)(XH)H_2$. However, integration of spectra acquired with a long pulse delay of 10 s showed that the ratio between the hydride signal and the resonance for the methyl groups of IMes was in fact 1:36, suggestive of the coordinatively unsaturated complex $Ru(IMes)_2(CO)(X)H$.

Initially, upfield hydride resonances of **2**, **3**, **4** and **5** in the ^1H NMR spectra were assigned to *trans* hydride ligands (-23.15, -23.51, -24.47 and -23.77 ppm respectively).[2, 3] It was reasoned that the IMes groups had sufficient steric bulk to stabilise *trans* hydride ligands similar to the bulky phosphine platinum complexes PtL_2H_2 (L = PPh^tBu_2, PCy_3 and P^iPr_3) reported by Yoshida.[19] However, *trans* hydride ligands appear over a large range of chemical shifts in the hydride region and do not necessarily even differ significantly from the related *cis* complexes.[19-24] For example, our group has prepared the 18-electron complex $Ru(PPh_3)_2(IEt_2Me_2)(CO)H_2$ with *trans* hydride ligands apparent at -4.90 ppm in the ^1H NMR spectrum in comparison to the *cis* isomer with shifts at -6.38 and -9.99 ppm.[25] In hindsight the chemical shifts reported for **2**, **3**, **4** and **5** are more diagnostic of the hydride ligand lying *trans* to a vacant site comparable to the complexes displayed in **Table 2.4**.

Complex	^1H NMR shift Ru-<u>H</u> (ppm)	Complex	^1H NMR shift Ru-<u>H</u> (ppm)
$Ru(P^tBu_2Me)_2(CO)(OH)H$ [26]	-22.3	**2** [2]	-23.15
$Ru(P^tBu_2Me)_2(CO)(OEt)H$ [26]	-24.2	**3** [2]	-23.51
$Ru(P^iPr_3)_2(CO)(SH)H$ [27]	-20.71	**4** [3]	-24.47
$Ru(P^tBu_2Me)_2(CO)(SPh)H$ [26]	-23.9	**5** [2]	-23.77

Table 2.4. Typical ^1H NMR spectroscopic values of complexes containing hydride ligands *trans* to a vacant site.

The structures were unequivocally confirmed as $Ru(IMes)_2(CO)(X)H$ by ^{13}C-^{1}H coupled NMR spectroscopy. Signals for the carbonyl and carbenic carbon atoms appeared as doublets (**Figure 2.3**) due to coupling to **one** hydride ligand rather than triplet signals, as would arise from coupling to two equivalent *trans*-hydride ligands. **Table 2.5** displays ^{13}C NMR spectroscopic shifts for carbonyl and carbenic atoms of the complexes **2**, **3** and **4** with their respective coupling constant values.

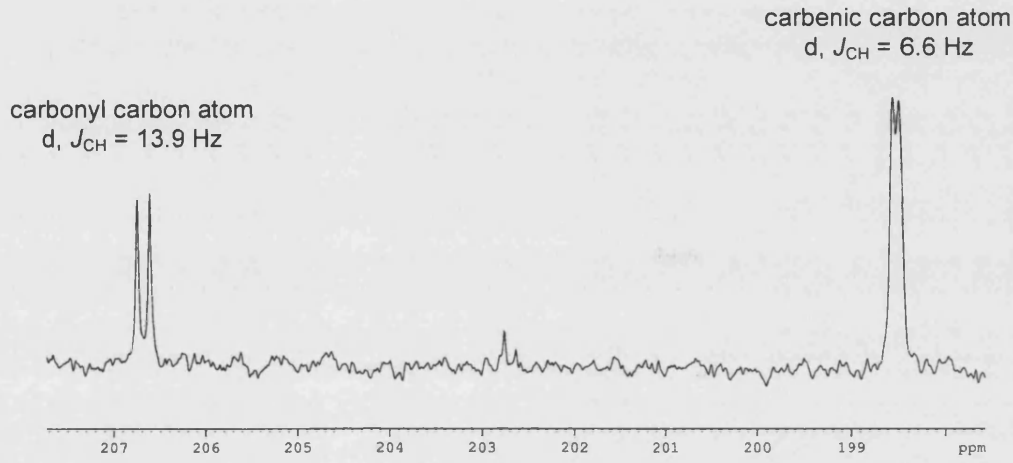

Figure 2.3 ^{13}C-^{1}H coupled NMR spectrum of $Ru(IMes)_2(CO)(OH)H$ (**2**) showing the doublet carbonyl and carbenic carbon resonances typical of $Ru(IMes)_2(CO)(X)H$ ($C_6D_5CD_3$, 298 K, 125.8 MHz).

$Ru(IMes)_2(CO)(X)H$	**^{13}C NMR shifts (ppm)**	
X =	**Ru-<u>C</u>O**	**Ru-<u>C</u>:**
OH [a]	206.7 (J_{CH} = 13.9 Hz)	198.6 (J_{CH} = 6.6 Hz)
OEt [a]	205.8 (J_{CH} = 13.0 Hz)	198.1 (J_{CH} = 6.1 Hz)
SH	203.2 [a] (J_{CH} = 11.6 Hz)	198.1 [b] br

Table 2.5 ^{13}C-^{1}H coupled NMR data for $Ru(IMes)_2(CO)(X)H$ ($C_6D_5CD_3$, [a]298 K, [b]233 K).

2.4 Formation of the hydride fluoride complex Ru(IMes)$_2$(CO)(F)H (6)

Preparation of the hydride fluoride complex Ru(IMes)$_2$(CO)(F)H (**6**) from the reaction of **1** with $Et_3N.3HF$ also served to confirm the characterisation of this class of complex. It would be unlikely that **6** would take on the structure Ru(IMes)$_2$(CO)(FH)H$_2$ as there are no known metal hydrogen fluoride complexes. An X-ray crystal structure of **6** was obtained but once again location of any possible hydrogen atom on fluorine remained unreliable. However, it was possible to obtain a neutron structure with assignments based on the X-ray crystallography results. By neutron diffraction it was apparent that there was definitely no Ru-F-H hydrogen atom. Additionally one hydride ligand was observed disordered over the two available sites in a ratio of 62:38.[4]

To summarise, **6** provided evidence against 18e$^-$, 6-coordinate-type complexes and consequently helped towards the assignment of our class of structures as 16e$^-$, 5-coordinate species, Ru(IMes)$_2$(CO)(X)H.

2.4.1 Synthesis and characterisation of Ru(IMes)$_2$(CO)(F)H (6)

Reaction of Ru(IMes)$_2$(CO)(OH)H (**2**) with a source of fluoride (eg. C_6F_6, $Et_3N.3HF$) produces Ru(IMes)$_2$(CO)(F)H (**6**). Spectroscopic and structural characterisation has been previously carried out by Jazzar *via* C-F bond activation of C_6F_6.[6] However, the preferred method of production was by reaction of Ru(AsPh$_3$)(IMes)$_2$(CO)H$_2$ (**1**) directly with $Et_3N.3HF$ without going *via* the hydroxide species, **2** (**Scheme 2.4**).[4]

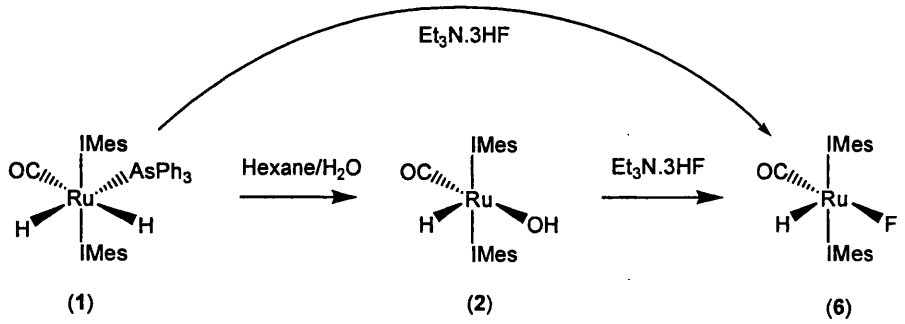

Scheme 2.4 Possible methods of preparation of Ru(IMes)$_2$(CO)(F)H.

One advantage of **6** over other $Ru(IMes)_2(CO)(X)H$ complexes is the extra characterisation handle that ^{19}F NMR spectroscopy provides. **6** was spectroscopically characterised by a diagnostic hydride resonance at -24.55 ppm and a broad singlet at -208.3 ppm in the ^{19}F NMR spectrum. The ^{19}F NMR resonance of **6** is similar to that of the coordinatively unsaturated species $Ru(PhOCH_2P^tBu_2\text{-}\kappa\text{-}P)_2(CO)(F)H$ (-203.0 ppm)[28] but differs dramatically from that for 16-electron $Ru(P^tBu_2Me)_2(CO)(F)H$ (-311 ppm).[26] In fact, the ^{19}F NMR shift for $Ru(P^tBu_2Me)_2(CO)(F)H$ is more comparable to 6-coordinate complexes (-270 to -391.3 ppm), than 5-coordinate species (-184.5 to -238.9 ppm), although the range for both is broad (>100 ppm).[29] An upfield ^{19}F NMR resonance also suggests that the fluoride is relatively electron rich.[29] Otherwise, spectral data for **6** are generally similar to that of related complexes as displayed in **Table 2.6**.

Complex	^1H and ^{19}F NMR shifts (ppm)		ν_{CO} (cm^{-1})
	Ru-H	Ru-F	
6	-24.55	-208.3	1873
$Ru(P^iPr_3)_2(CO)(F)H$ [29]	-23.7	-	-
$Ru(P^tBu_2Me)_2(CO)(F)H$ [26]	-24.0	-311	1892
$Ru(PhOCH_2P^tBu_2\text{-}\kappa\text{-}P)_2(CO)(F)H$ [28]	-24.20	-203.0	1898

Table 2.6 Examples of coordinatively unsaturated complexes analogous to $Ru(IMes)_2(CO)(F)H$ (**6**) and relevant spectroscopic data for comparison (- = not reported).

Doublet signals for the carbonyl (206.3 ppm, J_{CF} = 77.5 Hz) and carbenic (197.0 ppm, J_{CF} = 6.1 Hz) carbon atoms in the $^{13}C\{^1H\}$ NMR spectrum of **6** are consistent with *trans* and *cis* ^{13}C-^{19}F coupling respectively.

The IR spectrum of **6** displayed ν_{CO} at 1873 cm^{-1}, lower in frequency than the phosphine analogues shown in **Table 2.6** because of the increased electron donor capacity of IMes over phosphines. The carbonyl shift for **6** is consistent with the previously described bis IMes complexes $Ru(IMes)_2(CO)(X)H$ (X = OEt, OH, SH, S^{n}Pr) (1861 to 1886 cm^{-1}). A summary of 16-electron bis IMes systems is provided in section **2.10**.

2.5 Formation of the hydride chloride complex $Ru(IMes)_2(CO)(Cl)H$ (7)

There are various different ways that $Ru(IMes)_2(CO)(Cl)H$ (7) can be prepared as shown in **Scheme 2.5**. The main preparation involved simple dissolution of $Ru(IMes)_2(CO)(OH)H$ (**2**) in CH_2Cl_2. Both **2** and **7** are fully soluble in CH_2Cl_2 so solvent was removed *in vacuo* from the reaction mixture and the residue washed with hexane to precipitate **7** as a bright yellow powder in 98 % yield. Complete conversion to **7** was apparent by a new hydride signal in the ^1H NMR spectrum at -25.39 ppm. **7** has also been observed by the reaction of **2** with other chloride sources such as C_6Cl_6.[6] It is possible to produce **7** directly from reaction of a chloride source with $Ru(AsPh_3)(IMes)_2(CO)H_2$ (**1**) without going *via* **2**, but the resultant yellow powder was less microcrystalline than in the above reactions. Alternatively, **7** can be produced in 96 % yield from the reaction of $Ru(PPh_3)_3(CO)(Cl)H$ with three equivalents of IMes at 343 K for 1 h. The reaction is a harsher version of that reported by Nolan for the preparation of $Ru(PPh_3)(IMes)(CO)(Cl)H$.[30]

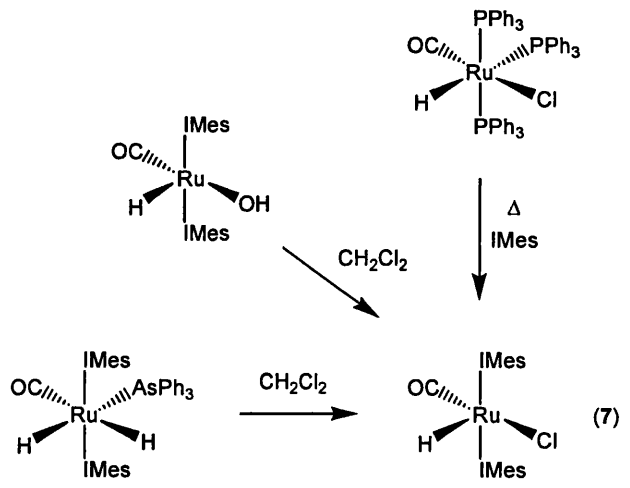

Scheme 2.5 Methods of preparation of $Ru(IMes)_2(CO)(Cl)H$.

In the $^{13}C\{^1H\}$ NMR spectrum of **7**, the carbonyl resonance was observed at 202.8 ppm and the peak for the carbenic carbon atom at 195.9 ppm, both values being

consistent with the other $Ru(IMes)_2(CO)(X)H$ complexes (**Table 2.5**, p. 34). Some related hydride chloride complexes are listed in **Table 2.7** below. All of the examples contain bulky ligands that help to stabilise the 16-electron configuration. For example $Ru(PPh_3)(IMes)(CO)(Cl)H$[30] is stabilised by the inclusion of an IMes ligand whereas the analogous bis phosphine complex $Ru(PPh_3)_2(CO)(Cl)H$ is not known. Presumably PPh_3 ligands do not protect the metal centre sufficiently to prevent binding of other ligands and coordinatively saturated systems such as $Ru(PPh_3)_3(CO)(Cl)H$ are formed instead. Conversely, the coordinatively unsaturated complex $Ru(PR_3)_3(Cl)H$ is known when R = Ph,[31] but not with bulkier phosphines such as when R = Cy or ^{t}Bu.

$RuL_2(CO)(Cl)H$ **L_2 =**	**^{1}H NMR shift (ppm)** **Ru-H**	**IR shift (cm^{-1})** **ν_{CO}**
$(IMes)_2$ (7)	-25.39	1882
$(PPh_3)(IMes)$ [30]	-23.89	1913
$(PCy_3)(IMes)$ [32]	-24.83	1896
$(PCy_3)_2$ [32-35]	-24.7	1907
$(P^iPr_3)_2$ [36, 37]	-24.20	1910
$(P^tBu_2Me)(P^iPr_3)$ [38]	-24.4	-
$(P^tBu_2Me)_2$ [26, 36, 38, 39]	-24.5	1904

Table 2.7 Examples of coordinatively unsaturated complexes analogous to $Ru(IMes)_2(CO)(Cl)H$ and relevant spectroscopic data for comparison. (- = data not provided).

Low temperature ^{1}H NMR spectroscopy showed separation of the three methyl proton resonances of **7** at 298 K (2.38, 2.16 and 2.05 ppm in $C_6D_5CD_3$) into six peaks at 230 K (2.39, 2.35, 2.27, 2.20, 2.11 and 1.96 ppm) each corresponding to two methyl groups. Initially the signals appear to collapse over the temperature range 298 – 250 K but sharpen at 230 K and below (down to 190 K) as illustrated in **Figure 2.4**.

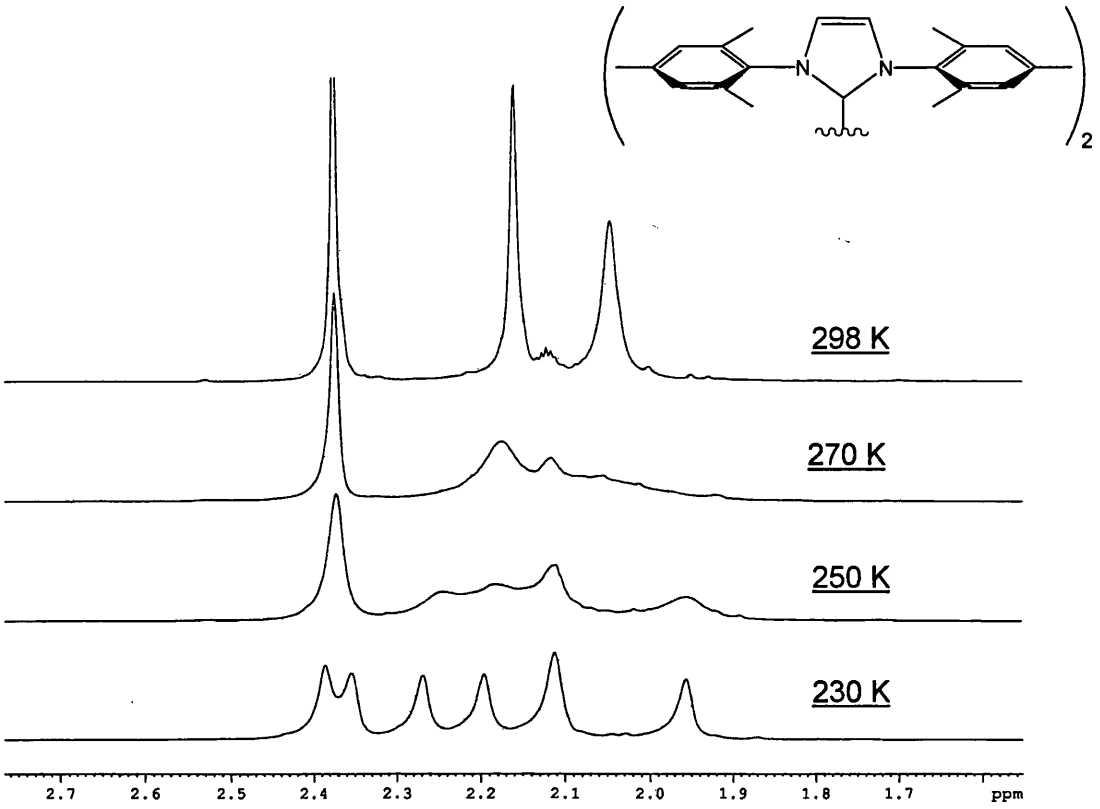

Figure 2.4 Variable temperature ^{1}H NMR spectra of the methyl region for **7** showing peaks associated with the methyl protons of the mesityl arms ($C_6D_5CD_3$, 400 MHz).

The backbone proton resonance at 6.24 ppm ($C_6D_5CD_3$) at 298 K divides into two signals at 210 K (5.95 and 5.92 ppm). The aryl protons of the mesityl arms also show splitting at 230 K, from two distinct signals observed at 298 K (6.82 and 6.79 ppm in $C_6D_5CD_3$) into four peaks at 210 K (6.84, 6.82, 6.80 and 6.77 ppm) (**Figure 2.5**).

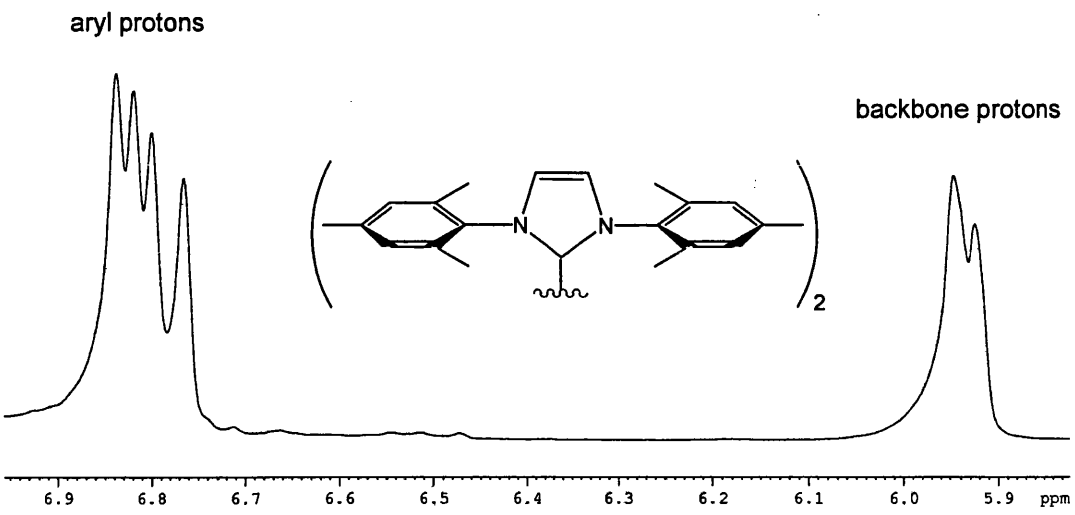

Figure 2.5 Low temperature ^{1}H NMR spectrum of the aryl region for **7** showing peaks associated with the backbone protons and aryl protons of the mesityl arms ($C_6D_5CD_3$, 210 K, 400 MHz).

Even at these low temperatures (down to 190 K), there are still only half of the possible signals apparent for **7** considering there are two IMes ligands, suggesting that two halves of the complex contain equivalent environments. Presumably it is the left and right sides of the complex that are equivalent rather than each of the IMes ligands individually, to account for the unsymmetrical geometry of square based pyramidal systems.

2.6 Electron donating ability of X in $Ru(IMes)_2(CO)(X)H$ (X = OH, OEt, SH, S^{n}Pr, F, Cl)

It has been established throughout the previous sections that the carbonyl stretching frequencies for $Ru(IMes)_2(CO)(X)H$ are consistently lower than equivalent bands for $Ru(PR_3)_2(CO)(X)H$ due to the increased electron donor ability of IMes over phosphine ligands. **Table 2.8** below shows ν_{CO} values of $Ru(IMes)_2(CO)(X)H$ for comparison with each other.

$Ru(IMes)_2(CO)(X)H$ X =	ν_{CO} (cm^{-1})
OEt [2] (3)	1886
S^nPr [2] (5)	1883
Cl (7)	1882
SH [3] (4)	1879
F [4] (6)	1873
OH [2] (2)	1861

Table 2.8 Carbonyl stretching frequencies for $Ru(IMes)_2(CO)(X)H$ (X = OH, OEt, SH, S^nPr) (nujol mulls).

The order of decreasing ν_{CO} in the complexes $Ru(IMes)_2(CO)(X)H$ occurs as X = OEt > S^nPr > Cl > SH > F > OH, suggesting that OEt is the worst electron donor in the series, and OH the best. Carbonyl stretching frequencies have been used to study composite ($\sigma + \pi$) electron donor ability of X in the complexes $Ru(P^tBu_2Me)_2(CO)(Y)H$ by Caulton.[40] In $Ru(P^tBu_2Me)_2(CO)(Y)H$ the electron donor ability of Y is reported as follows:

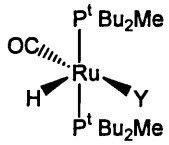

worse donor (higher ν_{CO})

H < I < Br < *C≡CPh* < Cl < SPh < OPh < NHPh < OH < OCH_2CF_3 < F < $OSiPh_3$ < $OSiMe_2Ph$ < $OSiMe_3$ < OEt

better donor (lower ν_{CO})

Although only limited comparisons can be made with Caulton's series (direct comparisons are underlined), the donor ability of X in $Ru(IMes)_2(CO)(X)H$ does not appear to mirror that of Y in $Ru(P^tBu_2Me)_2(CO)(Y)H$, notably when X = OEt. These findings support the growing body of evidence that electron-donation cannot be so

simply quantified.[41] For Y = C≡CPh (*italicised*) the analogous bis IMes complex has been prepared (ν_{CO} = 1887 cm^{-1}) and will be discussed further in Chapter 3.

2.7 Treatment of $Ru(IMes)_2(CO)(X)H$ (X= OH, SH, F, Cl) with H_2

The importance of the species $Ru(IMes)_2(CO)(X)(\eta^2\text{-}H_2)H$ has been outlined in the computational work at the beginning of this chapter. We attempted to form such as complex by reacting $Ru(IMes)_2(CO)(X)H$ {X = OH (**2**), SH (**4**), F (**6**), Cl (**7**)} with H_2. An atmosphere of H_2 was added to samples of **2**, **4**, **6** and **7** but no immediate change was observed by ^1H NMR spectroscopy over a range of temperatures (298 - 190 K); no new hydride signals were apparent and there was no sign of non-classical hydrogen. There was possible evidence of minor $Ru(IMes)_2(CO)(\eta^2\text{-}H_2)H_2$ formation from **2** reacting with H_2 after a week at 298 K, observed as a broad signal at -6.93 ppm in the ^1H NMR spectrum.

The reaction of H_2 with related complexes $Ru(P^tBu_2Me)_2(CO)(Y)H$ (Y = OH, F, Cl, I) showed varying reactivities.[40] (**Scheme 2.6**). When Y = OH or F, reaction with H_2 at 298 K yielded the dihydrogen dihydride complex $Ru(P^tBu_2Me)_2(CO)(\eta^2\text{-}H_2)H_2$, apparent by a broad resonance in the ^1H NMR spectrum at -6.95 ppm.

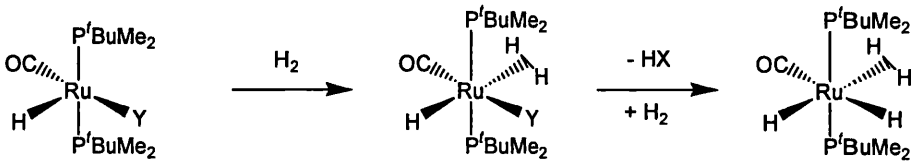

Scheme 2.6 Reaction of $Ru(P^tBu_2Me)_2(CO)(Y)H$ with H_2.[40]

Caulton observed no new hydride signal at room temperature when Y = Cl or I, but concluded that $\eta^2\text{-}H_2$ bonding probably did occur at room temperature by loss of the free H_2 signal. Low temperature ^1H NMR spectroscopy (166 K) showed new hydride resonances assigned to $Ru(P^tBu_2Me)_2(CO)(Cl)(\eta^2\text{-}H_2)H$ (-9.2 ppm) and

$Ru(P^tBu_2Me)_2(CO)(I)(\eta^2\text{-}H_2)H$ (-9.7 ppm).[40] Addition of the non-binding Brønsted base DBU to both systems caused formation of $Ru(P^tBu_2Me)_2(CO)(\eta^2\text{-}H_2)H_2$ from $Ru(P^tBu_2Me)_2(CO)(I)H$ but failed to change $Ru(P^tBu_2Me)_2(CO)(Cl)H$. Caulton concluded that increased donating power of X results in decreased propensity for H_2 to bond to the metal centre, although F appears to be an anomaly to this rule. The strength of the H-F bond formed as a byproduct (573 kJ mol^{-1} *cf.* H-Cl at 426 kJ mol^{-1}) may promote $Ru(P^tBu_2Me)_2(CO)(\eta^2\text{-}H_2)H_2$ production, along with the destabilising effect of filled M d_π and X p_π orbitals in $Ru(P^tBu_2Me)_2(CO)(\eta^2\text{-}H_2)(F)H$.

2.8 Treatment of $Ru(IMes)_2(CO)(X)H$ (X= OH, SH, F, Cl) with D_2

Upon exposure to D_2, $Ru(IMes)_2(CO)(X)H$ {X = OH (**2**), SH (**4**), F (**6**), Cl (**7**)} demonstrated incorporation of D into the hydride positions, implying that η^2-binding does in fact occur (**Scheme 2.7**).

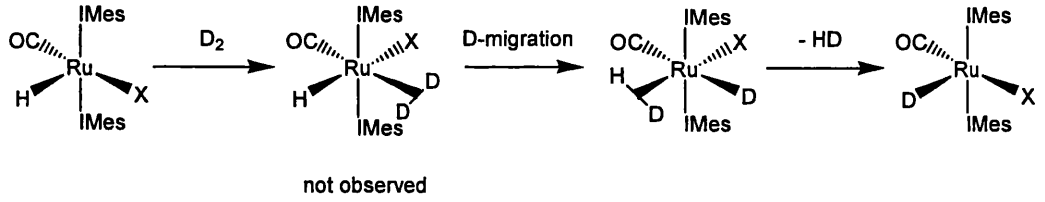

Scheme 2.7 H/D scambling in $Ru(IMes)_2(CO)(X)H$ (X = OH, SH, F, Cl) upon exposure to D_2.

The reaction of $Ru(IMes)_2(CO)(X)H$ {X = OH (**2**), SH (**4**), F (**6**), Cl (**7**)} with D_2 at 298 K showed decreased hydride resonances in the ^1H NMR spectra with respect to the backbone protons and an added external reference ferrocene (*ca.* 0.2 equiv.). **Figure 2.6** shows the relative % loss of hydride over time at 298 K, calculated by comparing integrals of the hydride resonance against the ferrocene reference (3.99 ppm) in the ^1H NMR spectra.

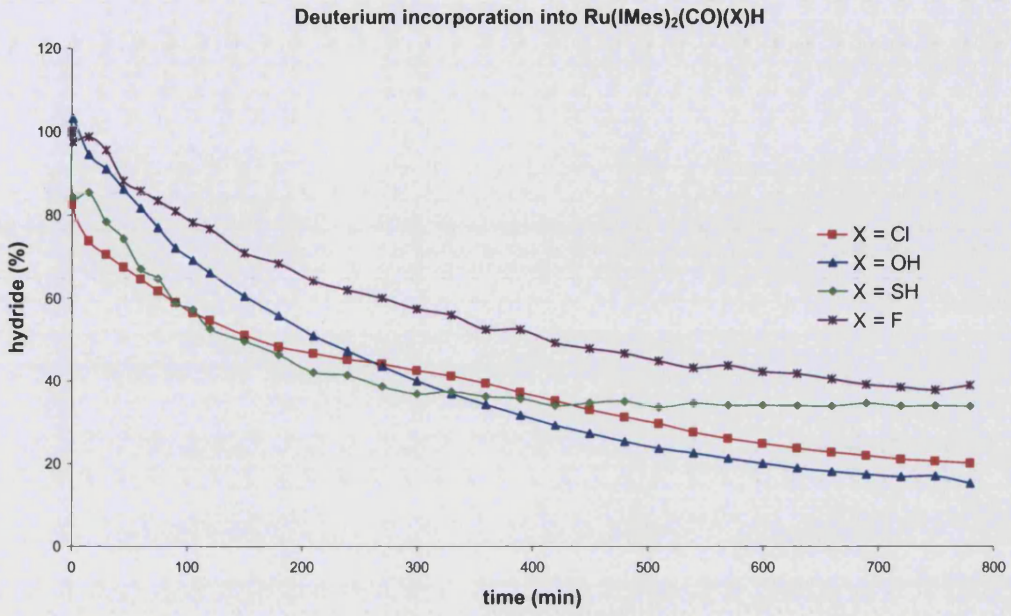

Figure 2.6 H/D exchange in the hydride positions of **2**, **4**, **6** and **7**, calculated by using ferrocene as a reference for integration (*ca.* 0.2 equiv.). (C_6D_6, 298 K, 400 MHz).

Initially **7** showed the fastest loss of its hydride resonance, although ultimately **2** showed the biggest decrease in its hydride (15 % hydride remained by ^{1}H NMR spectroscopy, 13 h, 298 K). **4** also displayed relatively quick loss of its hydride ligand over the first 3 hours of the reaction (46 % remaining hydride) but then the reaction slowed so that the hydride only decreased by a further 12 % over the remaining reaction time (resulting in 34 % hydride loss after 13 h). **6** showed consistently poor H-loss over the whole reaction concluding with the hydride ligand at 39 % of the original integral. These results are discussed in more detail later in the text.

Elimination of HD was evident in the reactions involving **6** and **4** by the appearance of a 1:1:1 triplet at 4.42 ppm (J_{HD} = 42.3 Hz) as well as H_2 (s, 4.45 ppm). The ratios of H_2:HD are given in **Table 2.9** below for these complexes. The intensities of the said peaks change throughout the reaction and it is unclear why H_2 was so prevalent in the reaction with **4** compared to **6**. Neither H_2 nor HD were observed in the spectra of **2** or **7** with D_2.

Reaction time	Ratio H_2:HD	
	4	**6**
Immediately after D_2 addition	3.5:1	0.3:1
1 h	0.8:1	0.9:1
2 h	0.2:1	-

Table 2.9 Ratios of free H_2:HD in the reaction of **4** and **6** with D_2. (C_6D_6, 298 K, 400 MHz).

^{2}H NMR spectra verified the incorporation of D into the hydride positions of **2**, **4**, **6** and **7**, and also revealed scrambling in the hydroxide ligand of **2** at 0.93 ppm. In contrast there was no apparent D-incorporation into the SH ligand of **4** in the ^{2}H NMR spectrum after 13 h 298 K, but the ^{1}H NMR spectrum of **4** with D_2 did show a new peak emerging at -0.60 ppm slightly upfield of the original SH peak at -0.59 ppm. After an hour the new resonance became more prominant and continued to grow over the course of the reaction (13 h).

It is important to note that the reaction of **2** with D_2 also resulted in the formation of Ru(IMes)$_2$(CO)(η^2-H_2)H_2 as observed in the ^{1}H NMR spectrum and presumably the deuterated analogue Ru(IMes)$_2$(CO)(η^2-D_2)D_2 is also produced (although this was not seen in the ^{2}H NMR spectrum, most likely due to broadness). Furthermore, there was evidence in the ^{2}H NMR spectrum of deuterium incorporation into the *ortho* methyl groups of IMes (2.12, 2.02 ppm), suggesting that C-H activation is also a source of hydrogen for the formation of Ru(IMes)$_2$(CO)(η^2-H_2)H_2.[42] Therefore the plot of hydride loss in **Figure 2.6** for **2** not only represents deuterium incorporation, but also takes into account the loss of hydride that contributes towards Ru(IMes)$_2$(CO)(η^2-H_2)H_2 formation and is further complicated by the involvement of C-H activation.

2.8.1 Geometry of Ru(IMes)$_2$(CO)(X)H for D-incorporation

In order for D-incorporation to occur D_2 must bind *cis* to the hydride to enable D-migration and therefore the geometry around the metal centre must change, either by

increasing the H-Ru-X angle (α) or the H-Ru-CO angle (β) as shown in **Figure 2.7**. Caulton calculated that increasing the H-Ru-Cl bond angle (α) in $Ru(PH_3)_2(CO)(Cl)H$ is energetically feasible, whereas increasing the H-Ru-CO angle (β) is energetically demanding. This was concluded by comparing *ab initio* values of the isomers **A** and **B** (where L = PH_3, X = Cl); 28.4 and 112.0 kJ mol^{-1} respectively.[40] **A** is lower in energy and therefore more feasible, perhaps due to the *trans* influence of CO and in addition, subsequent nucleophile binding would occur *trans* to π-accepting CO.

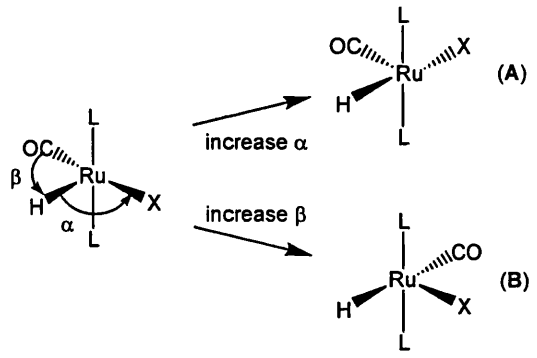

Figure 2.7 Increasing angles α or β so a nucleophile (e.g. D_2) can bind *cis* to the hydride ligand.

2.8.2 D-incorporation and the electron donating ability of X

The propensity for H/D exchange in complexes $Ru(IMes)_2(CO)(X)H$ is related to the electron-donating ability of X, with more strongly donating X resulting in inhibited D_2 binding. Alternatively, more Lewis acidic X ligands act in a more unsaturated manner resulting in more favourable D_2 binding. For example, the related complex $Ru(P^tBu_2Me)_2(CO)(Y)H$ (Y = I, Cl, F) displayed D exchange values (%) >95, 78, 27 respectively after 1 h at 298 K with 4 equiv. D_2, with the halide ligands demonstrating electron-donating ability I < Cl < F and Lewis acidity I > Cl > F.[40]

Based on υ_{CO} values, the electron-donating ability of $Ru(IMes)_2(CO)(X)H$ follows Cl (**7**) < SH (**4**) < F (**6**) < OH (**2**). The end of the 13 h reactions with D_2 furnished results consistent with the expected trend with the exception of $Ru(IMes)_2(CO)(OH)H$ (**2**). In comparison to the analogous complexes

$Ru(P^tBu_2Me)_2(CO)(Y)H$ (Y = Cl, F), **7** and **6** show slower D-incorporation (35 and 14 % exchange respectively after 1 h 298 K). **2** showed an unexpected propensity for hydride loss although the electron donating ability of OH should be relatively high, theoretically inhibiting D_2 binding. Perhaps the formation of $Ru(IMes)_2(CO)(\eta^2\text{-}H_2)H_2$ accounts for a lot of the hydride loss (although the $Ru(IMes)_2(CO)(OH)(\eta^2\text{-}H_2)H$ would need to be formed initially) or acts as a driving force for hydride loss from **2**.

In summary, the electron-donating ability of X affects exchange in the hydride position and has consequences for the ability of the complexes to lose HX and form the dihydrogen dihydride species $Ru(IMes)_2(CO)(\eta^2\text{-}H_2)H_2$. However, determining electron-donating ability is not trivial and does not appear to be as explicitly linked to υ_{CO} values as first suggested.[40, 41] Other factors that determine the equilibrium constant between $Ru(IMes)_2(CO)(X)(\eta^2\text{-}H_2)H$ and $Ru(IMes)_2(CO)(\eta^2\text{-}H_2)H_2$ include Ru-X bond dissociation energies, the formation energies of HX and molecular orbital arguments as discussed in the previous section in regard to **6**.

2.9 $Ru(IMes)_2(CO)(X)H$ (X = OH, SH, F, Cl) as hydrogenation catalysts

2.9.1 $Ru(IMes)_2(CO)(X)H$ in acetophenone hydrogenation

The coordinatively unsaturated nature of $Ru(IMes)_2(CO)(X)H$ {X = OH (**2**), SH (**4**), F (**6**), Cl (**7**)} complexes made them likely candidates for catalysis. Each system was tested as a hydrogenation catalyst for the reduction of acetophenone to phenethyl alcohol. For comparison, the mixed PR_3 / NHC complex $Ru(PPh_3)(IMes)(CO)(Cl)H$ (**8**) was also used for ketone hydrogenation. Nolan has successfully used **8** to catalyse hydrogenation of cyclooctene and cyclododecene,[30] but not shown its use for C=O hydrogenation.

The hydrogenation reactions were carried out using 0.4 mol % catalyst (*ca.* 10 mg) in 0.3 M ^{i}PrOH with respect to the substrate. The reaction mixture was transferred to an autoclave, into which *ca.* 10 atm H_2 was added and heated to 343 K for 20 h. The reaction conditions were based on previous hydrogenation work in the

Whittlesey group, with one major exception being the use of neat ^{i}PrOH for the reaction solvent.[43] Conversion of ketone to the corresponding alcohol was calculated by comparing the methyl integral of phenethyl alcohol (d, 1.41 ppm) with that of acetophenenone (s, 2.53 ppm) (**Table 2.10**).

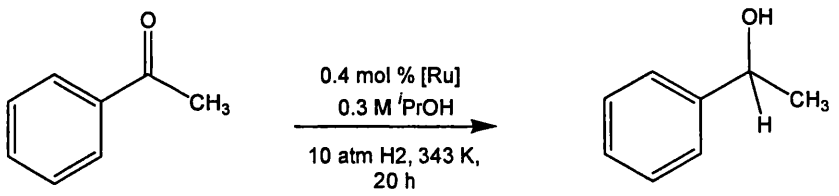

[Ru] = $Ru(IMes)_2(CO)(X)H$

$RuL_2(CO)(X)H$		Conversion to alcohol (%)
L_2 =	X =	
$(IMes)_2$	OH (**2**)	64
$(IMes)_2$	SH (**4**)	16
$(IMes)_2$	F (**6**)	95
$(IMes)_2$	Cl (**7**)	82
$(PPh_3)(IMes)$	Cl (**8**)	80

Table 2.10 Conversion (%) of acetophenone to phenethyl alcohol using the conditions outlined above.

All of the complexes in **Table 2.10** showed moderate catalytic activity with the exception of **4** (16 % conversion). Exchanging an IMes ligand for PPh_3, as in **7** and **8**, did not result in significantly different conversions to phenethyl alcohol (82 and 80 % respectively), suggesting that the potential for PPh_3 loss from **8** is not crucial in forming the active species for C=O hydrogenation under these conditions.

2.9.2 Investigating the hydrogenation reaction pathway using $Ru(IMes)_2(CO)(X)H$ as a catalyst

Stoichiometric reactions of acetophenone with $Ru(IMes)_2(CO)(X)H$ {X = OH (**2**), SH (**4**), F (**6**), Cl (**7**)} on an NMR-scale did not result in any identifiable new products being formed by ^1H NMR spectroscopy, at 343 K either under 1 atm of Ar or H_2. In addition, complex residues left on the stirrer at the end of the hydrogenation reactions were also tested to verify no complex transformations occurred. ^1H NMR spectra showed no new hydride peaks or significant changes to the complexes following the time in the autoclave.

As both H_2 and ^{i}PrOH can act as hydrogen donors {direct (DH) or transfer hydrogenation (TH)}, it was impossible to determine how the catalyst was regenerated in the reactions above. Consequently, the hydrogenation process was probed by changing the reaction conditions using **7** as a typical system (chosen for its relatively high conversion in the standard hydrogenation). Hydrogenation experiments were attempted with and without the presence of H_2 and in C_6H_6 rather than ^{i}PrOH. When the reaction was run under 1 atm Ar rather than *ca.* 10 atm H_2, only 3 % conversion to alcohol was observed suggesting that the catalyst is regenerated by H_2 in direct hydrogenation. However, the presence of ^{i}PrOH as the reaction solvent was also necessary, as in C_6H_6 the conversion was negligible even under 10 atm H_2. It has been suggested that ^{i}PrOH is such a good solvent for DH because it has a higher dielectric constant than aprotic solvents and aids the heterolytic splitting of H_2.[44] H-bonding may also be a factor in stabilising any intermediate species. Solvent choice is an important factor; for example, primary alcohols could not be used because the aldehyde dehydrogenation product is likely to deactivate the ruthenium catalyst via decarbonylation.[45]

The addition of base (1 equiv. NaOH) to the hydrogenation reaction with $Ru(IMes)_2(CO)(Cl)H$ (**7**) resulted in full conversion from acetophenone to phenethyl alcohol under standard conditions. In the absence of H_2 (under 1 atm Ar) the conversion was also increased from 3 % to 22 % using base in the reaction mixture. The effect of base addition to TH reactions is well precedented.[45, 46] Noyori's hydrogenation catalysts (TH and DH) rely on the inclusion of base to convert the chloride precatalysts into the

active hydride species.[47] Alternatively, the base serves to produce a more nucleophilic alkoxide ion which subsequently attacks the metal complex and is dehydrogenated. It has been reported that base increases conversion in both TH and DH with the disadvantage of decreasing enantioselectivity in TH cases, which is unimportant here as **7** did not display any enantioselectivity (*ca.* 50:50, R:S phenethyl alcohol by GC analysis).

2.9.3 Hydrogenation of other ketones

Ketones containing electron withdrawing or donating groups in the 4-position were investigated to check the affect of enhancing or removing electron density (**Table 2.11**). The effect of sterics was investigated through use of pinacolone (final entry in **Table 2.11**), a notoriously difficult ketone to reduce.

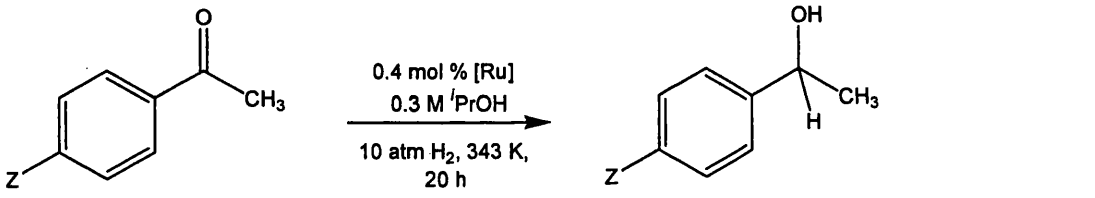

[Ru] = $Ru(IMes)_2(CO)(Cl)H$

Substrate Z =	Conversion to alcohol (%)
H	82
Me	48
OMe	33
F	49
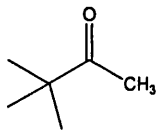	14

Table 2.11 Conversion (%) of ketone substrate to the corresponding alcohol using **7** as the catalyst under standard conditions outlined above.

Table 2.11 demonstrates that varying the groups on the 4-position of the phenyl ring has a pronounced effect on hydrogenation. However, there was no apparent correlation between electron-donating or withdrawing groups and conversion to alcohol. Hydrogenation of pinacolone to pinacolyl alcohol was poor (14 %) compared to the other substrates, suggesting steric factors are important in the reaction.

2.10 Summary of 16-electron complexes

The complexes $Ru(IMes)_2(CO)(XH)H_2$ have been reformulated as $Ru(IMes)_2(CO)(X)H$ based on computational work when X = SH/S by the Macgregor group and by reconsidering experimental analyses previously carried out by Jazzar.[2, 6, 48] The ^{13}C-^{1}H coupled spectra of $Ru(IMes)_2(CO)(X)H$ revealed $C_{carbonyl}$ and C_{NHC} atoms coupled to only one ^{1}H nuclei, consistent with the 16-electron description of the complexes. The synthesis of $Ru(IMes)_2(CO)(F)H$ and the subsequent structural characterisation of the complex by neutron diffraction, also helped in the recharacterisation of this class of complex by locating only one hydride ligand and by the absence of H bound to the fluoride ligand. In addition, comparisons with similar heteroatom containing 16-electron complexes supported reformulation of these complexes.

We have attempted to determine the electron-donating ability of X by studying υ_{CO} values of $Ru(IMes)_2(CO)(X)H$, however comparison with the υ_{CO} values of $Ru(P^tBu_2Me)_2(CO)(Y)H$ highlighted that electron-donating ability in these systems cannot be thought of in such a simple manner.

Attempted observation of the hydrogen transfer product $Ru(IMes)_2(CO)(X)(\eta^2\text{-}H_2)H$, in the transformation from $Ru(IMes)_2(CO)(XH)H_2$ to the actual product $Ru(IMes)_2(CO)(X)H$, was not successful retrospectively. Reaction of the 16-electron complexes $Ru(IMes)_2(CO)(X)H$ with H_2 resulted instead in the formation of $Ru(IMes)_2(CO)(\eta^2\text{-}H_2)H_2$ when X = OH or F and no reaction was observed when X = SH or Cl. H/D exchange was observed in the hydride position upon the analogous reaction with D_2, confirming that H_2 or D_2 binds to the metal centre of $Ru(IMes)_2(CO)(X)H$ as in $Ru(IMes)_2(CO)(\eta^2\text{-}H_2)H_2$.

The use of $Ru(IMes)_2(CO)(X)H$ as a hydrogenation catalyst for ketones has achieved reasonable conversions to the corresponding alcohols, with the exception of $Ru(IMes)_2(CO)(SH)H$. Although it was necessary to carry out the reactions in the donor solvent ^{i}PrOH, regeneration of the catalyst is achieved with H_2 (DH), based on very low conversions in the absence of H_2.

2.11 18-electron complexes

2.11.1 Reaction of $Ru(IMes)_2(CO)(X)H$ with CO

The reaction of complexes **2**, **3**, **4** and **5** with CO were all previously reported by Jazzar to yield $Ru(IMes)_2(CO)_2(X)H$ {although $Ru(IMes)_2(CO)_2(OEt)H$ was not isolated as it continued reacting to form $Ru(IMes)_2(CO)_3$}.[2] By ^{1}H NMR spectroscopy it was clear that the hydride ligands in $Ru(IMes)_2(CO)_2(X)H$ no longer lie *trans* to a vacant site as the diagnostic hydride resonances underwent a significant downfield shift from *ca.* -24 ppm to *ca.* -4 ppm. With the reformulation of $Ru(IMes)_2(CO)(XH)H_2$ as $Ru(IMes)_2(CO)(X)H$ the 18-electron dicarbonyl complexes can now be considered simply to result from direct bonding of CO into the vacant coordination site (**Scheme 2.8**).

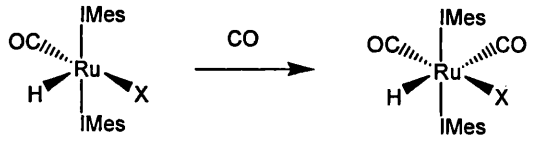

Scheme 2.8 Direct bonding of carbon monoxide into the vacant site of $Ru(IMes)_2(CO)(X)H$ (X = OH, OEt, SH and S^{n}Pr) to yield $Ru(IMes)_2(CO)_2(X)H$.

This was confirmed by use of ^{13}CO, which gave exclusively a *trans* ^{13}CO-Ru-H geometry on the basis of J_{HC} coupling patterns and constants (*ca.* 45 Hz) in $Ru(IMes)_2(CO)_2(X)H$.[2, 3] The presence of two inequivalent carbonyl ligands was confirmed by two low field resonances in the $^{13}C\{^1H\}$ NMR spectra and the appearance of two bands in the IR spectra (**Table 2.12**). The carbonyl ligand *trans* to the hydride

ligand also has an effect on the Ru-H stretching frequency such that it can be observed by IR spectroscopy by intensity stealing, whereas ν_{Ru-H} was not seen in the starting coordinatively unsaturated complexes, $Ru(IMes)_2(CO)(X)H$. Definitive confirmation of the structures of $Ru(IMes)_2(CO)_2(X)H$ were provided by X-ray crystallography.

$Ru(IMes)_2(CO)_2(X)H$ X =	Ru-CO $^{13}C\{^1H\}$ NMR shift (ppm)[a]	ν_{CO} (cm^{-1})[b]	Ru-H ^1H NMR shift (ppm)[a]	ν_{Ru-H} (cm^{-1})[b]
OH [2]	204.2 195.4	2019 1880	-4.27	1924
OEt [6 c]	- 195.2	-	-3.88	-
SH [3, 48]	203.1 197.4	2023 1892	-4.82	1931
S^{n}Pr [2]	202.9 199.0	2014 1896	-4.10	1946

Table 2.12 Spectroscopic data described by Jazzar and Chatwin for $Ru(IMes)_2(CO)_2(X)H$ (X = OH, OEt, SH and S^{n}Pr). [a]298 K, C_6D_6, 400 MHz. [b]Nujol mull. [c]Data are for $Ru(IMes)_2(^{13}CO)(CO)(OEt)H$, in which only the labelled CO resonance was detectable.

2.11.2 Formation of $Ru(IMes)_2(CO)_2(F)H$ (9)

Exposure of $Ru(IMes)_2(CO)(F)H$ (**6**) to 1 atm CO at room temperature yielded the expected dicarbonyl complex $Ru(IMes)_2(CO)_2(F)H$ (**9**) in the time taken to acquire an NMR spectrum.[6] (**Scheme 2.9**).

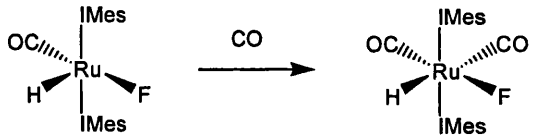

(6) (9)

Scheme 2.9 Formation of $Ru(IMes)_2(CO)_2(F)H$ (**9**).

The hydride doublet resonance (-3.80 ppm, J_{HF} = 3.8 Hz) is shifted significantly downfield from **6** (-24.55 ppm) as expected for hydride now lying *trans* to CO. Similar data has been reported by Caulton for $Ru(P^tBu_2Me)_2(CO)_2(F)H$ (-4.16 ppm, J_{HP} = 19 Hz, J_{HF} = 9 Hz).[26] By ^{19}F NMR spectroscopy, the fluoride ligand in **9** was located at -379.5 ppm, within the range expected for 6-coordinate complexes (-270 to -391.3 ppm).[29] In contrast, the resonance reported for Caulton's complex lies at -202 ppm (t, J_{PF} = 20 Hz)[26] more like the value for **6** (-208.3 ppm).

IR spectroscopy showed both symmetric and asymmetric carbonyl stretching frequencies for **9** (1880 and 1991 cm^{-1}) in accordance with the *cis* geometry of the CO ligands. The Ru-H stretch is also observed at 1930 cm^{-1}. All spectroscopic values are consistent with those shown in **Table 2.12** (p. 53) for other $Ru(IMes)_2(CO)_2(X)H$ systems.

2.11.3 Formation of $Ru(IMes)_2(CO)_2(Cl)H$ (10)

$Ru(IMes)_2(CO)(Cl)H$ (**7**) also reacts immediately with CO at room temperature (evident by a colour change from yellow to colourless) to yield $Ru(IMes)_2(CO)_2(Cl)H$ (**10**) (**Scheme 2.10**). The complex displayed a new hydride resonance at -4.30 ppm, with two carbonyl carbon signals in the $^{13}C\{^1H\}$ NMR spectrum at 204.4 ppm and 194.6 ppm. The IR spectrum of **10** contained both symmetric and asymmetric ν_{CO} stretching bands at 2037 and 1903 cm^{-1}, which are compared to other bis NHC dicarbonyl complexes in **Table 2.13**.

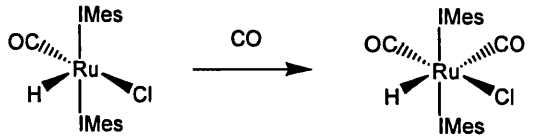

(7) (10)

Scheme 2.10 Formation of $Ru(IMes)_2(CO)_2(Cl)H$ (**10**).

Complex	ν_{CO} (cm^{-1}) n = 1	ν_{CO} (cm^{-1}) n = 2
$Ru(IMes)_2(CO)_n(Cl)H$ [a]	1882	2037 1903 (ν_{Ru-H} = 1938)
$Ru(IPr)_2(CO)_n(Cl)H$ [b]	1898 (ν_{Ru-H} = 1884)	2029 1934
$Ru(SIPr)_2(CO)_n(Cl)H$ [b]	1903	2032 1937

Table 2.13 IR spectroscopic values (cm^{-1}) for mono and bis carbonyl complexes $Ru(NHC)_2(CO)_n(Cl)H$ (IPr = 1,3-bis(2,4-diisopropylphenyl)imidazol-2-ylidene, SIPr = 1,3-bis(2,4-diisopropylphenyl)imidazolin-2-ylidene). [a] Nujol mull. [b] C_6D_6.

The structure of **10** was determined by X-ray crystallography, with the structure showing disorder between the chloride ligand and the *trans* carbonyl ligand in a ratio of 60:40 with the major component shown in **Structure 2.1**. A selection of relevant bond lengths and angles are given in **Table 2.14** including values for the related complexes $Ru(IMes)_2(CO)_2(OH)H$[2] and $Ru(IMes)_2(CO)_2(F)H$ (**9**).[4]

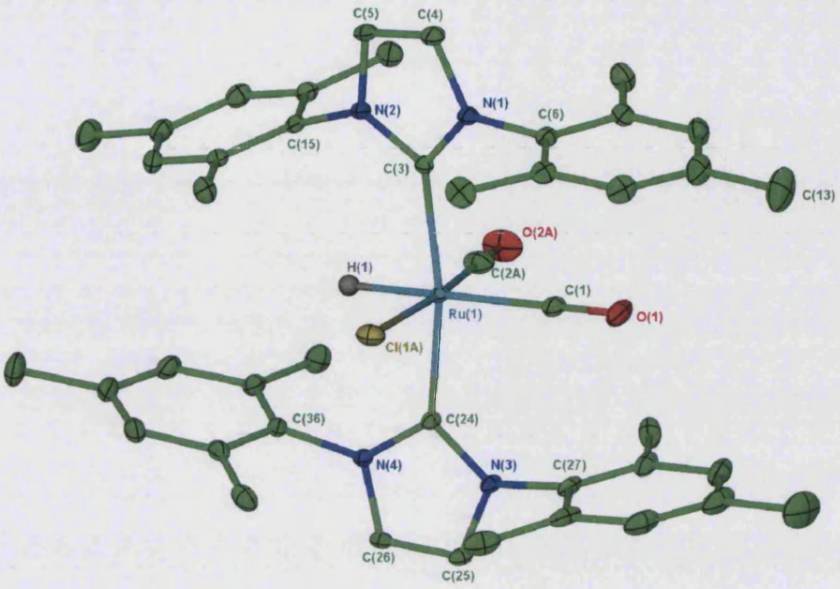

Structure 2.14 X-ray structure of $Ru(IMes)_2(CO)_2(Cl)H$ (**10**). Thermal ellipsoids are set at 30 % probability. Hydrogen atoms have been omitted for clarity (except the hydride).

	$Ru(IMes)_2(CO)_2(X)H$		
	X = Cl (10)	**X = OH** [2]	**X = F (9)** [4]
Ru-C(3)	2.1158(15)	2.113(2)	2.0998(15)
Ru-C(24)	2.1064(15)	2.101(2)	2.1074(16)
Ru-Cl(1A)	2.384(2)	-	-
Ru-C(1)	1.9840(19)	1.966(3)	1.988(2)
Ru-C(2A)	1.890(8)	1.873(6)	1.890(6)
C(3)-Ru-C(24)	168.81(6)	167.94(8)	167.67(6)

Table 2.14 Selected bond lengths (Å) and angles (°) for **10** with values for $Ru(IMes)_2(CO)_2(OH)H$[2] and $Ru(IMes)_2(CO)_2(F)H$ (**9**)[4] provided for comparison.

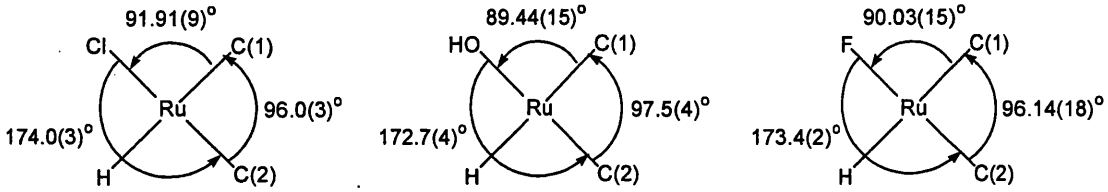

Figure 2.8 A pictorial representation of the equatorial ligands of **10**, $Ru(IMes)_2(CO)_2(OH)H$[2] and $Ru(IMes)_2(CO)_2(F)H$ (**9**)[4] with corresponding bond angles to display ligand distribution.

Comparison with the related bis CO complexes in **Table 2.14** and **Figure 2.8** reveals the metrics of **10** are typical of $Ru(IMes)_2(CO)_2(X)H$ systems. As such, the ligands *cis* to the hydride ligand {Cl, C(2), C(3), C(24)} tend to bend slightly towards the Ru-H side of the structure where it is less sterically crowded due to the small size of H. Consequently, the structure is distorted octahedral with the C(2)-Ru-Cl angle less than 180 ° at 174.0(3) ° and a C_{NHC}-Ru-C_{NHC} angle of 168.81(6) °.

2.11.4 Formation of $Ru(PPh_3)(IMes)(CO)_2(Cl)H$ (11)

For comparison with **10**, the known mixed phosphine/NHC complex $Ru(PPh_3)(IMes)(CO)(Cl)H$ (**8**) was treated with an atmosphere of CO at room temperature to immediately yield $Ru(PPh_3)(IMes)(CO)_2(Cl)H$ (**11**) (**Scheme 2.11**). The reaction occurred with a corresponding colour change from yellow to pale brown. **11** was characterised by a new doublet hydride resonance at -4.25 ppm (J_{HP} = 14.7 Hz) in the ^1H NMR spectrum and a singlet at 41.0 ppm in the $^{31}P\{^1H\}$ NMR spectrum. Chemical shifts for the starting complex appeared at -23.89 ppm (J_{HP} = 24.3 Hz) (Ru-H) and 42.1 ppm (Ru-P).[30]

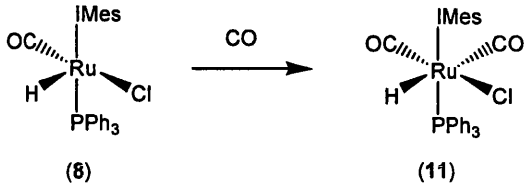

(8) (11)

Scheme 2.11 Coordination of CO into the vacant site of $Ru(PPh_3)(IMes)(CO)(Cl)H$ to yield $Ru(PPh_3)(IMes)(CO)_2(Cl)H$ (**11**).

The hydride resonance at -4.25 ppm is in line with the value obtained for $Ru(IMes)_2(CO)_2(Cl)H$ (**10**) (-4.30 ppm). A comparison of the shifts of the carbenic carbon atoms for the two complexes showed very little difference (184.9 and 185.7 ppm respectively). A large coupling constant of 96.5 Hz was seen for the carbenic carbon, typical of *trans* C-P as expected. $^{13}C\{^1H\}$ NMR shifts of the CO ligands also resembled the data obtained for **10** (201.8 and 194.5 ppm vs. 204.4 and 194.6 ppm respectively).

As expected, the reduced electron density as a result of having a phosphine ligand in **11** rather than second IMes ligand resulted in the CO stretching frequencies of this compound (2044, 1945 cm^{-1}) appearing at higher energies in the IR spectrum than those for **10** (2037, 1903 cm^{-1}). Selected spectroscopic values for **10** and some bis phosphine analogues are given in **Table 2.15** below for comparison with **11**.

$RuL_2(CO)_2(Cl)H$ L_2 =	^1H NMR shift (ppm) Ru-H	IR shift (cm^{-1})	
		ν_{CO}	ν_{Ru-H}
(PPh_3)(IMes) (**11**)	-4.25 (J_{HP} = 14.7 Hz)	2044 1945	1922
$(IMes)_2$ (**10**)	-4.30	2037 1903	1938
$(PPh_3)_2$ [49]	-4.5 (J_{HP} = 19 Hz)	2042 2032	1995 1982
$(PCy_3)_2$ [50]	-5.2 (J_{HP} = 20 Hz)	2030 1944	1960
P^iPr_3 ♠ [34]	-5.15 (J_{HP} = 20 Hz)	2030 1905	1970
$(P^nPr_2{}^tBu)_2$ [51]	-5.29 (J_{HP} = 19.9 Hz)	2025 1957	-
P^tBu_2Me [36]	-5.67 (J_{HP} = 19.7 Hz)	2042 1923	1967
P^tBu_2Et [36]	-5.48 (J_{HP} = 19.2 Hz)	2045 1922	1971
$(PMe_2Ph)_2$ [52]	-5.25 (J_{HP} = -23.1 Hz)	2045 1965	-
$(AsMe_2Ph)_2$ [52]	-5.04	2045 1965	-

Table 2.15 Spectroscopic values for complexes $RuL_2(CO)_2(Cl)H$ for comparison with **11**. (- = not provided)

♠ IR data for $Ru(P^iPr_3)(CO)_2(Cl)H$ was assigned differently in the literature: υ_{CO} = 1905, 1970 cm^{-1}; υ_{Ru-H} = 2030 cm^{-1}.[34]

11 was structurally characterised by X-ray crystallography with crystals grown from a solution of benzene-hexane (**Structure 2.2**). The high *trans* influence of the hydride ligand leads to two quite different Ru-CO distances (Ru-C(1) = 1.973(2) Å, Ru-C(2) = 1.848(2) Å).

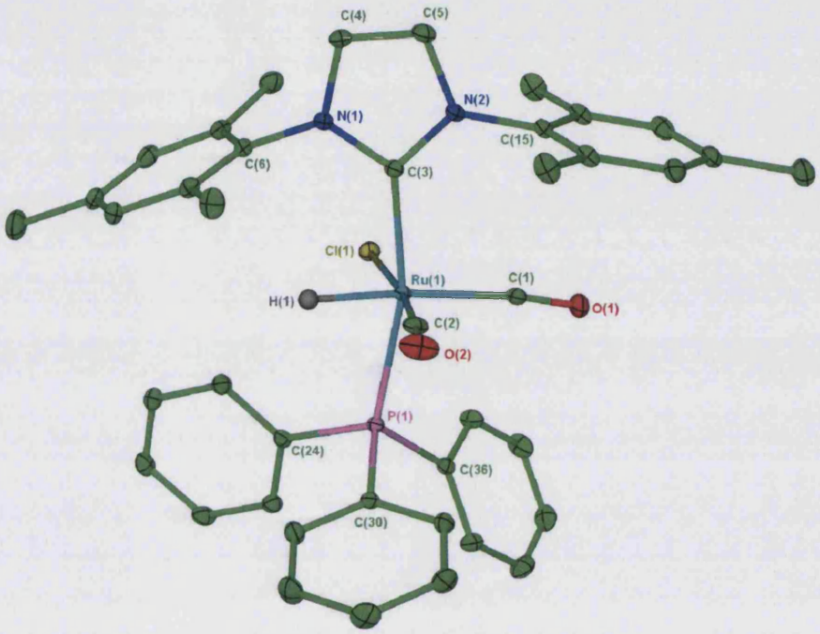

Structure 2.2 X-ray structure of $Ru(PPh_3)(IMes)(CO)_2(Cl)H$ (**11**). Thermal ellipsoids are set at 30 % probability. Hydrogen atoms have been omitted for clarity (except the hydride).

Bond lengths and angles of **11** (**Table 2.16** and **Figure 2.9**) have been compared with those acquired for **10** (**Table 2.14**, **Figure 2.8**, p. 56) and found to be generally similar. In both complexes, Ru-C(1) bond lengths are affected by lying *trans* to a hydride ligand, displaying longer bonds than the carbonyl ligand *trans* to a chloride ligand. Bond angles between the axial ligands in **11** and **10** are also similar (165.42(5) and 168.81(6) ° respectively).

	11
Ru-C(3)	2.0974(19)
Ru-P(1)	2.3529(5)
Ru-Cl(1)	2.4528(5)
Ru-C(1)	1.973(2)
Ru-C(2)	1.848(2)
C(3)-Ru-P(1)	165.42(5)

Table 2.16 Selected bond lengths (Å) and angles (°) for **11**.

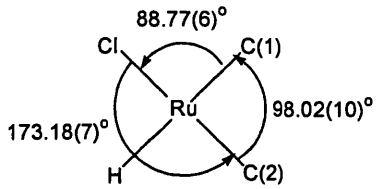

Figure 2.9 A pictorial representation of the equatorial ligands of **11** with corresponding bond angles to display ligand distribution.

It is clear from the X-ray structure of **11** (**Structure 2.2**) that the C(1) side of the complex is more open than the hydride side of the complex, which is attributed to the larger Cl and CO ligands finding steric relief by bending towards the small hydride ligand. The Cl(1)-Ru-C(2) bond angle of 173.18(7) ° supports this hypothesis. The axial ligands also bend away from this region as implied by the small C(3)-Ru-P(1) angle {165.42(5) °}. This is illustrated more effectively by comparing the angles between each *i*-C_{Mes} atom {C(6), C(15)} and the *i*-C_{Ph} atoms on the relevant sides of the structure {C(24), C(36)}; the C(6)-Ru-C(24) angle is significantly smaller at 94.5 ° than the C(15)-Ru-C(36) angle at 127.1 °.

2.11.5 Formation of $Ru(IMes)_2(CO)(NH_3)(Cl)H$ (12)

Exposure of $Ru(IMes)_2(CO)(Cl)H$ (7) to 1 atm ammonia in a C_6D_6 solution resulted in the formation of $Ru(IMes)_2(CO)(Cl)(NH_3)H$ (**12**) upon shaking (**Scheme 2.12**). The ^1H NMR spectrum of **12** showed a singlet hydride resonance at -13.94 ppm. The ammine protons were observed downfield from free NH_3 (t, -0.16 ppm, 31.7 Hz) at 1.60 ppm in a 3:1 ratio with the hydride resonance.

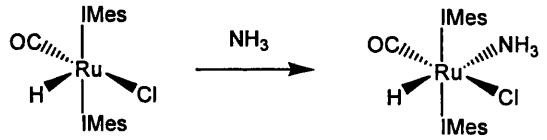

(7) (12)

Scheme 2.12 Reaction of $Ru(IMes)_2(CO)(Cl)H$ with ammonia to yield $Ru(IMes)_2(CO)(Cl)(NH_3)H$ (**12**).

The ^1H NMR spectrum of **12** displayed inequivalent resonances for the IMes ligands, including inequivalent back-bone protons (6.15 and 5.98 ppm) and six different environments for the methyl groups. The NOESY spectrum of **12** at 298 K was acquired to verify the static nature of the complex (**Figure 2.10**). The hydride ligand of **12** showed an NOE correlation with one of the methyl resonances (2.10 ppm). However, there was no NOE correlation between the ammine protons and the methyl protons of IMes, perhaps unsurprisingly once exchange between the bound NH_3 and free NH_3 was established.

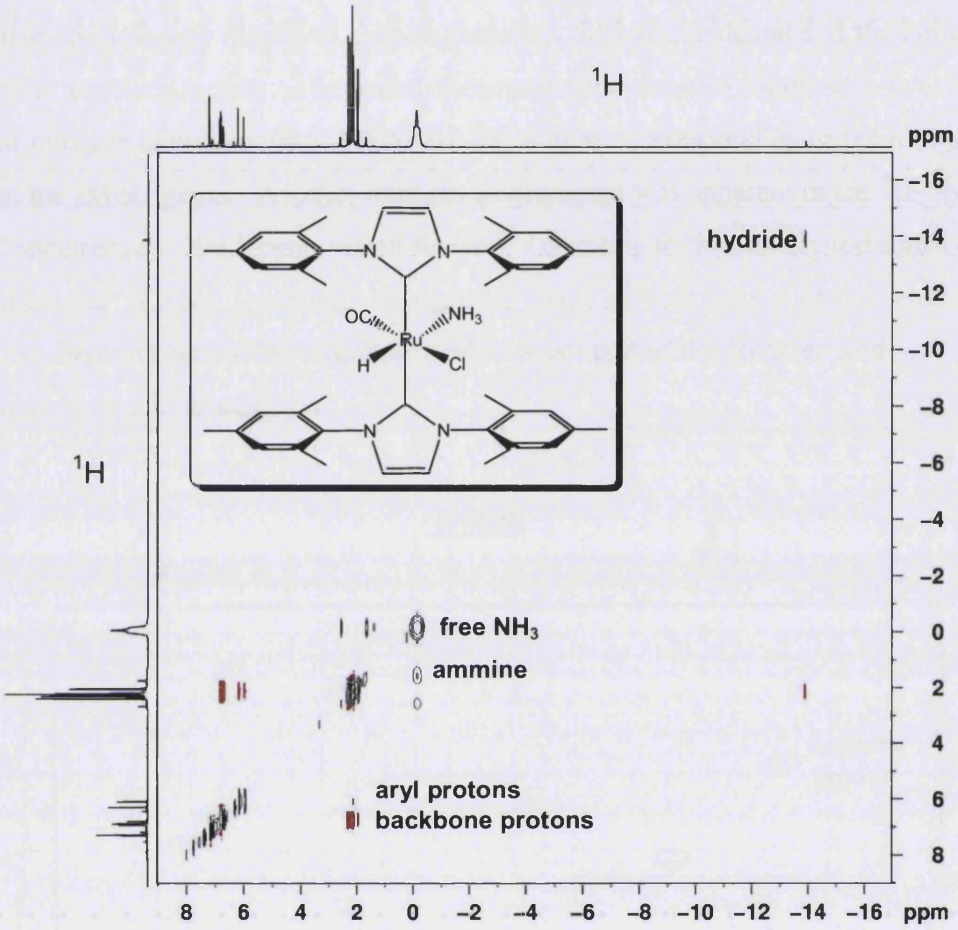

Figure 2.10 ^{1}H-^{1}H NOESY NMR spectrum of **12**, exchange crosspeaks in black and NOE crosspeaks in red (C_6D_6, 298 K, 400 MHz).

The ^{13}C{^{1}H} NMR spectrum of **12** also showed the backbone and mesityl carbon atoms to be inequivalent, verified by ^{1}H-^{13}C{^{1}H} HMQC spectroscopy. Attempts to assign the quaternary carbon atoms by ^{1}H-^{13}C{^{1}H} HMBC spectroscopy were thwarted by the large number and proximity of signals. This effect may well result from the marked difference in the nature of the equatorial ligands. These results are consistent with a significant barrier to rotation around the Ru-C_{NHC} and N-$C_{mesityl}$ axis. This barrier has been calculated as $\Delta H = 52.3$ kJ mol^{-1} in $Ru(PPh_3)_2(IMes)(CO)H_2$.[53]

^{1}H-^{15}N HMQC spectroscopy (**Figure 2.11**) showed coupling to the protons of the bound NH_3 moiety clearly, revealing the nitrogen atom of the ammine ligand at

-409.6 ppm, similar to the reported values for $[Ru(NH_3)_4(2\text{-bzpy})]^{2+}$.[54♦] Longer range correlation spectroscopy displayed coupling between the hydride ligand and the nitrogen atom of the ammonia moiety. The back-bone protons also showed coupling to two different nitrogen environments (-375.5 and -381.4 ppm), corresponding to the nitrogen atoms in the IMes ligands. Another nitrogen environment was apparent in the ^{1}H-^{15}N HMQC spectrum at –396.1 ppm, which showed ^{1}J coupling to the unassigned signal at 2.52 ppm in the ^{1}H NMR spectrum. No coupling to the hydride resonance was observed and it was therefore concluded that these peaks are not part of the complex and unfortunately remain unassigned.

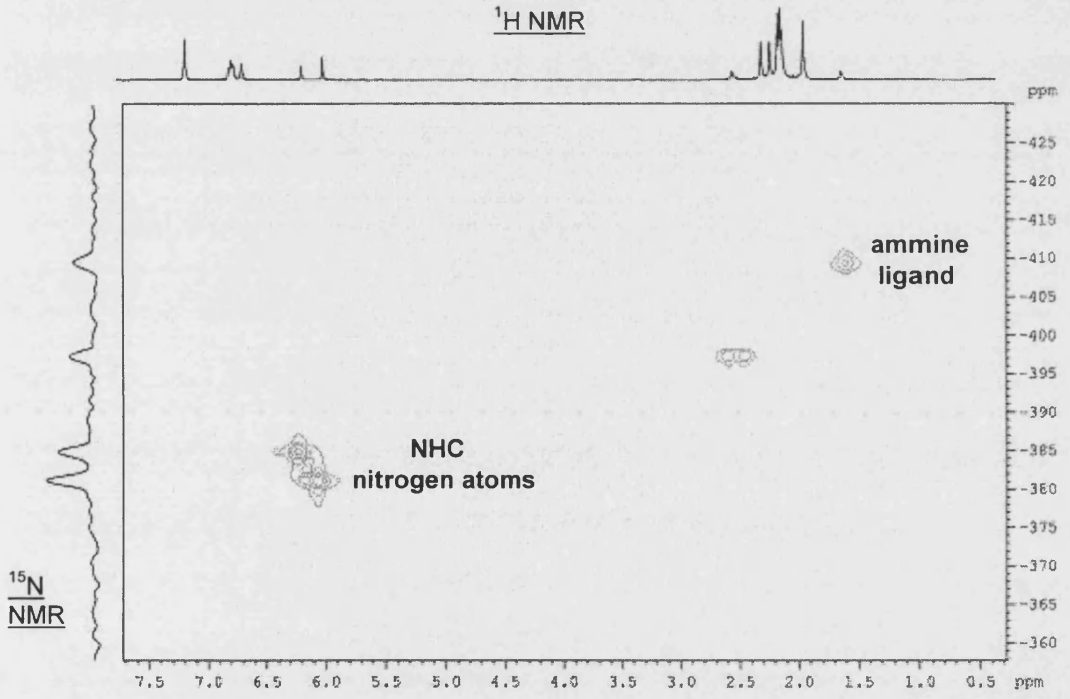

Figure 2.11 ^{1}H-^{15}N HMQC NMR spectrum of **12** (C_6D_6, 298 K).

Crystals of **12** were formed by layering a benzene solution with ammonia saturated hexane. Any removal of the solvent *in vacuo* or the ammonia atmosphere

♦ Free NH_3 was observed at -183.9 ppm in contrast to the IUPAC value of -380.2 ppm.[55] However, the reported data is based on liquid NH_3 as opposed to gaseous NH_3 in C_6D_6, as was used in these reactions.

resulted in dissociation of the ammonia ligand and regeneration of the starting complex $Ru(IMes)_2(CO)(Cl)H$, even with crystalline samples. It is acknowledged that ammonia ligands only coordinate weakly ($BDE_{Ru\text{-}NH_3}$ = 52.7 kJ mol^{-1}),[56] creating relatively unstable complexes. For example, NH_3 is easily lost from $Ru(PCP)(CO)(Cl)(NH_3)$ even as a solid.[56] Furthermore, NH_3 lability is likely to be increased by the NH_3 ligand located opposite the *trans* labilising hydride ligand in **12**. Consequently no elemental analysis was carried out on **12**.

The IR spectrum (C_6D_6) revealed that carbonyl stretching frequencies for **7** and **12** differ only slightly (ν_{CO} = 1887 and 1885 cm^{-1} respectively), consistent with the NH_3 being only weakly bound to the metal centre. This is in contrast to the analogous complexes Ru(PCP)(CO)Cl (ν_{CO} = 1923 cm^{-1}) and $Ru(PCP)(CO)(Cl)(NH_3)$ (ν_{CO} = 1900 cm^{-1}) prepared by Gunnoe *et al*, which differ significantly from each other.[56] However, bound NH_3 in **12** was observed by symmetrical and asymmetrical N-H stretching bands at 3232 and 3129 cm^{-1} and N-H deformation signal at 1619 cm^{-1}.[57]

The X-ray crystal structure of **12** showed disorder between the carbonyl and hydride ligands in a ratio of 80:20. Ripples of electron density were evident in the region of the bound nitrogen atom presumably caused by the hydrogen atoms on ammonia. However, attempted modelling of said difference peaks as hydrogen atoms yielded unsatisfactory U_{iso} values/ N-H distances. The structure determined for **12** indicated a distorted octahedral geometry with retention in arrangement of the equatorial ligands (Cl, CO and H) as shown in **Structure 2.3**.

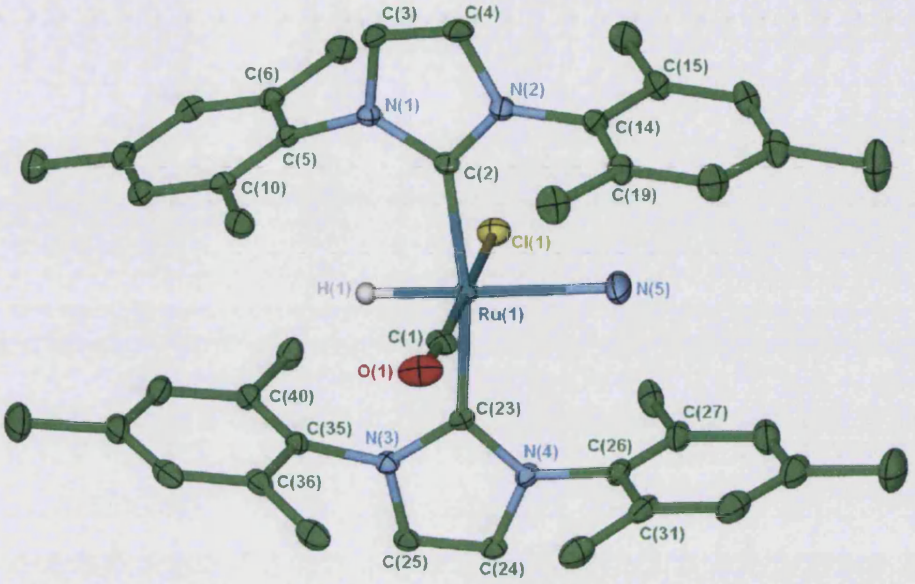

Structure 2.3 X-ray crystal structure of $Ru(IMes)_2(CO)(Cl)(NH_3)H$ (**12**). Thermal ellipsoids are set at 30 % probability. Hydrogen atoms have been omitted for clarity (except the hydride).

	12
Ru-C(2)	2.110(3)
Ru-C(23)	2.102(3)
Ru-Cl	2.488(2)
Ru-C(1)	1.822(9)
Ru-N(5)	2.314(3)
C(2)-Ru-C(23)	170.64(11)

Table 2.17 Selected bond lengths (Å) and angles (°) for **12**.

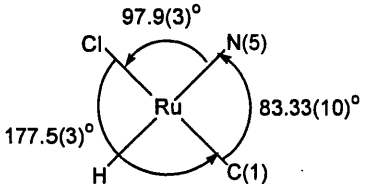

Figure 2.12 A pictorial representation of the equatorial ligands of **12** with corresponding bond angles to display ligand distribution.

12 has Ru-C_{NHC} bond lengths similar to other bis IMes species (**Table 2.17**). The Ru-Cl bond length is longer in **12** than in the analogous complex $Ru(IMes)_2(CO)_2(Cl)H$ (**10**) {2.488(2) vs. 2.384(2) Å}. This can be attributed to Cl lying *trans* to π-accepting CO in **10**, especially as the equivalent bond in the starting complex $Ru(IMes)_2(CO)(Cl)H$ (**7**) is similar to **12** {2.433(3) Å}.[6] The Ru-CO bond length in **12** {1.822(9) Å} is surprisingly shorter than the equivalent bond in **10** {1.890(8) Å} (*trans* to Cl). As with $Ru(IMes)_2(CO)_2(Cl)H$ (**10**) and $Ru(PPh_3)(IMes)(CO)_2(Cl)H$ (**11**), **12** shows Cl and C(1) atoms bending towards the hydride side of the complex, however it was noticeable in **12** that the largest angle between equatorial *cis* ligands was not between C(1)-Ru-N(5) {83.33(10) °} as expected from the related chloride complexes, but between Cl-Ru-N(5) {97.9(3) °} (**Figure 2.12**).

2.12 Summary of 18-electron complexes

The reaction between 16-electron complexes $Ru(IMes)_2(CO)(X)H$ and 2-electron donors (CO, NH_3) to form novel complexes **9**, **10**, **11** and **12** occurs by simple ligand coordination to the metal centre in the position of the original vacant site without any changes in geometry, as previously described. The hydride resonances for **9**, **10**, **11** and **12** are consistently > 10 ppm downfield of the coordinatively unsaturated analogues in the ^1H NMR spectra.[34]

Table 2.18 summarises the spectral data for the new 18-electron complexes reported in this section.

Complex	Ru-<u>C</u>O $^{13}C\{^1H\}$ NMR shift (ppm)[a]	ν_{CO} (cm^{-1})	Ru-<u>H</u> ^1H NMR shift (ppm)[a]	ν_{Ru-H} (cm^{-1})
$Ru(IMes)_2(CO)_2(F)H$ [b] (**9**)	205.7 194.3	1991 1880	-3.80	1930
$Ru(IMes)_2(CO)_2(Cl)H$ [b] (**10**)	204.4 194.6	2037 1903	-4.30	1938
$Ru(PPh_3)(IMes)(CO)_2(Cl)H$ [b] (**11**)	201.8 194.5	2044 1945	-4.25	1922
$Ru(IMes)_2(CO)(NH_3)(Cl)H$ [a] (**12**)	208.4 -	1885 -	-13.94	1863

Table 2.18 Spectroscopic data for novel 18-electron complexes described in this chapter. [a]298 K, C_6D_6. [b]Nujol mull. [c]C_6D_6 solvent cell (- = N/A).

The X-ray crystal structures of the 18-electron species have been compared with their 16-electron counterparts (where available). The effect of the filling the vacant site is noticeable in the X-ray crystal structures by a consistent decrease of *ca.* 10 ° of the C_{NHC}-Ru-C_{NHC} angles; for example, this angle decreases from 179.78(19) ° in $Ru(IMes)_2(CO)(Cl)H$ (**7**) to 168.81(6) and 170.64(11) ° in **10** and **12** respectively. This is due to the large axial ligands moving to the hydride side of the complexes to overcome steric hindrance. The same effect has been observed with equatorial ligands spreading towards the hydride region of the complexes. More detailed investigations into the axial ligands showed that the IMes twist angles decreased considerably (> 20 °) on addition of the sixth ligand and the mesityl arms 'flattened out' with respect to each other to a large extent (**Table 2.19**).

$Ru(IMes)_2(CO)_n(X)H$	C_{NHC}-Ru-C_{NHC}	IMes/IMes	Mes/Mes
X = OH; n = 1 (**2**)	175.43(9)	48.3	45.7, 39.4
n = 2	167.94(8)	21.7	17.6, 16.8
X = SH; n = 1 (**4**)	178.73(9)	52.3	46.2, 46.2
n = 2	168.37(6)	13.9	17.6, 16.4
X = F; n = 1 (**6**)	176.26(10)	47.4	46.2, 38.4
n = 2 (**9**)	167.67(6)	20.9	16.2, 16.4
X = Cl; n = 1 (**7**)	179.78(19)	53.3	45.6, 45.6
n = 2 (**10**)	168.81(6)	16.5	17.0, 16.1
$Ru(IMes)_2(CO)(NH_3)(Cl)H$ (**12**)	170.64(11)	16.0	18.7, 17.1

Table 2.19 Bond and twist angles (°) based on planes imposed on the imidazolium rings and the phenyl rings of the mesityl groups.

The changes in the bond angles displayed in **Table 2.19** remained reasonably uniform over the range of complexes. The consistent decrease in the angles between IMes ligands and the mesityl rings was expected as the metal centres became more sterically hindered, restricting the movement of the ligands.

2.14 References

1. Jazzar, R.F.R.; Macgregor, S.A.; Mahon, M.F.; Richards, S.P.; Whittlesey, M.K., *J. Am. Chem. Soc.*, **2002**, *124*, 4944.
2. Jazzar, R.F.R.; Bhatia, P.H.; Mahon, M.F.; Whittlesey, M.K., *Organometallics*, **2003**, *22*, 670.
3. Chatwin, S.L.; Diggle, R.A.; Jazzar, R.F.R.; Macgregor, S.A.; Mahon, M.F.; Whittlesey, M.K., *Inorg. Chem.*, **2003**, *42*, 7695.

4. Chatwin, S.L.; Davidson, M.G.; Doherty, C.; Donald, S.M.; Jazzar, R.F.R.; Macgregor, S.A.; McIntyre, G.J.; Mahon, M.F.; Whittlesey, M.K., *Organometallics*, **2006**, *25*, 99.
5. Caulton, K.G.; Huffman, J.C.; Renkema, K.B., *Polyhedron*, **1999**, *18*, 2575.
6. Jazzar, R.F.R., *PhD Thesis, University of Bath*, **2003**.
7. Dinelli, L.R.; Batista, A.A.; Wohnrath, K.; de Araujo, M.P.; Queiroz, S.L.; Bonfadini, M.R.; Oliva, G.; Nascimento, O.R.; Cyr, P.W.; MacFarlane, K.S.; James, B.R., *Inorg. Chem.*, **1999**, *38*, 5341.
8. Mahon, M.F.; Whittlesey, M.K.; Wood, P.T., *Organometallics*, **1999**, *18*, 4068.
9. Vinas, C.; Nunez, R.; Teixidor, F.; Kivekas, R.; Sillanaa, R., *Organometallics*, **1996**, *15*, 3850.
10. Abbenhuis, R.A.T.M.; del Rio, I.; Bergshoef, M.M.; Boersma, J.; Veldman, N.; Spek, A.L.; van Koten, G., *Inorg. Chem.*, **1998**, *37*, 1749.
11. Cheng, L.; Powell, D.R.; Khan, M.A.; Richter-Addo, G.B., *Inorg. Chem.*, **2001**, *40*, 125.
12. Kaplan, A.W.; Bergman, R.G., *Organometallics*, **1998**, *17*, 5072.
13. Hartwig, J.F.; Bergman, R.G.; Andersen, R.A., *J. Am. Chem. Soc.*, **1991**, *113*, 3404.
14. Gemel, C.; Mereiter, K.; Schmid, R.; Kirchner, K., *Organometallics*, **1997**, *16*, 5601.
15. Alkita, M.; Takahashi, Y.; Hikichi, S.; Moro-oka, Y., *Inorg. Chem.*, **2001**, *40*, 169.
16. Burn, M.J.; Fickes, M.G.; Hartwig, J.F.; Hollander, F.J.; Bergman, R.G., *J. Am. Chem. Soc.*, **1993**, *115*, 5875.
17. Albores, P.; Chaia, Z.D.; Baraldo, L.; Castellano, E.E.; Piro, O.E., *Acta Crystal. Sect. C - Cryst. Struct. Commun.*, **2002**, *58*, M235.
18. Yoshida, T.; Adachi, T.; Ueda, T.; Akao, H.; Tanaka, T.; Goto, F., *Inorg. Chim. Acta*, **1995**, *231*, 95.
19. Yoshida, T.; Otsuka, S., *J. Am. Chem. Soc.*, **1977**, *99*, 2134.
20. Shaw, B.L.; Uttley, M.F., *J. Chem. Soc., Chem. Commun.*, **1974**, 918.
21. Kudo, K.; Hidai, M.; Uchida, Y., *J. Organomet. Chem.*, **1973**, *56*, 417.

22. Paonessa, R.S.; Trogler, W.C., *J. Am. Chem. Soc.*, **1982**, *104*, 1138.
23. Fryzuk, M.D.; MacNeil, P.A., *Organometallics*, **1983**, *2*, 682.
24. Rybtchinski, B.; Ben-David, Y.; Milstein, D., *Organometallics*, **1997**, *16*, 3786.
25. Burling, S.; Mahon, M.F.; Paine, B.M.; Whittlesey, M.K.; Williams, J.M.J., *Organometallics*, **2004**, *23*, 4537.
26. Poulton, J.T.; Sigalas, M.P.; Folting, K.; Streib, W.E.; Eisenstein, O.; Caulton, K.G., *Inorg. Chem.*, **1994**, *33*, 1476.
27. Buil, M.L.; Elipe, S.; Esteruelas, M.A.; Onate, E.; Peinado, E.; Ruiz, N., *Organometallics*, **1997**, *16*, 5748.
28. Jung, S.; Ilg, K.; Brandt, C.D.; Wolf, J.; Werner, H., *Dalton Trans.*, **2002**, 318.
29. Huang, D.; Koren, P.R.; Folting, K.; Davidson, E.R.; Caulton, K.G., *J. Am. Chem. Soc.*, **2000**, *122*, 8916.
30. Nolan, S.P.; Fogg, D.E.; dos Santos, E.N.; Foucault, H.M.; Dharmasena, U.L., *Organometallics*, **2005**, *24*, 1056.
31. Hallman, P.S.; McGarvey, B.R.; Wilkinson, G., *J. Chem. Soc. A*, **1968**, 3143.
32. Lee, H.M.; Smith, J., D. C.; He, Z.; Stevens, E.D.; Yi, C.S.; Nolan, S.P., *Organometallics*, **2001**, *20*, 794.
33. Yi, C.S.; Lee, D.W.; Chen, Y., *Organometallics*, **1999**, *18*, 2043.
34. Esteruelas, M.A.; Werner, H., *J. Organomet. Chem.*, **1986**, *303*, 221.
35. Johnson, B.F.G.; Segal, J.A., *J. Chem. Soc., Dalton Trans.*, **1973**, *5*, 478.
36. Shaw, B.L.; Gill, D.F., *Inorg. Chim. Acta*, **1979**, *32*, 19.
37. Huang, D.; Streib, W.E.; Bollinger, J.C.; Caulton, K.G.; Winter, R.F.; Scheiring, T., *J. Am. Chem. Soc.*, **1999**, *121*, 8087.
38. Poulton, J.T.; Hauger, B.E.; Kuhlman, R.L.; Caulton, K.G., *Inorg. Chem.*, **1994**, *33*, 3325.
39. Poulton, J.T.; Folting, K.; Streib, W.E.; Caulton, K.G., *Inorg. Chem.*, **1992**, *31*, 3190.
40. Poulton, J.T.; Sigalas, M.P.; Eisenstein, O.; Caulton, K.G., *Inorg. Chem.*, **1993**, *32*, 5490.
41. Heyn, R.H.; Macgregor, S.A.; Nadasdi, T.T.; Ogasawara, M.; Eisenstein, O.; Caulton, K.G., *Inorg. Chim. Acta*, **1997**, *259*, 5.

42. Buskens, P.; Giunta, D.; Leitner, W., *Inorg. Chim. Acta.*, **2004**, *357*, 1969.
43. Burling, S.; Whittlesey, M.K.; Williams, J.M.J., *Adv. Synth. Catal.*, **2005**, *347*, 591.
44. Rautenstrauch, V.; Hoang-Cong, X.; Churland, R.; Abdur-Rashid, K.; Morris, R.H., *Chem.-Eur. J.*, **2003**, *9*, 4954.
45. Chowdhury, R.L.; Backvall, J.E., *J. Chem. Soc., Chem. Commun.*, **1991**, 1063.
46. Aranyos, A.; Csjernyik, G.; Szabó, K.J.; Backväll, J.E., *Chem. Commun.*, **1999**, 351.
47. Haack, K.J.; Hashiguchi, S.; Fujii, A.; Ikariya, T.; Noyori, R., *Angew. Chem. Int. Ed.*, **1997**, *36*, 285.
48. Chatwin, S.L., *MChem project*, **2003**.
49. James, B.R.; Markham, L.D.; Hui, B.C.; Rempel, G.L., *J. Chem. Soc., Dalton Trans.*, **1973**, 2247.
50. Moers, F.G.; Ten Hoet, R.W.N.; Langhout, J.P., *J. Inorg. Nucl. Chem.*, **1974**, *36*, 2279.
51. Gill, D.F.; Mann, B.E.; Shaw, B.L., *J. Chem. Soc., Dalton Trans.*, **1973**, 311.
52. Bray, J.M.; Mawby, R.J., *J. Chem. Soc., Dalton Trans.*, **1987**, 2989.
53. Burling, S.; Paine, B.M.; Nama, D.; Brown, V.S.; Mahon, M.F.; Prior, T.J.; Pregosin, P.S.; Whittlesey, M.K.; Williams, J.M.J., *J. Am. Chem. Soc.*, **2007**, *129*, 1987.
54. de Paula, A.S.A.T.; Mann, B.E.; Tfouni, E., *Polyhedron*, **1999**, *18*, 2017.
55. Mason, J., *Multinuclear NMR, Chap 12*, **1987**, *Plenum Press, NY.*
56. Conner, D.; Jayaprakash, K.N.; Cundari, T.R.; Gunnoe, T.B., *Organometallics*, **2004**, *23*, 2724.
57. Bellamy, L.J., *The Infrared Spectra of Complex Molecules*, **1975**, *1, 3rd Ed.*

Chapter 3

3. bis IMes acetylide complexes

3.1 Preamble

The hydroxide complex $Ru(IMes)_2(CO)(OH)H$ (**2**) is investigated as a useful precursor to other 16-electron complexes. This chapter comprises of two sections; in the first part we describe the formation of some novel bis IMes phenylacetylide complexes from **2** and investigate possible mechanisms for their formation, including the back reaction with H_2. The reaction between HC≡CPh and $Ru(IMes)_2(CO)(Cl)H$ (**7**) is used as a comparison to the reaction with **2**. Characterisation of the related trimethylsilylacetylide complex is also provided. The second section deals with the formation of 18-electron, phenylacetylide dicarbonyl complexes. The findings of both sections are compared and summarised at the end of the chapter.

3.2 $Ru(IMes)_2(CO)(OH)H$ (2) as a useful precursor

2 has proved to react readily with an array of small molecules, such that it is the starting material for the production of majority of the complexes described in Chapter 2, including **4**, **6** and **7**. The reaction of **2** with acetylenes serves three purposes. Firstly, to establish whether **2** is sufficiently reactive to undergo any change and, secondly, to determine if there is sufficient space for acetylide ligands to bind to the metal centre as it is considered to be sterically shielded by the bulky IMes ligands. The third and most significant reason is to prepare bis IMes acetylide complexes for comparison with reported phosphine systems. In general, monomeric acetylide complexes are sought after as models for polymeric systems, which are known for their interesting material and electronic properties.[1]

3.3 Formation of the hydroxide complex $Ru(IMes)_2(CO)(OH)H$ (2)

3.3.1 Synthesis and characterisation of 2

The synthesis of $Ru(IMes)_2(CO)(OH)H$ (**2**) has previously been described by Jazzar,[2] although small changes have been made in the preparation including the use of 1:1 water/hexane mixture to precipitate out the complex rather than just hexane allowing higher yields of **2** to be isolated.

It has also proved possible to produce **2** *via* metathesis of $Ru(IMes)_2(CO)(Cl)H$ (**7**) with KOH / MeOH following a modified preparation described by Esteruelas for preparation of $Os(P^iPr_3)_2(CO)(OH)H$ from $Os(P^iPr_3)_2(CO)(Cl)H$.[3] Chloride contamination was continually problematic in the preparation of **2**, readily forming **7**. This preparation was an effective and quick way to convert **7** back to **2**, ensuring clean samples of **2** could be achieved. (**Scheme 3.1**).

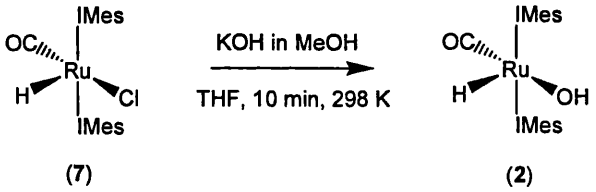

(7) (2)

Scheme 3.1 The metathesis reaction of **7** with KOH to form **2**.

Formation of **2** was characterised by a diagnostic hydride resonance at -23.15 ppm in the ^1H NMR spectrum. Caulton reported similar values for the analogous complex $Ru(P^tBu_2Me)_2(CO)(OH)H$ (-22.3 ppm, J_{HP} = 19 Hz) also produced by metathesis of the corresponding hydride chloride complex with KOH.[4]

3.4 16-electron acetylide complexes

3.4.1 Formation of the mono phenylacetylide complex Ru(IMes)$_2$(CO)(C≡CPh)H (13)

3.4.1.1 Synthesis and characterisation of 13

Ru(IMes)$_2$(CO)(OH)H (**2**) was reacted with one equivalent of HC≡CPh to produce the 16-electron mono phenylacetylide complex Ru(IMes)$_2$(CO)(C≡CPh)H (**13**) (**Scheme 3.2**) The reaction occurred immediately at ambient temperature as shown by the formation of a new singlet hydride resonance in the ^{1}H NMR spectrum at -28.33 ppm, indicative of a vacant *trans* coordination site. The coordination sphere is completed by a *trans* arrangement of the π-donating acetylide ligand opposite π-accepting CO.

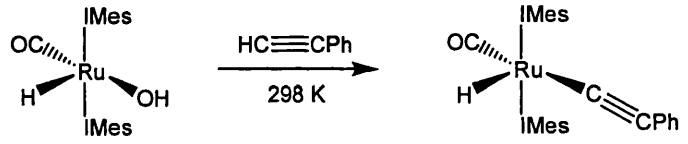

(2) (13)

Scheme 3.2 Formation of Ru(IMes)$_2$(CO)(C≡CPh)H (**13**).

The ^{13}C{^{1}H} NMR spectrum showed a signal for the carbenic carbon atoms at 197.8 ppm and the carbonyl carbon at 204.0 ppm. Two acetylide carbon signals were located at 145.9 and 116.5 ppm and assigned to C_α and C_β respectively on the basis of a crosspeak in the ^{1}H-^{13}C{^{1}H} HMBC spectrum between the resonance at 145.9 ppm and the hydride resonance. In related systems with phosphine ligands it is sometimes possible to differentiate between C_α and C_β resonances by the relative J_{CP} coupling constants, with J_{CP} for C_β usually smaller than C_α, so much so that C_β often appears as a simple singlet. It is notable that there is no consistency in the position of the chemical shift of C_α relative to C_β. (**Table 3.9**, p. 104 contains the relevant data for comparison).[5]

The carbonyl stretching frequency for **13** was observed at 1887 cm^{-1} in the IR spectrum, in contrast to 1906 cm^{-1} for the related phosphine complex

$Ru(P^tBu_2Me)_2(CO)(C{\equiv}CPh)H$, (which also contains the C≡C-Ru-CO *trans* arrangement).[4] The lower frequency for **13** is consistent with the higher σ-donor power of IMes compared to P^tBu_2Me. An absorption band was observed for the triple bond of **13** at 2062 cm^{-1} in comparison to 2072 cm^{-1} for Caulton's complex.

The filled π-orbitals of the acetylide ligand may act as a source of π-electron donation to the metal centre by forming the vinylidene-type zwitterion resonance structure shown in **Figure 3.1** for stabilisation.

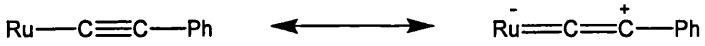

Figure 3.1 Possible resonance structures of **13**.

The propensity of the C≡C unit to undergo resonance stabilisation should be apparent in the crystal structures of these species, giving rise to shorter Ru-C_α distances and longer C_α-C_β bonds.[6] In this manner Carty concluded that $Ru(PEt_3)_2(CO)_2(C{\equiv}CPh)_2$ did not contain significant Ru-C multiple bonding.[7] The X-ray crystal structure of **13** (**Structure 3.1**) displayed bond lengths for Ru-C_α and C_α-C_β of 2.084(6) and 1.213(8) Å, which are similar to the data reported for $Ru(PEt_3)_2(CO)_2(C{\equiv}CPh)_2$ {2.074(3) and 1.200(4) Å respectively} and thus **13** is assigned as a typical acetylide complex with negligible contribution from the vinylidene zwitterion resonance structure. Other bond lengths of interest (**Table 3.1**) such as Ru-C_{NHC} were found to be similar to bis IMes complexes previously described, as was the case with bond angles.

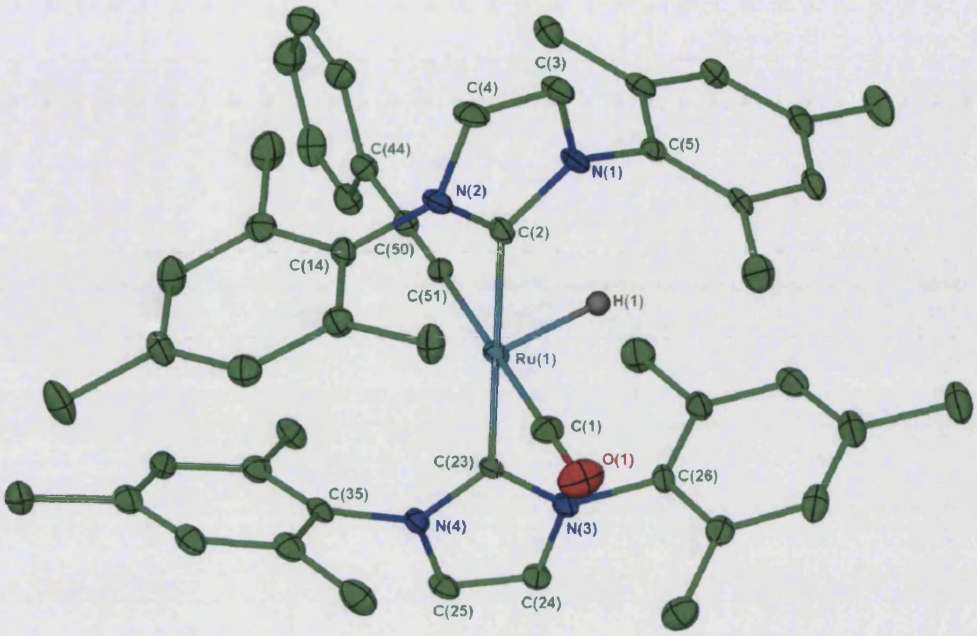

Structure 3.1 X-ray crystal structure of $Ru(IMes)_2(CO)(C{\equiv}CPh)H$ (**13**). Thermal ellipsoids are set at 30 % probability. Hydrogen atoms have been omitted for clarity (except the hydride).

	13
Ru-C(2)	2.071(5)
Ru-C(23)	2.066(5)
Ru-C(1)	1.847(6)
Ru-C(51)	2.084(6)
C(50)-C(51)	1.213(8)
C(2)-Ru-C(23)	177.9(2)
C(1)-Ru-C(51)	179.5(3)

Table 3.1 Selected bond lengths (Å) and angles (°) for **13**.

Comments on the orientation of the phenyl substituent will be considered later in the Summary section at the end of the chapter.

3.4.1.2 Possible mechanisms for the formation of Ru(IMes)$_2$(CO)(C≡CPh)H (13)

There are two possible mechanisms shown in **Scheme 3.3** that could readily account for the reaction of **2** with phenylacetylene. Following η^2-bonding of the acetylene substrate to the metal centre (**A**), the acidic proton could transfer to the hydroxide ligand producing an acetylide ligand and H_2O which is easily lost to form **13** upon isomerisation (pathway **a**). Alternatively, the hydride ligand could transfer to the hydroxide group to form bound H_2O (**B**), which is subsequently lost and the acetylide moiety could provide its proton to reinstate a hydride ligand (pathway **b**). The key difference between pathways **a** and **b** is the origin of the hydride ligand in **13**; either the original hydride (from **2**) remains or the hydride is obtained from the acetylide substrate. Loss of H_2O, consistent with both pathways **a** and **b**, was observed by a broad peak in the ^{1}H NMR spectrum at 0.63 ppm.

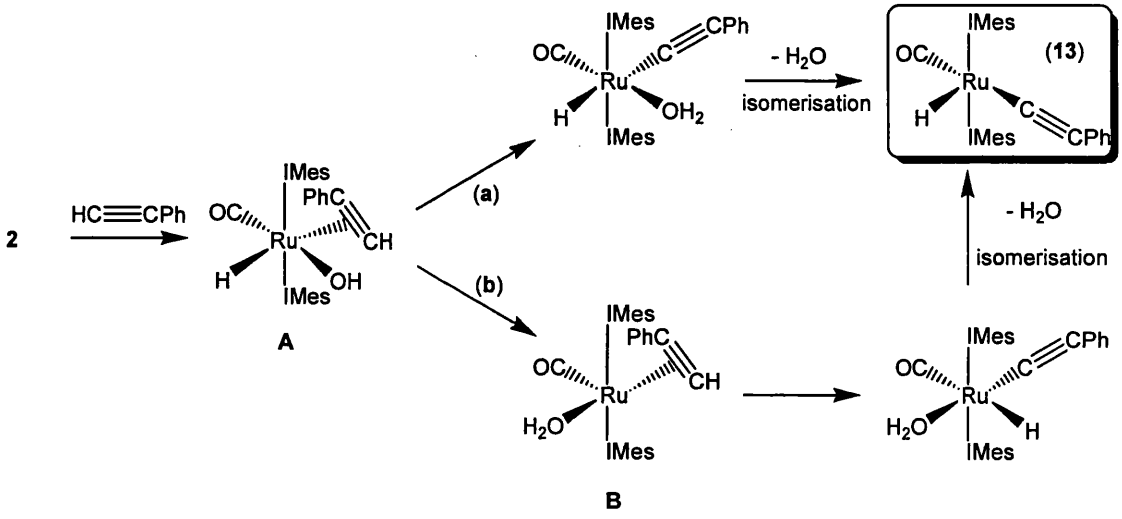

Scheme 3.3 Two possible mechanisms (**a** and **b**) for the production of **13** from **2**.

We have not attempted labelling studies to resolve the mechanism but labelling experiments by Caulton in the reaction of Ru(P^{t}Bu$_2$Me)$_2$(CO)(X)D (X = OR', SiOR''$_3$) with HC≡CPh support pathway **a** as a likely mechanism. Reaction of the labelled species Ru(P^{t}Bu$_2$Me)$_2$(CO)(X)D with HC≡CPh caused complete retention of deuterium by the metal, implying the proton lost in XH originates from the acetylide substrate.[8]

3.4.2 Formation of the bis phenylacetylide complex, $Ru(IMes)_2(CO)(C{\equiv}CPh)_2$ (14)

3.4.2.1 Synthesis and characterisation of 14

Treatment of $Ru(IMes)_2(CO)(OH)H$ (**2**) with excess HC≡CPh (10 equiv.) at room temperature led to the formation of the bis phenylacetylide complex $Ru(IMes)_2(CO)(C{\equiv}CPh)_2$ (**14**). The ^1H NMR spectrum recorded immediately after addition showed no remaining hydride resonance for **2** but full conversion to the mono acetylide complex $Ru(IMes)_2(CO)(C{\equiv}CPh)H$ (**13**). Over two days at 298 K the diagnostic **13** hydride signal at -28.33 ppm decreased until it was completely lost with total conversion to **14**. (**Scheme 3.4**). The phenylacetylide groups in **14** are equivalent as there are only three different proton environments for the phenyl moiety (*o*, *m* and *p*) observed in the ^1H NMR spectrum. The $^{13}C\{^1H\}$ NMR spectrum of **14** shows very little difference to that for **13**. In fact the only resonance differing by more than 1 ppm from **13**, are the two equivalent carbenic signals at 191.3 ppm (197.8 ppm for **13**).

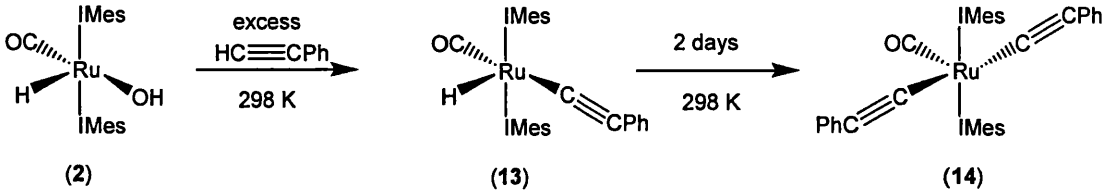

Scheme 3.4 Reaction of **2** with excess phenylacetylene to yield $Ru(IMes)_2(CO)(C{\equiv}CPh)_2$ (**14**) *via* the formation of **13**.

The IR spectrum of **14** shows the expected single carbonyl absorption band at 1954 cm^{-1}, moved to considerably higher frequency relative to **13** (ν_{CO} 1887 cm^{-1}). Not only is the second acetylide group a poorer donor than the original hydride ligand but, more importantly, the CO group in **14** lies *trans* to a vacant site, further decreasing the degree of backbonding. Caulton used the observation of a high frequency CO band in $Ru(P^tBu_2Me)_2(CO)(C{\equiv}CPh)_2$ (ν_{CO} 1933 cm^{-1}) to rationalise its geometry as having CO *trans* to the vacant site.[8] Werner reported the carbonyl

stretching frequency of another bis phenylacetylide system, $Ru(P^iPr_3)_2(CO)(C{\equiv}CPh)_2$ at 1925 cm^{-1} but without any structural discussion.[9] Interestingly the formation of $Ru(P^iPr_3)_2(CO)(C{\equiv}CPh)_2$ probably occurs in the same manner as **14** except in a one pot synthesis comprising of the chloride complex $Ru(P^iPr_3)_2(CO)(Cl)H$, a stoichiometric amount of KOH in MeOH {presumably producing $Ru(P^iPr_3)_2(CO)(OH)H$} and excess phenylacetylene.[9]

$RuL_2(CO)(C{\equiv}CPh)_2$[a] L =	IR shift (cm^{-1})	
	ν_{CO}	$\nu_{C\equiv C}$
IMes (**14**)[b]	1954	2068
P^tBu_2Me[8]	1933	2074
P^iPr_3[9, 10]	1925	2060
PCy_3[11]	1920	2074
13[b]	1887	2062

Table 3.2 Infra-red spectroscopic values for complexes $RuL_2(CO)(C{\equiv}CPh)_2$ for comparison with **14** [a](except **13**, which has the formula $Ru(IMes)_2(CO)(C{\equiv}CPh)H$). [b]Nujol mull.

Table 3.2 contains selected spectroscopic data for species similar to **14**. In the acetylide region of the IR spectrum of **14** a single band located at 2068 cm^{-1} was assigned to the acetylide groups similar to the reported values (ν_{CC} 2074 cm^{-1}) for $RuL_2(CO)(C{\equiv}CPh)_2$ (L = P^tBu_2Me, PCy_3).[8, 11] However, the carbonyl stretching frequency for **14** is unexpectedly higher than those reported for the phosphine analogues suggesting that ν_{CO} in **14** is affected by steric factors rather than being dominated just by electron considerations.

The X-ray crystal structure of **14** (**Structure 3.2**) confirmed without doubt that the CO ligand lies *trans* to the vacant site. The data revealed significantly shorter Ru-CO {1.803(5) Å} and C-O {1.163(6) Å} bond lengths than those reported for $Ru(P^tBu_2Me)_2(CO)(C{\equiv}CPh)_2$ {2.05(8) and 1.22(7) Å respectively}.[8] It is also significant that Ru-C-O in $Ru(P^tBu_2Me)_2(CO)(C{\equiv}CPh)_2$ deviates markedly from linearity at 143.0(5) °, whereas the carbonyl ligand in **14** remains linear (180 °). Metrics of **14** and $Ru(P^tBu_2Me)_2(CO)(C{\equiv}CPh)_2$ structures are compared in **Table 3.3** and show that the atoms bound directly to the ruthenium atom in **14** generally have

shorter bond lengths than in $Ru(P^tBu_2Me)_2(CO)(C{\equiv}CPh)_2$, suggesting that in the former they are held more tightly to the metal centre. The angle between the axial ligands (L) is marginally larger in $Ru(P^tBu_2Me)_2(CO)(C{\equiv}CPh)_2$ {176.3(10) Å} than in **14** {172.10(14) Å}, possibly due to the steric bulk imparted by phosphine ligands. The angle available to the vacant site is larger in **14** {175.06(17)°} than the comparative complex {169.0(15)°}, suggesting that coordination into the vacant site is sterically feasible.

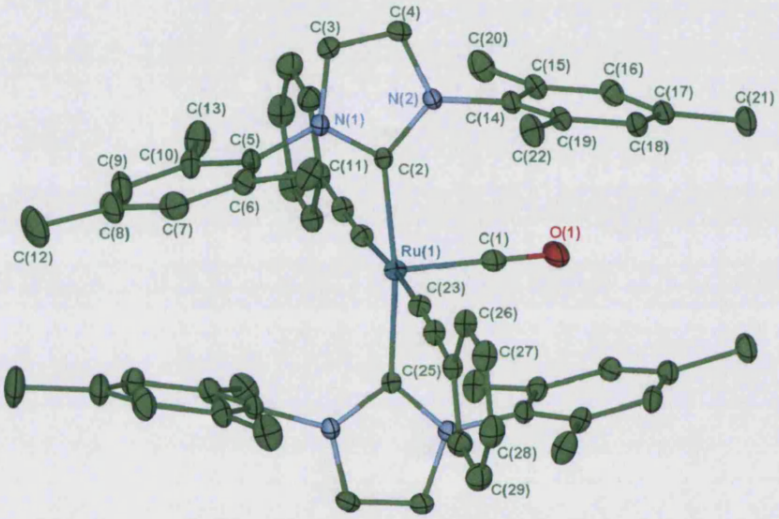

Structure 3.2 X-ray crystal structure of $Ru(IMes)_2(CO)(C{\equiv}CPh)_2$ (**14**). Thermal ellipsoids are set at 30 % probability. Hydrogen atoms have been omitted for clarity.

The structure of **14** is symmetrical with Ru and CO ligand atoms located on a 2-fold rotation axis, making both phenylacetylide groups equivalent (C_α denoted by C(23) and C(23') in **Table 3.3**).

	14	$Ru(P^tBu_2Me)_2(CO)(C{\equiv}CPh)_2$ [12]
Ru-C(2)	2.094(3)	-
Ru-C(1)	1.803(5)	2.05(8)
Ru-C(23)	2.047(3)	2.16(3), 2.08(4)
C(23)-C(24)	1.219(4)	1.18(5), 1.21(6)
L-Ru-L (L = IMes / $P^tBu_2Me)_2$)	172.10(14)	176.3(10)
C(23)-Ru-C(23')	175.06(17)	169.0(15)
C(23)-C(24)-Ph	177.6(3)	172.0(5)
C(23)-Ru-C(1)	92.47(8)	90.4

Table 3.3 Selected bond angles (°) and distances (Å) comparing **14** with the phosphine analogue $Ru(P^tBu_2Me)_2(CO)(C{\equiv}CPh)_2$.[6]

Little difference is seen in the metrics of $Ru(IMes)_2(CO)(C{\equiv}CPh)H$ (**13**) and **14**. The Ru-C_{NHC} bond lengths are slightly longer in **14** {2.094(3) vs. *ca.* 2.07 Å for **13**}. The Ru-CO bond length is a little shorter in **14** {1.803(5) Å} than **13** {1.847(6) Å} (negligible differences exist between the C≡O bond lengths at 1.163(6) and 1.170(7) Å respectively) contrary to what might be expected on the basis of CO being *trans* to a vacant site and acetylide respectively. The Ru-C_α bond lengths in **14** are surprisingly shorter than in **13** (2.047(3) vs. 2.084(6) Å respectively), implying that this bond is not lengthened by the absence of a *trans* CO ligand. **Structure 3.2** shows the phenyl rings staggered with respect to the IMes arms, hence sterics are not implicated in the Ru-C_α distances. Once again the orientation of the ligands will be discussed in more detail in the Summary section at the end of the chapter.

3.4.2.2 Investigating the formation of $Ru(IMes)_2(CO)(C{\equiv}CPh)_2$ (14)

14 can also be produced upon treatment of isolated $Ru(IMes)_2(CO)(C{\equiv}CPh)H$ (**13**) with excess phenylacetylene at room temperature. **Scheme 3.5** shows two possible mechanisms for the formation of **14**. One

mechanism (**a**) involves the formation of the alkenyl species $Ru(IMes)_2(CO)(C{\equiv}CPh)(HC{=}CHPh)$ (**A**) as a result of hydrogen migration but it could also be rationalised by insertion of phenylacetylene into the Ru-H bond. Pathway (**a**) also leads to the stoichiometric loss of styrene to produce **14**. In contrast pathway (**b**) is a simple metathesis reaction in which the acidic terminal proton of $HC{\equiv}CPh$ and the basic hydride ligand are lost as H_2, followed by isomerisation to achieve **14**.

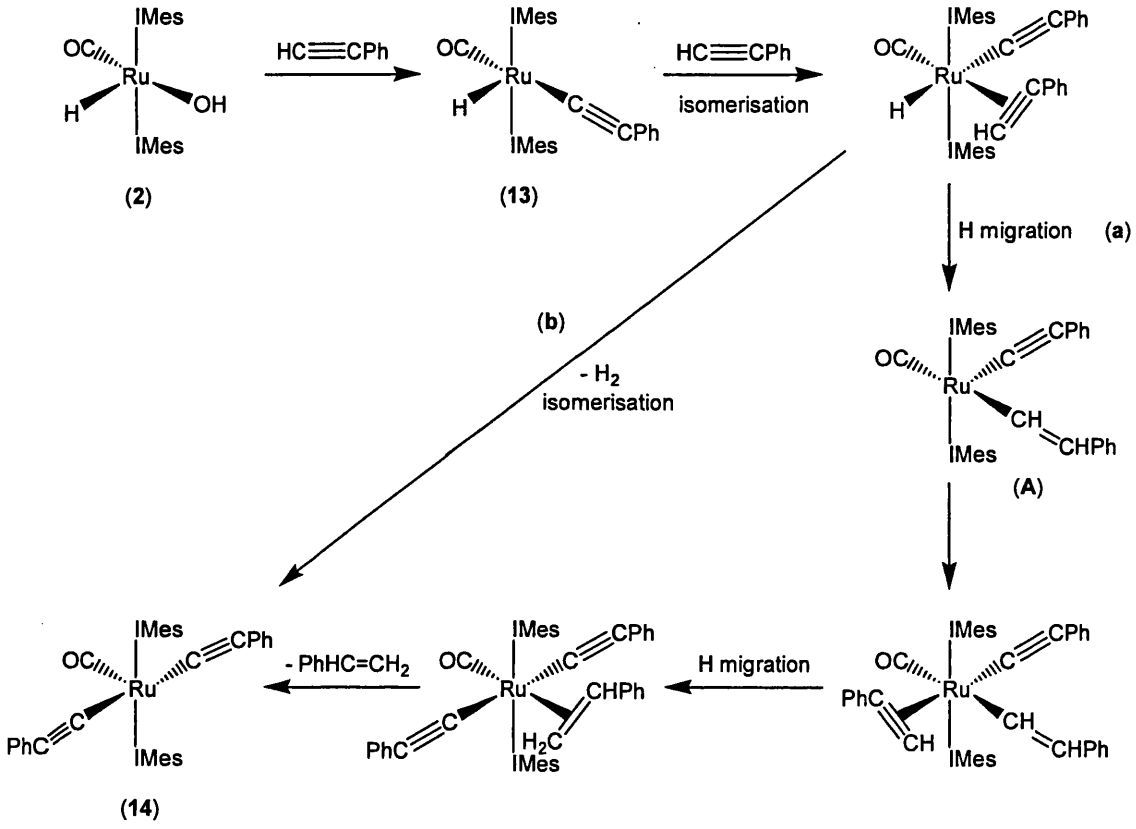

Scheme 3.5 Two proposed mechanisms (**a** and **b**) for the production of **14** from **13**.

In order to establish which pathway best describes the reaction, $Ru(IMes)_2(CO)(OH)H$ (**2**) was reacted with two equivalents of $HC{\equiv}CPh$ and the reaction followed at room temperature by ^1H NMR spectroscopy. If pathway **a** was correct, then **more than** two equivalents of substrate would be necessary to form **14** and the proposed intermediate complex $Ru(IMes)_2(CO)(C{\equiv}CPh)(HC{=}CHPh)$ should be produced instead. The ^1H NMR spectrum showed immediate conversion to **13**, followed by partial loss of the hydride resonance characteristic of the mono

phenylacetylide complex, **13**, overnight and appearance of the diagnostic backbone proton resonance for **14** (5.97 ppm). However, the spectrum also displayed two very small doublet resonances at 8.19 and 5.72 ppm (both J_{HH} = 13.6 Hz) tentatively assigned as α and β-bound protons of the vinyl ligand in $Ru(IMes)_2(CO)(C{\equiv}CPh)(HC{=}CHPh)$ {expected at *ca.* 8.65 and 6.4 ppm, based on values reported for $RuL_2(CO)(C{\equiv}CPh)(HC{=}CHPh)$ where L = P^tBu_2Me,[12] P^iPr_3[9]}. Over the course of the reaction these resonances remained as very minor signals in comparison to resonances associated with **14** and **13**. After a week at 298 K the ^1H NMR spectrum revealed **14** as the major product (>2:1 respectively with respect to **13**, based on backbone proton integrals), consistent with pathway **b** on the premise that only two equivalents of HC≡CPh are necessary to yield **14** from **2**.

Free styrene was evident in the sample by a characteristic doublet of doublet signals for the terminal alkenyl protons at 5.59 ppm (J_{HH} = 17.6, 0.9 Hz) and 5.06 ppm (J_{HH} = 11.0, 0.9 Hz). However, the ratio of styrene to **14** was far from stoichiometric at *ca.* 1:35 respectively. Presumably styrene formation was made possible by the presence of H_2 produced from metathesis pathway **b** rather than being formed as a byproduct of pathway **a**. An atmosphere of hydrogen was added to the reaction sample to investigate whether styrene production would be increased. On addition of H_2 to the reaction mixture (>2:1 **14**:**13**) at room temperature, increased amounts of styrene were observed but more remarkably H_2 caused the reverse reaction of **14** to **13** (resulting in 1:2 ratio) so that the mono phenylacetylide complex predominated the reaction mixture!

3.4.2.3 Investigating the back-reaction from $Ru(IMes)_2(CO)(C{\equiv}CPh)_2$ (14) to $Ru(IMes)_2(CO)(C{\equiv}CPh)H$ (13)

A clean sample of **14** was exposed to 1 atm of H_2 at 298 K to establish whether the reaction from **13** to **14** was reversible, as considered in **Scheme 3.6**. The reaction mixture was heated for 1 h at 333 K with ^1H NMR spectra taken at 15 min intervals (**Figure 3.2**).

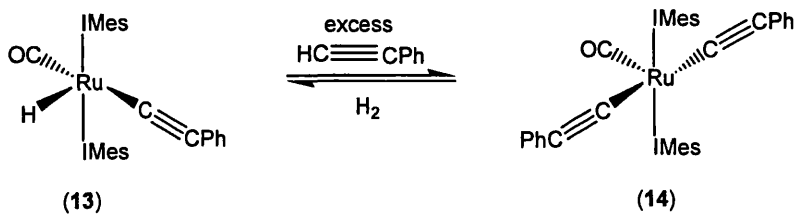

Scheme 3.6 Reversible reaction between **13** and **14** with the back-reaction occurring on addition of 1 atm H_2 at 298 K.

The reaction was followed by studying the formation of the diagnostic hydride resonance for **13** at -28.33 ppm and the relative magnitudes of the characteristic backbone proton signals for **14** and **13** at 5.97 and 6.22 ppm respectively. Immediately after exposure to H_2 (at 298 K) the ^{1}H NMR spectrum showed a 48 % conversion from **14** to **13**. After 1 h at 333 K the backbone proton resonance diagnostic of **14** diminished so that it was no longer observable and the spectrum showed only **13**.

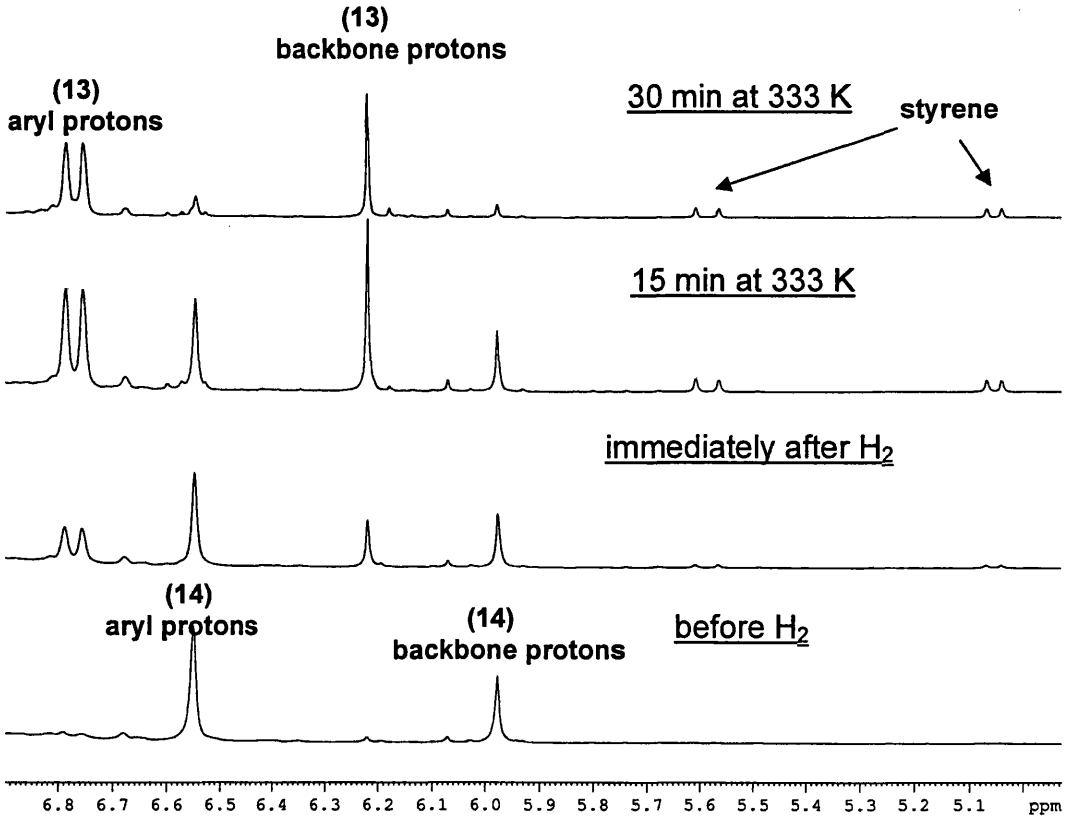

Figure 3.2 ^{1}H NMR spectra showing the reaction of **14** with H_2 heated at 333 K to form **13** (C_6D_6, 298 K, 400 MHz).

Free HC≡CPh was envisaged as a byproduct of the conversion from **14** to **13**, but evidence of it in the ^{1}H NMR spectrum was not clear (expected at 2.71 ppm). However, the formation of styrene was evident, which we suggest is formed subsequent to the loss of HC≡CPh. A mechanism to account for **13** and styrene formation is proposed in **Scheme 3.7**. The proposed pathway shows η^2-binding of H_2 into the vacant site of **14** (**A**) followed by H-migration to yield **13** and free HC≡CPh. Whilst free HC≡CPh is present the process is in equilibrium as the forward reaction can also occur (which also produces H_2). Hydrogenation to H_2C=CHPh removes HC≡CPh from the system, promoting the back-reaction. The production of styrene can be realised by subsequent insertion of HC≡CPh into the Ru-H bond of **13** yielding Ru(IMes)$_2$(CO)(C≡CPh)(HC=CHPh)* (**B**) to which η^2-H_2 can bind (**C**) and undergo H-migration to form η^2-H_2C=CHPh and a hydride ligand. Styrene is lost from the metal centre resulting in reformation of **13**.

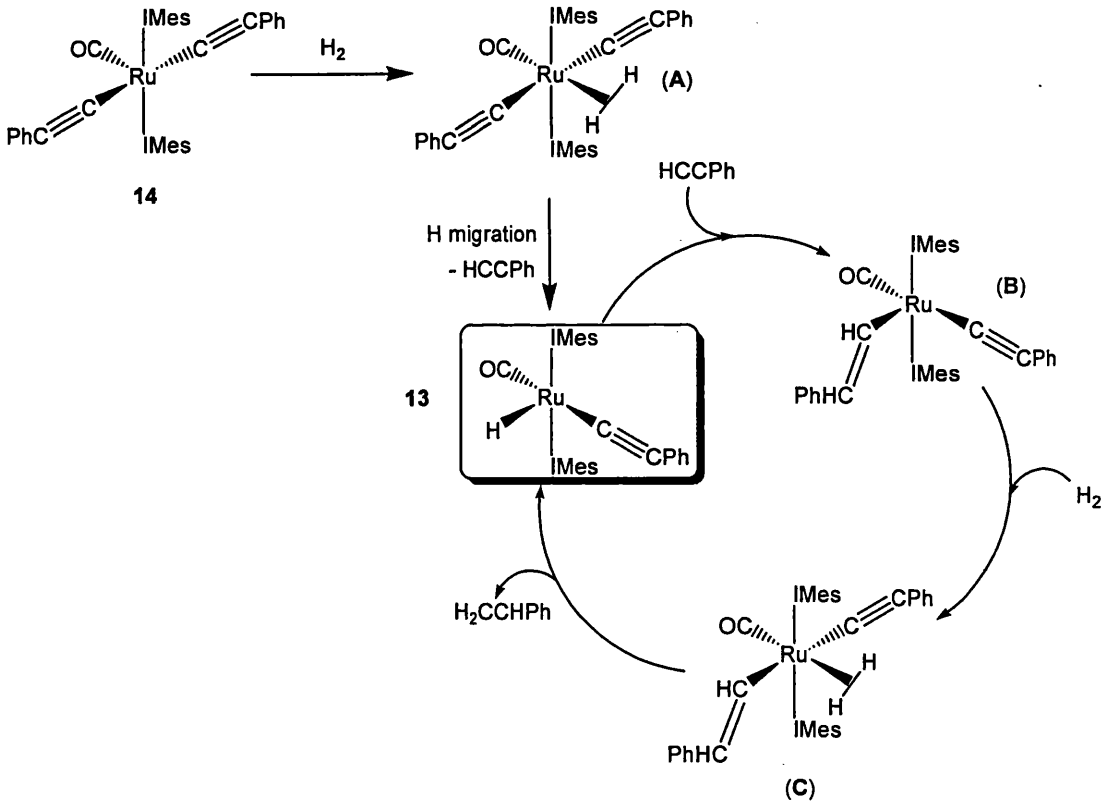

Scheme 3.7 A proposed mechanism for the reverse reaction of **14** to **13** (boxed) under 1 atm H_2 at 298 K to account for the side reaction which produces styrene as a byproduct.

* previously considered and discounted for its role in the forward reaction, p. 84.

3.4.2.4 Investigating the reaction of $Ru(IMes)_2(CO)(C{\equiv}CPh)H$ (13) with H_2

The NMR sample of **14** with H_2 was rechecked after a night at 298 K and the ^1H NMR spectrum revealed hydride resonances characteristic of $Ru(IMes)_2(CO)(OH)H$ (**2**) and $Ru(IMes)_2(CO)(Cl)H$ (**7**) as well as for **13**. These results imply that the back-reaction with H_2 does not stop at the mono acetylide complex **13** but also affects the acetylide ligand of **13**. Presumably the acetylide ligand in $Ru(IMes)_2(CO)(C{\equiv}CPh)H$ (**13**) is effectively fluxional until $HC{\equiv}CPh$ is removed from the system by hydrogenation, producing styrene. Without free $HC{\equiv}CPh$ to form **13** the species reacts with adventitious H_2O or 'Cl' from contamination to yield **2** and **7** as shown in **Scheme 3.8**. Of course, if free $HC{\equiv}CPh$ was added to the reaction mixture the hydroxide component (**2**) would react to form **13** or **14** (depending on the quantities used) and complete the cycle. The reaction of $Ru(IMes)_2(CO)(Cl)H$ (**7**) with $HC{\equiv}CPh$ is discussed in the next section.

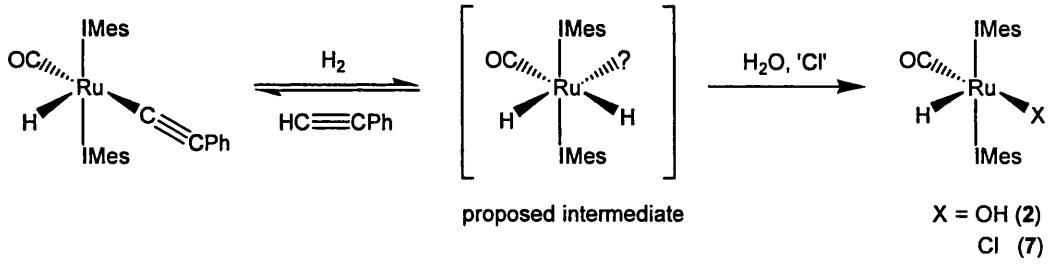

Scheme 3.8 Possible pathway for the reaction of **13** with H_2 (1 atm, 298 K).

A set of reactions were carried out to substantiate the conditions necessary for the formation of **2** and **7** from **13**, including possible intermediate species as implied in **Scheme 3.8.**

An NMR sample of **13** in C_6D_6 was treated with a large excess of H_2O (*ca.* 16 h, 323 K) to verify that a presence of H_2O did not result in production of **2**. However, upon exposure of the H_2O-saturated sample to H_2 at 298 K the ^1H NMR spectrum showed depletion of the hydride signal for **13** alongside significant broadening and a downfield shift to -27.87 ppm (previously -28.33 ppm). This coincided with the appearance of a new, relatively broad hydride signal at -23.93 ppm assigned to **2**. The slight upfield shift from the normal hydride

resonance for **2** at -23.15 ppm is attributed to possible interactions between **2** and H_2. After *ca.* 16 h at 298 K the diagnostic hydride signal for **13** was no longer present and the spectrum showed both **2** and **7** hydride resonances.

In a parallel experiment, **13** was treated with a large excess of CH_2Cl_2 (used a source of 'Cl'). In contrast to the reaction with H_2O, **13** does react with 'Cl' although only *ca.* 50 % conversion to **7** was observed after a night at 323 K. Consequently **7** in **Scheme 3.8** above could originate either from reaction of 'Cl' with **2** or **13**, although it is noteworthy that **2** is converted more readily to **7** and under milder conditions (100 % conversion at 298 K) than **13**.

Reaction of **13** with H_2 at 298 K under rigorously dry conditions (using $C_6D_5CD_3$ dried over potassium to minimise H_2O contamination) immediately resulted in severe depletion of the hydride peak at -28.43 ppm, a downfield shift to -27.67 ppm and broadening of the resulting resonance. Formation of styrene was also apparent immediately (in less than stoichiometric amounts). Low temperature ^1H NMR spectroscopy revealed two broad singlets at 230 K, which sharpened slightly by further decreasing the temperature to 190 K (-3.11 and -9.92 ppm) (**Figure 3.3**). The hydrides were tentatively assigned to an intermediate species such as that shown in **Scheme 3.8**. It is unlikely that the said complex contains a vacant site as there is excess H_2 present, which could facilitate the formation of the known dihydrogen dihydride complex $Ru(IMes)_2(CO)(\eta^2\text{-}H_2)H_2$ by binding to any available vacant site.

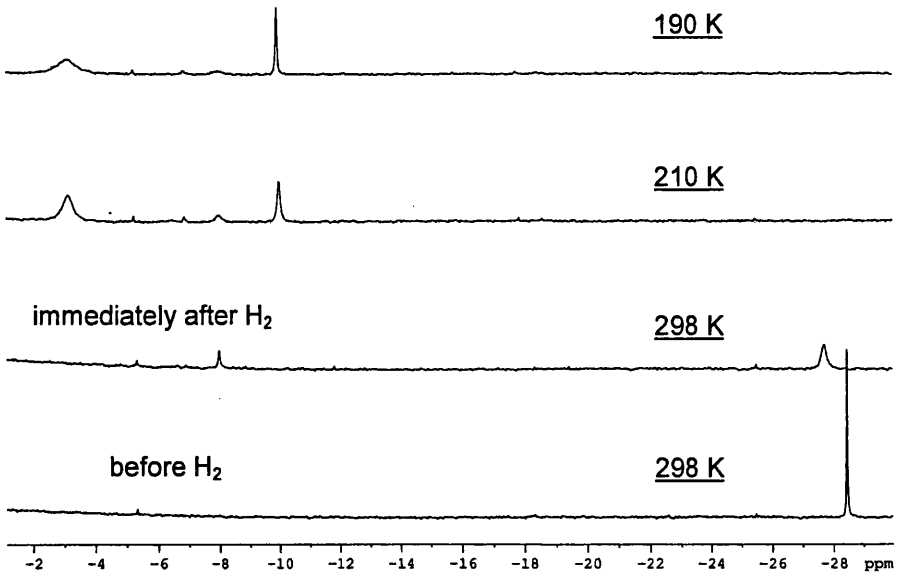

Figure 3.3 Variable temperature ^{1}H NMR spectra showing the reaction of **13** with H_2 ($C_6D_5CD_3$, 400 MHz).

In the absence of a characteristic resonance for $Ru(IMes)_2(CO)(\eta^2\text{-}H_2)H_2$ (br, -6 ppm) we propose that styrene binds to the metal centre to form $Ru(IMes)_2(CO)(\eta^2\text{-}H_2C{=}CHPh)H_2$. It is also significant that the corresponding alkane, EtPh is produced, as confirmed by the appearance of a quartet and triplet in the expected 2:3 ratio at 2.44 ppm (J_{HH} = 7.71 Hz) and 1.09 ppm (J_{HH} = 7.54 Hz) respectively. The formation of EtPh was observed immediately at 298 K in a *ca.* 3.5:1 ratio with free H_2C=CHPh, which further increased overnight at 298 K coinciding with total loss of free styrene from the system. This result is consistent with styrene binding to the metal centre to undergo hydrogenation to EtPh as shown in **Scheme 3.9**. We propose that the boxed complex corresponds to the two broad hydride resonances seen at 190 K in the ^{1}H NMR spectrum. The species occurring between EtPh loss and H_2C=CHPh binding is not known. Similarly, once all of the styrene has been hydrogenated the fate of the complex is uncertain; however a new hydride signal was apparent at -19.32 ppm.

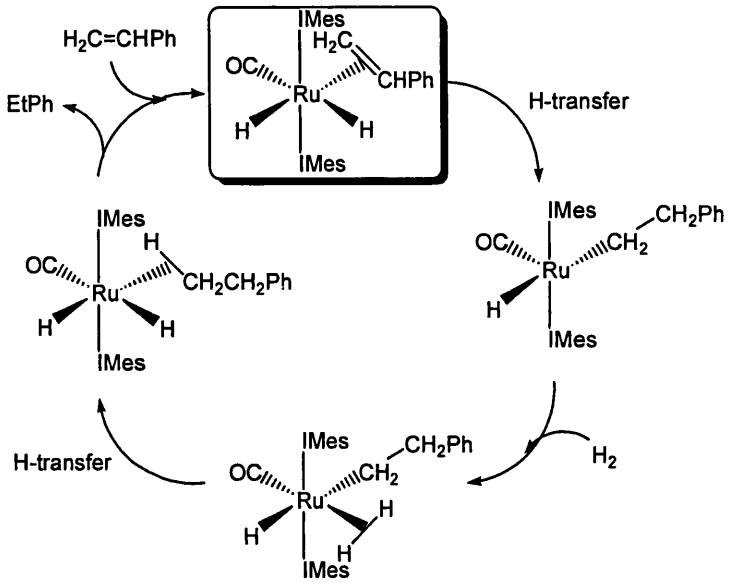

Scheme 3.9 Proposed mechanism for the hydrogenation of H_2C=CHPh to EtPh.

In comparison, Ru(P^{t}Bu$_2$Me)$_2$(CO)(C≡CPh)H reacts with H_2 at room temperature to yield Ru(P^{t}Bu$_2$Me)$_2$(CO)(η^2-H_2)H_2 after just 1 h as revealed by a broad resonance at -6.95 ppm.[8] Caulton detected the hydrocarbyl ligand as solely ethylbenzene with no free phenyacetylene or styrene observed. This information implied that the active hydrogenation species formed from **13** is a less active hydrogenation catalyst than the species using Ru(P^{t}Bu$_2$Me)$_2$(CO)(C≡CPh)H as a precursor, or maybe the active species is just formed more readily from the latter.

3.4.3 Treatment of Ru(IMes)$_2$(CO)(Cl)H (7) with phenylacetylene

3.4.3.1 Synthesis and characterisation of Ru(IMes)$_2$(CO)(Cl)(HC=CHPh) (15)

Ru(IMes)$_2$(CO)(Cl)H (**7**) was treated with phenylacetylene in comparison to the work with Ru(IMes)$_2$(CO)(OH)H (**2**). A stoichiometric amount of HC≡CPh was initially added to a yellow C_6D_6 sample of **7**, followed by another 3 equivalents to ensure that no starting material remained. A red solution of Ru(IMes)$_2$(CO)(Cl)(HC=CHPh) (**15**) was produced after 3 days at 333 K (**Scheme**

3.10), in comparison to just 15 min at 298 K necessary for the related complex $Ru(P^tBu_2Me)_2(CO)(Cl)(HC{=}CHPh)$.[8]

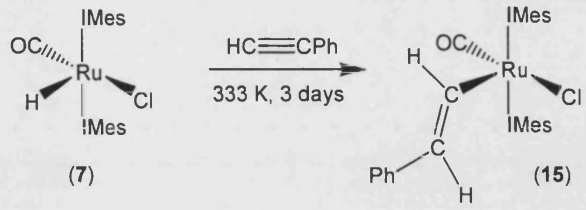

Scheme 3.10 Formation of $Ru(IMes)_2(CO)(Cl)(HC{=}CHPh)$ (**15**).

The formation of **15** was apparent in the ^1H NMR spectrum by the appearance of two characteristic medium to high frequency proton signals for the vinyl ligand at 8.27 ppm (C_α) and 5.82 ppm (C_β) (J_{HH} = 13.8 Hz for both resonances) in a 1:1 ratio. Their connectivity was further verified by a ^1H-^1H COSY spectrum (**Figure 3.4**).

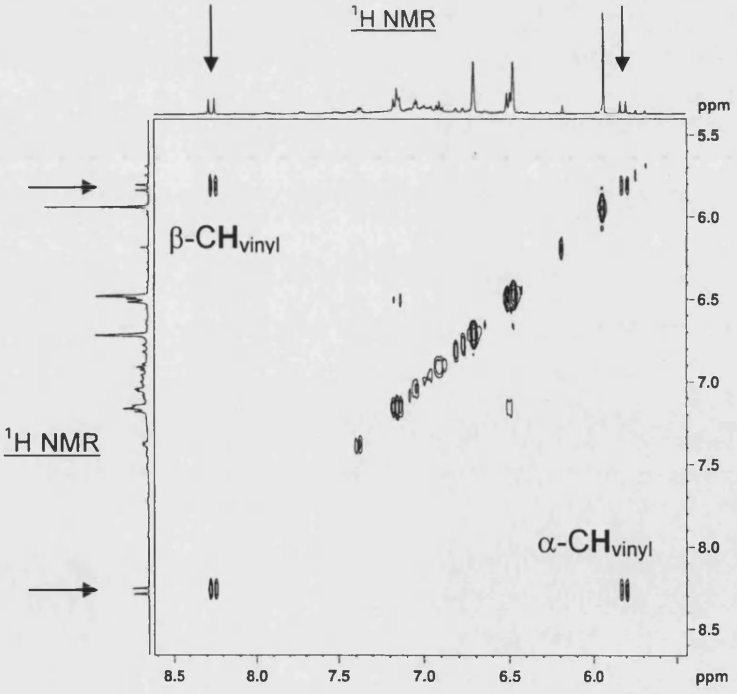

Figure 3.4 ^1H-^1H COSY spectrum for $Ru(IMes)_2(CO)(Cl)(CH{=}CHPh)$ (**15**) showing the regions containing vinyl proton resonances (highlighted by arrows) (C_6D_6, 298 K, 400 MHz).

At 2.29, 2.14 and 2.01 ppm the methyl proton peaks in the ^{1}H NMR spectrum of **15** are shifted upfield from the equivalent signals in **7** (2.32, 2.17 and 2.05 ppm) as displayed in **Figure 3.5**. Other resonances associated with the IMes ligands also differ between **15** and **7**, the signal for the backbone protons appeared at 5.94 ppm, upfield of the equivalent peak for **7** (6.18 ppm) and in contrast to **7**, the *m*-mesityl protons are inequivalent in **15**, appearing as two separate resonances (6.72 and 6.48 ppm)

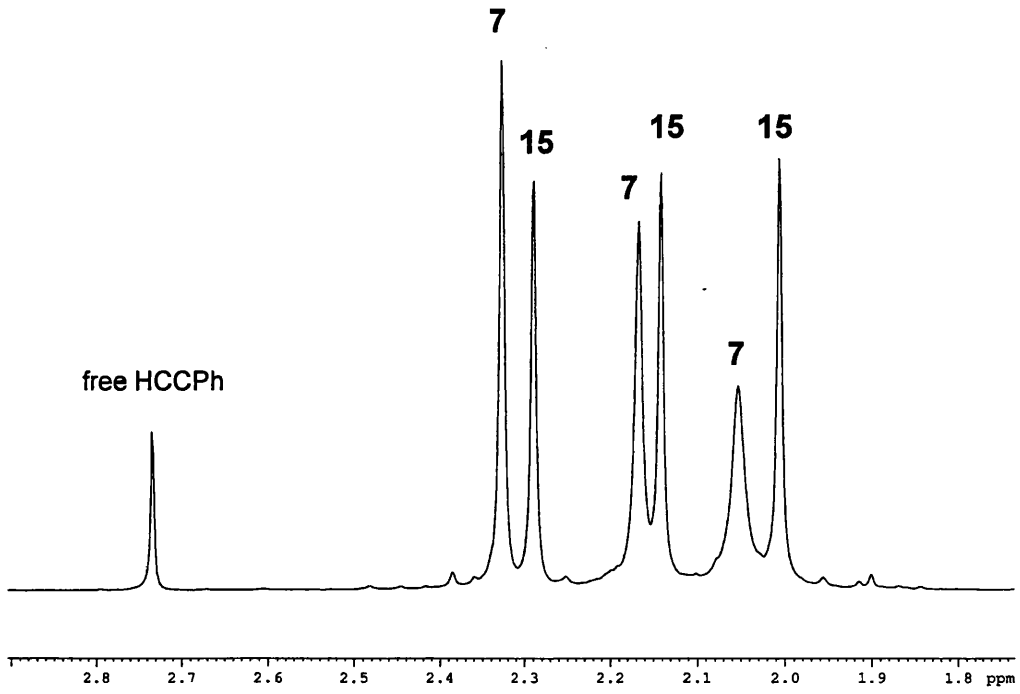

Figure 3.5 The methyl region of the ^{1}H NMR spectrum for the reaction of Ru(IMes)$_2$(CO)(Cl)H (**7**) with phenylacetylene to form Ru(IMes)$_2$(CO)(Cl)(HC=CHPh) (**15**) after 1 day at 333 K (C_6D_6, 298 K, 400 MHz).

By ^{13}C{^{1}H} NMR spectroscopy, the vinyl α and β-carbon atoms of **15** were observed at 155.9 and 133.4 ppm respectively. Their assignment was supported by crosspeaks in the ^{1}H-^{13}C{^{1}H} HMQC spectrum linking the two resonances with the doublet signals in the ^{1}H NMR spectrum as displayed in **Figure 3.6**.

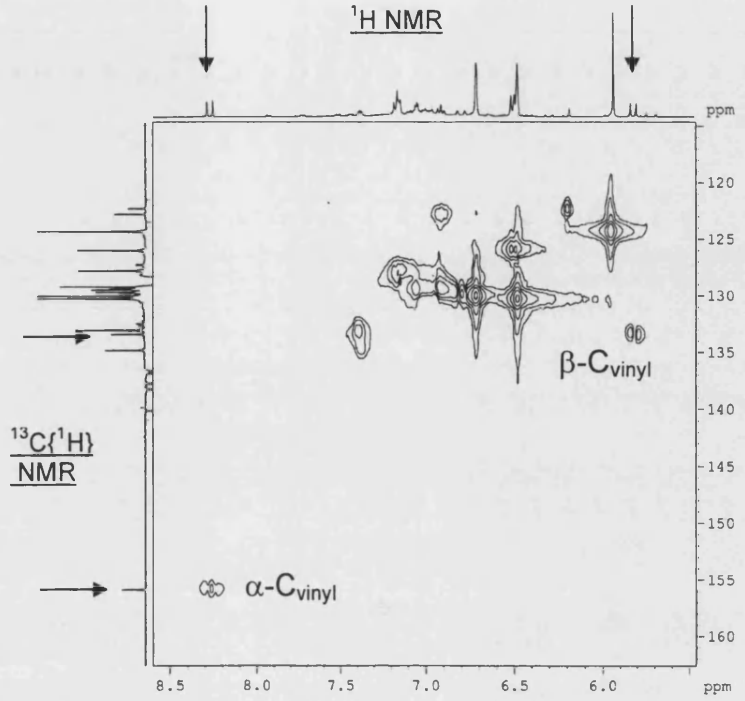

Figure 3.6 ^{1}H-^{13}C{^{1}H} HMQC spectrum for Ru(IMes)$_2$(CO)(Cl)(HC=CHPh) (**15**) showing the regions containing vinyl proton and carbon atom resonances (highlighted by arrows).

A variety of ruthenium vinyl complexes have been reported with bis phosphine ligands,[13-17] some of which are displayed in **Table 3.5** for comparison with **15**.

Complex	NMR shift (ppm)			
	^{1}H		^{13}C{^{1}H}	
	α-C<u>H</u>	β-C<u>H</u>	Ru-<u>C</u>$_\alpha$	Ru-<u>C</u>$_\beta$
15	8.27	5.82	155.9	133.4
Ru(P^{i}Pr$_3$)$_2$(CO)(Cl)(HC=CHPh) [15]	8.95	6.52	-	-
Ru(P^{t}BuMe)$_2$(CO)(Cl)(HC=CHPh) [17]	8.63	5.73	-	-
Ru(P^{t}Bu$_2$Me)$_2$(CO)$_2$(Cl)(HC=CHSiMe$_3$) [16]	8.80	5.54	-	-
Ru(PMe$_2$Ph)$_2$(CO)$_2$(Cl)(HC=CHPh) [14]	8.17	6.76	189.4	141.6

Table 3.5 Spectroscopic values for **15** and other vinyl complexes for comparison. (- = value not provided).

The structure of **15** was confirmed by X-ray crystallography on crystals grown from a hexane solution at low temperature (255 K) (**Structure 3.3**). The asymmetric unit of **15** consisted of a molecule of the complex and one and a half molecules of hexane, with the half molecule of hexane straddling an inversion centre and showing disorder. Consequently, the hydrogen atoms on the latter were not reliably located and omitted from the final least-squares refinements. From the X-ray crystal structure it was possible to characterise the vinyl protons as having *E* geometry, consistent with other reported vinyl species prepared from hydride chloride complexes (as in **Table 3.5**).[14-19]

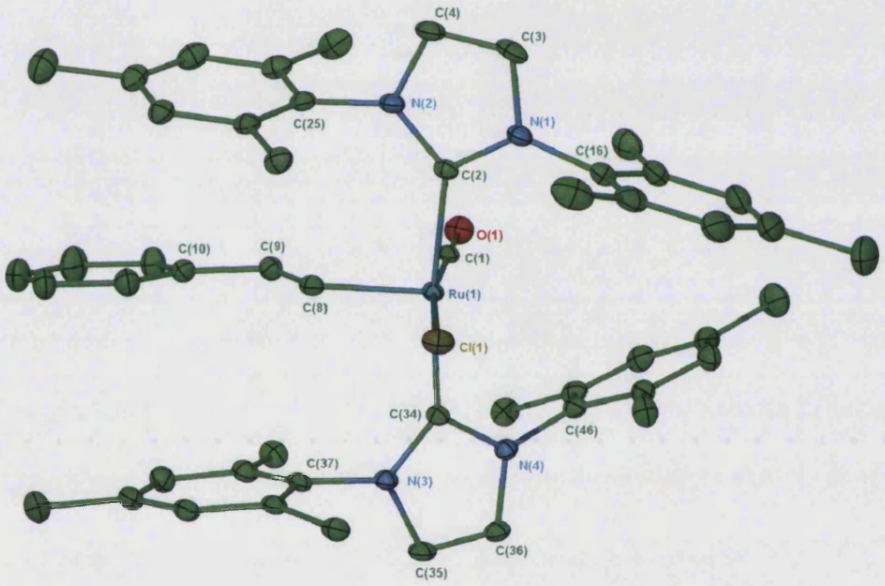

Structure 3.3 X-ray crystal structure of $Ru(IMes)_2(CO)(Cl)(HC{=}CHPh)$ (**15**). Thermal ellipsoids are set at 30 % probability. Hydrogen atoms have been omitted for clarity.

The metrics of **15** (**Table 3.4**) are similar to related systems in the literature,[18-20] with the only exception being the Ru-C=C bond angle in the $Ru(P^iPr_3)_2(CO)(Cl)(NC_5H_4\text{-}o\text{-}CH{=}CH)$ {118.2(6) °} which is constrained due to the bidentate nature of the ligand.[18]

	15
Ru-C(2)	2.119(2)
Ru-C(34)	2.117(2)
Ru-C(1)	1.864(3)
Ru-Cl	2.4128(6)
Ru-C(8)	2.011(2)
C(8)-C(9)	1.333(3)
C(2)-Ru-C(34)	170.78(9)
Ru-C(1)-C(2)	134.9(3)
C(1)-Ru-Cl	169.98(7)
C(1)-Ru-C(8)	87.11(10)
C(8)-Ru-Cl	102.81(7)

Table 3.4 Selected bond lengths (Å) and angles (°) for **15**.

There are clear differences between the reactions of HC≡CPh with **7** and $Ru(IMes)_2(CO)(OH)H$ (**2**). The former contains a Cl ligand, which does not take part in the reaction because of low Brønsted basicity and so is retained in the product, consistent with the related complexes $Ru(P^tBu_2Me)_2(CO)(X)(HC{=}CHPh)$ (X = F, Cl, I) prepared from $Ru(P^tBu_2Me)_2(CO)(X)H$.[8, 9] In these examples HC≡CPh inserts into the Ru-H bond to generally form HC=CHPh ligands. This was demonstrated by labelling studies by Caulton using $Ru(P^tBu_2Me)_2(CO)(X)D$ (**Scheme 3.11**).[8] {When X = F there is evidence of other products in addition to the formation of $Ru(P^tBu_2Me)_2(CO)(X)(HC{=}CHPh)$, namely acetylide insertion can occur with a different regiochemistry to yield a $PhC{=}CH_2$ ligand **and** HF elimination to form $Ru(P^tBu_2Me)_2(CO)(C{\equiv}CPh)H$}.[8]

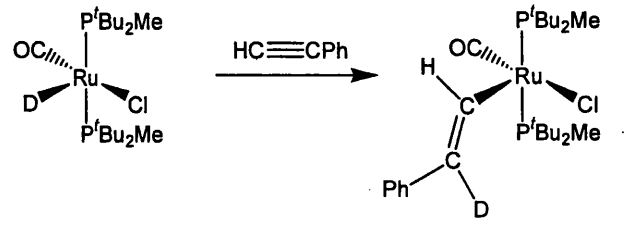

Scheme 3.11 Labelled reaction of Ru(P^{t}Bu$_2$Me)$_2$(CO)(Cl)D with phenylacetylene to form the conventional *syn* alkenyl-bound complex Ru(P^{t}Bu$_2$Me)$_2$(CO)(Cl)(HC=CDPh).[8]

The insertion of an HC≡CPh into Ru-H could occur directly or subsequent to η^2-binding of HC≡CPh to the metal centre. Binding HC≡CPh into the available vacant site results in the wrong stereochemistry for reduction (*trans* H-Ru-C_2HPh). However, it has been reported that Ru(PMe$_2$Ph)$_2$(CO)$_2$(Cl)H reacts with HC≡CPh although there is no vacant site available (5 days, 298 K),[14] thus implying that a vacant site is not necessary for the reaction to proceed, either because the reaction occurs *via* direct insertion into Ru-H or that HC≡CPh binds to the metal centre once the H-Ru-Cl angle has opened up, ensuring *cis* H-acetylide geometry. The second situation would account for the increased reaction time necessary for Ru(PMe$_2$Ph)$_2$(CO)$_2$(Cl)H compared to unsaturated systems, in which the chloride ligand can undergo migration more easily. This is supported by computational work showing that increasing the H-Ru-Cl bond angle in Ru(PH$_3$)$_2$(CO)(Cl)H costs less than 41.8 kJ mol^{-1}.[16] Furthermore, Caulton illustrated the propensity of HC≡CH (as a model acetylene) to insert into Ru-H of Ru(PH$_3$)$_2$(CO)(Cl)H once bound to the metal centre; the vinyl product is thermodynamically favoured over Ru(PH$_3$)$_2$(CO)(Cl)(η^2-HC≡CH)H by 121.6 kJ mol^{-1}.[21]

3.4.4 Formation of the trimethylsilylacetylide complex, Ru(IMes)$_2$(CO)(C≡CSiMe$_3$)H (16)

3.4.4.1 Synthesis and characterisation of 16

Ru(IMes)$_2$(CO)(OH)H (**2**) was treated with HC≡CSiMe$_3$ as a comparison to the reaction with HC≡CPh. One equivalent of HC≡CSiMe$_3$ was added to a benzene solution of **2** to yield the mono trimethylsilylacetylide complex

$Ru(IMes)_2(CO)(C{\equiv}CSiMe_3)H$ (**16**) (**Scheme 3.12**). Presumably $HC{\equiv}CSiMe_3$ reacts with **2** in the same manner as proposed for the formation of $Ru(IMes)_2(CO)(C{\equiv}CPh)H$ (**13**) (**Scheme 3.3**, p. 78) with loss of a molecule of water.

(2) (16)

Scheme 3.12. Formation of $Ru(IMes)_2(CO)(C{\equiv}CSiMe_3)H$ (**16**).

The ^1H NMR spectrum of **16** showed a new hydride peak at -28.44 ppm. The $^{13}C\{^1H\}$ NMR spectrum for **16** is very similar to that obtained for **13** with carbenic and carbonyl carbon signals located at 197.6 and 203.7 ppm respectively. ^1H-$^{13}C\{^1H\}$ HMBC spectroscopy revealed the C_α resonance at 167.8 ppm. **16** displayed a carbonyl stretching band at 1893 cm^{-1} in the IR spectrum, again similar to the value for **13** (ν_{CO} 1887 cm^{-1}).

Red crystals of **16** suitable for X-ray crystallography were grown from benzene-ethanol. (**Structure 3.4**). Two molecules of benzene were present in the asymmetric unit as well as one molecule of **16**.

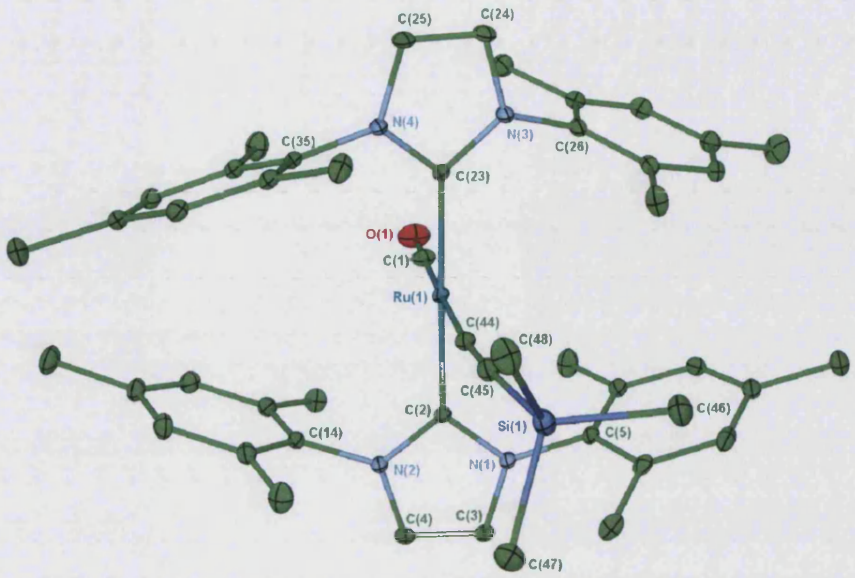

Structure 3.4 X-ray crystal structure of $Ru(IMes)_2(CO)(C{\equiv}CSiMe_3)H$ (**16**). Thermal ellipsoids are set at 30 % probability. Hydrogen atoms have been omitted for clarity.

	16
Ru-C(2)	2.0740(13)
Ru-C(23)	2.0725(13)
Ru-C(1)	1.8612(16)
Ru-C(44)	2.0874(15)
C(44)-C(45)	1.221(2)
C(45)-Si	1.8204(16)
C(2)-Ru-C(23)	175.99(5)
C(1)-Ru-C(44)	178.59(6)

Table 3.6 Selected bond lengths (Å) and angles (°) for **16**.

The structure and metrics of **16** (**Table 3.6**) proved to be similar to those found in **13** and **14** and generally the bond lengths and angles in **16** were in good agreement with the other species. Thus, the C_α-C_β bond length in **16** {1.221(2) Å} is consistent with the values in the other acetylide complexes (*ca.* 1.2 Å). The C-Si

bond length (1.8204(16) Å) is similar to that in the bis acetylide dicarbonyl system $Ru(PEt_3)_2(CO)_2(C{\equiv}CSiMe_3)_2$ {1.812(2) Å}, in which the authors suggest that there is some contribution from the zwitterionic resonance structure $Ru^{-}{=}C{=}^{+}C\text{-}SiMe_3$.[6] Other factors indicative of multiple bond character of Ru-C such as low frequency ν_{CO} and ν_{CC} values and a relatively downfield $^{13}C\{^1H\}$ NMR C_α resonance are not conclusive for **16**.

The formation of $Ru(IMes)_2(CO)(C{\equiv}CSiMe_3)_2$, analogous to **14**, was not observed. Excess $HC{\equiv}CSiMe_3$ (10 equiv.), prolonged reaction times and increased reaction temperature (up to 343 K) were used to try to promote formation of $Ru(IMes)_2(CO)(C{\equiv}CSiMe_3)_2$, but to no avail. Analogous bis trimethylsilylacetylide complexes are known {e.g. *trans*-$Ru(P^iPr_3)_2(CO)(C{\equiv}CSiMe_3)_2$[22]} and even the dicarbonyl systems *cis*-$Ru(P^iPr_3)_2(CO)_2(C{\equiv}CSiMe_3)_2$[22] and *trans*-$Ru(PEt_3)_2(CO)_2(C{\equiv}CSiMe_3)_2$[8] have been reported. It is noteworthy that there is a change of geometry (based on υ_{CO} data) in going from $Ru(P^iPr_3)_2(CO)(C{\equiv}CSiMe_3)_2$ (*trans*) to the dicarbonyl analogue (*cis*), maybe to minimise the steric repulsion between the bulky phosphine and $SiMe_3$ groups when there is no vacant site available. Presumably it is the collective steric effects of the bulky trimethylsilyl moiety and the large IMes ligands that result in the metal centre being too sterically hindered in **16** for another $C{\equiv}CSiMe_3$ ligand to bind and form $Ru(IMes)_2(CO)(C{\equiv}CSiMe_3)_2$.

3.5 18-electron acetylide complexes

3.5.1 Treatment of $Ru(IMes)_2(CO)(C{\equiv}CPh)H$ (13) with CO

The coordinatively unsaturated nature of Ru(IMes)(CO)(C≡CPh)H (**13**) allowed an immediate reaction to take place with 1 atm CO to yield the 18-electron $Ru(IMes)_2(CO)_2(C{\equiv}CPh)H$ (**17**) (**Scheme 3.13**). The reaction was accompanied by a colour change from red-brown to very pale yellow. The hydride ligand of **17** is observed at -5.24 ppm, shifted significantly downfield from **13** (-28.33 ppm), consistent with a *trans* H-Ru-CO arrangement.[23]

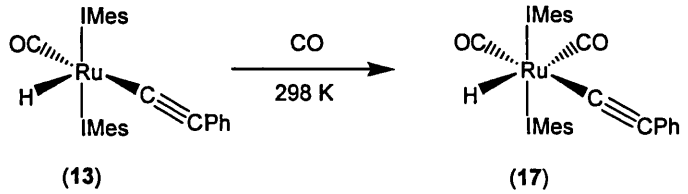

(13) (17)

Scheme 3.13. Formation of $Ru(IMes)_2(CO)_2(C{\equiv}CPh)H$ (**17**).

The carbenic carbon was detected at 186.3 ppm in the $^{13}C\{^1H\}$ NMR spectrum, lower frequency than the analogous resonance for **13** (197.8 ppm). Unfortunately only one of the quaternary acetylide carbon atoms could be detected at 111.5 ppm. (cf. Mawby reported values of 111.7 (C_α) and 113.6 ppm (C_β) for the acetylide resonances in $Ru(PMe_2Ph)_2(CO)_2(C{\equiv}CPh)H$).[14]

Two inequivalent carbonyl carbon resonances were seen at 205.2 and 196.9 ppm consistent with a *cis*-$Ru(CO)_2$ geometry. This was confirmed by the IR spectrum of **17**, which showed two carbonyl stretching bands at 2017 and 1903 cm^{-1}. The acetylide triple bond was observed by an absorption band at 2094 cm^{-1} (*cf.* 2062 cm^{-1} for **13**). These spectroscopic values are consistent with analogous complexes as displayed in **Table 3.7** overleaf.

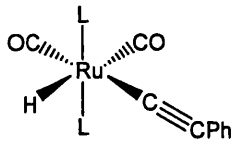

$RuL_2(CO)_2(C{\equiv}CPh)H$

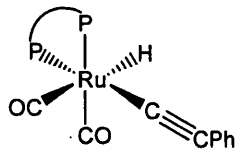

$Ru(d^tbpe)(CO)_2(C{\equiv}CPh)H$
(d^tbpe = $^tBu_2PC_2H_4P^tBu_2$)

$RuL_2(CO)_2(C{\equiv}CPh)H$[a]	^1H NMR (ppm)	IR shift (cm^{-1})		
L_2	Ru-H	ν_{CO}	$\nu_{C\equiv C}$	ν_{Ru-H}
IMes (**17**) [b]	-5.24	2017 1903	2094	1939
PMe_2Ph [14]	-6.30	-	-	-
P^tBu_2Me [24]	-6.63	2020 1958	2103	1919
P^iPr_3 [25]	-6.75	2012 1958	2105	1912
PCy_3 [25]	-6.43	2010 1958	2101	1916
d^tbpe [26]	-7.20	2027 1989	2108	-
13 [b]	-28.33	1887	2062	-

Table 3.7 ^1H NMR and infra-red spectroscopic values for comparison with **17** described by $RuL_2(CO)_2(C{\equiv}CPh)H$ [a](except **13**, which is formulated as $Ru(IMes)_2(CO)(C{\equiv}CPh)H$). [b]Nujol mull. (- = N/A or not reported).

X-ray quality crystals of **17** were grown from benzene-ethanol (**Structure 3.5**). Each asymmetric unit contained two molecules of complex and three molecules of benzene. **Table 3.8** displays selected bond lengths and angles for one of the molecules of **17** {containing the metal centre labelled Ru(1)}. The geometries of both complex molecules in the unit cell are very similar with bond lengths and angles of no considerable difference, with the exception of the arrangement of equatorial ligands, which differ between Ru(1) and Ru(2) by *ca.* 3° at the most. For

example, OC-Ru-CO bond angles of 97.31(10) and 95.46(13)° for Ru(1) and Ru(2) respectively.

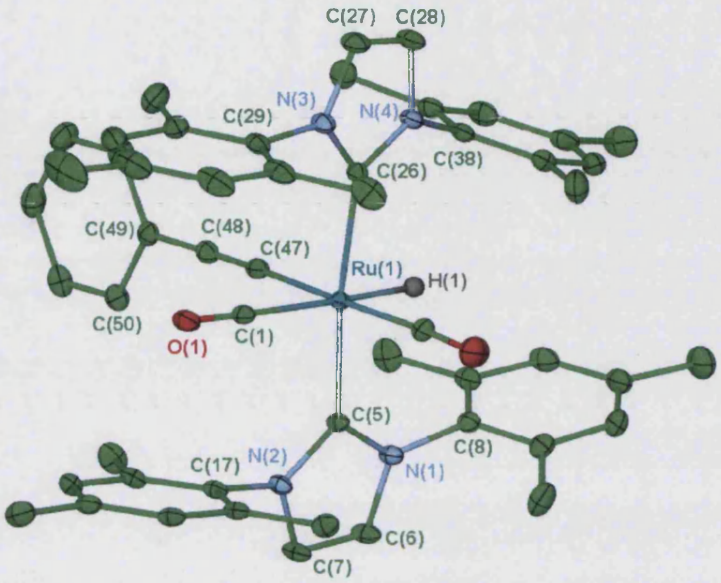

Structure 3.5 X-ray crystal structure of $Ru(IMes)_2(CO)_2(C{\equiv}CPh)H$ (**17**). Thermal ellipsoids are set at 30 % probability. Hydrogen atoms have been omitted for clarity (except the hydride).

	17
Ru-C(26)	2.109(2)
Ru-C(5)	2.109(2)
Ru-C(1)	1.961(2)
Ru-C(2)	1.883(2)
Ru-C(47)	2.085(2)
C(47)-C(48)	1.220(3)
C(26)-Ru-C(5)	166.93(8)
C(1)-Ru-C(2)	97.31(10)

Table 3.8 Selected bond lengths (Å) and angles (°) for **17** based on the complex molecule containing Ru(1).

Addition of CO affects the X-ray crystal structure not only by expected lengthening of the Ru-carbonyl bonds consistent with decreased backbonding, but also slightly increased Ru-C_{NHC} bond length (2.109(2) vs. *ca.* 2.07 Å in **13**), perhaps due to the more sterically hindered metal centre in **17**. This idea is enforced by the C_{NHC}-Ru-C_{NHC} bond angle in **17** being more acute than the equivalent value for **13** (166.93(8) and 177.9(2)° respectively). The acetylide group appears unaffected by comparison with **13**.

3.5.2 Treatment of $Ru(IMes)_2(CO)(C{\equiv}CPh)_2$ (14) with CO

$Ru(IMes)_2(CO)(C{\equiv}CPh)_2$ (**14**) was treated with CO to demonstrate that there is sufficient room at the vacant site to accommodate another ligand (**Scheme 3.14**). Immediate formation of $Ru(IMes)_2(CO)_2(C{\equiv}CPh)_2$ (**18**) was found upon exposure of **14** to 1 atm CO at room temperature as shown by the disappearance of methyl proton signals for **14** at 2.38 and 2.16 ppm and formation of comparable resonances for **18** at 2.34 and 2.04 ppm.

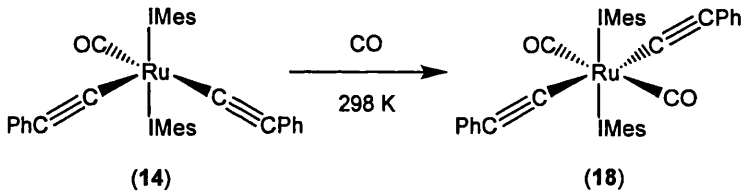

(14) (18)

Scheme 3.14 Formation of $Ru(IMes)_2(CO)_2(C{\equiv}CPh)_2$ (**18**).

A single carbonyl resonance at 198.9 ppm was observed in the $^{13}C\{^1H\}$ NMR spectrum of **18**, indicating equivalent carbonyl environments. Likewise, the IR spectrum showed only one carbonyl stretching band at 1995 cm^{-1}, consistent with a *trans* arrangement of the two CO groups. *Trans* carbonyl moieties are quite unusual but their manifestation in bis acetylide complexes is well precedented, for example, in $Ru(P^iPr_3)_2(CO)_2(C{\equiv}CCy)_2$,[22] $Ru(PEt_3)_2(CO)_2(C{\equiv}CPh)_2$[7] and $Ru(PEt_3)_2(CO)_2(C{\equiv}CSiMe_3)_2$.[6] In contrast to the latter example, $Ru(P^iPr_3)_2(CO)_2(C{\equiv}CSiMe_3)_2$ displays a *cis* acetylide arrangement, perhaps due to the greater bulk of P^iPr_3.[22] Furthermore, $Ru(P^iPr_3)_2(CO)_2(C{\equiv}CPh)_2$ is reported with

both *cis* and *trans* carbonyl ligand geometries apparently depending on how it is synthesised.[10,27] **Table 3.9** below gives some spectroscopic data of *trans* and *cis* bis-acetylide dicarbonyl complexes for comparison with **18**.

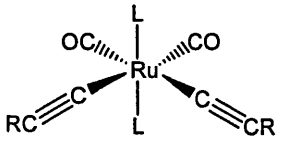

cis CO ligands

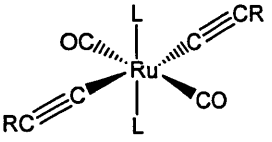

trans CO ligands

$RuL_2(CO)_2(C{\equiv}CR)_2$		*c* or	$^{13}C\{^1H\}$ NMR shifts (ppm)			IR (cm^{-1})	
L_2	R	*t* CO	Ru-<u>C</u>O	Ru-<u>C</u>$_\alpha$	Ru-<u>C</u>$_\beta$	ν_{CO}	$\nu_{C\equiv C}$
IMes (**18**)[a]	Ph	*t*	198.9	-	-	1995	2086
PEt_3	Ph [7]	*t*	198.6	104.9	111.2	1987	2093
PEt_3	$SiMe_3$ [6]	*t*	198.1	128.4	116.1	1986	2021
dppe	Ph [28]	*t*	-	-	-	-	2061
P^nBu_3	Ph [29]	*t*	-	-	-	1987	2093
P^iPr_3	Cy [22]	*t*	203.5	86.43	115.4	1975	-
P^iPr_3	Ph [27]	*t*	202.5	107.2	114.5	1970	2090
P^iPr_3	Ph [10]	*c*	-	-	-	1972 1955	2095
P^iPr_3	$SiMe_3$ [22]	*c*	202.0	132.0	119.0	2015 1980	2060

Table 3.9 Spectroscopic values for complexes to compare with **18** described by $RuL_2(CO)_2(C{\equiv}CR)_2$. (- = N/A or not reported). [a]Nujol mull.

The $^{13}C\{^1H\}$ NMR data for α and β-$C_{acetylide}$ atoms in **Table 3.9** illustrates their unsystematic nature, which makes assignment of the equivalent resonances for **18** difficult.

The all *trans* geometry in **18** was verified by growing small crystals from a benzene solution layered with hexane and determining their structure by X-ray crystallography at Daresbury Laboratories (**Structure 3.6**). The structure of **18** displayed some disorder, mostly because of the symmetrical nature of the complex.

The asymmetric unit consists of ½ a molecule of complex with Ru(1), C(2) and O(2) located on a crystallographic 2-fold rotation axis and subsequently there is 50:50 disorder in the carbonyl ligand based on C(1). Additionally there is 70:30 disorder apparent in the NHC ring and in the mesityl unit based on C(16). C-C and C-N bond distances in the minor component were refined subject to constraints, as were the ADPs in the major fraction of the mesityl group.

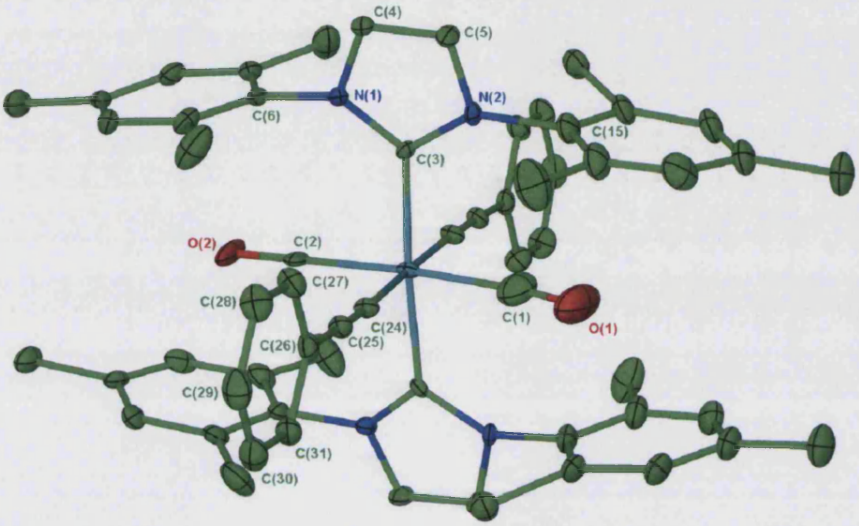

Structure 3.6 X-ray crystal structure of $Ru(IMes)_2(CO)_2(C{\equiv}CPh)_2$ (**18**). Thermal ellipsoids are set at 30 % probability. Hydrogen atoms have been omitted for clarity.

	18
Ru-C(3)	2.081(17)
Ru-C(1)	2.008(14)
Ru-C(2)	1.876(7)
Ru-C(24)	2.135(5)
C(24)-C(25)	1.266(7)
C(3)-Ru-C(3')	171.0(10)
C(1)-Ru-C(2)	165.5(5)
C(24)-C(25)-C(26)	178.2(5)

Table 3.10 Selected bond angles (°) and distances (Å) for **18**.

There is a significant difference between the two Ru-CO bond lengths in **18** {2.008(14) and 1.876(7) Å}, which can be reasoned by considering the disorder in the structure making the Ru-C(2) distance the most reliable and similar to other Ru-CO bond lengths (*ca.* 1.8-9 Å). The most striking difference in comparison with **13**, **14** and **17** is the bond lengths associated with the acetylide ligands in **18**. At 2.135(5) Å, the Ru-$C_{acetylide}$ bond lengths are significantly longer than in $Ru(IMes)_2(CO)(C{\equiv}CPh)_2$ (**14**) {2.047(3) Å} and longer than mono phenylacetylide systems **13** and **17** (*ca.* 2.08 Å). Furthermore, the C≡C bond lengths of 1.266(7) Å are longer than the typical values for bound acetylide complexes (*ca.* 1.22 Å). This does not fit with the zwitterion resonance structure argument, or with the expected affect of adding a second π-accepting CO ligand.

3.6 Chapter Summary

$Ru(IMes)_2(CO)(OH)H$ (**2**) has proved to be a useful precursor to the acetylide complexes $Ru(IMes)_2(CO)(C{\equiv}CPh)H$ (**13**), $Ru(IMes)_2(CO)(C{\equiv}CPh)_2$ (**14**) and $Ru(IMes)_2(CO)(C{\equiv}CSiMe_3)H$ (**15**). In contrast, the treatment of $Ru(IMes)_2(CO)(Cl)H$ with HC≡CPh resulted in the vinyl-bound complex $Ru(IMes)_2(CO)(HC{=}CHPh)(Cl)$ (**16**). The phenylacetylide complexes **13** and **14** were treated with CO to form 18-electron complexes $Ru(IMes)_2(CO)_2(C{\equiv}CPh)H$ (**17**) and $Ru(IMes)_2(CO)_2(C{\equiv}CPh)_2$ (**18**). **Table 3.11** shows comparative spectroscopic values for both the 16 and 18-electron acetylide complexes discussed in this chapter.

Complex	^{1}H NMR shift (ppm)[a]	^{13}C{^{1}H} NMR shift (ppm)[a]			IR shift (cm^{-1})[b]	
	Ru-H	Ru-CO	Ru-C:	Ru-C_α	ν_{CO}	ν_{CC}
13	-28.33	204.0	197.8	149.5	1887	2062
14	-	203.9	191.3	-	1954	2068
16	-28.44	203.7	197.6	167.8	1893	2042
17	-5.24	205.2 196.9	186.3	111.5	2017 1903	2094
18	-	198.9	180.2	-	1995	2086

Table 3.11 Comparative spectroscopic values for acetylide complexes **13**, **14**, **16**, **17** and **18**. [a]C_6D_6, 298 K, 400 MHz. [b]Nujol mull. (- = N/A or not provided).

In the coordinatively unsaturated systems the hydride ligand lies *trans* to the vacant site and the CO ligand *trans* to the acetylide ligand (**13**, **16**). In **14**, the acetylide groups oppose each other, causing the CO to lie opposite the vacant site resulting in a relatively high ν_{CO} band. The ligand arrangement in the phenylacetylide complexes is retained upon addition of CO into the vacant site to form 18-electron complexes **17** and **18** (**Figure 3.7**).

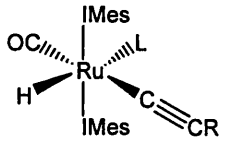

R = Ph L = vacant site (**13**)
R = $SiMe_3$ L = vacant site (**16**)

R = Ph L = CO (**17**)

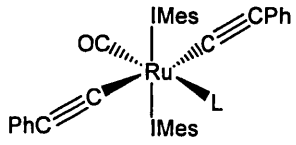

L = vacant site (**14**)

L = CO (**18**)

Figure 3.7 Geometry of the acetylide complexes in this chapter.

The geometry of the equatorial ligands in these systems is paramount in reducing steric repulsion with the bulky axial IMes ligands. All of the acetylide crystal structures demonstrated IMes ligands rotated so that they are perpendicular to the most sterically demanding axis (C_α-Ru-CO or C_α-Ru-C_α). This particular

orientation could not minimise steric repulsion if the acetylide ligands appeared mutually *cis* in **14** and **18**. **Figure 3.8** displays **13** viewed down the C_{NHC}-Ru-C_{NHC} axis to show in which the mesityl arms are located preferentially over the Ru-H containing axis to maximise the staggered conformation.

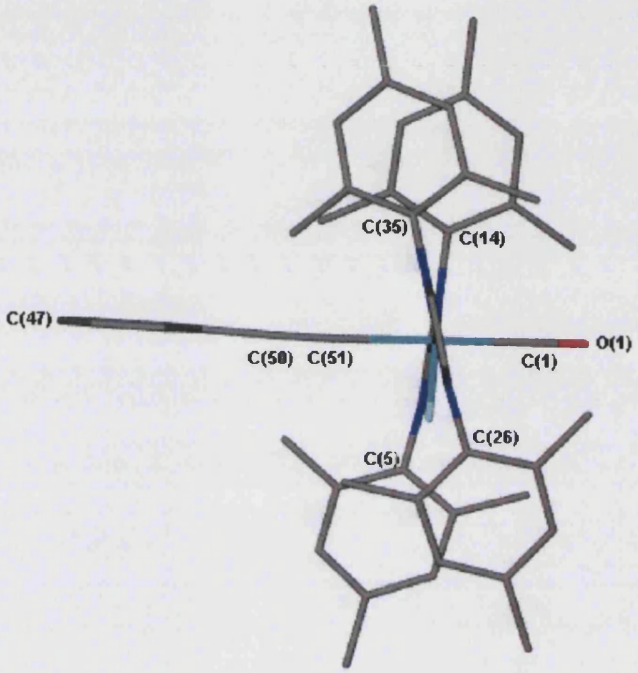

Figure 3.8 Bird's eye view of **13** down the C_{NHC}-Ru-C_{NHC} axis.

A study of the series of acetylide complexes revealed that the IMes ligands are staggered with respect to the acetylide ligands in the range 75-88 ° and the IMes ligands are relatively coplanar with the maximum twists exhibited for **13** (20.0 °) and **16** (20.9 °). The bis phenylacetylide complexes **14** and **18** show notably smaller IMes / IMes twist angles (6.5 and 8.0 ° respectively) than the other systems, probably as a result of being constrained by the *trans* C≡CPh ligands. The mesityl rings (within the same IMes ligand) are most coplanar in the more sterically hindered systems **14**, **17** and **18** falling in the range 14 to 22 °, whereas the mono acetylide, mono CO complexes **13** and **16** display angles over 30 °. **Table 3.12** shows the twist angles in more detail, calculated using planes based on the imidazole ring of IMes and the phenyl rings of phenylacetylide ligands and mesityl arms.

Complex	IMes / IMes		IMes / Ph		Ph / Ph	Mes / Mes
13	20.0		84.8 75.3		-	32.7 34.7
14	6.5		86.6 86.9	86.6 86.9	3.6	19.7 19.7
16	20.9		-		-	35.3 35.8
17 (2 molecules per unit cell)	Ru(1)	13.5	83.7 84.4		-	17.9 12.8
	Ru(2)	14.7	82.8 87.8		-	20.5 14.3
18	8.0		84.9 87.0	83.2 81.5	2.5	14.1 21.8

Table 3.12 Twist angles (°) based on planes imposed on imidazolium and phenyl rings. (Values at the top of split cells refer to N(1) and N(2) containing IMes; bottom values, the other IMes ligand. Data to the left and right of split cells correspond with C(n) and C(n') respectively).

To further minimise repulsion in the equatorial region, the phenyl rings in **13**, **14**, **17** and **18** lie approximately perpendicular to the mesityl arms of IMes. In contrast, the $SiMe_3$ group in **16** has more three-dimensional bulk compared to the more two-dimensional nature of C≡CPh bearing complexes but lies further from the metal centre so there were no noticeable affects on the structure.

3.7 References

1. Cifuentes, M.P.; Humphrey, M.G., *J. Organomet. Chem.*, **2004**, *689*, 3968.
2. Jazzar, R.F.R.; Bhatia, P.H.; Mahon, M.F.; Whittlesey, M.K., *Organometallics*, **2003**, *22*, 670.
3. Esteruelas, M.A.; Edwards, A.J.; Elipe, S.; Lahoz, F.J.; Oro, L.A.; Valero, C., *Organometallics*, **1997**, *16*, 3828.
4. Poulton, J.T.; Sigalas, M.P.; Folting, K.; Streib, W.E.; Eisenstein, O.; Caulton, K.G., *Inorg. Chem.*, **1994**, *33*, 1476.
5. Conner, D.; Jayaprakash, K.N.; Cundari, T.R.; Gunnoe, T.B., *Organometallics*, **2004**, *23*, 2724.
6. Sun, Y.; Taylor, N.J.; Carty, A.J., *Organometallics*, **1992**, *11*, 4293.
7. Sun, Y.; Taylor, N.J.; Carty, A.J., *J. Organomet. Chem.*, **1992**, *423*, C43.
8. Poulton, J.T.; Sigalas, M.P.; Eisenstein, O.; Caulton, K.G., *Inorg. Chem.*, **1993**, *32*, 5490.
9. Werner, H.; Esteruelas, M.A.; Otto, H., *Organometallics*, **1986**, *5*, 2295.
10. Werner, H.; Meyer, U.; Esteruelas, M.A.; Sola, E.; Oro, L.A., *J. Organomet. Chem.*, **1989**, *366*, 187.
11. Tsuda, T.; Moto-o, S., *Organometallics*, **1999**, *18*, 2741.
12. Pedersen, A.; Tilset, M.; Folting, K.; Caulton, K.G., *Organometallics*, **1995**, *14*, 875.
13. Waugh, M.P.; Mawby, R.J., *Dalton Trans.*, **1996**, 21.
14. Mawby, R.J.; Bray, J.M., *J. Chem. Soc., Dalton Trans.*, **1989**, 589.
15. Marchenko, A.V.; Huffman, J.C.; Valerga, P.; Jimenez Tenorio, M.; Carmen Puerta, M.; Caulton, K.G., *Inorg. Chem.*, **2001**, *40*, 6444.
16. Marchenko, A.V.; Gerard, H.; Eisenstein, O.; Caulton, K.G., *New J. Chem.*, **2001**, *25*, 1244.
17. Werner, H.; Meyer, U.; Peters, K.; von Schnering, H.G., *Chem. Ber.*, **1989**, *122*, 2097.
18. Buil, M.L.; Esteruelas, M.A.; Goni, E.; Oliván, M.; Oñate, E., *Organometallics*, **2006**, *25*, 3076.
19. Maruyama, Y.; Yamamura, K.; Sagawa, T.; Katayama, H.; Ozawa, F., *Organometallics*, **2000**, *19*, 1308.

20. Torres, M.R.; Vegas, A.; Santos, A., *J. Organomet. Chem.*, **1986**, *309*, 169.
21. Marchenko, A.V.; Gerard, H.; Eisenstein, O.; Caulton, K.G., *New J. Chem.*, **2001**, *25*, 1382.
22. Bohanna, C.; Esteruelas, M.A.; Herrero, J.; López, A.M.; Oro, L.A., *J. Organomet. Chem.*, **1995**, *498*, 199.
23. Esteruelas, M.A.Werner, H., *J. Organomet. Chem.*, **1986**, *303*, 221.
24. Ogasawara, M.; Macgregor, S.A.; Streib, W.E.; Folting, K.; Eisenstein, O.; Caulton, K.G., *J. Am. Chem. Soc.*, **1996**, *118*, 10189.
25. Chunbang, L.; Ogasawara, M.; Nolan, S.P.; Caulton, K.G., *Organometallics*, **1996**, *15*, 4900.
26. Gottschalk-Gaudig, T.; Huffman, J.C.; Gerard, H.; Eisenstein, O.; Caulton, K.G., *Inorg. Chem.*, **2000**, *39*, 3957.
27. Esteruelas, M.A.; Lahoz, F.J.; Lopez, A.M.; Onate, E.; Oro, L.A., *Organometallics*, **1994**, *13*, 1669.
28. Raithby, P.R.; Atherton, Z.; Faulkner, C.W.; Ingham, S.L.; Kakkar, A.K.; Khan, M.S.; Lewis, J.; Long, N.J., *J. Organomet. Chem.*, **1993**, *462*, 265.
29. Raithby, P.R.; Khan, M.S.; Kakkar, A.K.; Ingham, S.L.; Lewis, J.; Spencer, B.; Wittmann, F.; Friend, R.H., *J. Organomet. Chem.*, **1994**, *472*, 247.

Chapter 4

4. Attempted formation of the dihydride complexes $RuL_2(CO)H_2$ {L = $(IMes)_2$, $(PPh_3)(IMes)$}

4.1 Preamble

The importance of hydride complexes has already been covered in Chapter 1. The aim of this chapter is to report our attempts to form 16-electron dihydride complexes $RuL_2(CO)H_2$ {L = $(IMes)_2$, $(PPh_3)(IMes)$}. The first and major section of this chapter is concerned with the reduction of $RuL_2(CO)(Cl)H$ with $NaBH_4$ to produce the borohydride complexes $RuL_2(CO)(\eta^2\text{-}BH_4)H$. Characterisation and reactions of $RuL_2(CO)(\eta^2\text{-}BH_4)H$ are described with a view to understanding the reactivity of these complexes and the resistance met towards dihydride complex formation. The use of $RuL_2(CO)(\eta^2\text{-}BH_4)H$ complexes as catalysts for the hydrogenation of acetophenone is also briefly investigated.

In the latter sections of the chapter, some other possible methods of achieving the desired dihydride complex $RuL_2(CO)H_2$ are considered; reduction of $RuL_2(CO)(Cl)H$ with $LiAlH_4$ and the 'super hydride' $LiEt_3BH$, metathesis with $KN(SiMe_3)_2$ and silyl transfer from Et_3SiH to $RuL_2(CO)(F)H$.

4.2 Introduction to borohydride (BH_4^-) complexes

The reducing agent $NaBH_4$ has been known since 1942 and has proved so important that it was the subject of the Nobel Lecture given by Brown in 1979.[1,2] It is very widely recognised as a mild reducing agent, specifically affecting aldehydes, ketones and acid chlorides. Importantly, reduction by $NaBH_4$ is not just limited to organic compounds but also used on metal complexes containing halide ligands to achieve hydride complexes. The halide ligand is removed as NaHal, whose production is the driving force behind the reaction.[3]

BH_4^- complexes have been observed as intermediates en-route to hydride containing products. The BH_4^- moiety binds to the metal centre after the abstraction of the chloride ligand and it is possible to isolate some complexes at this 'intermediate'

stage. The first transition metal BH_4^- complex was produced in 1949, not from reaction with $NaBH_4$ but with $Al(BH_4)_3$. The first Ru-BH_4^- complex $Ru(\eta^5\text{-}C_5H_5)(PPh_3)_2(BH_4)$ was reported in 1971 by Stone.[4] A comprehensive review was later compiled by Marks and Kolb in 1977.[5]

Suzuki prepared trihydridoruthenium(IV) complexes $Ru(IV)(\eta^5\text{-}C_5Me_5)(P)H_3$ ($P = PMe_3$, PEt_3, P^iPr_3, PCy_3, PPh_2Me, PPh_3) by reducing $Ru(III)(\eta^5\text{-}C_5Me_5)(P)\mathbf{Br_3}$ and $Ru(\eta^5\text{-}C_5Me_5)(P)\mathbf{Cl_2}$ with excess $NaBH_4$ in EtOH.[6] Synthesis of the corresponding BH_4^- species $Ru(\eta^5\text{-}C_5Me_5)(P)(\eta^2\text{-}BH_4)$ was undertaken by Suzuki to clarify the reaction mechanism and successfully achieved by altering the reaction solvent to THF, preventing protonolysis to the trihydride product.[6] **Table 4.1** shows some other examples of Ru-BH_4^- complexes and their hydride counterparts.

In the majority of the examples expressed in **Table 4.1**, the production of either the BH_4^- or the hydride product can be controlled by solvent selection. It therefore follows that once the BH_4^- analogues are isolated, conversion into the hydride analogues is feasible simply by treating with protic solvents or removal of BH_3. For example, Suzuki's BH_4^- intermediates are easily converted into the trihydride products by either stirring with EtOH or by filtration through alumina.[6]

Starting material	Ru-BH_4 analogue	Ru-H analogue	ref
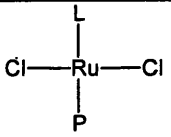	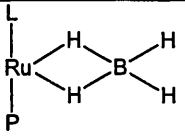	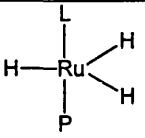	
L = η^5-C_5Me_5			
P = PMe_3,	y	y	6
PEt_3,	y	y	
P^iPr_3,	y	y	
PCy_3,	y	y	
PPh_2Me,	y	y	
PPh_3	y	y	
L = η^6-C_6Me_6			
P = PMe_2Ph, P^tBuMe_2	y	y	7
	y	y	
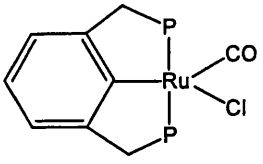	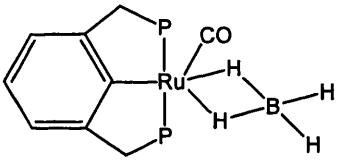	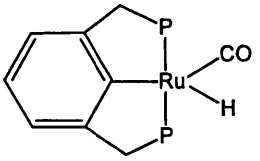	8
P = P^tBu_2			
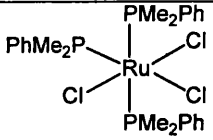	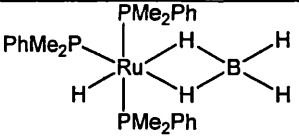	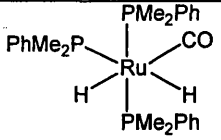	◊ [9]
$[RuCl_2(ttp)]_x$	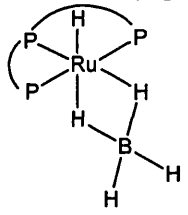	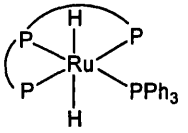	10
ttp =			
$PhP\{(CH_2)_3PPh_2\}_2$			

Table 4.1 Selected Ru-BH_4 complexes and their directly analogous Ru-H counterparts.

◊ $Ru(PMe_2Ph)_3(\eta^2\text{-}BH_4)H$ was refluxed in EtOH to achieve conversion to the dihydride product; decarbonylation of EtOH accounts for the formation of new CO ligand.[9]

4.2.1 Coordination of BH_4^- ligands

Not all halide containing complexes react with $NaBH_4$. For example, difficulties were encountered in reactions between Suzuki's bromide complexes $Ru(\eta^5\text{-}C_5Me_5)(PR_3)\mathbf{Br_3}$ containing the bulky phosphines PCy_3 and $P\textit{i}\text{-}Pr_3$, and $NaBH_4$.[6] No reduction was observed and it was postulated that the reducing agent could not get close enough to the metal centre to react. This problem was overcome by using a less sterically hindered Ru(III) chloride analogue, $Ru(\eta^5\text{-}C_5Me_5)(PR_3)Cl_2$, to successfully produce $Ru(\eta^5\text{-}C_5Me_5)(PR_3)H_3$.[6]

Steric factors also influence the way that the BH_4^- ligand can bind to the metal centre. A variety of different coordination modes are possible as shown in **Figure 4.1**, but the actual coordination mode depends on the amount of vacant sites available and the bulk of other ligands. For example, when L = $PMePh_2$[11] or PMe_3[12] in $Ru(L)_3(BH_4)$, the borohydride ligand is bound in an η^2 fashion, whereas η^1 binding occurs when L = PPh_3.[13]

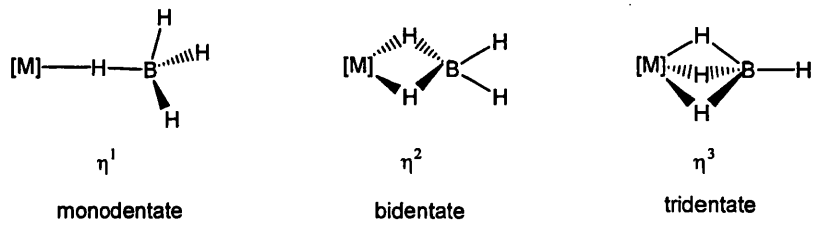

Figure 4.1 The different coordination modes available to the BH_4^- ligand.

As well as steric factors, electronic contributions are involved in deciding the coordination mode. There are two main approaches that are used to describe the bonding in BH_4^- complexes; a covalent approach (each B-H-M bond considered as a three-centre-two-electron bond) and a molecular orbital perspective {which considers symmetry based combinations of B and H atomic valence orbitals (**Figure 4.2**)}.[14] In the latter model each B-H unit is considered as a σ-donor providing a dative bond to the metal centre. Consequently, when BH_4^- is η^1-bound it acts as a two-electron donor, in the case of η^2 and η^3-bound ligands they are four and six electron donors respectively.

Alternatively, when BH_4 is regarded as neutral, it acts as a one (η^1), three (η^2) or five (η^3) electron donor. This is important in ensuring that the 18-electron rule is fulfilled for stable borohydride complexes.

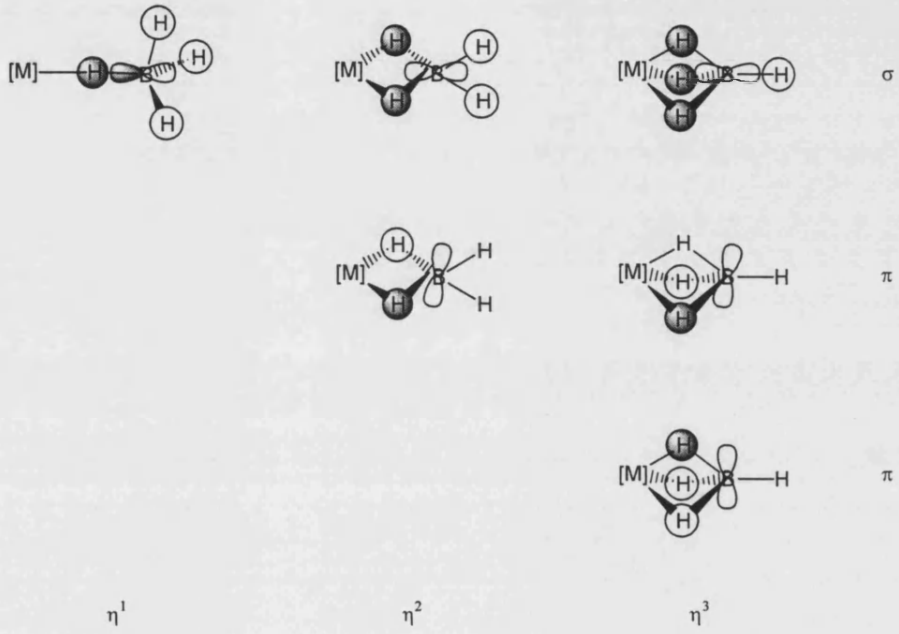

Figure 4.2 The BH_4^- orbitals involved in η^1, η^2 and η^3 coordination modes.

The molecular orbital diagram displayed in **Figure 4.2** explains how the B and H atomic valence orbitals can interact to account for the types of bonding seen in borohydride complexes. Each coordination mode has one orbital combination that results in a metal-ligand σ-molecular orbital as mentioned above. The other molecular orbital combinations create metal-ligand π-orbitals (one for η^2-BH_4^- and two for η^3).

4.2.2 Fluxionality between BH_4^- ligand coordination modes

It is possible for the BH_4^- ligand to change between coordination modes if there is sufficient opportunity (sterically and electronically). Indeed the ligand has been described as a 'gate keeper,' by Marks and Kolb.[5] The ability to switch between

coordination modes helps to preserve the stability of the complex by retaining coordinative saturation and fulfilling the 18-electron rule.

This feature makes η^2-BH_4^- complexes especially desirable as they are relatively stable but able to create a vacant site, which is generally good for catalysis. So, not only are BH_4^- complexes relatively stable potential precursors to their hydride counterparts, they are also useful in their own right.

There have been many reported examples of η^2-BH_4^- complexes used in catalytic reactions, although it is clear that not all of the examples retain the BH_4^- moiety (particularly when any nucleophilic reagents are present to cause BH_3 abstraction).[10, 11, 15]

4.2.3 Transformation from borohydride to hydride complexes

Examples in the text above (especially those in **Table 4.1**) give the impression that it is possible to achieve hydride containing species from any BH_4^- complex. However, this is not the case as some BH_4^- complexes are so stable that the hydride analogues are not achieved. For example, $RuH(BH_4)$(tripod) does not react with MeOH to yield a dihydride complex, but instead produces the tetrahydroborate bridged complex $[(tripod)HRu(\mu,\eta^2\text{-}BH_4)RuH(tripod)]^+$.[16]

It is not clear why some BH_4^- complexes are viable precursors to their hydride-containing analogues and others are not. One major consideration is that the loss of BH_3 may create an unstable hydride product in going from an 18 to a 16-electron system with a vacant site. An example is given in **Scheme 4.1**. The Whittlesey group and other authors have successfully isolated 16-electron mono hydride complexes but there are very few known 16-electron bis hydride complexes of this type.[17-20]

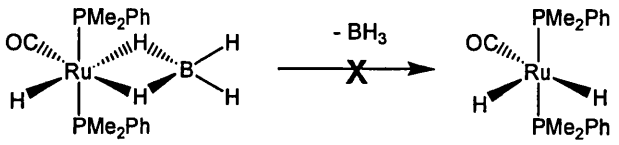

Scheme 4.1 BH_3-loss from $Ru(PMe_2Ph)_2(CO)(\eta^2\text{-}BH_4)H$ is not observed.[21]

Additionally, it is important to understand how BH_3 is lost from BH_4^- complexes. It was considered unlikely that BH_3 can be lost directly from η^2-BH_4^- complexes and more likely the coordination mode switches to a η^1-BH_4^- arrangement first so that BH_3 can be abstracted by a Lewis base to form an adduct. This is the process that occurs when BH_4^- complexes react in protic solvents like EtOH (essentially a weak Lewis base) to afford hydride products. Furthermore, if a sufficiently strong Lewis base is not present BH_3 cannot be abstracted from the complex. For example, $Ru(PR)_3(\eta^2\text{-}BH_4)H$ (R = $MePh_2$[11] or Me_3[22]) reacts with CO to form $Ru(PR_3)_3(CO)H_2$ but only in the presence of NEt_3, which acts to remove BH_3 as the adduct $Et_3N.BH_3$. However, there is also the possibility that the Lewis base can bind to the metal centre filling the newly acquired vacant site. Unlike the former examples, CO operates as both the BH_3 abstracter **and** a new ligand to form $M(P^iPr_3)_2(CO)_2H_2$ (M = Ru, Os) from $M(P^iPr_3)_2(CO)(\eta^2\text{-}BH_4)H$.[23] The dual role of the Lewis base overcomes the problems associated with losing BH_3 to form unstable coordinatively unsaturated products as discussed earlier.

The contrasting reactivity of CO in the examples given above demonstrates that substrates can act differently depending on the complex. From this information two important points were concluded: i) it is not possible to employ a common Lewis base to remove BH_3 from all BH_4^- complexes, and ii) the formation of a stable adduct is not sufficient driving force to ensure that a reaction will occur.

In summary, halide containing complexes can be reduced by $NaBH_4$ to potentially afford a hydride product, however in some cases the reaction gets 'stuck' at an 'intermediate' BH_4^- complex. The propensity to lose BH_3 from a BH_4^- complex as an adduct of a Lewis base is not a consistent route for Ru-H production.

4.3 Formation of the borohydride complex $Ru(IMes)_2(CO)(\eta^2\text{-}BH_4)H$ (19)

4.3.1 Synthesis and characterisation of 19

The reaction of $Ru(IMes)_2(CO)(Cl)H$ (**7**) with excess $NaBH_4$ in EtOH at 298 K afforded the BH_4^- complex, $Ru(IMes)_2(CO)(\eta^2\text{-}BH_4)H$ (**19**) shown in **Scheme 4.2**. **19** can also be produced from $Ru(IMes)_2(CO)(F)H$ (**6**) under the same conditions. All samples of **19** documented here were produced from **7**.

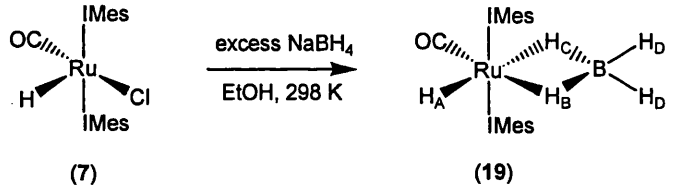

(7) (19)

Scheme 4.2 Formation of $Ru(IMes)_2(CO)(\eta^2\text{-}BH_4)H$ (**19**).

Formation of **19** caused the reaction mixture to change colour from yellow to off-white and the ^1H NMR spectrum in $C_6D_5CD_3$ showed loss of the starting complex (-25.39 ppm) and the appearance of new, higher frequency signals at -16.28 ppm and at *ca.* -7 ppm (v br). Upon cooling to 228 K, the broad signal separated out into three signals in a 2:1:1 ratio for the terminal and bridging BH_4^- hydrogen atoms respectively (**Figure 4.3**).

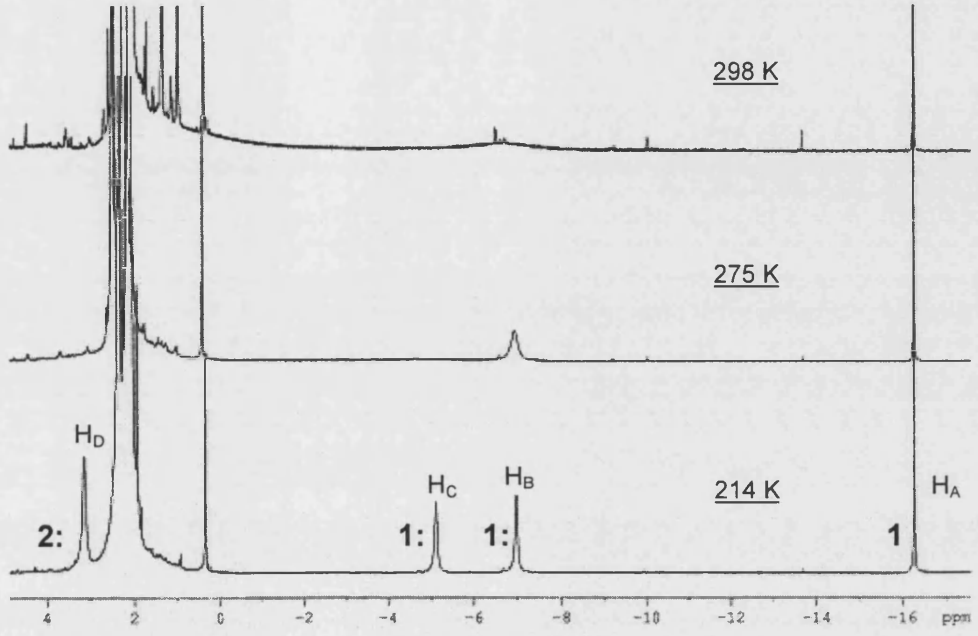

Figure 4.3 The effect of temperature on the ^1H NMR spectra of **19** ($C_6D_5CD_3$, 400 MHz).

It was important to differentiate between the bridging hydrogen atoms (labelled H_B and H_C) for complete assignment and more importantly, for subsequent mechanistic studies. Attempts to locate H_B and H_C using ^1H-$^{13}C\{^1H\}$ HMBC spectroscopy were unsuccessful as no coupling was observed between either hydride with the carbonyl or the carbenic carbon atoms. However, ROESY data enabled H_B and H_C to be correctly assigned. The ^1H ROESY and 1D ROE NMR spectra link H_A and H_B together revealing their *cis* relationship (**Figure 4.4**).

Initially the location of the H_C resonance downfield from H_B was surprising as mutually *trans* hydrides are generally expected at higher shifts because of the *trans* influence of hydride ligands. However, the location of H_C *trans* to H_A is consistent with the resonances assigned to $Ru(PMe_2Ph)_2(CO)(\eta^2\text{-}BH_4)H$, also determined by ROE spectroscopy.[21]

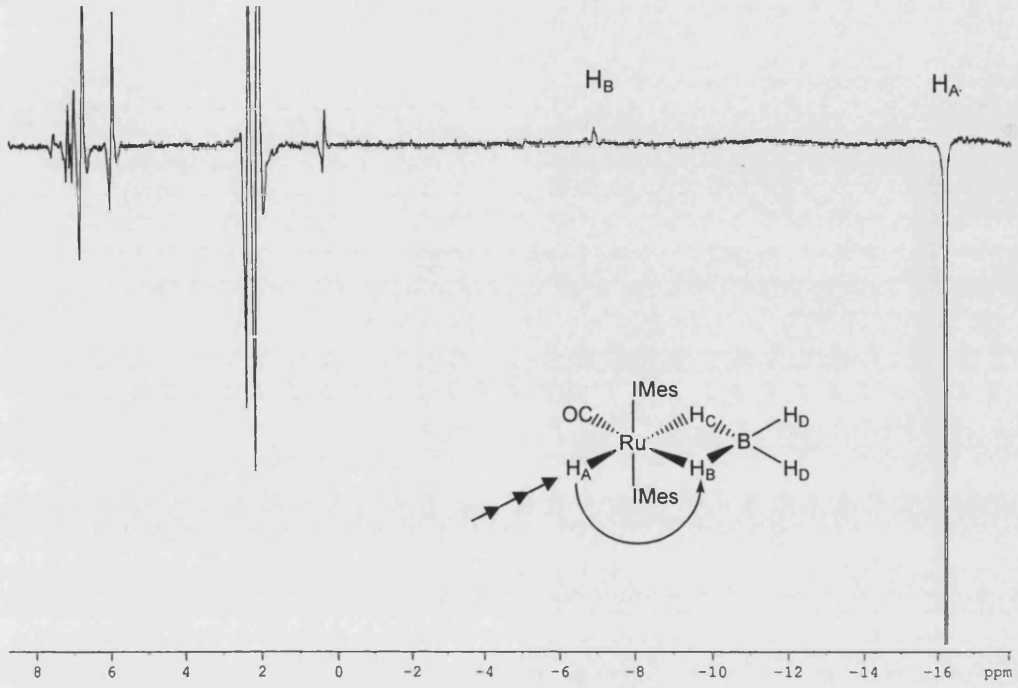

Figure 4.4 ^{1}H ROE NMR spectrum of **19** showing the signal for H_B out of phase with respect to the irradiated H_A resonance (214 K, $C_6D_5CD_3$, 400 MHz).

Spin-lattice relaxation (T_1) measurements using the standard inversion-recovery pulse sequence were carried out on **19** at 214 K (**Table 4.2**). Unfortunately T_1 values could not be successfully determined for the H_D protons due to their proximity to other signals in the spectrum. As expected, T_1 values showed the bridging hydrides H_B and H_C exhibiting faster relaxation time than the classical hydride H_A (214 K). Comparable T_1 values were obtained for $Ru(PMe_2Ph)_2(CO)(\eta^2\text{-}BH_4)H$ by Lowe at 213 K.[21, 24]

Hydride	^{1}H NMR shift (ppm)	T_1 (ms)
H_A	-16.28	994
H_B	-6.98	145
H_C	-5.12	130
H_D (2H)	3.13	-

Table 4.2 ^{1}H NMR shifts and T_1 values for hydrides associated with $Ru(IMes)_2(CO)(BH_4)H$ (**19**) ($C_6D_5CD_3$, 214 K, 400 MHz).

Major characteristic peaks in the $^{13}C\{^1H\}$ NMR spectrum of **19** such as the resonances for carbenic, carbonyl and methyl carbon atoms, were similar to other bis IMes systems seen in previous chapters. A broad ^{11}B resonance was detected at -2.79 ppm at 298 K, which broadened further at low temperatures so that it was no longer observable.

The IR spectrum of **19** showed the CO absorption band at 1900 cm^{-1}, higher than the starting complex **7** (1882 cm^{-1}). Peaks at 2425 and 2400 cm^{-1} correspond to the terminal B-H stretches and absorption for the B-H deformation was observed at 1156 cm^{-1}, similar to assignments reported for related complexes (**Table 4.3**).

Crystals of **19** were grown for structure determination by X-ray crystallography. Two types of crystals of the same unit cell were produced (cuboid and platelets as the majority). Unfortunately the resulting structures proved to be too disordered about the equatorial positions to determine bond length or bond angle values. More specifically, the electron density for the disordered carbonyl carbon was seen over four sites, each containing peak heights that were equivalent to 1.5 electrons (not much bigger than a hydrogen atom).

Structure solution problems are not uncommon in these systems because of the close proximity of the hydrogen atoms to the metal centre.[5] The small number of electrons involved means that the observed diffraction intensity is very difficult to see. In fact there are only very few ruthenium η^2-tetrahydroborate complexes listed on the Cambridge Crystallographic Database, including $Ru(PMe_3)_3(\eta^2\text{-}BH_4)H$,[12] and a cationic

bimetallic species $[(tripod)HRu(\mu,\eta^2\text{-}BH_4)RuH(tripod)]^+$ {tripod = $MeC(CH_2PPh_2)_3$}, in which the BH_4^- ligand bridges the two metal centres.[16]

complex	$\nu_{terminal\ B\text{-}H}$	$B\text{-}H_{deformation}$	$B\text{-}H_B\text{-}Ru$	ν_{CO}
19	2425 2400	1156	1658 1609 1595	1900
$Ru(PMe_2Ph)_2(CO)(\eta^2\text{-}BH_4)H$ [21]	2435 2413	1172	-	1952
$Ru(PMePh_2)_3(\eta^2\text{-}BH_4)H$ [11]	2395 2375 2315	1180	1945 1370	-
$Ru(ttp)(\eta^2\text{-}BH_4)H$ [10]	2390 2380 2330	1180	-	-
$Ru(triphos)(\eta^2\text{-}BH_4)H$ [25]	2382 2310	1169	1919 1395	-

Table 4.3 Relevant IR shifts (cm^{-1}) for $Ru(IMes)_2(CO)(BH_4)H$ (**19**) and similar complexes for comparison. (- = N/A or not provided).

4.3.2 Attempted formation of $Ru(IMes)_2(CO)H_2$ from $Ru(IMes)_2(CO)(\eta^2\text{-}BH_4)H$ (19)

In contrast to the BH_4^- complexes shown in **Table 4.1** (p. 114), **19** showed no evidence of conversion to the dihydride species $Ru(IMes)_2(CO)H_2$ even though the reaction solvent was protic. Although various different forcing conditions were used reaction of $Ru(IMes)_2(CO)(Cl)H$ (**7**) with $NaBH_4$ did not furnish $Ru(IMes)_2(CO)H_2$ at any point {long reaction times (overnight) and increased temperatures (343 K)}.

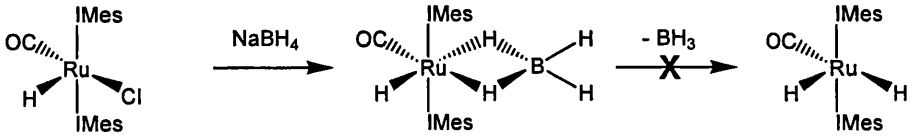

Scheme 4.3 The reaction of **7** with $NaBH_4$.

Werner was able to produce a dihydrogen dihydride species $Ru(PMe_3)_3(\eta^2\text{-}H_2)H_2$ by reacting $Ru(PMe_3)_3(\eta^2\text{-}BH_4)H$ directly with hydrogen in MeOH.[22] This method echoes the work previously described by Caulton.[26] Bubbling H_2 continuously through the reaction of **7** with $NaBH_4$ did not produce $Ru(IMes)_2(CO)H_2$ or $Ru(IMes)_2(CO)(\eta^2\text{-}H_2)H_2$. In hindsight this outcome was not surprising as the reaction mixture itself evolved hydrogen providing sufficient opportunity for any change to occur. Reaction of an isolated sample of **19** with H_2 produced the same result. Similarly, no change was evident after stirring **19** in MeOH or in a mixture of H_2O/THF overnight.

4.3.3 Establishing fluxionality in $Ru(IMes)_2(CO)(\eta^2\text{-}BH_4)H$ (19)

The fact that **19** does not react to form the dihydride species $Ru(IMes)_2(CO)H_2$ may be related to the propensity of the η^2-BH_4 ligand to 'open up' to form η^1-BH_4. This is a well established process (first suggested in 1961)[27] and a key factor in the protonolysis route from BH_4^- to hydride-containing complexes.[28] We proposed that in determining whether the η^2-BH_4 ligand in **19** 'opens up' readily, it may be possible to explain why BH_3 is not easily lost.

The ^1H NMR spectrum of **19** at 298 K implies that the BH_4^- protons are rapidly exchanging as they are observed as one broad peak. Exchange in other η^2-BH_4 systems is well established and most likely takes place as shown in **Scheme 4.4**.[5, 10, 12, 21] The BH_4^- ligand 'opens up' to η^1-BH_4 so that the three terminal hydrogen atoms can rotate freely about the bridging hydride bond. When the BH_4^- ligand returns to the η^2-coordination mode it is not necessarily the original hydrogen that returns to the bridging position. This process is continuous so eventually all of the BH_4^- hydrogen

atoms undergo exchange. Other hydrogen exchange mechanisms have been proposed, such as coordination *via* η^3-BH_4. However, the switch between η^2 and η^1-coordination modes (**Scheme 4.4**) is considered the most likely as a decrease to 16 valence electrons has more precedence than increasing the electron count to 20 for η^3-BH_4.[28]

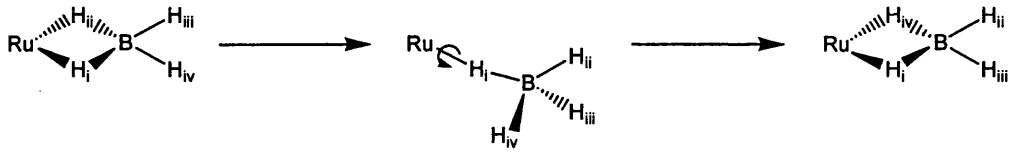

Scheme 4.4 The fluxional nature of the BH_4^- ligand, causing exchange of BH_4^- hydrogen atoms.

4.3.4 Treatment of Ru(IMes)$_2$(CO)(η^2-BH$_4$)H (19) with D$_2$

Although exchange was expected in **19** between the BH_4^- hydrogen atoms, we wanted to investigate whether new atoms could be incorporated into the system. Consequently **19** was reacted with D_2, exposing another major question; whether the BH_4^- hydrogen atoms in **19** can undergo exchange with protons that are introduced from outside the system. Two samples of **19** were prepared, one in $C_6D_5CD_3$ and the other in $C_6H_5CH_3$, and both were treated identically throughout so that each reaction could be followed by both ^1H and ^2H NMR spectroscopy in parallel. The samples were exposed to 1 atm D_2 at 298 K and followed over 2 weeks by ^1H and ^2H NMR spectroscopy at 238 K.

A small decrease in the hydride resonance H_A (20 % with respect to the backbone protons) was apparent in the ^1H NMR spectrum after 6 days at 298 K under an atmosphere of D_2. After 2 weeks under the same conditions, the H_A integral had reduced to half whilst H_B and H_C resonances remained unchanged (**Figure 4.5**). It is noteworthy that a 50 % decrease in the H_A resonance of **19** could be achieved after only 2 days at the higher temperature 323 K. The ^2H NMR spectrum revealed the formation of Ru-D as a broadened resonance at -16.28 ppm, implying that the hydride position had undergone H/D exchange to form Ru(IMes)$_2$(CO)(η^2-BH$_4$)D (**19-d$_1$**).

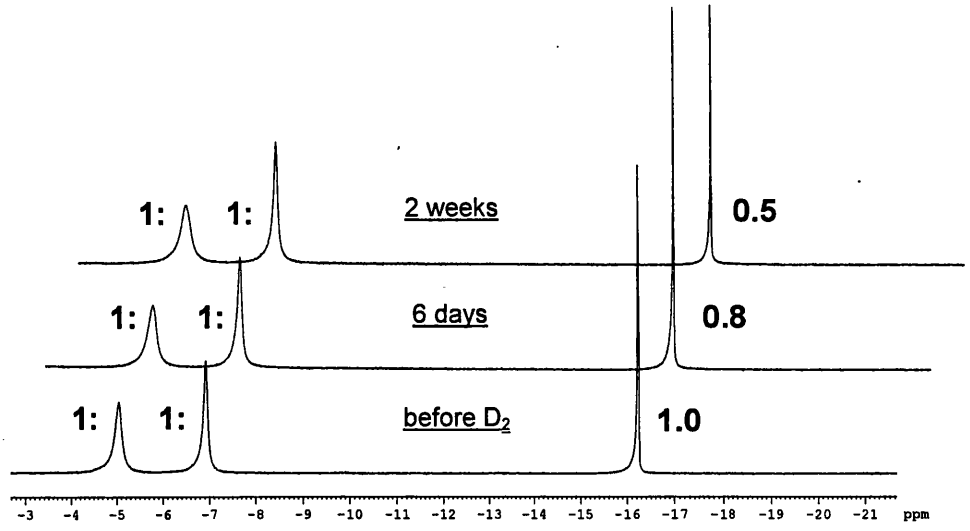

Figure 4.5 ^{1}H NMR spectra for the reaction of **19** with D_2 at 298 K ($C_6D_5CD_3$, 238 K, 400 MHz).

Formation of the partially deuterated complex **19-d$_1$** can be easily reasoned by the proposed mechanism shown in **Scheme 4.5**. The proposed mechanism only serves to address the *cis* geometry necessary for deuterium to undergo migration. Non-classical binding of D_2 into the vacant site of the η^1-BH_4 species *cis* to the hydride, is followed by transfer of a deuterium atom to the hydride ligand. HD is lost to recreate the vacant site and the borohydride ligand can return to the η^2-coordination mode. Unfortunately, there was no clear evidence of free HD in the ^{1}H NMR spectrum of **19** with D_2.

The mechanism described below is consistent with work done by Lowe, in which $Ru(PMe_2Ph)_2(CO)(\eta^2\text{-}BH_4)H$ was reacted with a para-enriched H_2 in order to probe the exchange process between free H_2 and hydrogen atoms in the complex.[24] Lowe's study implied that a ruthenium (IV) trihydride species with three inequivalent hydride ligands $Ru(PMe_2Ph)_2(CO)(\eta^1\text{-}BH_4)H_3$, was involved in the reaction. $Ru(IMes)_2(CO)(\eta^1\text{-}BH_4)(D_2)H$ shown in **Scheme 4.5** may be related to Lowe's intermediate. These results are also consistent with H/D exchange results obtained for the 16-electron complexes $Ru(IMes)_2(CO)(X)H$ (X = OH, SH, F, Cl) in Chapter 2, although significantly slower. Thus, **19** demonstrated some characteristics of a

coordinatively unsaturated complex, suggesting that $Ru(IMes)_2(CO)(\eta^1\text{-}BH_4)H$ is a feasible species.

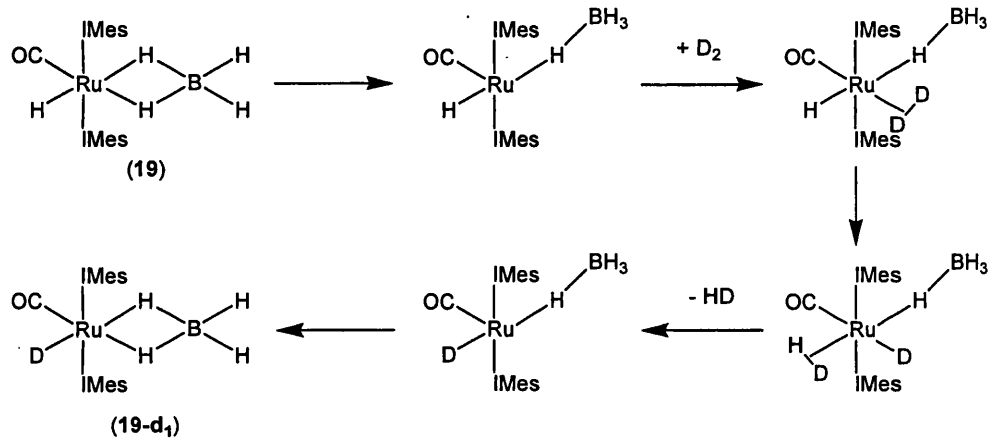

Scheme 4.5 The proposed mechanism for the incorporation of deuterium into the 'hydride' position of **19** to yield **19-d_1**. NB. This scheme is not meant to be indicative of the manner in which the BH_4^- ligand opens up.

4.3.5 Deuterium incorporation into the borohydride ligand of 19

The ^1H and ^2H NMR spectra (228 K) for the reaction of **19** with D_2 were inconclusive in determining whether H/D exchange occurred within the BH_4^- ligand. By ^1H NMR spectroscopy the integrals corresponding to H_B, H_C and H_D remained unchanged over a month at 298 K and resonances for D_B, D_C and D_D were not apparent in the ^2H NMR spectra. The quadrupolar nature of ^2H nuclei (I = 1) may cause such broadening that the signals were not observed in the ^2H NMR spectrum especially as the signals for H_B, H_C and H_D were broad even in the ^1H NMR spectrum. For more clarity, the borodeuteride analogue $Ru(IMes)_2(CO)(\eta^2\text{-}BD_4)H$ (**19-d_4**) was prepared for reaction with H_2.

4.4 Formation of the borodeuteride complex $Ru(IMes)_2(CO)(\eta^2\text{-}BD_4)H$ (19-d_4)

The deuterated analogue of **19** $Ru(IMes)_2(CO)(\eta^2\text{-}BD_4)H$ (**19-d_4**) was prepared by reaction of $Ru(IMes)_2(CO)(Cl)H$ (**7**) with $NaBD_4$, following the method used to produce **19**. It noteworthy that the reaction was carried out in EtOH rather than EtOD without detriment to the BD_4 ligand and that the hydride ligand remained unchanged.

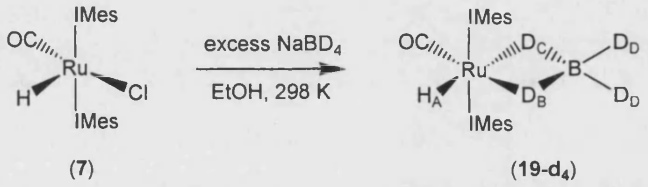

(7) (19-d_4)

Scheme 4.6 Formation of $Ru(IMes)_2(CO)(BD_4)H$ (**19-d_4**).

The H_A signal showed the expected ratio to the IMes protons in the ^1H NMR spectrum (1:4, Ru-**H**:NC**H**); the BD_4^- resonances were located in the ^2H NMR spectrum at the same chemical shifts as in the ^1H NMR spectrum of **19** (230 K) (**Fig. 4.6**).

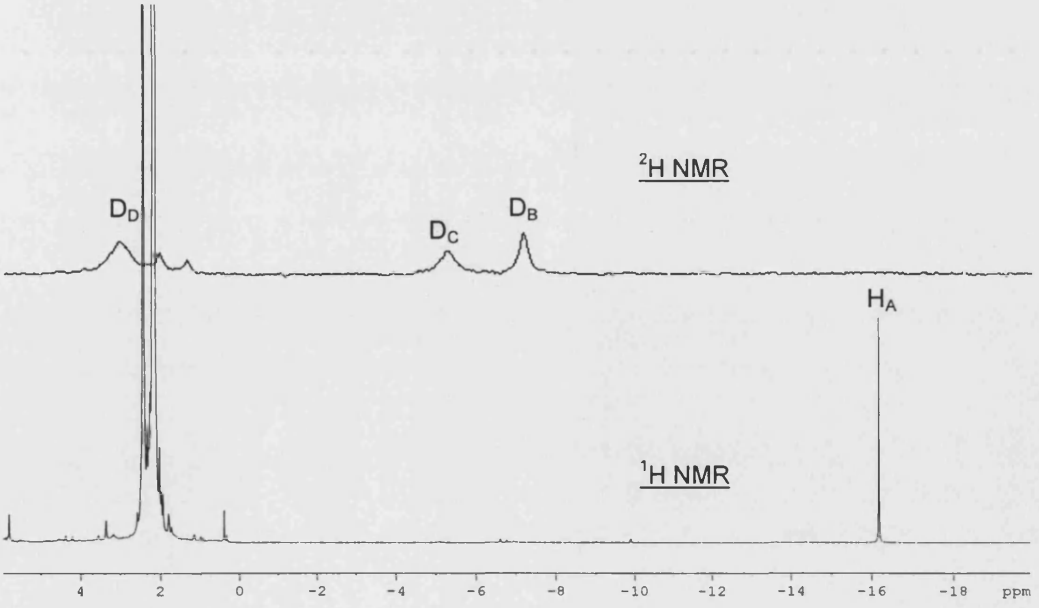

Figure 4.6 ^1H and ^2H NMR spectra of **19-d_4** ($C_6D_5CD_3$ and $C_6H_5CH_3$ respectively, 230 K).

All of IR spectroscopic bands associated with BD_4^- in **19-d$_4$** varied dramatically from the equivalent BH_4^- values for **19** due to heavier D atoms incorporated into **19-d$_4$**. IR bands for BD_4^- in **19-d$_4$** were observed at 1826, 1765 and 1712 cm^{-1} ($\upsilon_{terminal\ B\text{-}D}$); 1079, 1034 and 1161 cm^{-1} (B-D_B-Ru) and at 846 cm^{-1} (B-$D_{deformation}$). Doubling the atomic mass number (Z) from H to D has a large effect on the resulting vibration frequency as these factors are related to each other by ($1/\sqrt{}$reduced mass). Therefore BD_4^- IR shifts consistently lie hundreds of wavenumbers below their BH_4^- analogues.[10, 11] In contrast υ_{CO} was essentially unchanged between **19** and **19-d$_4$** (1900 and 1898 cm^{-1} respectively).

4.4.1 Treatment of Ru(IMes)$_2$(CO)(η^1-BD$_4$)H (19-d$_4$) with H$_2$

A sample of **19-d$_4$** was exposed to 1 atm H_2 at 298 K and followed by ^{1}H NMR spectroscopy at 230 K in order to detect growth of H_B, H_C and H_D resonances. Exchange between the BD_4^- ligand and free H_2 was not evident when the sample was kept at 298 K (even over 3 weeks). However, heating at 323 K resulted in a slow increase in the integral values. After 21 days at 323 K the integral ratio of bridging hydrogens (H_B, H_C) to the hydride integral (H_A) stood at 1:1:3. The ratio 1:1:2 was achieved after 28 days at 323 K. Free HD gas was also observed, characterised by the appearance of a diagnostic 1:1:1 signal at 4.44 ppm (J_{HD} = 43 Hz).

Comparing the integrals between H_B, H_C and H_A may be misleading if deuterium was transferred from the bridging positions to the hydride (pathway **a**, **Scheme 4.7**). The mechanism of **a** relies on the BD_4^- ligand splitting to produce a deuteride ligand and a BD_3 moiety, which Esteruelas and coworkers have investigated computationally (with BH_4^-).[28] The BD_3 ligand then reattaches *via* the hydride. It is noteworthy that, in the analogous reaction between **19** and D_2 deuterium was not observed in the hydride position by ^{2}H NMR spectroscopy and therefore, the data did not support exchange between Ru-H and B-D, although this may be explained by the large excess of hydrogen in the system.

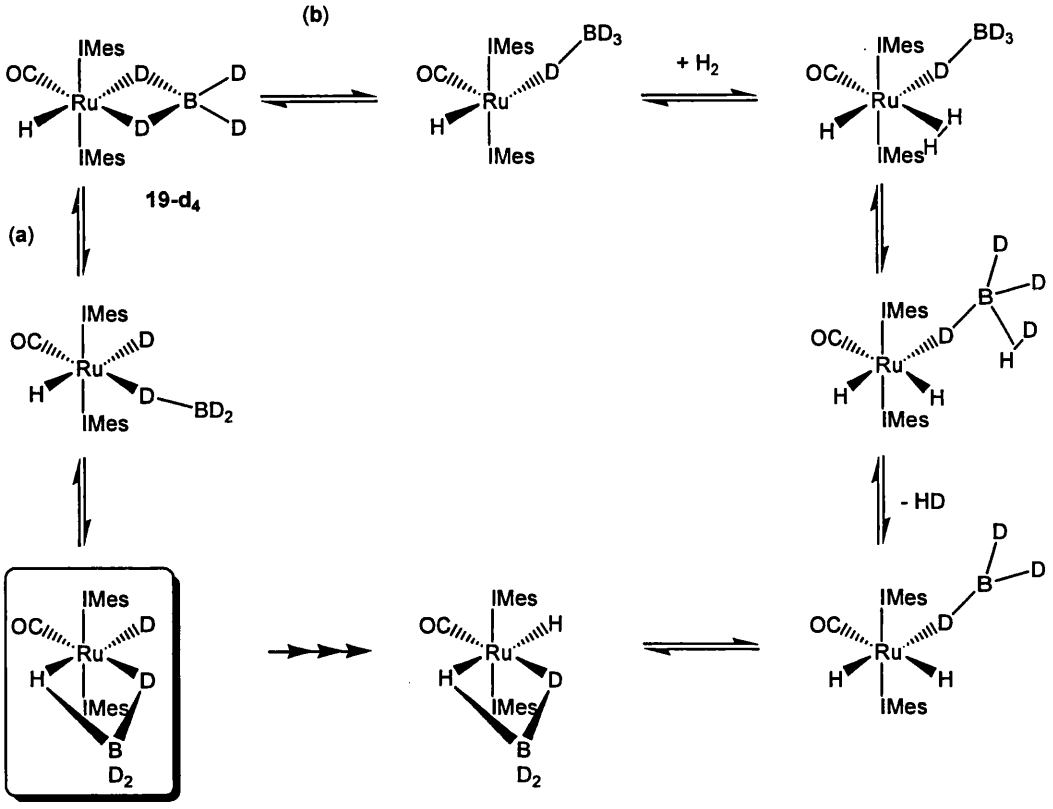

Scheme 4.7 Two possible mechanisms (**a** and **b**) for H-incorporation into the BD_4^- ligand of **19-d$_4$**.

Alternatively H/D scrambling could occur *via* the η^2-bound H_2 (**b**). In pathway **b**, H_2 binds to the metal centre *cis* to the BD_4^- ligand so that H can migrate into it, at which point a second Ru-H ligand is formed. HD is lost from the system and the remaining BD_3 ligand reattaches *via* the deuteride.

As the reaction took place, changes were observed in the hydride region of the ^{1}H NMR spectrum; four resonances were apparent in the location associated with Ru-H rather than just one for **19-d$_4$**. To establish the origin of the hydride signals isotopic perturbation of resonances was carried out; equimolar amounts of **19** and **19-d$_4$** were mixed together and the ^{1}H NMR spectrum acquired. With subsequent addition of another equivalent of **19** it was possible to establish that the **19-d$_4$** hydride lies 0.03 ppm downfield of the **19** signal and comparison with the original spectrum meant that two of

the peaks could be assigned (**Figure 4.7**). Presumably, the other signals denoted the isotopomers in between **19** and **19-d_4**.

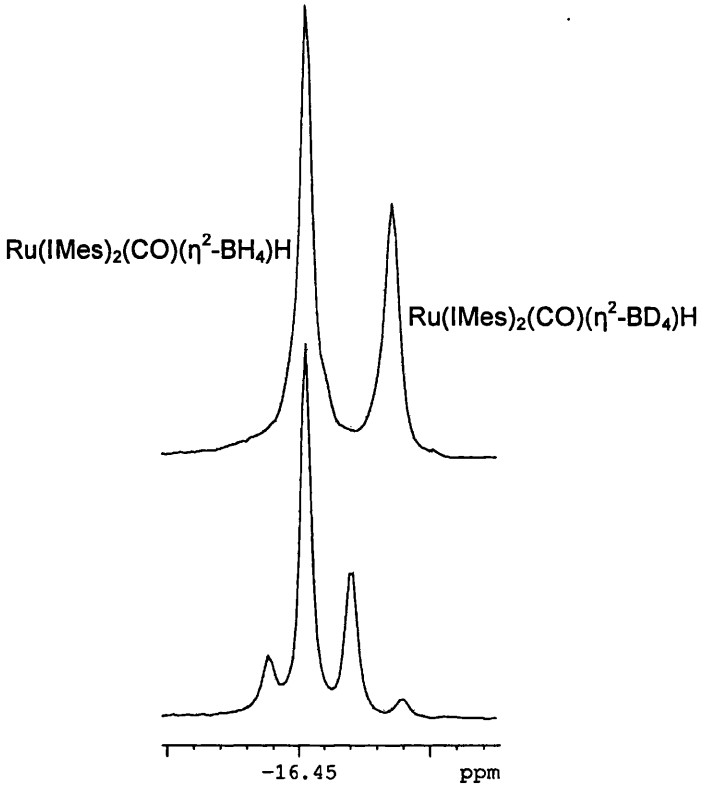

Figure 4.7 ^{1}H NMR spectra for **19** / **19-d_4** 2:1 mix (top) for comparison with the reaction of **19-d_4** with H_2 (bottom) ($C_6D_5CD_3$, 298 K, 400 MHz).

As expected the major hydride resonance was associated with the starting complex **19-d_4** and the smallest with the resulting product **19**, located in the most upfield position. It was not possible to extrapolate this data based on frequency and deuterium content as the spectra contained a resonance downfield of **19**, suggesting that the resonance corresponded to a complex containing more hydrogen atoms than the fully protio complex $Ru(IMes)_2(CO)(\eta^2\text{-}BH_4)H$! Furthermore, only four hydride signals are observed although there are many more possible isotopomers as shown in **Figure 4.8**. So, not every possible H/D combination of the complex causes a shift in the position of the hydride.

There are a number of ways that the shifts can be accounted for but none of the options seem to completely justify the spectral data as described above: i) the isotopes can be grouped according to the number of H/D atoms they contain, resulting in five possible hydride shifts. However, this approach does not account for the *trans* effect that would cause the BD_3H isotopes to differ from each other; or ii) another possibility that does account for the *trans* effect, is to assume that the hydride resonance is only affected by exchange of the bridging atoms and not by that of the terminal atoms. Therefore all of the isotopes described by BD_2H_2 and BDH_3 would be equivalent by ^1H NMR spectroscopy. This rule would also extend to BH_4, rendering comparison with the authentic spectrum inconclusive.

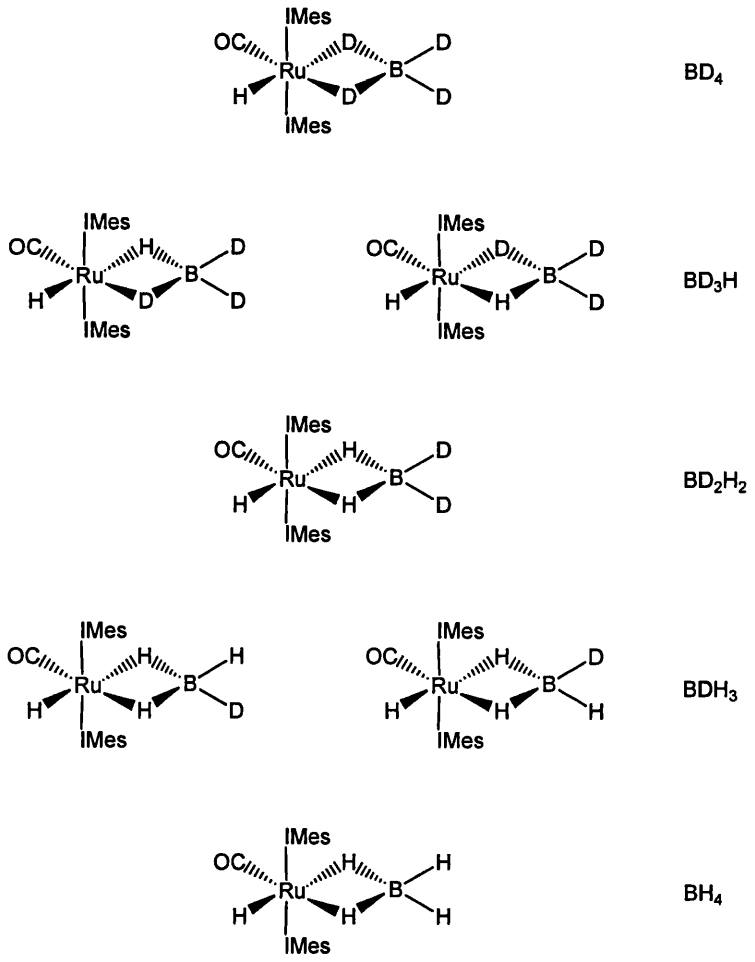

Figure 4.8 The possible isotopomers available from the reaction of **19-d_4** with H_2.

Another shortcoming of this model is that it assumes that the complex is static on the NMR timescale, although it is has already been established this is not so.

4.5 Thermal degradation of $Ru(IMes)_2(CO)(\eta^2\text{-}BH_4)H$ (19)

4.5.1 Formation of IMes.BH_3 (20)

The stability of $Ru(IMes)_2(CO)(\eta^2\text{-}BH_4)H$ (**19**) to heat was investigated over a range of temperatures (up to 358 K) and revealed that thermal decomposition occurred at 358 K to form the adduct IMes.BH_3 (**20**) (**Scheme 4.8**). Decomposition of **19** was apparent by the loss of the diagnostic hydride resonance after a day at 358 K. On cooling to 298 K the solution deposited small colourless platelets of **20**. The ^1H NMR spectrum of **20** (THF-d_8) showed no hydride resonances but protons associated with an IMes ligand remained present. A new 1:1:1:1 quartet at 0.44 ppm was also observed, consistent with protons coupled to a ^{11}B nuclei and the ^{11}B NMR spectrum showed a resonance at -37.4 ppm consistent with the formation of a BH_3 adduct.[21, 29-31] The fate of the metal complex was not determined.

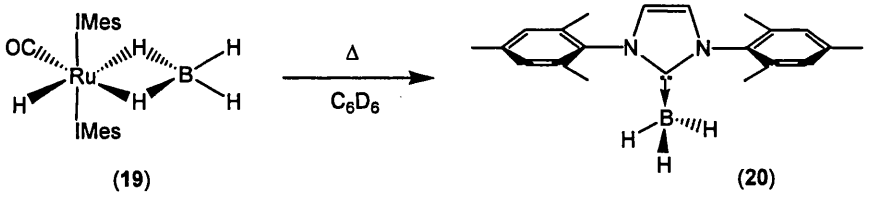

Scheme 4.8 Formation of IMes.BH_3 (**20**).

X-ray crystallography was used to verify the structure of **20** by comparison with the published unit cell data.[32] Although the structure has been previously published, no spectroscopic data was reported.

The IR spectrum of **20** showed terminal B-H stretches at 2362 and 2336 cm^{-1} and a band corresponding to B-H deformation was apparent at 1155 cm^{-1}. These values are similar to those obtained for BH_4^- complexes and reported BH_3-adducts.[33-35]

4.6 Reactions of $Ru(IMes)_2(CO)(\eta^2\text{-}BH_4)H$ (19) with small molecules

H/D exchange reactions on $Ru(IMes)_2(CO)(\eta^2\text{-}BH_4)H$ (**19**) and the deuterated analogue **19-d_4** have indicated that the BH_4^- ligand in **19** does open up. This section investigates the propensity of small molecules to coordinate in the vacant site of $Ru(IMes)_2(CO)(\eta^1\text{-}BH_4)H$. The ultimate aim of this work was to observe a trapped η^1-bound borohydride complex in order to understand the opening up process more fully.

4.7 Treatment of $Ru(IMes)_2(CO)(\eta^2\text{-}BH_4)H$ (19) with $H_2C{=}CH_2$

The coordination of alkenes to metal centres has often been quoted as a significant step in many innersphere-type catalytic cycles involving alkenes. Herein lay the opportunity for ethene to bind to the metal centre in **19** when the BH_4^- ligand is bound in an η^1-fashion.

Addition of 1 atm $H_2C{=}CH_2$ to a sample of **19** at room temperature caused a decrease in the resonance for H_A, however no new hydride signals appeared. Initially free $H_2C{=}CH_2$ was seen in the ^1H NMR spectrum at 5.35 ppm, but after 16 h at 343 K, hydrogenation of ethene to ethane was apparent by a new signal at 0.90 ppm. Loss of hydride and conversion of ethene to ethane suggested that the ethene moiety binds to the metal centre as proposed in the mechanism shown in **Scheme 4.9** before being lost as ethane and causing complex decomposition.

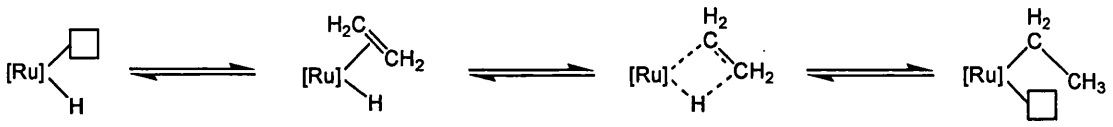

Scheme 4.9 Conversion of ethene to ethane after coordination of ethene to the metal centre. [Ru] = $Ru(IMes)_2(CO)(\eta^1\text{-}BH_4)$.

Low temperature ^1H NMR spectroscopy was employed in an attempt to observe a molecule of ethene inserted in to the $\eta^1\text{-}BH_4^-$ intermediate species (down to 200 K) but no protons characteristic of bound ethene were seen nor any new hydride signals ($\eta^2\text{-}C_2H_4$ expected at *ca.* 2 ppm).[21,36]

It has been noted that carbonyl bearing complexes are more likely to undergo alkane elimination than systems devoid of CO ligands, due to the stabilising effect of the CO ligand. However, Lowe suggested that the gate-keeping effect of the BH_4^- ligand in $Ru(PMe_2Ph)_2(CO)(\eta^2\text{-}BH_4)H$ hindered this process and the new complex $Ru(PMe_2Ph)_2(CO)(\eta^2\text{-}BH_4)(Et)$ was formed upon reaction of the former with ethene at room temperature (**Scheme 4.10**).[21,37] Low temperature studies of the reaction revealed an intermediate $\eta^1\text{-}BH_4^-$ complex in which the ethene ligand was bound to the metal centre in an η^2-fashion (**Scheme 4.10**), consistent with the mechanism proposed above in **Scheme 4.9**.

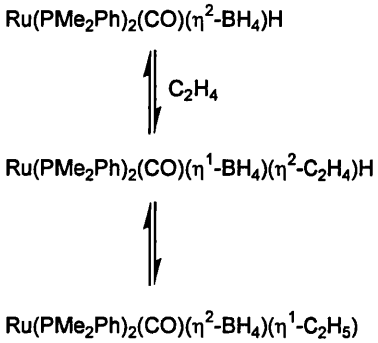

Scheme 4.10 Reaction of $Ru(PMe_2Ph)_2(CO)(\eta^2\text{-}BH_4)H$ with ethene.[21]

Unlike $Ru(PMe_2Ph)_2(CO)(\eta^2\text{-}BH_4)H$, the BH_4^- ligand in **19** did not hinder the elimination of ethane in the reaction of **19** with ethane maybe because of the steric difference between IMes and PMe_2Ph. The elimination process occurring in the reaction of **19** with ethene clearly caused complex decomposition. With this in mind evidence of the possible decarbonylation product propanal was sought, but no diagnostic resonances for propanal were observed (s, q, t, at *ca.* 9.8, 2.5, 1.1 ppm respectively).

4.8 Treatment of $Ru(IMes)_2(CO)(\eta^2\text{-}BH_4)H$ (19) with $H_2C{=}CH(SiMe_3)$

The treatment of **19** with excess $H_2C{=}CH(SiMe_3)$ (5-10 equiv.) was carried out as a comparison to the reaction of **19** with $H_2C{=}CH_2$ and met with similar results. There was no reaction of **19** with $H_2C{=}CH(SiMe_3)$ at 298 or 323 K, but on heating the sample at 343 K for 16 h there was a colour change from yellow to red. The ^1H NMR spectrum showed a decrease in the hydride resonance of **19** but no new hydride signals and a decrease in the intensity of the methyl peak for free $H_2C{=}CH(SiMe_3)$ {0.00 ppm}. The volatiles were collected and the corresponding ^1H NMR revealed conversion from $H_2C{=}CH(SiMe_3)$ to $CH_3CH_2SiMe_3$ by a quartet at 0.44 ppm and a triplet at 0.93 ppm (both J_{HH} = 7.7 Hz).

4.9 Treatment of $Ru(IMes)_2(CO)(\eta^2\text{-}BH_4)H$ (19) with CO

$Ru(IMes)_2(CO)(\eta^2\text{-}BH_4)H$ (**19**) reacted rapidly with CO at 298 K to produce the previously reported *cis* dicarbonyl complex $Ru(IMes)_2(CO)_2H_2$ (**22**), characterised by a diagnostic resonance at -6.53 ppm.[38] A day under an atmosphere of CO resulted in the formation of the tricarbonyl complex $Ru(IMes)_2(CO)_3$ (**23**), which is discussed in more detail in section **4.10**. (**Scheme 4.11**).

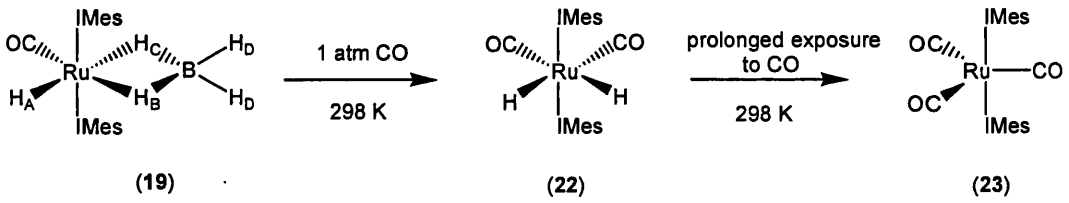

(19) (22) (23)

Scheme 4.11 Formation of **22** followed by **23** from the treatment of **19** with 1 atm CO.

4.9.1 Investigating the transformation of $Ru(IMes)_2(CO)(\eta^2\text{-}BH_4)H$ (19) into $Ru(IMes)_2(CO)_2H_2$ (22)

An atmosphere of CO was added to a cold sample of $Ru(IMes)_2(CO)(\eta^2\text{-}BH_4)H$ (**19**) (195 K, $C_6D_5CD_3$) to slow down the formation of **22**. The sample was allowed to warm slowly to 273 K in the NMR probe, at which point the formation of the intermediate species $Ru(IMes)_2(CO)_2(\eta^1\text{-}BH_4)H$ (**21**) was observed (**Scheme 4.12**) with the appearance of a new, very broad borohydride signal at *ca.* -2 ppm and a singlet at -5.53 ppm. The sample was subsequently cooled to 228 K to prevent production of **22**. This reduction in temperature also resulted in enhanced resonances for **21**, observed as a singlet at -5.23 ppm (1H, Ru-H), which integrated in a 1:4 ratio with the broad signal at *ca.* -2 ppm corresponding to all four BH_4^- hydrogen atoms.

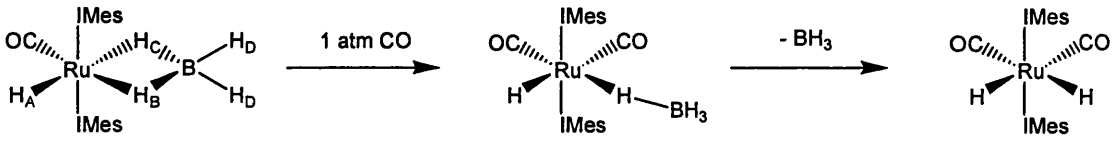

(19) (21) (22)

Scheme 4.12 Formation of **22** from **19** *via* the intermediate $\eta^1\text{-}BH_4^-$ species **21**.

At even lower temperatures (190 K) it was possible to distinguish between the bridging hydride and the terminal BH_3 protons of **21**. The previously broad signal of the

η^1-BH_4^- ligand (*ca.* -2 ppm) split into two new signals at -10.33 ppm (μ-H) and 0.91 ppm ($BH_{terminal}$, 3H), consistent with other intermediate η^1-BH_4^- species and stable η^1-BH_4^- complexes such as those in **Table 4.4**.

complex	$\underline{H}BH_3$ shift (ppm)	$HB\underline{H}_3$ shift (ppm)	Temperature (K)
21	-10.33	0.91	190
$Ru(PMe_2Ph)_2(CO)_2(\eta^1\text{-}BH_4)H$ [21]	-10.9	1.6	210
$Ru(PP_3)(\eta^1\text{-}BH_4)H$ [39a] $[P = (CH_2CH_2PPh_2)_3]$	-10.28	*ca.* 1.35	173
$Fe(dmpe)_2(\eta^1\text{-}BH_4)H$ [40]	-22.4	0.8	190

Table 4.4 ^1H NMR spectroscopic values for the bridging and terminal hydrogen atoms of some η^1-BH_4^- species ($C_6D_5CD_3$ except [a] in CD_2Cl_2).

The ^1H-$^{13}C\{^1H\}$ HMBC NMR spectrum of $Ru(IMes)_2(CO)_2(\eta^1\text{-}BH_4)H$ (**21**) at 228 K revealed two different $^{13}C\{^1H\}$ signals for the carbonyl ligands, consistent with inequivalent CO ligands and a *cis* arrangement (**Figure 4.9**).

The *cis* arrangement of CO ligands in **21** could result from either i) opening up of the BH_4^- ligand to produce a vacant site *trans* to hydride and trapping by direct CO insertion (pathway **a**, **Scheme 4.13**), or ii) if a vacant site was generated *trans* to CO and isomerisation followed before the binding of CO (pathway **b**, **Scheme 4.13**). Isomerisation in pathway **b** should be relatively facile to overcome the unfavourable *trans* arrangement of the *trans* labilising ligands H and η^1-BH_4^-.

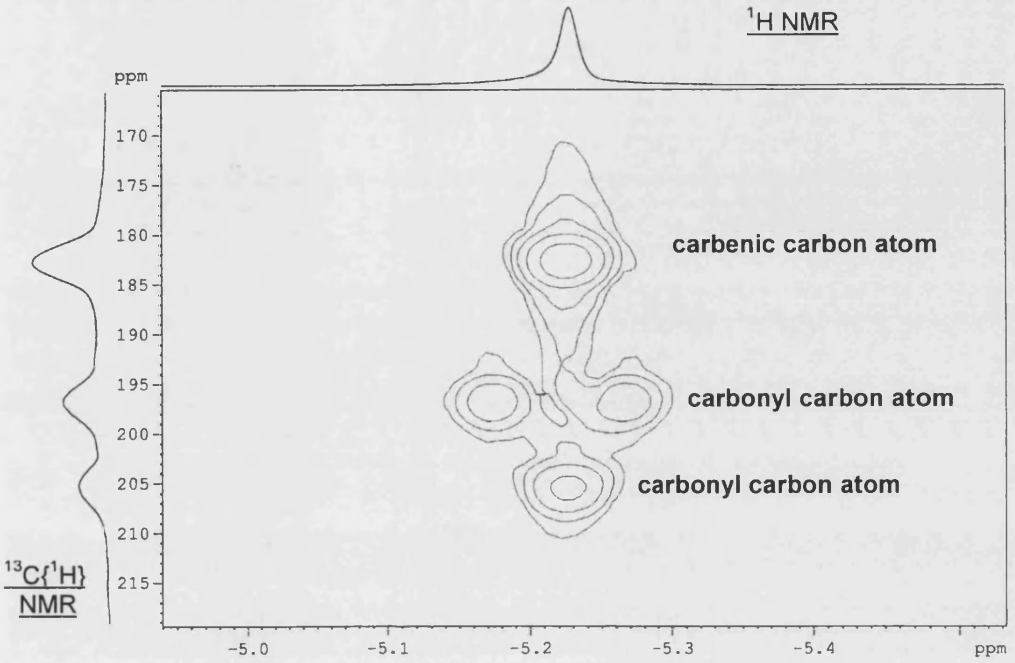

Figure 4.9 ^{1}H-^{13}C{^{1}H} HMBC spectrum of the intermediate species **21** ($C_6D_5CD_3$, 228 K).

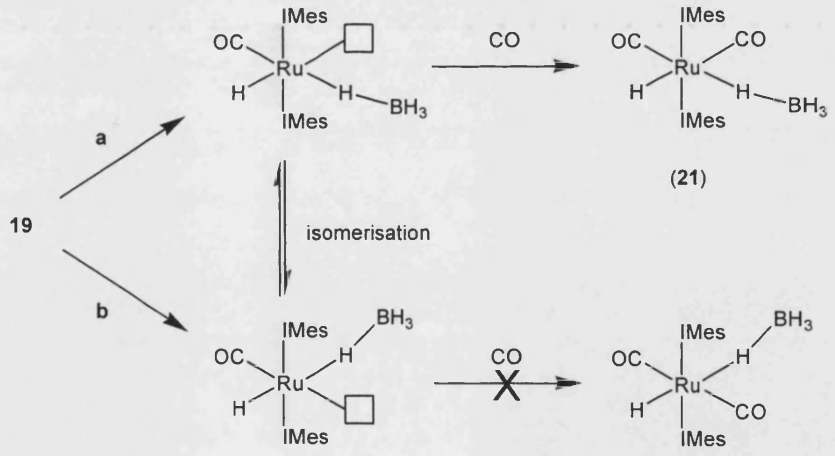

Scheme 4.13 Proposed mechanism including two possible pathways (**a** and **b**) to account for *cis* CO ligand arrangement in **21**.

4.9.2 Treatment of $Ru(IMes)_2(CO)(\eta^2\text{-}BH_4)H$ (19) with ^{13}CO

The reaction of **19** with CO was repeated with ^{13}CO to follow the incorporation of the labelled ligand into $Ru(IMes)_2(CO)(\eta^1\text{-}BH_4)H$ to form $Ru(IMes)_2(CO)(^{13}CO)(\eta^1\text{-}BH_4)H$ (**21***). ^{13}CO was added to a cold sample of **19** (195 K, $C_6D_5CD_3$), which was then allowed to warm to 273 K in the NMR probe. With warming (273 K) the ^1H NMR spectrum showed the hydride resonance of **21*** as two interpenetrating doublets consistent with binding of only **one** labelled carbon monoxide moiety (inclusion of two ^{13}CO ligands would have resulted in a d of d pattern). However, ^{13}CO is incorporated both *cis* and *trans* to the hydride in **21*** resulting in two doublet resonances rather than one (**Figure 4.10**). The resulting $^1H\text{-}^{13}C$ coupling constant values are characteristic of *cis* and *trans* couplings (6.6 and 37.9 Hz respectively). The $^{13}C\{^1H\}$ NMR spectrum of **21*** (228 K) showed enhanced resonances corresponding to ^{13}CO at 205.5 and 196.7 ppm, which was verified by $^1H\text{-}^{13}C\{^1H\}$ HMBC data, consistent with ^{13}CO incorporation into both carbonyl positions.

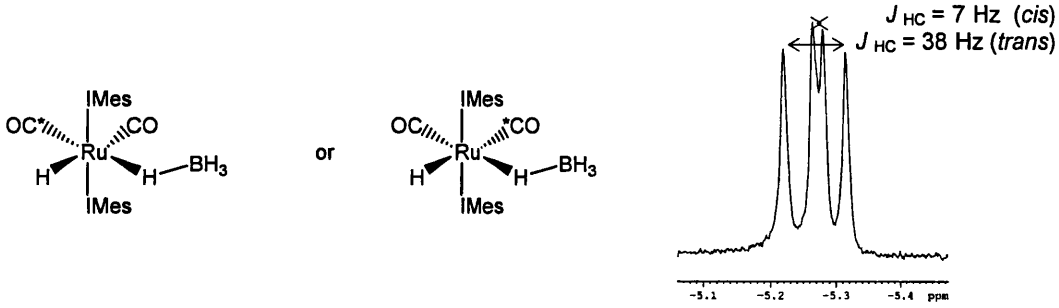

Figure 4.10 Isotopomers of **21*** that account for the hydride region of the ^1H NMR spectrum shown (273 K, $C_6D_5CD_3$, 400 MHz).

Insertion of ^{13}CO into two different positions of **21*** can be rationalised if the mechanism shown in **Scheme 4.13** involved another isomerisation step. **Scheme 4.13** only accounts for two possible isomers of $Ru(IMes)_2(CO)(\eta^1\text{-}BH_4)H$ **Ia** and **Ib** (**Scheme 4.14**) and it has been established that CO does not insert directly into the vacant site of **Ia**. A third isomer **Ic** must also exist, in which the vacant site is *cis* to the

hydride ligand (**Scheme 4.14**). Direct addition of ^{13}CO to the isomers **Ib** and **Ic** results in the species that were observed in the ^{1}H NMR spectrum as interpenetrating doublets.

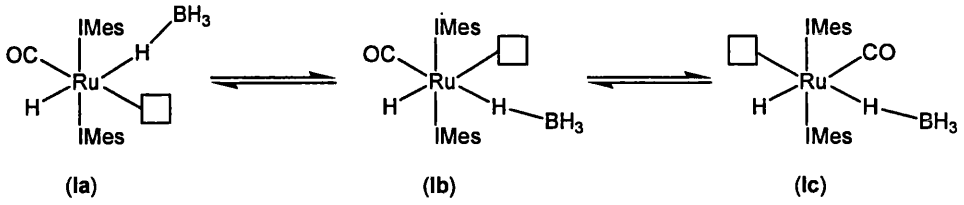

Scheme 4.14 Possible isomers of the intermediate species $Ru(IMes)_2(CO)(\eta^1\text{-}BH_4)H$ (**I**).

Another possible way to explain the location of ^{13}CO is by considering the 'opened up' species as a trigonal bipyramidal. This has been previously suggested by Lowe for reaction between $Ru(PMe_2Ph)_2(CO)(\eta^2\text{-}BH_4)H$ and ethene to form $Ru(PMe_2Ph)_2(CO)(\eta^2\text{-}BH_4)(Et)$.[24] However, the isolated 16-electron bis IMes complexes in this thesis are consistently characterised as square based pyramidal, suggesting that this extends to $Ru(IMes)_2(CO)(\eta^1\text{-}BH_4)H$ and the intermediate containing a vacant site.[41]

In conclusion, the reaction of **19** with CO was studied at low temperature and with labelling reactions leading to **22** as the final product *via* the intermediate species **21**. A mechanism for the reaction has been proposed based on these results. Although it has been possible to explain the steps in which **21** is formed, the reactions did not serve to differentiate between the initial possible 'opening-up' routes. The mono CO, $\eta^1\text{-}BH_4$ species $Ru(IMes)_2(CO)(\eta^1\text{-}BH_4)H$ was not detected at any point in the reaction so the mechanism could not be confirmed directly.

4.9.3 Attempted isolation of $Ru(IMes)_2(CO)_2(\eta^1\text{-}BH_4)H$ (21)

In an attempt to isolate the $\eta^1\text{-}BH_4$ complex **21**, an alternative preparation was used involving reaction of the dicarbonyl complex $Ru(IMes)_2(CO)_2(Cl)H$ (**10**) with excess $NaBH_4$. The absence of excess CO was considered advantageous in preventing BH_3 abstraction. However, BH_3 was lost during the reaction to produce the dihydride

complex $Ru(IMes)_2(CO)_2H_2$ (**22**), verifying that **10** was not too sterically hindered to prevent reduction by $NaBH_4$. The formation of **21** was not observed but we propose that **21** was involved in the reaction pathway but not seen due to facile loss of BH_3 (**Scheme 4.15**).

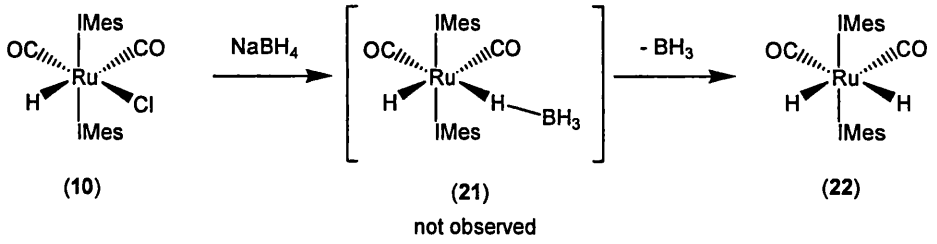

(10) (21) not observed (22)

Scheme 4.15 Proposed route for the reaction of **10** with excess $NaBH_4$ in EtOH.

4.10 Structural characterisation of $Ru(IMes)_2(CO)_3$ (23)

The production of $Ru(IMes)_2(CO)_3$ (**23**) was apparent in the reaction of $Ru(IMes)_2(CO)(\eta^2\text{-}BH_4)H$ (**19**) with excess CO subsequent to the formation of $Ru(IMes)_2(CO)_2H_2$ (**22**). After a day at 298 K, the ^1H NMR spectrum of the reaction mixture revealed a reduction in the hydride signal for **22**. The formation of **23** was confirmed by comparing $^{13}C\{^1H\}$ NMR and IR spectroscopic data with that obtained by Jazzar for the same complex (made by reaction of $Ru(IMes)_2(CO)(OH)H$ (**2**) with CO, 5 days, 298 K).[38] Briefly, the $^{13}C\{^1H\}$ NMR spectrum for **23** showed the carbonyl carbon atom resonance at 217.6 ppm and the IR spectrum contained three inequivalent ν_{CO} values (1950, 1879 and 1830 cm^{-1}).[38] X-ray quality crystals of **23** were grown from a solution of **22** under CO (**Structure 4.1**).

The bond lengths in **23** are comparable to the analogous mixed PPh_3/NHC system $Ru(PPh_3)(IMes)(CO)_3$ (**29**).[18,42] However, the angles between the carbonyl groups differ substantially between **23** and **29** as shown in **Figure 4.11** below, with **23** differing more markedly from the ideal trigonal bipyramidal geometry.[18,42] However, unlike **29** all of the carbonyl ligands in **23** lie in the same plane and the sum of the equatorial ligands was 360° so the values given in **Table 4.5** are not ambiguous.

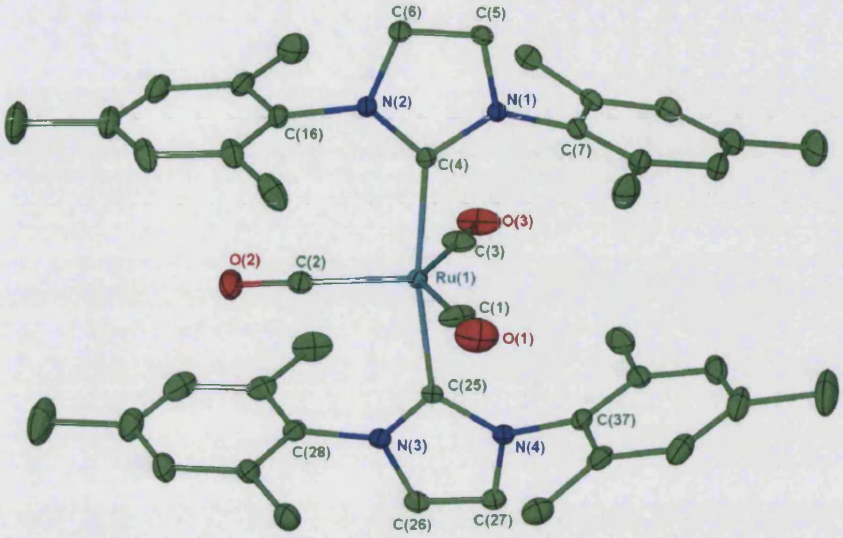

Structure 4.1 X-ray structure of $Ru(IMes)_2(CO)_3$ (**23**). Thermal ellipsoids are set at 30 % probability. Hydrogen atoms have been omitted for clarity.

	23	**29** [42]	**29** [18]
Ru-C(1)	1.944(3)	1.906(3)	1.91(2)
Ru-C(2)	1.927(2)	1.918(3)	1.92(2)
Ru-C(3)	1.900(3)	1.924(2)	1.93(2)
Ru-C(4)	2.1093(19)	2.111(2)	2.12(2)
Ru-C(25)	2.1125(19)	-	-
C(4)-Ru-L_{axial}	169.16(7)	174.77(6)	171.4(3)

Table 4.5 Selected bond lengths (Å) and angles (°) for **23** and **29** with[42] and without[18] a benzene molecule with half site occupancy.

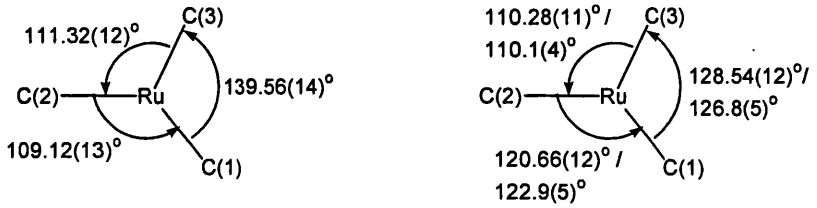

23 **29**

Figure 4.11 A pictorial representation of the equatorial ligands of **23** and **29** with corresponding bond angles to display ligand distribution. (Top values given for **29** refer to the structure containing a molecule of benzene).

The relatively large angle of 139.56(14)° between C(1) and C(3) in **23** may be due to steric constraints. The IMes arms lie over the Ru-C(3) axis, consequently the carbonyl on C(3) lies away from the methyl arms of IMes (3.846-4.130 Å $O_{carbonyl}$-C_{methyl} distance through space). In contrast C(1) and C(3) carbonyl ligands lie closer in space to the methyl groups of IMes (3.034-3.288 Å $O_{carbonyl}$-C_{methyl}), so are probably more affected by steric effects. Additionally, the IMes ligands are also bent in slightly toward the C(1) and C(3) side of the complex {C(4)-Ru-C(25) = 169.16(7)°}, further enhancing the role of steric factors. By comparison the mono NHC complex **29** (with[42] and without[18] a molecule of benzene with half site occupancy) only suffers slightly from increased bond angle between the equivalent C(1) and C(3) sites (128.54(12)° and 126.8(5)° respectively), presumably because there is one less IMes group to cause steric crowding. It is relevant that **29** adopts a staggered orientation of the R groups relative to the $Ru(CO)_3$ core, consistent with related bis phosphine complexes $Ru(PR_3)_2(CO)_3$ (R = Me_3,[43] Ph_3,[44] Cy_3[45]). This method of relieving steric tension cannot apply to **23** as the mesityl arms produce a 2-fold axis incompatible with the 3-fold axis of the carbonyl ligands.

Morris acknowledged the effects of steric tension in the structure of $Ru(PPh_3)(IMes)(CO)_3$, noting that two of the carbonyl ligands are affected by being positioned directly below one of the mesityl arms. To 'relieve steric tension' they bend away from the IMes ligand causing OC-Ru-C_{NHC} angles to exceed 90°{93.7(4) and

96.3(4)° vs. 84.8(4)° for the third CO ligand}.[18] In the structure of **29** by Jazzar, C(2) and C(3) each lie below a mesityl arm and consequently the OC-Ru-C_{NHC} values for these angles are also greater than 90° {96.45(10) and 93.45(10) vs. 88.02(10) for C(1)}. In comparison, the carbonyl ligands in **23** cannot bend way from both IMes ligands, instead the response to steric bulk is probably accounted for by the equatorial spread of the carbonyl groups.

4.11 Treatment of $Ru(IMes)_2(CO)(\eta^2\text{-}BH_4)H$ (19) with ^{t}BuNC

$Ru(IMes)_2(CO)(\eta^2\text{-}BH_4)H$ (**19**) was reacted with excess ^{t}BuNC as a comparison to the reaction with CO. Addition of ^{t}BuNC at 298 K did not cause immediate full conversion to a new product, but required long periods at 298 K for any significant changes in the ^{1}H NMR spectrum to be observed (**Figure 4.12**). The ^{1}H NMR spectrum showed a decrease in the diagnostic **19** hydride resonance and the appearance of four new hydride signals, the major one being a singlet at -8.01 ppm. Other signals were relatively weak in comparison but included two doublets at -6.47 and -8.05 ppm (both J_{HH} = 5.6 Hz) and a singlet (-6.64 ppm). It was anticipated that the two minor doublet signals were the expected product $Ru(IMes)_2(CO)(CN^tBu)H_2$, but this could not be confirmed as conversion remained very low at 298 K.

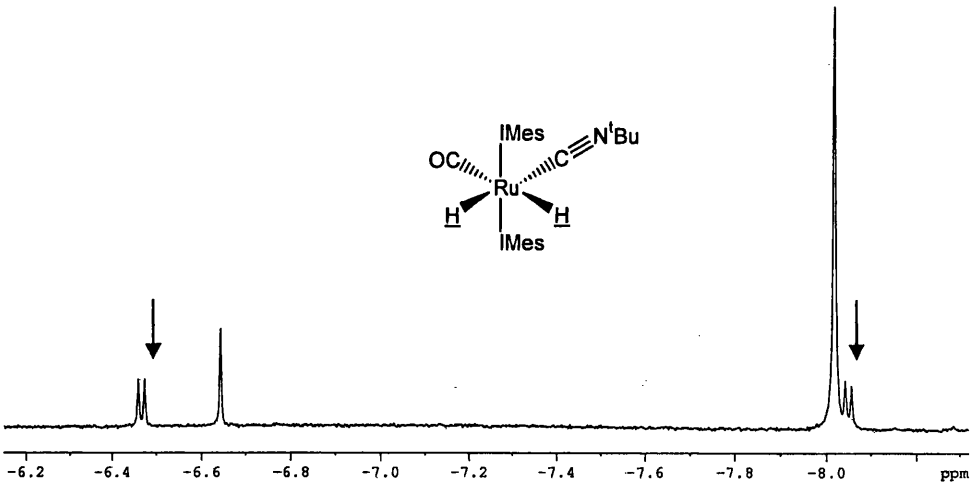

Figure 4.12 ^{1}H NMR spectrum of the reaction of **19** with tBuNC after 16 h and proposed assignment of the doublet resonances ($C_6D_5CD_3$, 298 K, 400 MHz).

A clear contrast between the reaction of **19** with CO and the reaction with ^{t}BuNC is the retention of the hydride ligand in the latter case. On this basis it was believed that identification of the intermediate η^1-BH_4^- speces $Ru(IMes)_2(CO)(\eta^1\text{-}BH_4)(CN^tBu)H$ might be likely. However, low temperature ^{1}H NMR spectra of the reaction between 298 and 228 K showed the bridging BH_4^- hydrogen atoms for the starting complex **19** in addition to the resonances displayed in **Figure 4.12**, but no evidence of the hoped for intermediate η^1-bound species.

The reaction of **19** with ^{t}BuNC was followed over a period of 5 days at 298 K and the ^{1}H NMR spectra showed continuing decrease in the amount of **19** and subsequent increase in the integrals of the reaction products (the intensities of all four signals remained relatively consistent over the time with respect to each other). Signals in the methyl region of the spectrum were integrated to reveal a correlation between the new major hydride signal (-8.01 ppm, 1H) and methyl resonances of IMes at 2.22 and 1.87 ppm (36H). Additionally, the ^{1}H-^{13}C{^{1}H} HMBC spectrum displayed crosspeaks linking the major hydride resonance with four ^{13}C{^{1}H} chemical shifts at 201.6, 182.1, 146.9 and 143.7 ppm. The first two ^{13}C values can be attributed to the $C_{carbonyl}$ and C_{NHC} carbon atoms respectively. However, the two remaining crosspeaks are consistent with two bound ^{t}BuNC moieties rather than one as expected.[46]

Small crystals of the major product (-8.01 ppm) were formed from toluene layered with hexane. The IR spectrum contained bands at 1965 and 1954 cm^{-1}, which correspond to either υ_{CO} or $\upsilon_{Ru\text{-}H}$ and bands at 2150 and 2123 cm^{-1}, consistent with other complexes containing bis ^{t}BuNC ligands.[47] The X-ray structure of the crystals revealed that the complex is cationic with a chloride anion and contained two ^{t}BuNC ligands in a *cis* geometry (**Structure 4.2**). The asymmetric unit contained one molecule of the complex and two toluene molecules with an additional toluene disordered over two sites in a 35:65 ratio.

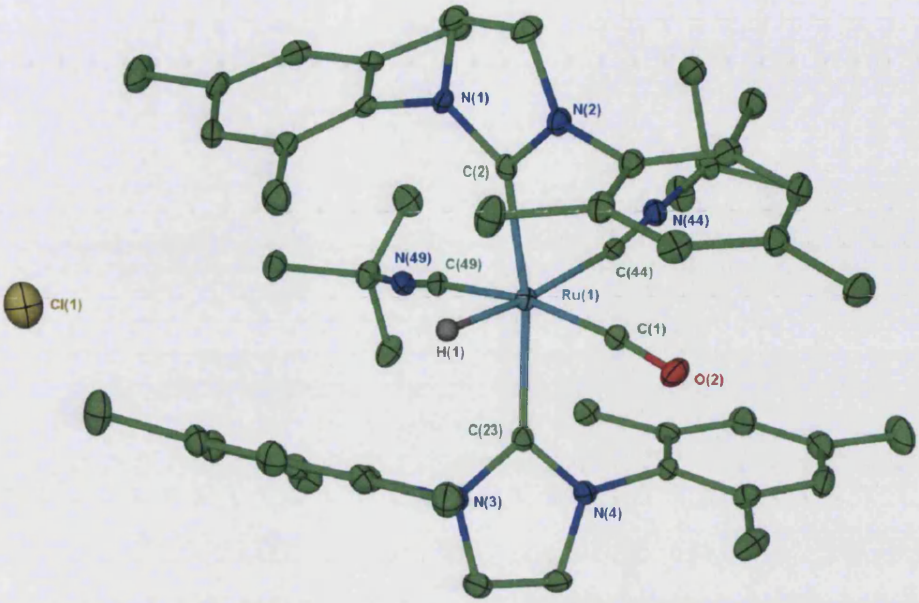

Structure 4.2 X-ray structure of $[Ru(IMes)_2(CO)(CN^tBu)_2H]^+Cl^-$ (**24**). Thermal ellipsoids are set at 30 % probability. Hydrogen atoms have been omitted for clarity (except the hydride).

	24
Ru-C(2)	2.100(5)
Ru-C(23)	2.126(5)
Ru-C(1)	1.872(6)
Ru-C(44)	2.034(6)
C(44)-N(44)	1.160(6)
Ru-C(49)	2.071(6)
C(49)-N(49)	1.141(6)
C(2)-Ru-C(23)	165.42(18)

Table 4.6 Selected bond lengths (Å) and angles (°) for **24**.

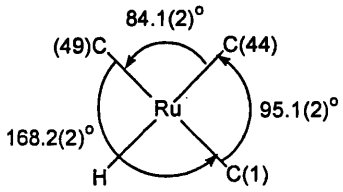

Figure 4.13 A pictorial representation of the equatorial ligands of **24**.

As with all of the 6-coordinate complexes in this thesis, the ligands of **24** bend towards the hydride ligand to overcome steric repulsion. The IMes twist angle is relatively high (67.1 °) due to the bulky *cis* ^{t}BuNC ligands. Otherwise, the metrics of **24** are typical of bis IMes complexes.

4.12 Treatment of $Ru(IMes)_2(CO)(\eta^2\text{-}BH_4)H$ (19) with Lewis bases

This section of work involved the use of reagents considered likely to abstract BH_3 from **19** as adducts. Although some of the substrates that have been previously discussed can also be described as nucleophiles they were chosen moreso for their small size. There is precedence for the use of Lewis bases in removing BH_3,[48] and it has been developed as a method for producing more active catalysts especially in *in situ* reactions.[10, 11, 49] Lewis bases can be used to extract BH_3 so that the complex species is susceptible to attack by another substrate {for example, NEt_3 was used to abstract BH_3 from $Ru(PR)_3(\eta^2\text{-}BH_4)H$ (R = $MePh_2$[11] or Me_3[22]) to create a vacant site for CO to occupy}.

4.13 Treatment of $Ru(IMes)_2(CO)(\eta^2\text{-}BH_4)H$ (19) with N-containing nucleophiles: NEt_3; 4-picoline (4-Mepy); MeCN

19 was treated with various N-containing nucleophiles to investigate whether BH_3 could be extracted from $Ru(IMes)_2(CO)(\eta^2\text{-}BH_4)H$ to form the dihydride complex $Ru(IMes)_2(CO)H_2$. However, no reactions occurred between **19** and NEt_3, 4-Mepy and

MeCN respectively on addition of 1-5 equiv. of the substrates over prolonged periods (up to a week) and at increased temperatures (up to 343 K).

4.14 Treatment of $Ru(IMes)_2(CO)(\eta^2\text{-}BH_4)H$ (19) with IMes

Adding IMes to a sample of **19** was proposed to act as a nucleophile and subsequently remove BH_3 as the IMes.BH_3 adduct. Initially only one equivalent of IMes was used, sufficient for adduct formation but not enough to bind to the metal centre. There are no *tris* or *cis* bis ruthenium IMes complexes known, (probably due to steric factors) suggesting that once a vacant site is produced it would remain vacant. However, treating **19** with IMes did not afford a dihydride product. In fact no change was observed by ^{1}H NMR spectroscopy acquired at 298 K. Only the characteristic hydride signal of **19** at -16.28 ppm was apparent even after prolonged periods of time and heating to 343 K. Increasing the number of equivalents of IMes used (up to 10 equiv.) did not affect the outcome.

4.15 Treatment of $Ru(IMes)_2(CO)(\eta^2\text{-}BH_4)H$ (19) with PMe_2Ph

A similar approach was attempted using phosphine to remove BH_3 as a $PMe_2Ph.BH_3$ adduct. However, phosphines are known to act as both a Lewis base for BH_3 abstraction and a ligand. For example, reacting PMe_3 with $Ru(PMe_3)_3(\eta^2\text{-}BH_4)H$ affords $Ru(PMe_3)_4H_2$[22] and the reaction of $Ru(PMe_2Ph)_2(CO)(\eta^2\text{-}BH_4)H$ with two equivalents of the corresponding free phosphine yields $Ru(PMe_2Ph)_3(CO)H_2$.[21]

No reaction was observed between **19** and PMe_2Ph at room temperature or at 323 K. However, increasing the reaction temperature to 343 K for two days resulted in the formation of a new complex (**25**). The ^{1}H NMR spectrum displayed two new resonances in the hydride region at -6.78 and -7.97 ppm, each as a doublet of doublets of doublets (**Figure 4.14**). This extensive coupling suggested that the complex is comprised of more than one phosphorus atom, confirmed by the $^{31}P\{^1H\}$ NMR spectrum having two ^{31}P signals at 5.7 and 18.4 ppm (each a doublet with J_{PP} = 21.6 Hz). So treatment of **19** with PMe_2Ph did not simply produce

$Ru(PMe_2Ph)(IMes)_2(CO)H_2$ as expected but another species containing two phosphine ligands, namely $Ru(PMe_2Ph)_2(IMes)(CO)H_2$ (**25**).

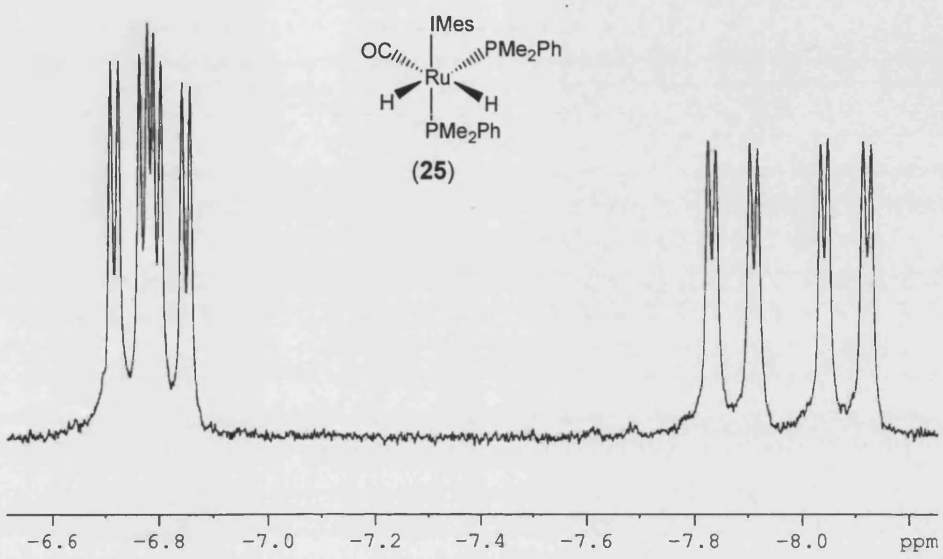

Figure 4.14 Hydride signals in the ^1H NMR spectrum of **25** (298 K, C_6D_6, 400 MHz).

The ^1H-^{31}P coupling constant values helped to determine the structure of **25** as that shown in **Figure 4.14**, by studying the relative positions of the hydride and phosphine ligands. The more downfield signal (-6.78 ppm) has coupling constant values consistent with a hydride lying mutually *cis* to two ^{31}P nuclei (J_{HP} = 32.4 and 31.5 Hz) and *cis* to the other hydride ligand (J_{HH} = 6.0 Hz). The hydride represented by the signal at -7.97 ppm appears to be both *trans* (J_{HP} = 84.5 Hz) and *cis* (J_{HP} = 30.7 Hz) to a phosphorus atom, with a small coupling constant attributable to H-H *cis* coupling (J_{HH} = 6.0 Hz). These assignments are similar to those for $Ru(PPh_3)_2(IMes)(CO)H_2$ {-6.36 ppm (J_{HP} = 26.8, 23.6 Hz; J_{HH} = 6.0 Hz), -8.08 ppm (J_{HP} = 81.2, 33.6 Hz; J_{HH} = 6.0 Hz)}.[50]

Similarities were also apparent in the ^{13}C NMR spectroscopic data for **25** and $Ru(PPh_3)_2(IMes)(CO)H_2$. Carbonyl and carbenic carbon atom resonances for **25** appeared at 205.9 ppm (t, J_{CP} = 8.3 Hz) and 197.8 ppm (d,d, J_{CP} = 75.4 and 9.2 Hz)

respectively. Comparative values for $Ru(PPh_3)_2(IMes)(CO)H_2$ are 205.2 ppm (t, J_{CP} = 8.8 Hz) and 197.7 ppm (d,d, J_{CP} = 75.5 and 6.7 Hz).[50]

Formation of **25** from **19** implies that an IMes ligand has been replaced by a phosphine ligand. Phosphine substitution of an NHC has been previously described by the Whittlesey group en-route to the C-C activated complex and also by others.[51, 52] However, here this is likely to be a gross oversimplification. It is important to note that only a slight excess of PMe_2Ph (1.2 equiv.) was used but each molecule of complex contains two phosphine ligands! Therefore, some degradation of the complex may take place before **25** is produced.

The NMR spectra taken after the reaction of **19** with PMe_2Ph showed resonances in line with the literature values for $PMe_2Ph.BH_3$[24, 53] providing evidence for the first option. A broad lump at 0.54 ppm by ^1H NMR spectroscopy related to the BH_3 protons of the phosphine adduct $PMe_2Ph.BH_3$, and further study of the ^{31}P NMR spectrum showed a quartet at 3.06 ppm. However there is also evidence of $IMes.BH_3$ (**20**) being formed. Attempted crystallisation of **25** from benzene layered with hexane precipitated powder with ^1H and $^{11}B\{^1H\}$ NMR spectroscopic data consistent with $IMes.BH_3$, while **25** remained in solution. Alternatively **25** can also be prepared by reaction of $Ru(IMes)(PPh_3)_2(CO)H_2$ with PMe_2Ph but the complex is incredibly soluble in a range of solvents including hexane, EtOH and EtO, preventing isolation.

4.16 Formation of the mixed NHC/phosphine borohydride complex $Ru(PPh_3)(IMes)(CO)(\eta^2\text{-}BH_4)H$ (26)

Reaction of $Ru(PPh_3)(IMes)(CO)(Cl)H$ with excess $NaBH_4$ at 298 K produced the mixed NHC/phosphine complex $Ru(PPh_3)(IMes)(CO)(\eta^2\text{-}BH_4)H$ (**26**). It was anticipated that moving away from the umbrella-like steric protection of the bis IMes ligands in $Ru(IMes)_2(CO)(\eta^2\text{-}BH_4)H$ (**19**) to a mono NHC species such as **26** might alter reactivity and perhaps result in more facile loss of BH_3 and the production of the dihydride complex $Ru(PPh_3)(IMes)(CO)H_2$.

The mixed NHC/phosphine BH_4^- system **26**, not only served as a natural comparison to **19**, but is the 'missing link' between our bis IMes BH_4^- system and the array of bis phosphine BH_4^- complexes that have been prepared by other groups.[6-12, 21, 23, 25]

4.16.1 Synthesis and characterisation of $Ru(PPh_3)(IMes)(CO)(\eta^2\text{-}BH_4)H$ (27)

$Ru(PPh_3)(IMes)(CO)(\eta^2\text{-}BH_4)H$ (**26**) was prepared by the same method described for **19**, by reaction of $Ru(PPh_3)(IMes)(CO)(Cl)H$ (**8**) with excess $NaBH_4$ in EtOH at 298 K (**Scheme 4.16**). The reaction took place with a corresponding colour change from yellow to straw. In the ^1H NMR spectrum there was loss of the starting complex (-23.89 ppm, J_{HP} = 24.3 Hz)[54] and the appearance of a new doublet hydride at -13.36 ppm (J_{HP} = 23.1 Hz).

The PPh_3 ligand in **26** provided an extra characterisation handle (over **19**), so reactions of **26** were also followed by $^{31}P\{^1H\}$ NMR spectroscopy. The $^{31}P\{^1H\}$ NMR spectrum of **26** displayed a new singlet at 52.0 ppm, (downfield from the starting material **8** at 42.1 ppm)[54] as confirmed by locating a crosspeak in the $^{31}P\{^1H\}$-^1H HMQC spectrum relating to the hydride shift. Unfortunately it was not possible to observe coupling between the bridging BH_4^- hydrogen atoms and the phosphorus atom by $^{31}P\{^1H\}$-^1H correlation spectroscopy.

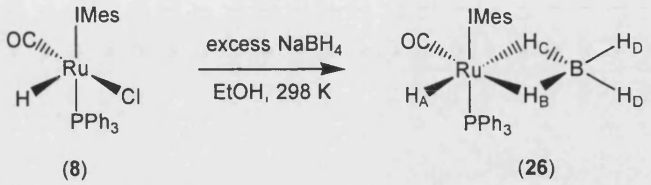

(8) (26)

Scheme 4.16 Formation of $Ru(PPh_3)(IMes)(CO)(BH_4)H$ (**26**).

In contrast to $Ru(IMes)_2(CO)(\eta^2\text{-}BH_4)H$ (**19**), the bridging and terminal hydrogen atoms of the BH_4^- in **26** were observed by ^1H NMR spectroscopy at 298 K, although cooling does make the spectrum clearer (**Figure 4.15**). Pronounced H_B, H_C and H_D signals for **26** at ambient temperatures suggested that the BH_4^- hydrogen atoms in the mixed IMes/PPh_3 complex were less fluxional than those in **19**. This notion is covered in more detail later in section **4.18**.

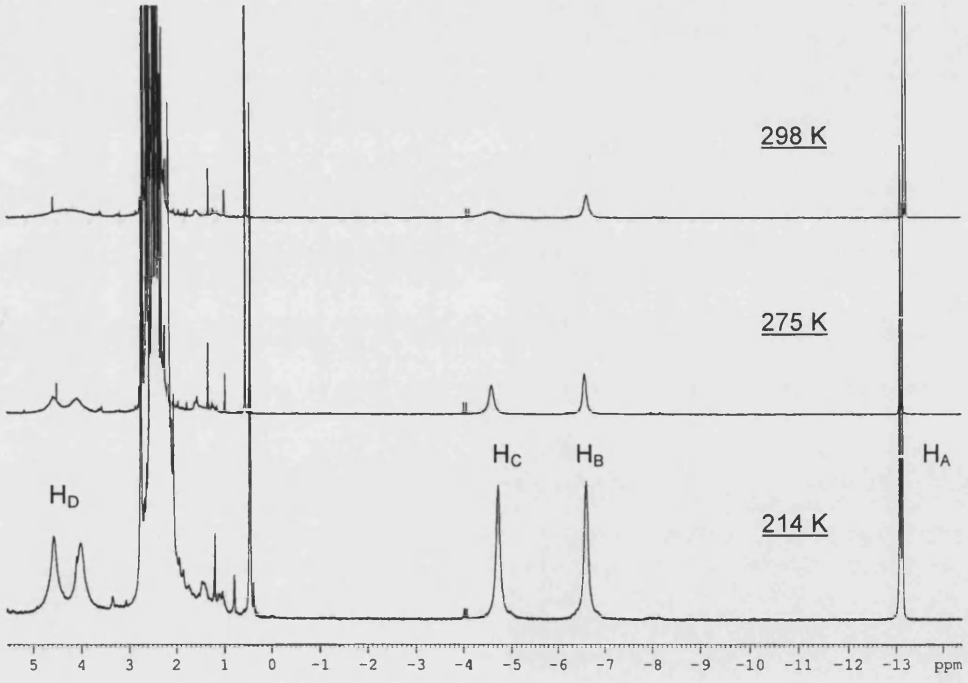

Figure 4.15 The effect of temperature on the ^1H NMR spectrum of **26** ($C_6D_5CD_3$, 400 MHz).

Figure 4.15 shows the terminal hydrogen signal (H_D) splitting into two separate resonances (4.56 and 4.09 ppm) at 275 K, whereas the equivalent H_D resonance in **19**

did not split at even 214 K. Decreasing the temperature affected the position of the resonance for H_A in **26** causing a slight downfield shift, noticeable in **Figure 4.15**.

T_1 measurements for the hydrogen atoms of Ru-H and BH_4^- in **26** (**Table 4.7**) are similar to those determined for **19** (**Table 4.2**, p. 122), although the T_1 values for the H_D nuclei indicate a faster rate of relaxation than the bridging hydrogen atoms, consistent with the equivalent value for $Ru(PMe_2Ph)_2(CO)(\eta^2\text{-}BH_4)H$ (97 ms, 213 K). This effect is most likely due to the fact that terminal B-H bonds are generally shorter than their bridging counterparts.

Hydride	^{1}H NMR shift (ppm)	T_1 (ms) (214 K)
H_A	-13.11 (22.5 Hz)	853
H_B	-6.62	129
H_C	-4.72	131
H_D (2H)	4.00, 4.56	104, 106

Table 4.7 ^{1}H NMR shifts and T_1 values for hydrogen atoms associated with $Ru(PPh_3)(IMes)(CO)(\eta^2\text{-}BH_4)H$ (**26**) (214 K, $C_6D_5CD_3$, 400 MHz).

The $^{13}C\{^1H\}$-^{31}P coupling constants for **26** are consistent with a *cis* (CO)-(PPh_3) ligand arrangement (J_{CP} = 14.7 Hz) and IMes *trans* to PPh_3 (J_{CP} = 90.1 Hz). **Table 4.8** below displays the $^{13}C\{^1H\}$ NMR resonances for BH_4^- systems containing a decreasing number of IMes ligands [**19** > **26** > $\{Ru(PMe_2Ph)_2(CO)(\eta^2\text{-}BH_4)H\}$] and some of the corresponding starting materials. The $^{13}C\{^1H\}$ values suggest that the $^{13}C_{carbonyl}$ resonances do not vary significantly over the range of complexes and that the $^{13}C_{NHC}$ signals move slightly downfield with exchange of IMes for PR_3.

$RuL_2(CO)(X)H$	$X = \eta^2\text{-}BH_4$		X = Cl	
L_2 =	CO	Ru-C	CO	Ru-C
$(IMes)_2$ (19) / (7)	205.6	194.1	202.8	195.9
(PPh_3)(IMes) (26) / (8)	205.6 (14.7 Hz)	190.9 (90.1 Hz)	201.4 (14.4 Hz)	189.7 (103.6 Hz)
$(PMe_2Ph)_2$ [21]	203.7	-	-	-

Table 4.8 $^{13}C\{^1H\}$ NMR data (ppm) for $C_{carbonyl}$ and C_{NHC} atoms of a series of BH_4^- and chloride complexes with a decreasing number of IMes ligands going downwards.

The $^{11}B\{^1H\}$ NMR spectrum of **26** was inconclusive; an incredibly broad signal at *ca.* 1 ppm did not sharpen by altering the acquisition temperature (190 - 323 K, $CD_3C_6D_5$).

The IR spectrum of **26** was similar to that obtained for $Ru(IMes)_2(CO)(\eta^2\text{-}BH_4)H$ (**19**), the only value of any notable difference being υ_{CO} at 1927 cm^{-1} in contrast to 1900 cm^{-1}. This shift to a higher wave number is expected as phosphines have reduced donor capacity compared to NHCs.

Although crystals of **26** were formed readily in a range of different solvent mixtures, the resultant crystals were fine needle-like structures and not of X-ray quality.

4.17 Attempted formation of $Ru(PPh_3)(IMes)(CO)H_2$ from $Ru(IMes)(PPh_3)(CO)(\eta^2\text{-}BH_4)H$ (26)

It was anticipated that **26** may be a more reactive species than **19** and possibly lead to the dihydride complex $Ru(PPh_3)(IMes)(CO)H_2$. However, **26** was the only species observed upon reaction with either protic solvents or with H_2, as was the case for **19** (298 K). Upon degradation at 323 K in MeOH (16 h), the well-known complex $Ru(PPh_3)_3(CO)H_2$ was observed in the ^1H NMR spectrum.

4.18 Investigating fluxionality and the 'opening up' process in $Ru(PPh_3)(IMes)(CO)(\eta^2\text{-}BH_4)H$ (26)

VT studies have been essential in investigating the 'opening up' processes in related BH_4^- complexes.[10, 12, 21, 23] The BH_4^- hydrogen resonances of **26** were readily apparent by ^1H NMR spectroscopy over a range of temperatures (unlike **19**), so **26** was considered a reliable candidate for VT studies. As depicted previously, the ^1H NMR spectrum of **26** (**Figure 4.15**, p. 153) displayed a broader resonance for H_C at 298 K than the other bridging hydrogen resonance H_B, with peak widths of 168.0 and 47.2 Hz respectively at half height. The relative broadness' of H_B and H_C remained consistent down to 214 K, implying that H_C is the more fluxional bridging hydrogen. Thus, 'opening up' appears to take place at H_C *trans* to the hydride ligand leaving H_B, as a bridging atom (**Scheme 4.17**). This qualitative approach has also been used by other authors.[10, 12, 21, 23] For example, Wilkinson reported that exchange between the terminal B-H atoms (H_D) and μ-H-B *trans* to the hydride ligand (H_C) in $Ru(PMe_3)_3(\eta^2\text{-}BH_4)H$ occurred at 353 K, whereas further exchange with μ-H-B *trans* to the phosphine ligand (H_B) required higher temperatures (383 K),[12] thus, implying that the Ru-H_C bond breaks more readily than its Ru-H_B. Meek reported similar behaviour for $Ru(ttp)(\eta^2\text{-}BH_4)H$, with the collapse of the signal for H_C occurring at lower temperatures than that for H_B.[10]

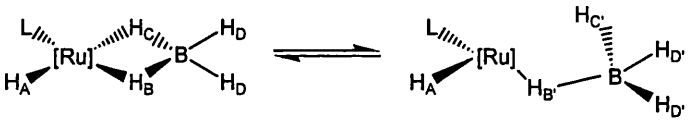

Scheme 4.17 The proposed route to an $\eta^1\text{-}BH_4^-$ opened up intermediate. [Ru] represents the metal centre with bound axial ligands and L = CO (**26**, **19**), PMe_3,[12] ttp[10] or $PMePh_2$.[21]

Lowe supported his experimental findings with a quantitive study on the T_1 values calculated for the BH_4^- hydrogen atoms in $Ru(PMe_2Ph)_2(CO)(\eta^2\text{-}BH_4)H$ over a range of temperatures.[24] At higher temperatures, the T_1 values for H_C become similar to those calculated for the terminal hydrogen atoms (H_D), suggesting that H_D and H_C are becoming more alike and therefore that H_C is fluxional. **Table 4.9** shows the effect of

increasing temperature on the T_1 values calculated for **26**. The results mimic those observed by Lowe and the similarity in the T_1 values at 275 K between H_C and the terminal H_D atoms endorses the idea that it is the B-H_C bond that is broken to achieve a η^1-BH_4^- intermediate.

Temperature (K)	H_A	H_B	H_C	H_D
214	853	129	131	104, 106
235	649	92	94	69, 77
255	790	84	80	64, 79
275	765	100	79	73, 76

Table 4.9 T_1 values (ms) calculated for hydrogen atoms associated with $Ru(PPh_3)(IMes)(CO)(\eta^2\text{-}BH_4)H$ (**26**) (shown) over a range of temperatures ($C_6D_5CD_3$, 400 MHz).

Selective irradiation of the hydride and BH_4^- resonances (at 273 K) of Lowe's complex $Ru(PMe_2Ph)_2(CO)(\eta^2\text{-}BH_4)H$ also provided evidence for the preferential breaking of Ru-H_C over Ru-H_B, as irradiation of the terminal hydrogen nuclei (H_D) affected the intensity of the signal for H_C but not H_B. The same approach was used to study **26** with similar results. The only effect seen occurred on irradiation of H_C at 275 K. This experiment caused H_D signals to collapse slightly into the baseline implying that H_C and H_D hydrogen atoms are undergoing exchange. However, at 235 K where H_D peaks are more pronounced, no evidence of collapse was seen.

Lowe was also able to use ^1H-^{31}P correlation data to further establish that the Ru-H_C bond is broken in $Ru(PMe_2Ph)_2(CO)(\eta^2\text{-}BH_4)H$ to form the η^1-BH_4^- intermediate, whilst Ru-H_B remains intact. Lowe found evidence of correlation (at 203 K) between the phosphorus nuclei and the bridging non-fluxional hydrogen in his system (H_B). Meek was also able to observe retention of *trans* ^{31}P-^1H coupling (due to H_B) in $Ru(ttp)(\eta^2\text{-}BH_4)H$ in the range 338-348 K (presumably J_{PHcis} from H_C was not seen).[10] In contrast, **26** did not show any correlation between PPh_3 and either of the bridging

hydrogen atoms (H_B or H_C) in the ^1H-^{31}P HMQC spectrum, even at low temperature (190 K).

Our findings for **26** are in agreement with majority of the work done on the initial switch in coordination modes from η^2 to η^1-BH_4^-. Wilkinson, Meek and Lowe both concluded that B-H bonds *trans* to the hydride ligands are preferentially broken. A notable exception is the study carried out by Werner on $Ru(L)_2(CO)(BH_4)H$ (L = P^iPr_3, PMe^tBu_2).[23] Although the NMR spectroscopic data are similar to that of others Werner claimed that it is the B-H bond *trans* to the carbonyl ligand that breaks preferentially. This argument was based on the relative broadening behaviour of the bridging hydride resonances with the more downfield shift broadening more rapidly. It is important to note that the bridging hydrogen atoms were assigned the opposite way round to other examples of this type, although the basis of this assignment was unclear.

In summary, the experimental evidence suggests that 'opening up' in **26** occurs at H_C leaving H_B as a bridging hydride and creating a vacant site *trans* to the hydride ligand, consistent with majority of related BH_4^- systems. These findings are mainly based upon the effect of VT on the bridging B-H hydrogen atoms of **26** and on the T_1 values calculated for relevant hydrogen atoms of **26**. The selective irradiation of H_C slightly affecting H_D resonances at 275 K is not totally conclusive but follows the other results well.

4.18.1 Treatment of $Ru(PPh_3)(IMes)(CO)(\eta^2\text{-}BH_4)H$ (26) with D_2

Samples of $Ru(PPh_3)(IMes)(CO)(\eta^2\text{-}BH_4)H$ (**26**) in C_6D_6 and C_6H_6 were exposed to 1 atm of D_2 at 298 K and followed by ^1H and ^2H NMR spectroscopy, to investigate whether D-incorporation occurs more readily than in the analogous reactions with $Ru(IMes)_2(CO)(\eta^2\text{-}BH_4)H$ (**19**). Unlike **19** the ^1H NMR spectra of **26** did not exhibit any significant integral decreases with respect to the backbone protons; in fact, after 2 weeks at 298 K all of the BH_4^- hydrogen signals had decreased by only *ca.* 20 %. The ^1H NMR spectra did imply that D-incorporation was occurring in some way by

mutations in the resonances for isotopomers of **26**, especially one of the H_D signals, H_C and H_A as displayed in **Figure 4.16**.

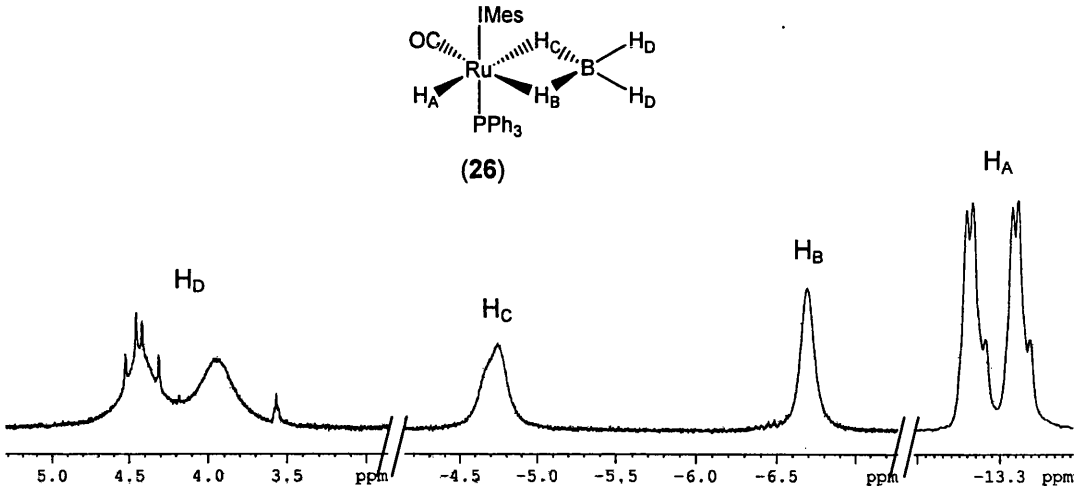

Figure 4.16 ^1H NMR spectrum of $Ru(PPh_3)(IMes)(CO)(\eta^2\text{-}BH_4)H$ (**26**) with D_2 after 10 days at 298 K (C_6D_6, 280 K, 400 MHz).

The ^2H NMR spectra were more revealing, showing evidence of H/D scrambling in the H_A position of **26** after 2-3 days at 298 K. After 10 days the spectrum showed resonances for D in the other BH_4^- positions H_B, H_C and H_D, consistent D-incorporation into the BH_4^- ligand.

4.19 Formation of the borodeuteride complex $Ru(PPh_3)(IMes)(CO)(\eta^2\text{-}BD_4)H$ (26-d_4)

The borodeuteride complex $Ru(PPh_3)(IMes)(CO)(\eta^2\text{-}BD_4)H$ (**26-d_4**) was prepared by reacting $Ru(PPh_3)(IMes)(CO)(Cl)H$ (**8**) with excess $NaBD_4$ in ethanol, analogous to the formation of **26-d_4** (**Scheme 4.18**).

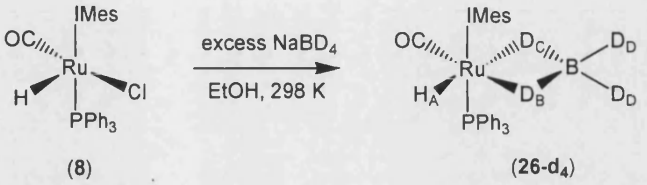

(8) (26-d_4)

Scheme 4.18 Formation of $Ru(PPh_3)(IMes)(CO)(BD_4)H$ (**26-d_4**).

The ^1H NMR spectrum of **26-d_4** at 280 K shown in **Figure 4.17** served to confirm the continued presence of a hydride ligand at -13.36 ppm (H_A) and showed very small BH_4^- signals from incomplete deuteration. The integral ratios between H_C, H_D and H_A were considered low enough to disregard (*ca.* 0.02 with respect to the backbone protons). Deuterium resonances of BD_4^- were seen in the ^2H NMR spectrum as expected at 4.56 and 4.09 (D_D), -4.62 (D_C) and -6.57 ppm (D_B) at 280 K (also **Figure 4.17**). By ^2H NMR spectroscopy at 280 K the difference in broadness for peaks D_B and D_C was incredibly noticeable; the same effect was apparent in the ^1H NMR spectrum for **26** but less pronounced. It is interesting to note that there is a small amount of deuteration of the hydride of **26-d_4**.

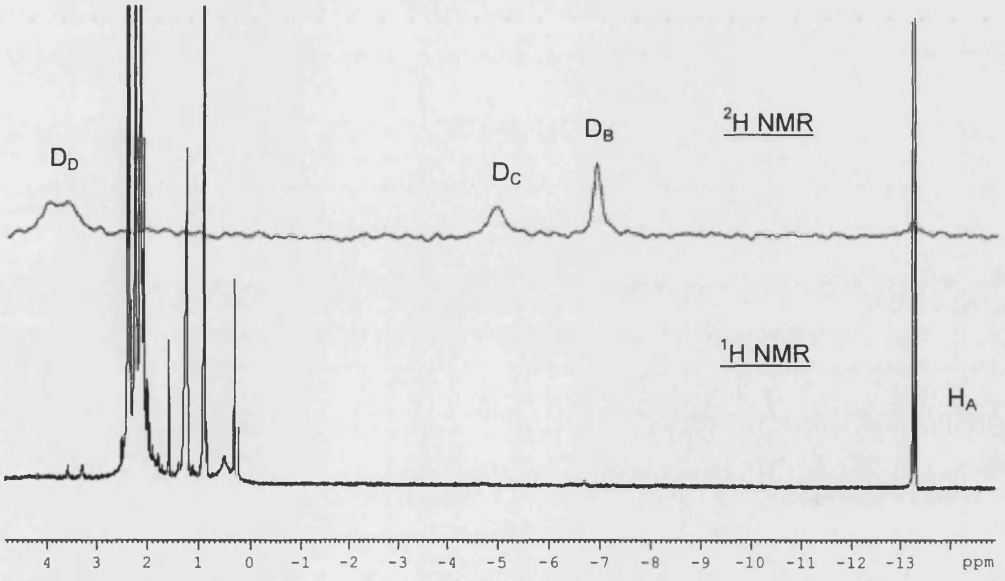

Figure 4.17 ^2H and ^1H NMR spectra for **26-d_4** (C_6D_6, 280 K).

The $^{31}P\{^1H\}$ NMR resonance remains totally unchanged between **26** and **26-d$_4$** remaining as a singlet at 52.0 ppm although a 1:1:1 triplet was expected, due to ^{31}P-^2H coupling. However, it was not possible to observe splitting due to J_{PD}, perhaps unsurprisingly as the expected splitting would be *ca.* 7 times smaller of that seen for J_{PH}. This comes about because of the relationship between coupling constant values and the gyromagnetic constant (γ).

$$J_{AB} \propto \gamma_A\gamma_B$$

γ is so much smaller for D than for H (4.11 x 10^7 rad T^{-1} s^{-1} and 26.75 x 10^7 rad T^{-1} s^{-1}) that J_{PD} would easily be lost in the broadness of the resonance (*ca.* 4 Hz line width at half height).

IR spectroscopy is the most clear spectroscopic technique to show changes brought about by the borodeuteride group. The carbonyl stretch is relatively unaffected by the switch from BH_4^- to a BD_4^- moiety (1927 and 1924 cm^{-1} respectively), as was also the case for **19** and **19-d$_4$**. Major differences occur in the frequencies associated with the borodeuteride/borohydride groups as discussed earlier in the text with respect to **19** and **19-d$_4$**. Bands at 1825, 1764 and 1715 cm^{-1} correspond to the terminal B-D stretches, $B\text{-}D_{deformation}$ was observed at 855 cm^{-1} and $B\text{-}D_B$-Ru bending at 1028, 1091 and 1156 cm^{-1}.

4.19.1 Treatment of Ru(PPh$_3$)(IMes)(CO)(η^2-BD$_4$)H (26-d$_4$) with H$_2$

A sample of **26-d$_4$** was treated with 1 atm H_2 at 298 K and spectra were recorded over 3 weeks at 280 K to allow clear observation of the BH_4^- resonances (**Figure 4.18**). The H_D signal was not followed quantitively as the chemical shift for free H_2 lay in the same region, complicating the integrals. After 1 day under H_2 there was a slight increase in the H_B and H_C signals in the ^1H NMR spectrum, but most noticeably, the H_A signal had decreased in intensity by *ca.* 25 % (with respect to the backbone protons,

which were used as a constant reference of 2 protons). The spectrum acquired after 4 days displayed H_A with half its original intensity and resonance H_B and H_C having grown to 0.15. In the subsequent spectra (6, 10, 21 days), the H_A integral did not decline much more but isotopomers of H_A were apparent, whereas resonances H_B and H_C continued to grow, to reach *ca.* 0.3 after 21 days. At this time, the ^2H NMR spectrum showed a large quantity of D-incorporation into the hydride position, consistent with decrease of the Ru-hydride integral over the 3 week reaction time. It was concluded that D lost from the BD_4^- moiety is incorporated into the hydride position. The ^1H NMR spectra failed to show significant amounts of HD formation throughout the experiment, perhaps implying that H/D exchange may have occurred *via* the hydride ligand or that D-incorporation into the hydride position is rapid.

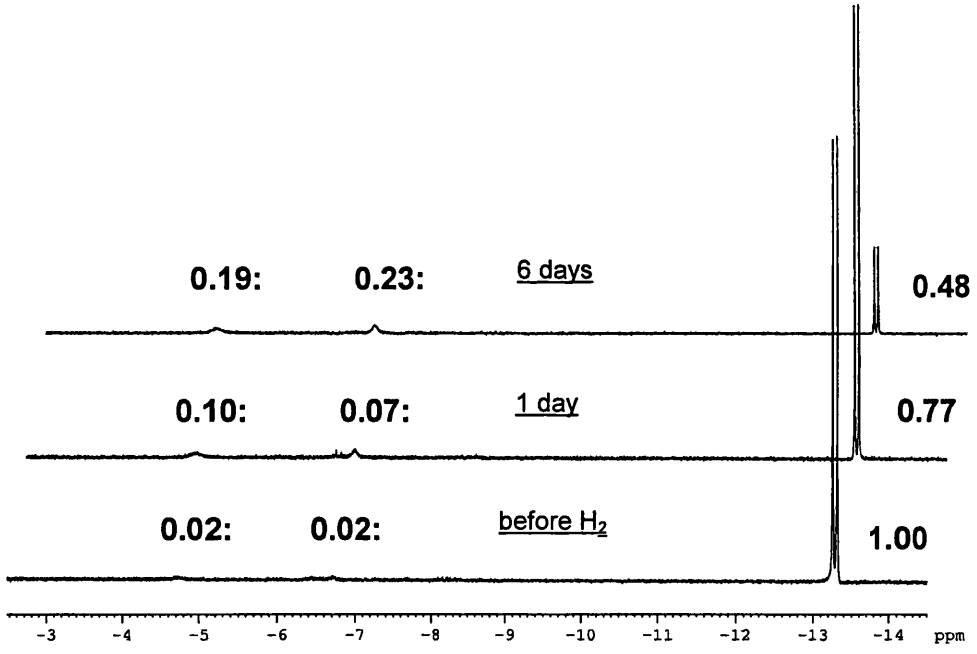

Figure 4.18 ^1H NMR spectra for the room temperature reaction of **26-d$_4$** with H_2 (C_6D_6, 280 K, 400 MHz).

4.20 Reactions of $Ru(PPh_3)(IMes)(CO)(\eta^2\text{-}BH_4)H$ (26) with small molecules

4.21 Treatment of $Ru(PPh_3)(IMes)(CO)(\eta^2\text{-}BH_4)H$ (26) with C_2H_4

The treatment of $Ru(IMes)_2(CO)(\eta^2\text{-}BH_4)$ H (**26**) with ethene at 298 K caused no change to the ^1H NMR spectrum of the sample, although at 323 K, overnight conversion of ethene to ethane was observed alongside reduction in the hydride signal of **26**, but without the appearance of any new hydride peaks. These results are consistent with the results obtained for **19**. Low temperature ^1H NMR spectroscopy (298 – 200 K) was used in an attempt to observe the ethene moiety bound to the metal centre of **26** but no new hydride signals were apparent, neither was there any evidence of protons from a bound $\eta^2\text{-}C_2H_4$ (expected at *ca.* 2 ppm).[21, 36]

4.22 Treatment of $Ru(PPh_3)(IMes)(CO)(\eta^2\text{-}BH_4)H$ (26) with CO

The room temperature reaction of $Ru(PPh_3)(IMes)(CO)(\eta^2\text{-}BH_4)H$ (**26**) with 1 atm of CO occurred in the same manner as for **19** (**Scheme 4.19**). $Ru(PPh_3)(IMes)(CO)_2H_2$ (**28**) was produced initially, evidenced by a doublet in the ^1H NMR spectrum at -6.56 ppm with J_{HP} = 26.4 Hz and by ^{31}P NMR spectroscopy, which showed a singlet at 60.5 ppm. At 298 K, **28** continued to react with CO to form $Ru(PPh_3)(IMes)(CO)_3$ (**29**), which displayed a $^{31}P\{^1H\}$ NMR resonance at 65.5 ppm.[42] The boron byproduct, $BH_3.CO$ was detected by a singlet in the $^{11}B\{^1H\}$ NMR spectrum at 41.4 ppm. This signal correlates to a 1:1:1:1 quartet in the ^1H NMR spectrum at 3.91 ppm (J_{HB} = 132 Hz).

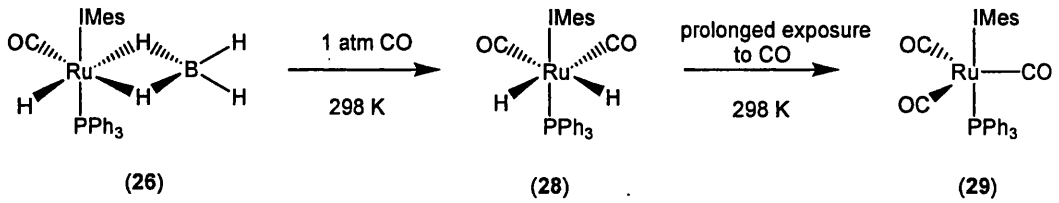

Scheme 4.19 Formation of **28** followed by **29** from the treatment of **26** with CO.

Both **28** and **29** have previously been observed upon reaction of $Ru(PPh_3)_2(IMes)(CO)H_2$ with CO at 298 K.[42] **29** has been structurally and spectroscopically characterised as previously discussed,[18,42] whereas **28** was characterised by comparison with reported ^1H NMR data for analogous species such as $Ru(PPh_3)_2(CO)_2H_2$.[55] Full characterisation of **28** is provided in section **4.23.**

4.22.1 Investigating the reaction pathway for conversion of $Ru(PPh_3)(IMes)(CO)(\eta^2\text{-}BH_4)H$ (26) to $Ru(PPh_3)(IMes)(CO)_2H_2$ (28)

The reaction between **26** and CO (**Scheme 4.20**) was followed at low temperature by ^1H NMR spectroscopy. The intermediate $Ru(PPh_3)(IMes)(CO)_2(\eta^1\text{-}BH_4)H$ (**27**) could be clearly seen at 230 K by the appearance of a doublet hydride signal at -5.33 ppm (J_{HP} = 24.7 Hz) (**Figure 4.19**).

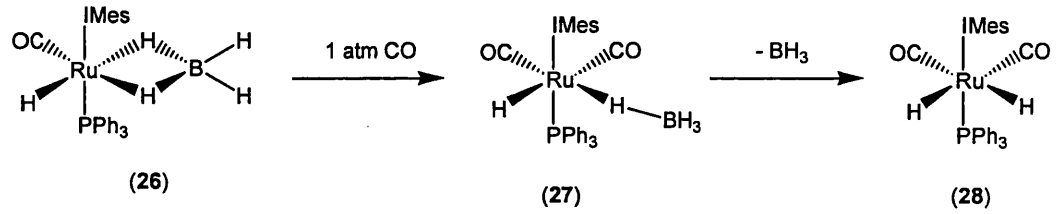

Scheme 4.20 Formation of **28** from **26** *via* the intermediate η^1-BH_4 species **27**.

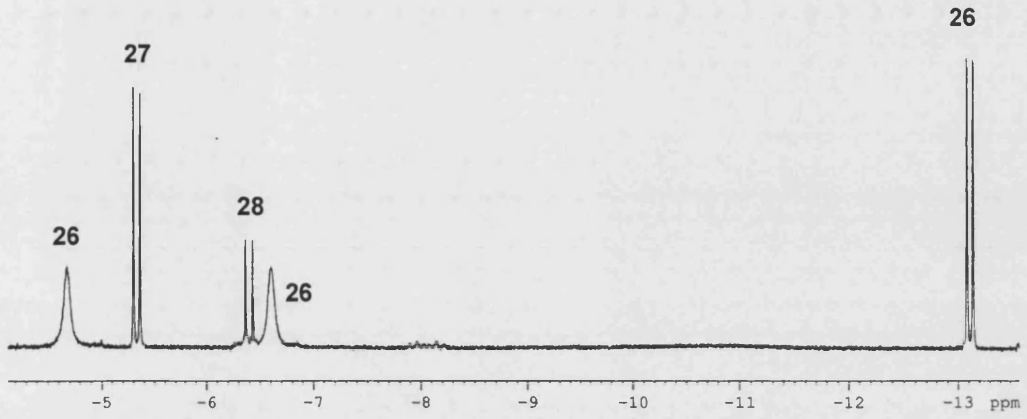

Figure 4.19 ^{1}H NMR spectrum of the reaction of **26** with CO to form **28** *via* the intermediate η^{1}-BH_4 species **27** ($C_6D_5CD_3$, 230 K, 400 MHz).

As with $Ru(IMes)_2(CO)_2(\eta^{1}\text{-}BH_4)H$ (**21**), the bridging and the terminal BH_4^- hydrogen atoms of **27** could be seen at 190 K at -10.68 ppm and 1.19 ppm respectively. In the $^{31}P\{^{1}H\}$ NMR spectrum at 190 K, **27** appeared as a singlet at 47.6 ppm. This was confirmed by $^{31}P\{^{1}H\}$-^{1}H HMQC spectroscopy (**Figure 4.20**). However, the correlation spectrum failed to show any cross peaks between the phosphorus atom and the borohydride protons.

^{1}H-$^{13}C\{^{1}H\}$ HMBC spectroscopy at 230 K revealed the $C_{carbonyl}$ and C_{NHC} resonances at 202.1 and 181.4 ppm respectively. The sample was allowed to warm in the probe to 273 K resulting in total loss of starting material and leaving only **27** and **28** resonances in the hydride region. Further heating to 298 K resulted in only **28** being observed.

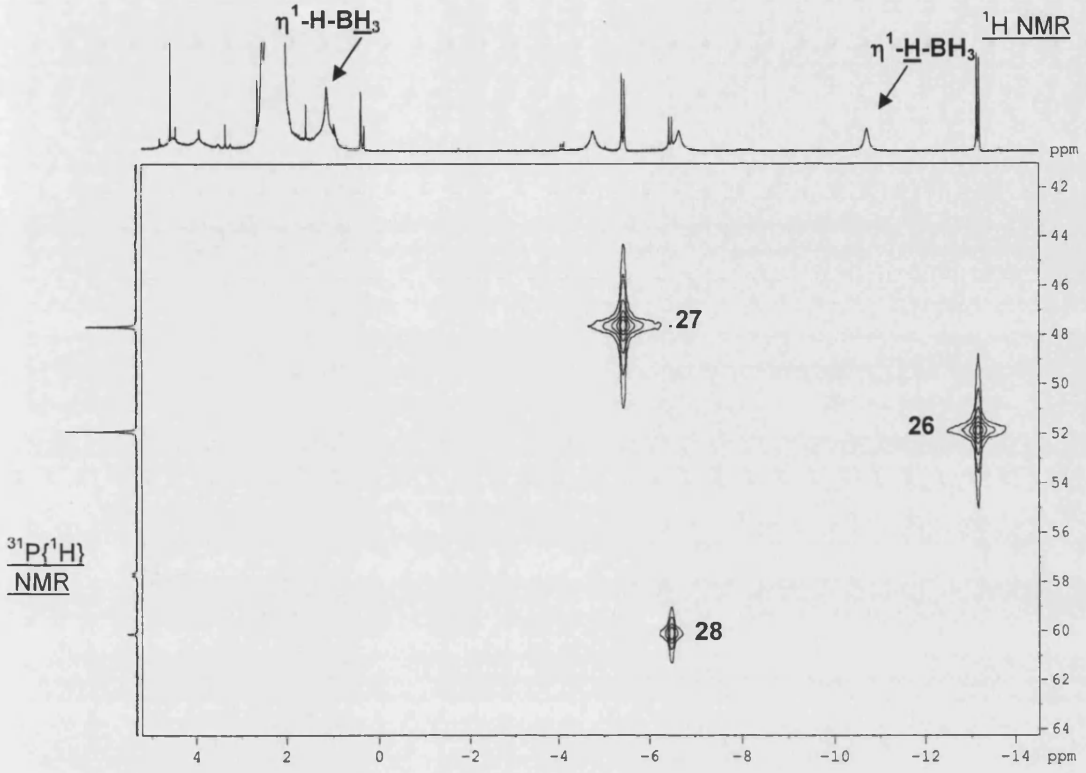

Figure 4.20 Low temperature $^{31}P\{^1H\}$-^1H HMQC spectrum of the reaction between **26** and CO ($C_6D_5CD_3$, 190 K).

4.23 Formation of $Ru(PPh_3)(IMes)(CO)_2H_2$ (28)

The isolation of **28** was important as it can be viewed as a CO trapped form of the dihydride complex $Ru(PPh_3)(IMes)(CO)H_2$. However, clean formation of **28** was hindered by further reaction to give **29**. In order to overcome this problem, **28** was produced instead by reaction of $Ru(PPh_3)(IMes)(CO)_2(Cl)H$ (**11**) with $NaBH_4$.

4.23.1 Synthesis and characterisation of 28

A sample of $Ru(PPh_3)(IMes)(CO)_2(Cl)H$ (**11**) was reduced with excess $NaBH_4$ in EtOH at 298 K over an hour to yield $Ru(PPh_3)(IMes)(CO)_2H_2$ (**28**) (**Scheme 4.21**). The

compound was characterised by a doublet at -6.56 ppm (J_{HP} = 26.4 Hz) in the ^{1}H NMR spectrum, which integrated in a ratio of 2:4 to the backbone protons of IMes. **28** showed a singlet at 60.5 ppm in the $^{31}P\{^{1}H\}$ NMR spectrum.

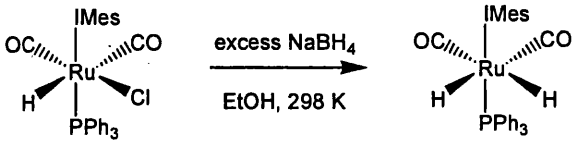

(11) (28)

Scheme 4.21 Clean formation $Ru(PPh_3)(IMes)(CO)_2H_2$ (**28**).

The $^{13}C\{^{1}H\}$ NMR spectrum of **28** verified that the CO ligands were equivalent with a single $C_{carbonyl}$ resonance at 203.1 ppm displaying coupling typical of *cis* OC-Ru-PPh_3 groups (J_{CP} = 8.5 Hz). The carbenic carbon atom showed a relatively large J_{CP} (72.5 Hz) in line with the *trans* arrangement of C_{NHC}-Ru-PPh_3 ligands. As expected, the IR spectrum of **28** displayed both υ_{COsymm} and $\upsilon_{COasymm}$ bands (1995, 1947 cm^{-1}). Spectroscopic data for **28** and related complexes is summarised in **Table 4.10**.

$RuL_2(CO)_2H_2$ L_2 =	^1H NMR Ru-H (ppm)	$^{31}P\{^1H\}$ NMR PR_3 (ppm)	^{13}C NMR CO (ppm)	IR shift (cm^1)	
				υ_{CO}	υ_{Ru-H}
$(IMes)_2$ [38] (22)	-6.53	-	204.3	1973 1936	-
$(IMes)(PPh_3)$ (28)	-6.56 J_{HP} = 26.4 Hz	60.5	203.1 J_{CP} = 8.5	1995 1947	1879
$(PMe_3)_2$ [56]	-7.32 J_{HP} = 26.4 Hz	-2.6	202.7 J_{CP} = 10.0	2010 1960	-
$(PPh_3)_2$ [55]	-6.90 J_{HP} = 23 Hz	-	-	2011 1974	1878 1823
$(PCy_3)_2$ [45]	-8.25 J_{HP} = 26 Hz	69.4	205.0 J_{CP} = 7	-	-
$\{P(tolyl)_3\}_2$ [45]	-6.04 J_{HP} = 23 Hz	55.4	-	-	-
$(PMe_2Ph)_2$ [57]	-7.01 J_{HP} = 25.9 Hz	12.1	202.8 J_{CP} = 8.9	2010 1965	1920
$(AsMe_2Ph)_2$ [57]	-7.29	-	-	2040 2010	1960 1920

Table 4.10 Spectroscopic data for complexes $RuL_2(CO)_2H_2$ for comparison with **28**. (- = N/A or not provided).

The structure of $Ru(PPh_3)(IMes)(CO)_2H_2$ (**28**) was confirmed by X-ray crystallography (**Structure 4.3**), which showed that the crystal consisted of a 90:10 mix of **28** and **11**.

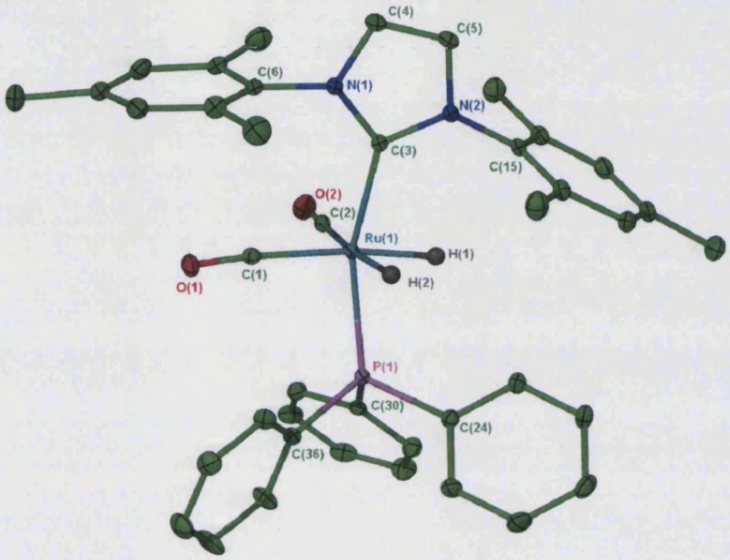

Structure 4.3 X-ray structure of $Ru(PPh_3)(IMes)(CO)_2H_2$ (**28**). Thermal ellipsoids are set at 30 % probability. Hydrogen atoms have been omitted for clarity (except the hydride ligands).

The bond lengths in **28** (**Table 4.11**) are generally similar to equivalent bonds seen in previous examples; Ru-C(O) bond lengths are typical of Ru-C bonds *trans* to a hydride ligand (slightly longer than *trans* to a vacant site) and the Ru-C_{NHC} bond length is slightly shorter at 2.0874(17) Å than in bis IMes complexes (*ca.* 2.10 Å). There is a large deviation from linearity in the axial ligands C(3)-Ru-P {158.42(5) °}, which shifts the PPh_3 ligand away from the dicarbonyl side of the complex and staggers the mesityl groups of IMes with respect to the phenyl groups of the phosphine ligand.

	28
Ru-C(1)	1.9202(18)
Ru-C(2)	1.9315(19)
Ru-C(3)	2.0874(17)
Ru-P(1)	2.3228(4)
C(3)-Ru-P(1)	158.42(5)
C(1)-Ru-C(2)	93.58(7)

Table 4.11. Selected bond lengths (Å) and angles (°) for **28**.

4.24 Treatment of $Ru(PPh_3)(IMes)(CO)(\eta^2\text{-}BH_4)H$ (26) with 4-picoline (4-Mepy)

$Ru(PPh_3)(IMes)(CO)(\eta^2\text{-}BH_4)H$ (**26**) reacted with 4-Mepy (1-5 equiv.) immediately at 298 K to form $Ru(PPh_3)(IMes)(CO)(4\text{-Mepy})H_2$ (**30**) (**Scheme 4.22**). The reaction between **26** and 4-Mepy did not result in full conversion to **30** even with a large excess of 4-Mepy, prolonged reaction times and heating (up to 323 K).

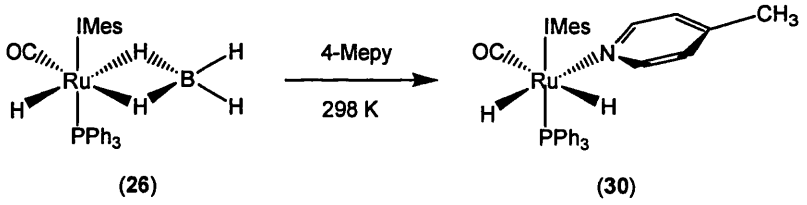

(26) (30)

Scheme 4.22 Formation of $Ru(PPh_3)(IMes)(CO)(4\text{-Mepy})H_2$ (**30**).

The product showed two new doublet of doublet hydride resonances consistent with one hydride (-4.15 ppm) lying *trans* to a carbonyl ligand and the other (-14.94 ppm) lying *trans* to the 4-picoline moiety. Additionally, the coupling constant values are typical of *cis* ^1H-^{31}P coupling (30.5 and 25.7 Hz respectively) and *cis* ^1H-^1H coupling (6.0 Hz). Both of the hydride resonances for **30** correlated with a new ^{31}P

signal at 69.3 ppm. **30** can alternatively be produced by a simple exchange reaction between $Ru(PPh_3)_2(IMes)(CO)H_2$ and 4-Mepy although again, not cleanly.

The chemical shifts of the 4-Mepy ligand in **30** were shifted upfield in comparison to the free substrate and were, furthermore, all inequivalent (8.09, 7.99, 6.05 and 5.75 ppm, all d, J_{HH} = 6.0 Hz) (**Figure 4.21**) consistent with hindered rotation about the Ru-N bond. The carbonyl and carbenic carbon resonances for **30** were located in the ^1H-$^{13}C\{^1H\}$ HMBC spectrum at 205.8 and 197.5 ppm respectively.

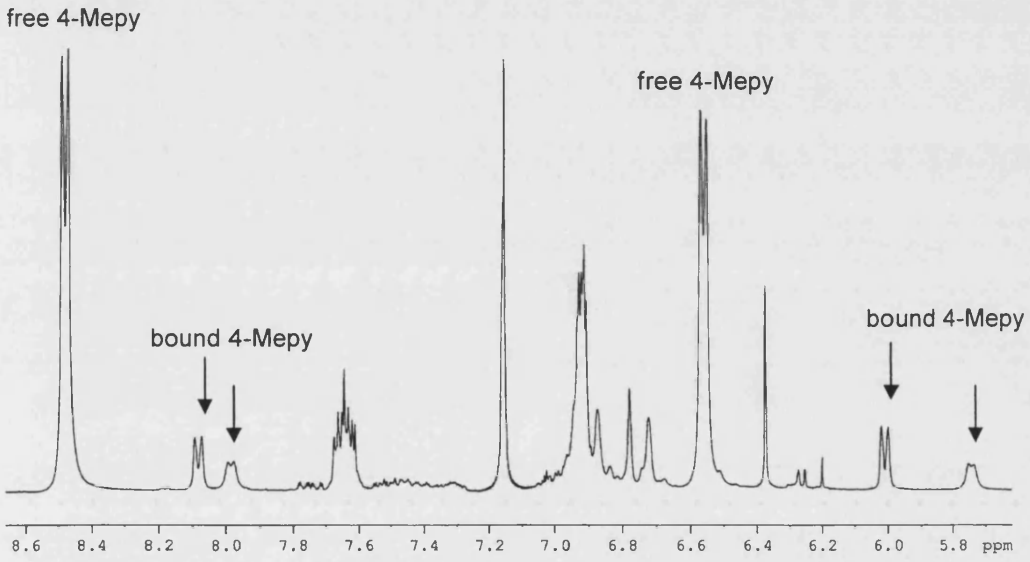

Figure 4.21 ^1H NMR spectrum showing the aryl region for the reaction between **26** and excess 4-Mepy to form **30** (C_6D_6, 298 K, 300 MHz).

Crystallisation of **30** by was attempted without success. Isolation appears to be commonly problematic for this class of complex; for example, in the related systems $Ru(PMePh_2)_2(CO)(4\text{-Mepy})H_2$ and $Ru(^tBu_2Me)_2(CO)(py)H_2$.[19, 53] The reversible nature of py-binding is one factor attributed to problems with the latter. However, importantly, Caulton also noted that isolating the 16-electron species $Ru(^tBu_2Me)_2(CO)H_2$ (in the absence of a py ligand) would be very unlikely due to lack of π-donation from the hydride.[19]

The reaction of **26** with 4-Mepy also yielded the adduct 4-Mepy.BH_3, which appeared as a very broad 1:1:1:1 proton resonance at 3.58 ppm and more clearly, in the $^{11}B\{^1H\}$ NMR spectrum as a sharp signal at -11.19 ppm (supported by ^{11}B-^1H correlation spectroscopy). These values are consistent with the values reported by Stott for the adduct following the reaction of $Ru(PMePh_2)_2(CO)(\eta^2\text{-}BH_4)H$ with 4-Mepy.[21]

4.24.1 Investigating the reaction pathway from $Ru(PPh_3)(IMes)(CO)(\eta^2\text{-}BH_4)H$ (26) to $Ru(PPh_3)(IMes)(CO)(4\text{-}Mepy)H_2$ (30)

The formation of **30** was treated as another opportunity to probe the 'opening up' process in **26**. We propose that 4-Mepy coordinates to the metal centre as the coordination mode of the BH_4^- in **26** switches from η^2 to η^1 creating a vacant site. BH_3 is lost to form 4-Mepy.BH_3 and the reaction affords **30** (**Scheme 4.23**).

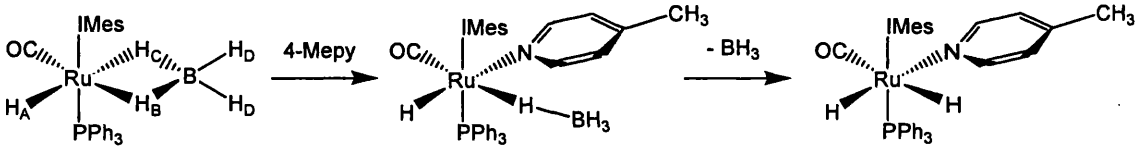

(26) (30)

Scheme 4.23 Reaction of **26** with 4-Mepy to form **30** *via* the η^1-BH_4^- bound intermediate species.

It has been established that the 4-Mepy ligand lies *trans* to a hydride ligand in **30**, but the 4-Mepy moiety may coordinate directly into the vacant site *trans* to the hydride or after isomerisation resulting in $Ru(PPh_3)(IMes)(CO)(\eta^1\text{-}BH_4)(4\text{-}Mepy)H$ shown in **Scheme 4.23** above. VT and T_1 studies on **26** support the former option, with the data implying that η^2-BH_4^- 'opens up' at H_C to create a vacant site *trans* to H_A. Work described in the following sections was aimed at testing this hypothesis.

4.24.2 Attempted observation of the intermediate species $Ru(PPh_3)(IMes)(CO)(\eta^1\text{-}BH_4)(4\text{-}Mepy)H$

4-Mepy was added to a sample of **26** at 195 K in $C_6D_5CD_3$ and followed by low temperature ^1H NMR spectroscopy in an attempt to observe the η^1-BH_4^- intermediate complex $Ru(PPh_3)(IMes)(CO)(\eta^1\text{-}BH_4)(4\text{-}Mepy)H$. At 250 K, a new tiny triplet peak appeared in the ^1H NMR spectrum at -12.20 ppm (J_{HP} = 22.5 Hz), which we tentatively assign to $Ru(PPh_3)(IMes)(CO)(\eta^1\text{-}BH_4)(4\text{-}Mepy)H$. The hydride peak transformed into a doublet (J_{HP} = 21.4 Hz) in the $^1H\{^{31}P\}$ spectrum, indicative of the hydride ligand coupling to a bridging hydrogen atom. The hydrogen atoms of the presumed η^1-BH_4^- ligand were not seen by ^1H NMR spectroscopy. $^{31}P\{^1H\}$ NMR spectroscopy revealed a singlet at 44.4 ppm, which was correlated by $^{31}P\{^1H\}$-^1H HMQC spectroscopy. In contrast, Stott was able to spectroscopically characterise the intermediate complex $Ru(PMe_2Ph)_2(CO)(\eta^1\text{-}BH_4)(4\text{-}Mepy)H$ in full, which showed a hydride resonance at -11.43 ppm at 250 K.[21, 53] Further cooling to 174 K allowed the bridging hydrogen atom to be located at -8.48 ppm.[53]

4.24.3 Treatment of $Ru(PPh_3)(IMes)(CO)(\eta^2\text{-}BD_4)H$ (26-d_4) with 4-Mepy

Two samples of **26-d_4** were treated with 4-Mepy (one in C_6D_6, the other in C_6H_6) and followed by both ^1H and ^2H NMR spectroscopy. Low frequency signals at -4.15 and -14.94 ppm were observed in both the ^1H **and** ^2H NMR spectra (**Figure 4.22**).

The spectra imply that the product contained both H and D in both possible 'hydride' positions (*trans* to the vacant site and *trans* to the carbonyl ligand). This is consistent with the intermediate species $Ru(PPh_3)(IMes)(CO)(\eta^1\text{-}BH_4)H$ undergoing isomerisation before the coordination of 4-Mepy as shown in **Scheme 4.24.**

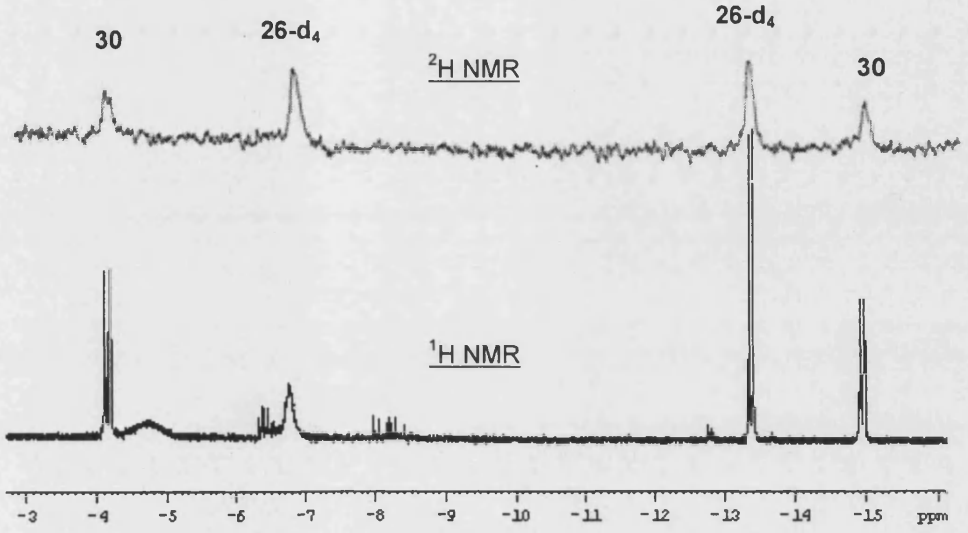

Figure 4.22 Characteristic hydride resonances for **30**, apparent in both ^{2}H and ^{1}H NMR spectra following the reaction of **26-d$_4$** with 4-Mepy after 1 day at 298 K (298 K, C_6D_6)

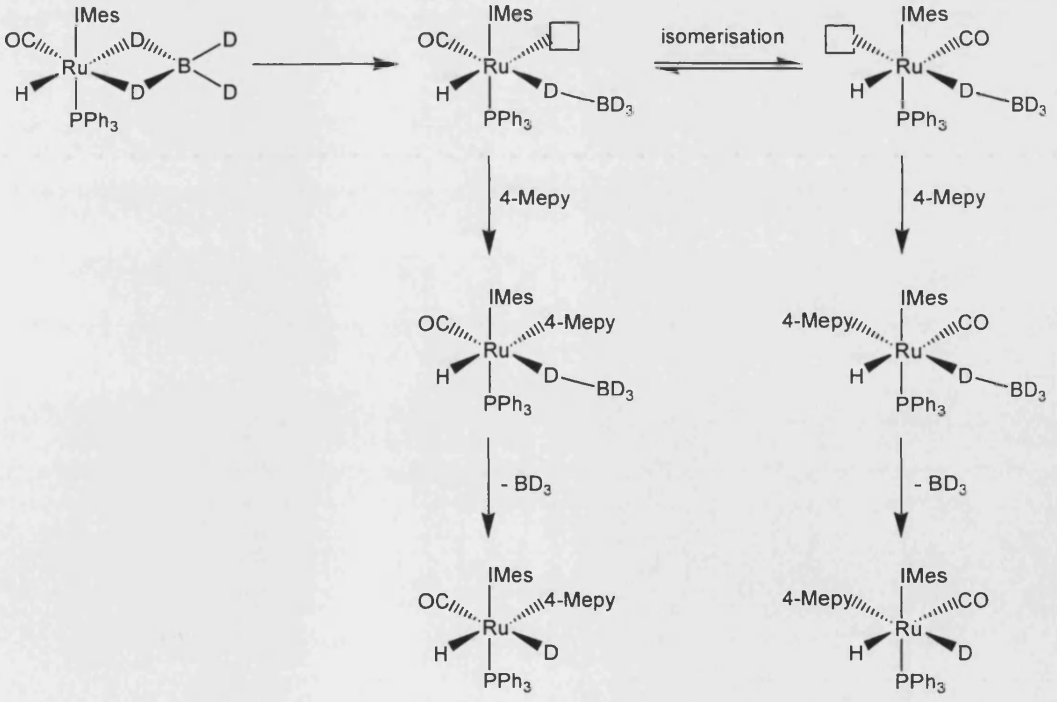

Scheme 4.24 Proposed mechanism to account for H and D atoms located both *trans* to the vacant site and *trans* to the carbonyl ligand.

4.25 Preparation of $Ru(PPh_3)(IMes)(CO)(Cl)(4\text{-}Mepy)H$ (31)

For comparison with $Ru(PPh_3)(IMes)(4\text{-}Mepy)H_2$ (**30**), the hydride chloride analogue $Ru(PPh_3)(IMes)(Cl)(4\text{-}Mepy)H$ (**31**) was prepared by reaction of 4-Mepy with $Ru(PPh_3)(IMes)(CO)(Cl)H$ (**8**) (**Scheme 4.25**).

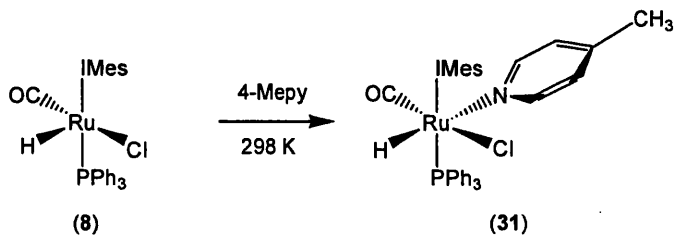

(8) (31)

Scheme 4.25 Formation of $Ru(PPh_3)(IMes)(CO)(Cl)(4\text{-}Mepy)H$ (**31**).

The ^1H NMR spectrum of **31** contained a broad hydride signal at -12.99 ppm and a broad signal in the aryl region attributed to the 4-Mepy moiety (8.46 ppm) (**Figure 4.23**). The broadness is most likely due to the fluxional nature of the complex, as in $Ru(^tBu_2Me)_2(CO)(Cl)(py)H$,[19] and is unchanged by removal of free 4-Mepy. The low temperature ^1H-^1H NOESY spectrum of **31** reflected the fluxional nature of the 4-Mepy ligand in **31** with crosspeaks observed between free and bound 4-Mepy.

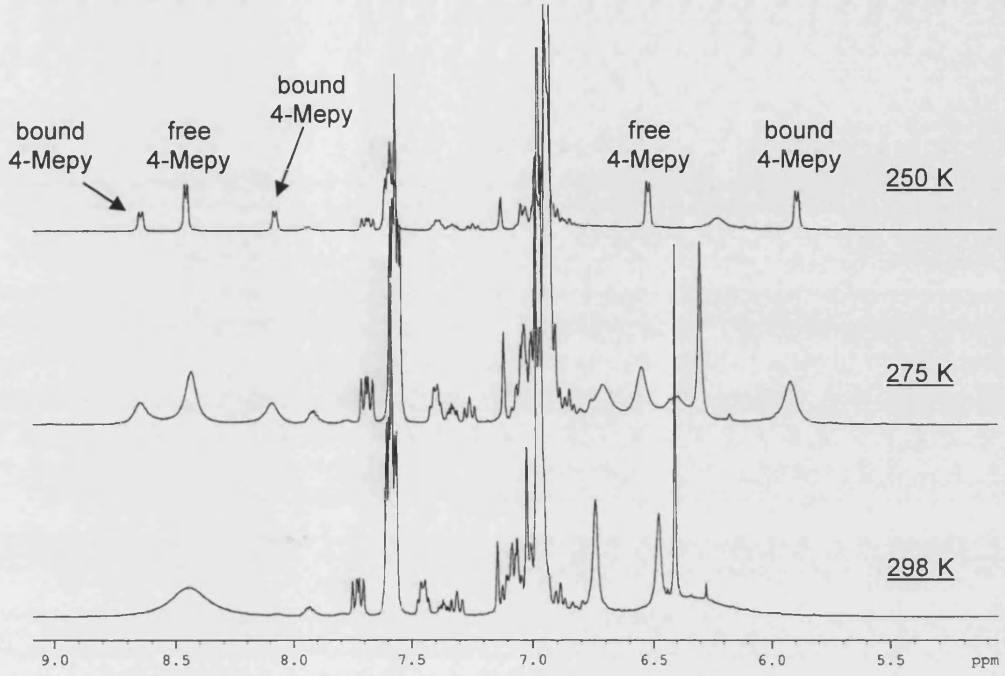

Figure 4.23 VT ^{1}H NMR spectra of **31** ($C_6D_5CD_3$, 400 MHz).

Cooling to 275 K made it possible to observe some splitting of the broad hydride resonance, while the aryl signal at 8.46 ppm separated completely into two resonances. Decreasing the temperature further to 250 K sharpened and split Ru-H into a doublet (-12.72 ppm, J_{HP} = 20.3 Hz), while the aryl resonances sharpened into three very clear doublets at 8.61, 8.04 and 5.84 ppm (J_{HH} = 4.4 Hz each) in a ratio of 1:1:2 (**Figure 4.23** above). The correlation of these signals was confirmed by ^{1}H COSY (**Figure 4.24**). Inequivalence of the aryl signals of the IMes ligand was also observed by the appearance of three resonances at 6.94 ppm (within the multiplet phenyl signal), 6.72 and 6.41 ppm in a ratio of 2:1:1 (275 K).

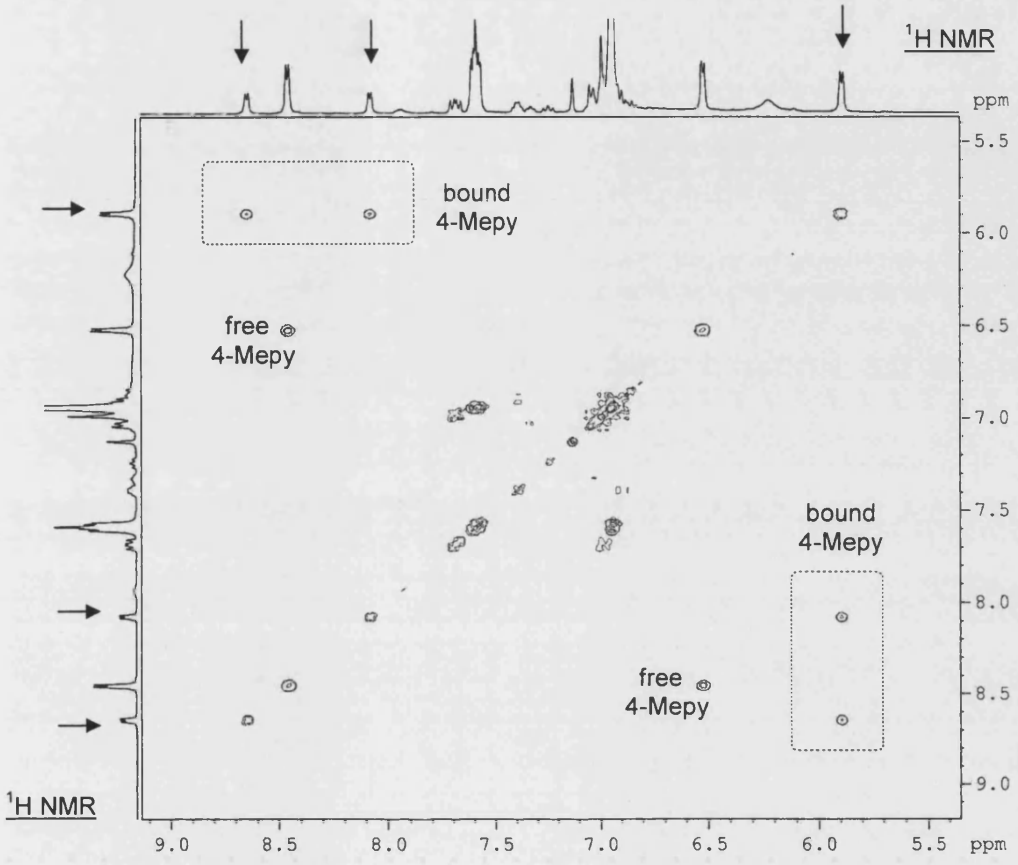

Figure 4.24 ^{1}H-^{1}H COSY spectrum of **31** ($C_6D_5CD_3$, 250 K, 400 MHz).

Pale yellow pyramidal crystals of **31** were produced from a mixture of benzene and hexane (**Structure 4.4**). The X-ray crystal structure showed mutual disorder between CO and Cl ligands in a 65:35 ratio and a phenyl ring {bound *via* C(23)} disordered over two sites with 50:50 occupancy in each.

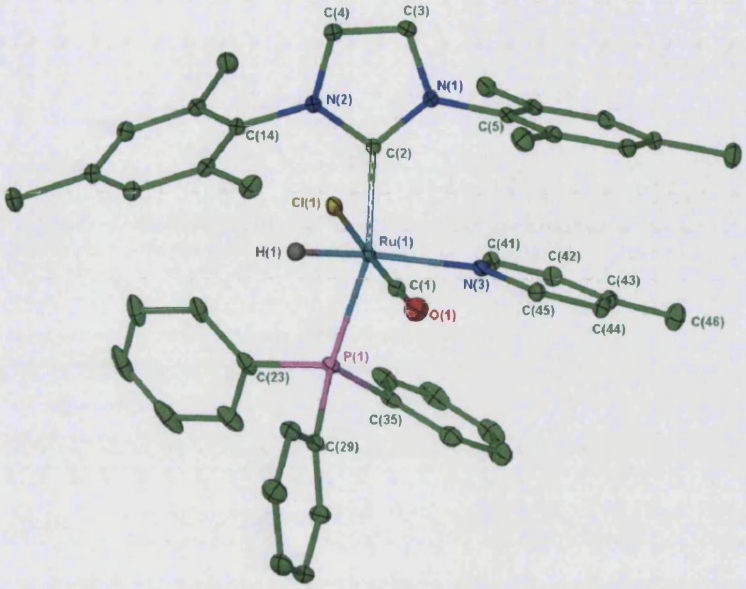

Structure 4.4 X-ray structure of $Ru(PPh_3)(IMes)(CO)(4\text{-}Mepy)(Cl)H$ (**31**). Thermal ellipsoids are set at 30 % probability. Hydrogen atoms have been omitted for clarity (except the hydride).

The X-ray crystal structure of **31** showed one mesityl arm, the 4-picoline ring and a phenyl ring in an eclipsed conformation, all exhibiting short interactions of 3.557 and 3.586 Å respectively (centroid-centroid distances). The rings are not stacked directly on top of each other, with twist angles of 15.25 and 21.97 ° respectively; neither do the rings lie exactly parallel to each other, tilting by 7.98 and 11.32 ° respectively. Similar interactions have been reported in $[Ir(PPh_3)_2(bq\text{-}R)H]PF_6$ (R = ^{i}Pr, ^{t}Bu); described as 'aromatic parallel stacking' although it is noted that the stacking could not be perfectly parallel.[58] These interactions have been found to be significant as they compete with and prevent agostic interactions in the case of R = ^{i}Pr, which displays two such interactions (centroid-centroid distances = 3.765 Å twice) whereas, when R = ^{t}Bu there is only one interaction and the complex is agostic.[58] The complex $Ru(PPh_3)_2(CO)(4\text{-}Mepy)Cl_2$ appears as though it may also contain stacking interactions between the 4-Mepy and a phenyl ring on each of the *trans* PPh_3 ligands, however no information was available to support this hypothesis.[59]

Selected bond lengths and angles for **31** are shown in **Table 4.12** below. The metrics for **31** are similar to those acquired for $Ru(PPh_3)(IMes)(CO)_2(Cl)H$ (**11**). The Ru-N bond length is a little longer {(2.2901(13) Å} than the same bond in $Ru(PPh_3)_2(CO)(4\text{-Mepy})Cl_2$ {(2.202(1) Å},[59] probably due to the *trans* influence of the hydride ligand in **31**.

	31
Ru-C(2)	2.1049(15)
Ru-P	2.3395(4)
Ru-N(3)	2.2901(13)
Ru-Cl(1)	2.4842(12)
Ru-C(1)	1.812(4)
C(2)-Ru-P	164.70(4)
Cl(1)-Ru-C(1)	178.06(9)
Cl(1)-Ru-N(3)	87.65(4)
N(3)-Ru-C(1)	92.23(9)

Table 4.12 Selected bond lengths (Å) and angles (°) for **31**.

4.26 Alternative substrates to 4-Mepy

It is clear that 4-Mepy is capable of abstracting BH_3 from $Ru(PPh_3)(IMes)(CO)(\eta^2\text{-}BH_4)H$ (**26**), however 4-Mepy also coordinates to the metal centre filling the vacant site to produce $Ru(PPh_3)(IMes)(CO)(4\text{-Mepy})H_2$ (**30**). Hindered rotation of the pyridine ligand in **30** implies that the 4-Mepy group causes significant steric hindrance in the complex. We aimed to manipulate the steric bulk of the substrate so that BH_3 could be removed from **26** but prevent ligand binding in an effort to form the dihydride complex $Ru(PPh_3)(IMes)(CO)H_2$. **26** was reacted with 2,6-lutidine (2,6-Mepy), which is more sterically hindered around the nitrogen atom than 4-Mepy, but no reaction was found even at elevated temperatures (up to 343 K).

4.27 Treatment of $Ru(PPh_3)(IMes)(CO)(\eta^2\text{-}BH_4)H$ (26) with PMe_2Ph

Upon treatment of $Ru(PPh_3)(IMes)(CO)(\eta^2\text{-}BH_4)H$ (**26**) with a slight excess of PMe_2Ph (1.2 equiv.), two new doublet of doublet of doublet hydride signals were detected at -6.69 and -7.75 ppm consistent with the formation of the mixed phosphine complex $Ru(PPh_3)(IMes)(CO)(PMe_2Ph)H_2$ (**32**) (**Scheme 4.26**).

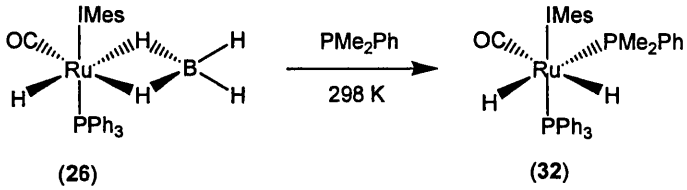

(26) (32)

Scheme 4.26 Formation of **32**.

The coupling patterns in the ^1H NMR spectrum for **32** mirrored those already described for $Ru(PMe_2Ph)_2(IMes)(CO)H_2$ (**25**) and for $Ru(PPh_3)_2(IMes)(CO)H_2$,[50] suggesting that the two phosphine ligands lie in a *cis* arrangement. The $^{31}P\{^1H\}$ NMR spectrum showed doublet resonances for **32** (both with J_{PP} = 16.7 Hz); importantly these occurred at different chemical shifts to **25**, verifying that the product contained both PPh_3 and PMe_2Ph ligands. However, it was unclear the exact arrangement of the ligands; PMe_2Ph may coordinate directly *trans* to a hydride ligand or lie *trans* to IMes following isomerisation. Formation of $PMe_2Ph.BH_3$ was also apparent in the $^{31}P\{^1H\}$ NMR spectrum with a 1:1:1:1 quartet at 3.1 ppm (J_{PB} = 56.7 Hz).[21]

Complete conversion to **32** was achieved after a day at 298 K. No further attempts were made to isolate or fully characterise **32** due to time constraints, but the reaction served to highlight important differences in reactivity between **26** and $Ru(IMes)_2(CO)(\eta^2\text{-}BH_4)H$ (**19**).

4.28 $RuL_2(CO)(\eta^2\text{-}BH_4)H$ as potential catalysts for C=O hydrogenation reactions

As previously mentioned, borohydride complexes have been used in catalysis but it is generally unclear whether they perform as the active species or just as precatalysts to hydride-containing species. Werner has reported a good example of the latter, with the addition of $NaBH_4$ to the TH catalyst $Os(P^iPr_3)_2(CO)(Cl)H$ resulting in significantly increasing catalytic activity.[56] It was postulated that $Os(P^iPr_3)_2(CO)H_2$ was formed, which operated as the active catalyst.[60, 61] The BH_4^- species $Os(P^iPr_3)_2(CO)(\eta^2\text{-}BH_4)H$ was later isolated and found to react with the transfer reagent ^{i}PrOH to produce $Os(P^iPr_3)_2(CO)(\eta^2\text{-}H_2)H_2$ (**Scheme 4.27**).[62]

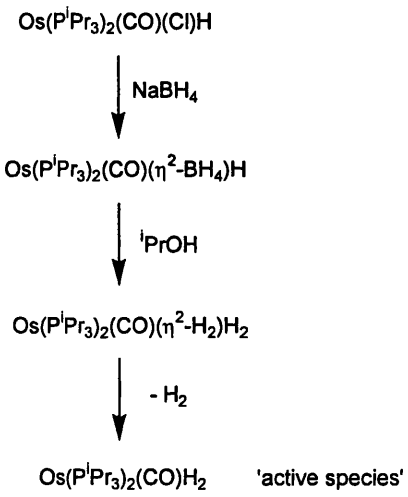

Scheme 4.27 Increasing the catalytic activity of the TH system $Os(P^iPr_3)_2(CO)(Cl)H$ by the addition of $NaBH_4$.[56, 62]

In contrast, when the related system $Ru(P^iPr_3)_2(CO)(\eta^2\text{-}BH_4)H$ was used as a catalyst for cyclotrimerisation of methyl propiolate (HC_2CO_2Me), the BH_4^- complex was retrieved at the end of the reaction, suggesting that it was the active catalyst.[63]

Following the hydrogenation work described in Chapter 2, the BH_4^- complexes $RuL_2(CO)(\eta^2\text{-}BH_4)H$ {L_2 = $(IMes)_2$ (**19**); $(PPh_3)(IMes)$ (**26**)} were tested for catalytic activity in the hydrogenation of acetophenone to phenethyl alcohol.

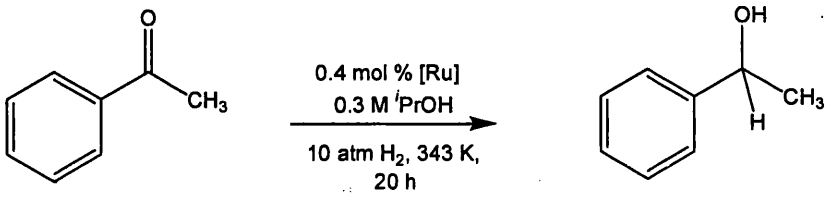

[Ru] = $RuL_2(CO)(\eta^2\text{-}BH_4)H$

Complex	Conversion (%) $L_2 = (IMes)_2$	Conversion (%) $L_2 = (PPh_3)(IMes)$
$RuL_2(CO)(Cl)H$	84	80
$RuL_2(\eta^2\text{-}BH_4)H$	85	74

Table 4.13 Conversion (%) of acetophenone to phenethyl alcohol using the conditions outlined above.

Table 4.13 shows that the catalytic activity for the BH_4^- systems **19** and **26** are comparable with their hydride chloride precursors $Ru(IMes)_2(CO)(Cl)H$ (**7**) and $Ru(PPh_3)(IMes)(CO)(Cl)H$ (**8**). Direct comparison with the coordinatively unsaturated species implies that **19** and **26** act like they have a vacant site, consistent with the fluxional nature of the BH_4^- ligands, established throughout this chapter. There was no evidence of increased catalytic activity in using **19** and **26**, which would suggest that neither a polyhydride system such as $RuL_2(CO)(\eta^2\text{-}H_2)H_2$ nor the dihydride complex $RuL_2(CO)H_2$ is formed. Furthermore, residue left on the stirrer following the hydrogenation reactions only showed hydride resonances diagnostic of **19** and **26** in the ^1H NMR spectra.

4.29 Attempted reduction of halide complexes with $LiAlH_4$ or $LiHBEt_3$

4.29.1 Treatment of $Ru(IMes)_2(CO)(Cl)H$ (7) with $LiAlH_4$

Reducing agents other than $NaBH_4$ were studied briefly in an effort to prepare $RuL_2(CO)H_2$ {L = $(IMes)_2$, $(PPh_3)(IMes)$}. In the reaction between $Ru(IMes)_2(CO)(Cl)H$ (**7**) and $LiAlH_4$ (4 equiv. in THF), spectroscopic data suggested formation of the aluminohydride complex $[(IMes)_2(CO)HRu(\mu\text{-}H)_2Al(H)(\mu\text{-}H)_2Al(H)(\mu\text{-}H)_2RuH(CO)(IMes)_2]$ (**33**) (**Figure 4.25**).

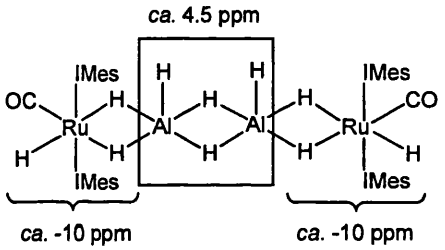

Figure 4.25 The proposed structure of **33** with diagnostic ^1H NMR spectroscopic values.

The ^1H NMR spectrum showed loss of the starting material hydride and appearance of two very broad signals around 4.5 and -10 ppm, consistent with the formation of an aluminohydride complex. Although incredibly broad, the resonances are in line with those reported for other aluminohydride complexes.[64, 65] The downfield signal corresponds with hydrogen atoms bridging the aluminium nuclei and the aluminium-hydride, whereas the upfield peak is characteristic of hydrogen atoms directly bound to the ruthenium metal centres. When less than 1 equiv. $LiAlH_4$ was used (*ca.* 0.8 equiv.), no colour change was observed in the reaction mixture and only the starting complex was shown in the ^1H NMR spectrum, suggesting that **33** contains more than one AlH_4^- moiety.

The broadness of the resonances made accurate integration impossible either due to overlapping signals or extreme broadness, such that signals were lost in the base-line.

This feature was attributed to the quadrupolar moment of ^{27}Al (I = 5/2) and the incredibly labile AlH_4^- hydrogen atoms undergoing exchange with each other and with the hydride ligand. A series of ^1H NMR spectra were acquired for **33** over a range of temperatures (298–190 K) in an attempt to sharpen or split the major characteristic signals by reducing fluxionality. However, even at the lowest temperature the hyride signal did not significantly change, although the peak at *ca.* 4 ppm did split into two overlapping resonances at 210 K.

The ^{27}Al NMR spectrum of **33** also displayed a broad resonance, situated at 69.7 ppm, also similar to analogous complexes. Unfortunately the use of NMR spectroscopy is severely limited for this system and not much in the way of characterisation could be achieved apart from by comparison with other reported aluminohydride complexes. IR bands for **33** were detected at 1743 cm^{-1} and at 1609 cm^{-1}. The former is consistent with terminal Al-H stretches and the latter could relate to either bridging hydrogen atoms or the Ru-H stretching frequency.[64, 65] **33** was not isolated due to its high reactivity, in line with other aluminohydride species.[64, 66-68]

4.29.2 Treatment of $Ru(PPh_3)(IMes)(CO)(Cl)H$ (8) with $LiAlH_4$

8 was also treated with $LiAlH_4$ but suffered from the same problems as **33**. The ^1H NMR spectrum showed four discreet new hydride signals within the same region (-8.03, -9.24 (br), -9.59 and -12.06 ppm), the latter two showed phosphorus coupling to a signal at 51.2 ppm in the $^{31}P\{^1H\}$ NMR spectrum. The J_{HP} values (65.7 and 21.9 Hz) concurred with the expected *cis* relationships between the two nuclei. Over time (3 days) at 298 K more hydride signals appeared and the previously major signals collapsed into the same broad resonance seen for $[(IMes)_2(CO)HRuAlH_4]_2$. In decomposition, phosphine ligands were lost and the ^{27}Al peak changed from 99.3 to 69.1 ppm in the ^{27}Al NMR spectrum.

4.29.3 Reduction of chloride complexes with $LiHBEt_3$

7 was reacted with a THF solution of 'super hydride' $LiHBEt_3$, with no reaction occurring over 3 days (up to 343 K). In contrast, the analogous complex **8** reacted immediately at room temperature producing an array of hydride complexes including the established species $Ru(PPh_3)_2(IMes)(CO)H_2$.

4.30 Reduction of chloride complexes with $KN(SiMe_3)_2$

4.30.1 Formation of the dihydrogen dihydride complex $Ru(IMes)_2(CO)(\eta^2\text{-}H_2)H_2$ (34)

The dihydrogen dihydride complex $Ru(IMes)_2(CO)(\eta^2\text{-}H_2)H_2$ (**34**) was formed upon reaction of $Ru(IMes)_2(CO)(Cl)H$ (**7**) with stoichiometric amounts of $KN(SiMe_3)_2$ in the presence of 1 atm H_2 (**Scheme 4.28**). A very broad signal was observed in the ^1H NMR spectrum at around -6 ppm for all four hydrogen atoms. Low temperature ^1H NMR spectroscopy (down to 190 K) of **34** did not result in any splitting of the broad resonance. Furthermore, $^1H\text{-}^{13}C\{^1H\}$ HMBC spectroscopy did not exhibit any cross-peaks between the hydride signal and the carbenic or carbonyl carbon atoms, consistent with fast exchange between the classical and non-classical hydrogens so that coupling is not observed. Nemeh reported a similar dehydrohalogenation reaction, in which Rh(PCP)(Cl)H was treated with $NaN(SiMe_3)_2$ to afford a very reactive 14-electron species, which reacted in the presence of H_2 to form $Rh(PCP)(\eta^2\text{-}H_2)$.[69]

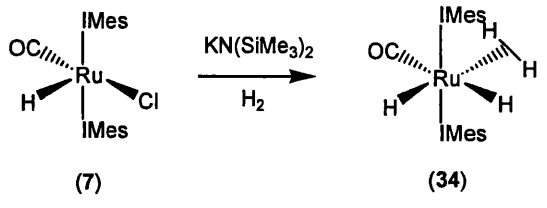

(7) (34)

Scheme 4.28 Preparation of $Ru(IMes)_2(CO)(\eta^2\text{-}H_2)H_2$ (**34**).

It is likely that this type of transformation (**Scheme 4.28**) occurred in the reaction of $Ru(P^tBu_2Me)_2(CO)(Cl)H$ with H_2 to form $Ru(P^tBu_2Me)_2(CO)(\eta^2\text{-}H_2)(H)_2$, in the presence of KOH. Presumably the hydroxide species $Ru(P^tBu_2Me)_2(CO)(OH)H$ is formed before the dihydrogen dihydride is produced.[70] Similar results have also been reported for the related complex $Ru(PPh_3)_3Cl_2$.[71]

Reduction of **7** in the absence of hydrogen gas, gave a ^1H NMR spectrum resembling that of the starting complex **7**. As previously discussed in Chapter 2, Caulton was able to react $Ru(P^tBu_2Me)_2(CO)(I)H$ with H_2 to produce $Ru(P^tBu_2Me)_2(CO)(\eta^2\text{-}H_2)(H)_2$ but only in the presence of DBU (1,8-diazabicyclo[5.4.0]undec-7-ene) a non-coordinating Brønsted base {without success for $Ru(P^tBu_2Me)_2(CO)(Cl)H$}.[26] Reaction of $Ru(P^tBu_2Me)_2(CO)(I)H$ with solely DBU does not produce any change so the authors proposed that the reagent deprotonates H_2 from the intermediate $Ru(P^tBu_2Me)_2(CO)(I)(\eta^2\text{-}H_2)H$ to produce $[Ru(P^tBu_2Me)_2(CO)(I)H_2^-][H\text{-}DBU^+]$ which subsequently loses I^- and adds another molecule of H_2.[26]

The X-ray crystal structure of **34** was previously obtained within the Whittlesey group, following reaction of $Ru(AsPh_3)(IMes)_2(CO)H_2$ (**1**) with H_2 under rigorously anhydrous conditions. This approach was generally considered unreliable and difficult, requiring incredibly dry solvents as both the starting material and product will go on to react with any adventitious water to produce the hydroxide complex $Ru(IMes)_2(CO)(OH)H$ (**2**), (equally, if any source of 'Cl' was present, **7** was formed). In correlation with the results described in Chapter 2 involving treatment of **2** with H_2 to produce **34**, we conclude that the reaction between **34** and **2** is in equilibrium where the formation of **2** is much more favourable (**Scheme 4.29**).

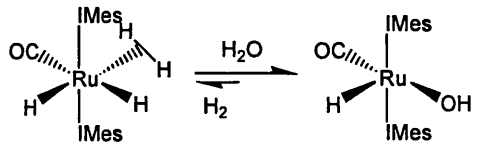

(34) (2)

Scheme 4.29 Equilibrium between $Ru(IMes)_2(CO)(\eta^2\text{-}H_2)H_2$ (**34**) and $Ru(IMes)_2(CO)(OH)H$ (**2**).

4.31 Attempted formation of the dihydride complex $RuL_2(CO)H_2$ using silyl transfer reagents

We proposed that the 16-electron dihydride complex $RuL_2(CO)H_2$ {L_2 = $(IMes)_2$, $(PPh_3)(IMes)$} could be formed from the reaction of $RuL_2(CO)(X)H$ {X = Cl, F and OH in the case of L_2 = $(IMes)_2$} with the silyl transfer agent Et_3SiH (**Scheme 4.30**).[26, 72 73] The driving force behind the reaction is the formation of a new strong Si-X bond.[72]

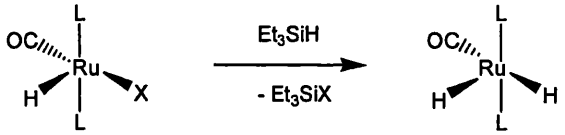

Scheme 4.30 Proposed formation of $RuL_2(CO)H_2$.

On reaction of $Ru(IMes)_2(CO)(X)H$ {X = OH (**2**), F (**6**), Cl (**7**)} with Et_3SiH the corresponding ^1H NMR spectra did not show any change. The lack of reactivity may be attributed to the steric bulk of the IMes groups, resulting in a protected metal centre. To determine whether this was the case the less sterically hindered, mixed phosphine-NHC complexes $Ru(PPh_3)(IMes)(CO)(X)H$ {X = Cl (**8**), F (**35**)} were investigated. **35** was prepared following preparations devised in the Whittlesey group *via* two routes (**a** and **b**, **Scheme 4.31**), both including PR_3 / IMes exchange and fluorination by $Et_3N.3HF$.[74]

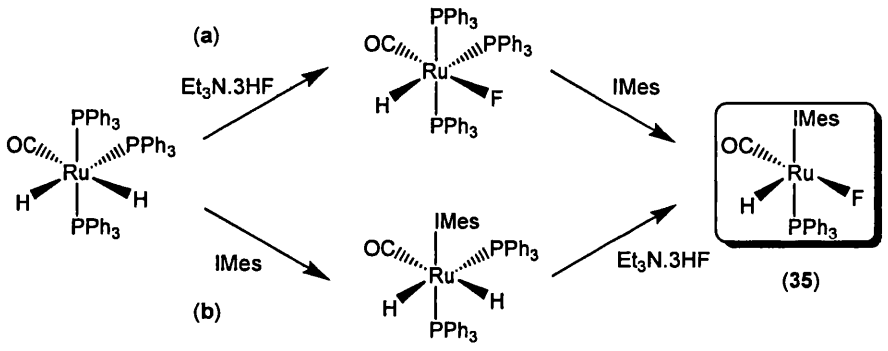

Scheme 4.31 Preparation of $Ru(PPh_3)(IMes)(CO)(F)H$ (**35**).

Following route **a** (**Scheme 4.31**) conversion of $Ru(PPh_3)_3(CO)H_2$ to $Ru(PPh_3)_3(CO)(F)H$ with 3 equiv. $Et_3N.3HF$ occurred at 358 K over 4-6 h and subsequent PPh_3 / NHC exchange occurred in *ca.* 1 h at 298 K upon addition of 3 equiv. IMes. **35** was characterised by a very broad signal at *ca.* -21.9 ppm in the ^1H NMR spectrum and 40.5 ppm (br d, J_{PF} = 28.3 Hz) in the $^{31}P\{^1H\}$ NMR spectrum. The bis IMes species $Ru(IMes)_2(CO)(F)H$ (**6**) was also produced, becoming the major product when the reaction was continued past an hour at 298 K, even when only stoichiometric amounts of IMes were used. In order to optimise the amount of **35** it was necessary to follow the reaction carefully and use the sample for reactions immediately as isolation was not feasible.

The alternative route (**b**) involved harsher reaction conditions, with the formation of $Ru(PPh_3)_2(IMes)(CO)H_2$ requiring heating at 353 K for 4 days before fluorination with stoichiometric amounts of $Et_3N.3HF$. $Ru(PPh_3)_2(IMes)(CO)H_2$ also proved difficult to isolate cleanly especially with respect to free PPh_3.

Treatment of $Ru(PPh_3)(IMes)(CO)(Cl)H$ (**8**) with Et_3SiH did not result in any changes in the ^1H NMR spectrum even after heating (up to 343 K). In contrast,[26] when the fluoride analogue **35** was treated with 1 equiv. Et_3SiH at room temperature the coordinatively saturated complex $Ru(PPh_3)_2(IMes)(CO)H_2$ (**36**) was formed immediately (**Scheme 4.32**) as determined by characteristic doublet of doublet of doublet resonances in the ^1H NMR spectrum at -6.36 and -8.08 ppm (H_a and H_b respectively).

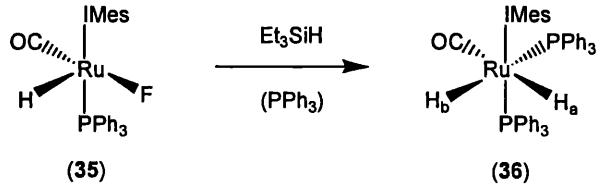

(35) (36)

Scheme 4.32 F/H ligand exchange in **35** using Et_3SiH as a transfer agent.

The $^{31}P\{^1H\}$ NMR spectrum of **36** revealed diagnostic chemical shifts at 59.0 and 47.8 ppm (both d, J_{PP} = 14.8 Hz). The second phosphine ligand in **36** originates

from free PPh_3 in the reaction mixture, suggesting that $Ru(PPh_3)(IMes)(CO)H_2$ is unstable as a 16-electron complex, requiring a 2-electron donor such as PPh_3 for stability. The ^{19}F NMR spectrum showed evidence of the byproduct Et_3SiF at -175.0 ppm. This work has verified that the methodology using Et_3SiH as a transfer agent works and this work is ongoing.[74]

4.32 Chapter Summary

The attempted reduction of $RuL_2(CO)(Cl)H$ {L_2 = $(IMes)_2$, $(PPh_3)(IMes)$} with $NaBH_4$ failed to afford the dihydride complex $RuL_2(CO)H_2$, instead producing the borohydride complexes $RuL_2(CO)(\eta^2\text{-}BH_4)H$, which are relatively stable and do not lose BH_3 to form $RuL_2(CO)H_2$. The fluxional behaviour of the BH_4^- ligands in both species was verified by VT, T_1 and labelling studies. Furthermore, their use as catalysts in the hydrogenation of acetophenone gave conversions consistent with the coordinatively unsaturated chloride starting complexes. Both complexes show a propensity for the BH_4^- ligand to 'open up' creating a vacant site *trans* to the hydride ligand, consistent with the majority of analogous systems. However, labelling experiments revealed that isomerisation does occur resulting in the coordination of small molecules in several different sites. With low temperature studies, it was possible to observe $\eta^1\text{-}BH_4^-$ as the dicarbonyl species $RuL_2(CO)_2(\eta^1\text{-}BH_4)H$.

The mixed PPh_3 / IMes borohydride complex (**26**) displayed significantly higher reactivity than the bis IMes analogue (**19**). The former reacted with PMe_2Ph at room temperature, whereas **19** required heating for 2 days at 343 K for a reaction to occur, suggesting that the second IMes ligand in **19** helps to stabilise the complex. Also, in contrast to **19**, **26** reacted with 4-Mepy, whereby 4-Mepy acted to remove BH_3 and coordinate as a ligand to form an 18-electron dihydride complex.

Reduction of $RuL_2(CO)(Cl)H$ with $LiAlH_4$ and superhydride met with limited success, mostly due to high reactivity of aluminohydride complexes and the many products formed in the reaction with the latter. Although the dihydrogen dihydride complex $Ru(IMes)_2(CO)(\eta^2\text{-}H_2)H_2$ (**34**) was formed upon the reaction of

$Ru(IMes)_2(CO)(Cl)H$ with $KN(SiMe_3)_2$ in the presence of H_2, we are still no closer to finding a reasonable method for the isolation of **34** because of its very reactive nature. The reaction of the mixed PPh_3 / IMes fluoride complex $Ru(PPh_3)(IMes)(CO)(F)H$ (**35**) with the silyl transfer agent Et_3SiH resulted in F/H ligand exchange, establishing that the methodology was successful.

4.33 References

1. Schlesinger, H.I.; Brown, H.C.; Hoekstra, H.R.; Rapp, L.R., *J. Am. Chem. Soc.*, **1953**, *75*, 199.
2. Brown, H.C., *Nobel Lecture*, **1979**.
3. Brown, H.C.; Brown, C.A., *J. Am. Chem. Soc.*, **1962**, *84*, 1493.
4. Blackmore, T.; Bruce, M.I.; Stone, F.G.A., *J. Chem. Soc. A*, **1971**, 2376.
5. Marks, T.J.; Kolb, J.R., *Chem. Rev.*, **1977**, *77*, 263.
6. Suzuki, H.; Lee, D.H.; Oshima, N.; Morooka, Y., *Organometallics*, **1987**, *6*, 1569.
7. Bennett, M.A.; Latten, J., *Aust. J. Chem.*, **1987**, *40*, 841.
8. Gusev, D.G.; Dolgushin, F.M.; Antipin, M.Y., *Organometallics*, **2000**, *19*, 3429.
9. Bruno, J.W.; Huffman, J.C.; Caulton, K.G., *Inorg. Chim. Acta-Articles and Letters*, **1984**, *89*, 167.
10. Letts, J.B.; Mazanec, T.J.; Meek, D.W., *J. Am. Chem. Soc.*, **1982**, *104*, 3898.
11. Crabtree, R.H.; Pearman, A.J., *J. Organomet. Chem.*, **1978**, *157*, 335.
12. Statler, J.A.; Wilkinson, G.; Thorntonpett, M.; Hursthouse, M.B., *J. Chem. Soc., Dalton Trans.*, **1984**, 1731.
13. Holah, D.G.; Hughes, A.N.; Hui, B.C., *Can. J. Chem.*, **1976**, *54*, 320.
14. Xu, Z.T.Lin, Z.Y., *Coord. Chem. Rev.*, **1996**, *156*, 139.
15. Esteruelas, M.A.; Garcia, M.P.; Lopez, A.M.; Oro, L.A.; Ruiz, N.; Schlunken, C.; Valero, C.; Werner, H., *Inorg. Chem.*, **1992**, *31*, 5580.
16. Rhodes, L.F.; Venanzi, L.M.; Sorato, C.; Albinati, A., *Inorg. Chem.*, **1986**, *25*, 3335.
17. Nolan, S.P.; Belderrain, T.R.; Grubbs, R.H., *Organometallics*, **1997**, *16*, 5569.
18. Abdur-Rashid, K.; Fedorkiw, T.; Lough, A.J.; Morris, R.H., *Organometallics*, **2004**, *23*, 86.
19. Poulton, J.T.; Sigalas, M.P.; Folting, K.; Streib, W.E.; Eisenstein, O.; Caulton, K.G., *Inorg. Chem.*, **1994**, *33*, 1476.
20. Heyn, R.H.; Macgregor, S.A.; Nadasdi, T.T.; Ogasawara, M.; Eisenstein, O.; Caulton, K.G., *Inorg. Chim. Acta*, **1997**, *259*, 5.

21. Chamberlain, B.; Duckett, S.B.; Lowe, J.P.; Mawby, R.J.; Stott, J.C., *Dalton Trans.*, **2003**, 2603.
22. Kohlmann, W.; Werner, H., *Z. Naturforsch.*, **1993**, *48*, 1499.
23. Werner, H.; Esteruelas, M.A.; Meyer, U.; Wrackmeyer, B., *Chem. Ber.*, **1987**, *120*, 11.
24. Lowe, J.P., *PhD Thesis, University of York*, **1999**.
25. Rhodes, L.F.; Venanzi, L.M., *Inorg. Chem.*, **1987**, *26*, 2692.
26. Poulton, J.T.; Sigalas, M.P.; Eisenstein, O.; Caulton, K.G., *Inorg. Chem.*, **1993**, *32*, 5490.
27. Williams, R.E., *J. Inorg. Nucl. Chem.*, **1961**, *20*, 198.
28. Demachy, I.; Esteruelas, M.A.; Jean, Y.; Lledos, A.; Maseras, F.; Oro, L.A.; Valero, C.; Volatron, F., *J. Am. Chem. Soc.*, **1996**, *118*, 8388.
29. Merle, N.; Koicok-Kohn, G.; Mahon, M.F.; Frost, C.G.; Ruggiero, G.D.; Weller, A.S.; Willis, M.C., *Dalton Trans.*, **2004**, *22*, 3883.
30. Bourumeau, K.; Gaumont, A.C.; Denis, J.M., *J. Organomet. Chem.*, **1997**, *529*, 205.
31. Jaganyi, D.; Mzinyati, A., *Polyhedron*, **2006**, *25*, 2730.
32. Ramnial, T.; Jong, H.; McKenzie, I.D.; Jennings, M.; Clyburne, J.A.C., *Chem. Commun.*, **2003**, 1722.
33. Perdigon-Melon, J.A.; Auroux, A.; Cornu, D.; Miele, P.; Toury, B.; Bonnetot, B., *J. Organomet. Chem.*, **2002**, *657*, 98.
34. Bolano, S.; Albinati, A.; Bravo, J.; Gonslavi, L.; Peruzzini, M., *Inorg. Chem. Comm.*, **2006**, *9*, 360.
35. Tellenbach, A.; Jansen, M., *Eur. J. Chem.*, **2003**, 3759.
36. Jazzar, R.F.R.; Mahon, M.F.; Whittlesey, M.K., *Organometallics*, **2001**, *20*, 3745.
37. Lowe, J.P.; Lowe, J.C.; Duckett, S.B.; Mawby, R.J., *Dalton Trans.*, **2004**, 3788.
38. Jazzar, R.F.R.; Bhatia, P.H.; Mahon, M.F.; Whittlesey, M.K., *Organometallics*, **2003**, *22*, 670.
39. Bianchini, C.; Perez, P.J.; Peruzzini, M., *Inorg. Chem.*, **1991**, *30*, 279.
40. Baker, M.V.; Field, L.D., *Chem. Commun.*, **1984**, 997.

41. Chatwin, S.L.; Davidson, M.G.; Doherty, C.; Donald, S.M.; Jazzar, R.F.R.; Macgregor, S.A.; McIntyre, G.J.; Mahon, M.F.; Whittlesey, M.K., *Organometallics*, **2006**, *25*, 99.
42. Jazzar, R.F.R., *PhD Thesis, University of Bath*, **2003**.
43. Jones, R.A.; Wilkinson, G.; Galas, A.M.R.; Hursthouse, M.B.; Malik, K.M.A., *J. Chem. Soc., Dalton Trans.*, **1980**, 1771.
44. Chaudret, B.; Sabo, S.; Dahan, F., *Acta Cryst. Sect. C - Cryst. Struct. Commun.*, **1984**, *40*, 786.
45. Dunne, J.P.; Blazina, D.; Aiken, S.; Carteret, H.A.; Duckett, S.B.; Jones, J.A.; Poli, R.; Whitwood, A.C., *Dalton Trans.*, **2004**, 3616.
46. Lindner, E.; Pautz, S.; Fawzi, R.; Steimann, M., *Organometallics*, **1998**, *17*, 3006.
47. King, R.B.; Saran, M.S., *Inorg. Chem.*, **1974**, *13*, 74.
48. James, B.D.; Nanda, R.K.; Wallbridge, M.G.H., *Inorg. Chem.*, **1967**, *6*, 1979.
49. Green, M.L.H.; Munakata, H., *J. Chem. Soc., Dalton Trans.*, **1974**, 269.
50. Jazzar, R.F.R.; Macgregor, S.A.; Mahon, M.F.; Richards, S.P.; Whittlesey, M.K., *J. Am. Chem. Soc.*, **2002**, *124*, 4944.
51. Titcomb, L.r.; Caddick, S.; Cloke, F.G.N.; Wilson, D.J.; McKerrecher, D., *Chem. Commun.*, **2001**, 1388.
52. Simms, R.W.; Drewitt, M.J.; Baird, M.C., *Organometallics*, **2002**, *21*, 2958.
53. Stott, J.C., *PhD Thesis, University of York*, **2001**.
54. Nolan, S.P.; Fogg, D.E.; dos Santos, E.N.; Foucault, H.M.; Dharmasena, U.L., *Organometallics*, **2005**, *24*, 1056.
55. L'Eplattenier, F.; Calderazzo, F., *Inorg. Chem.*, **1968**, *7*, 1290.
56. Whittlesey, M.K.; Perutz, R.N.; Mawby, R.J., *Organometallics*, **1995**, *14*, 3268.
57. Bray, J.M.; Mawby, R.J., *J. Chem. Soc., Dalton Trans.*, **1987**, 2989.
58. Clot, E.; Eisenstein, O.; Dubé, T.; Faller, J.W.; Crabtree, R.H., *Organometallics*, **2002**, *21*, 575.
59. Wohnrath, K.; Batista, A.A.; Gilberto Ferreira, A.; Zuckerman-Schpector, J.; de Oliveira, L.A.A.; Castellano, E.E., *Polyhedron*, **1998**, *17*, 2013.

60. Esteruelas, M.A.; Valero, C.; Oro, L.A.; Meyer, U.; Werner, H., *Inorg. Chem.*, **1991**, *30*, 1159.

61. Aracama, M.; Esteruelas, M.A.; Lahoz, F.J.; Lopez, J.A.; Meyer, U.; Oro, L.A.; Werner, H., *Inorg. Chem.*, **1991**, *30*, 288.

62. Esteruelas, M.A.; Jean, Y.; Lledós, A.; Oro, L.A.; Ruiz, N.; Volatron, F., *Inorg. Chem.*, **1994**, *33*, 3609.

63. Bohanna, C.; Esteruelas, M.A.; Herrero, J.; López, A.M.; Oro, L.A., *J. Organomet. Chem.*, **1995**, *498*, 199.

64. Barron, A.R.; Wilkinson, G., *Polyhedron*, **1986**, *5*, 1897.

65. Bulychev, B.M., *Polyhedron*, **1990**, *9*, 387.

66. Barron, A.R.; Lyons, D.; Wilkinson, G.; Motevalli, M.; Howes, A.J.; Hursthouse, M.B., *J. Chem. Soc., Dalton Trans.*, **1986**, 279.

67. Lin, W.; Wilson, S.R.; Girolami, G.S., *Organometallics*, **1997**, *16*, 2987.

68. Bel'sky, V.K.; Sizov, A.I.; Bulychev, B.M.; Soloveichik, G.L., *J. Organomet. Chem.*, **1985**, *280*, 67.

69. Nemeh, S.; Jensen, C.; Binamirasoriaga, E.; Kaska, W.C., *Organometallics*, **1983**, *2*, 1442.

70. Esteruelas, M.A.; Sola, E.; Oro, L.A.; Werner, H.; Meyer, U., *J. Mol. Cat.*, **1988**, *45*, 1.

71. Aranyos, A.; Csjernyik, G.; Szabó, K.J.; Backväll, J.E., *Chem. Commun.*, **1999**, 351.

72. Cooper, A.C.; Huffman, J.C.; Caulton, K.G., *Inorg. Chim. Acta*, **1998**, *270*, 261.

73. Vela, J.; Smith, J.M.; Yu, Y.; Ketterer, N.A.; Flaschenriem, C.J.; Lachicotte, R.J.; Holland, P.L., *J. Am. Chem. Soc.*, **2005**, *127*, 7857.

74. Reade, S.P., *unpublished results*, **2007**.

Chapter 5

5 Experimental

5.1 General Procedures

All reactions and manipulations were carried out under argon using standard Schlenk line techniques or in a moisture-free M. Braun glovebox unless otherwise stated. Glassware was oven-dried at 413 K overnight or flame-dried *in vacuo*.

Solvents, generally purchased from Fisher, were used dried and degassed. The solvents hexane, pentane, CH_2Cl_2, diethylether, THF, MeOH were dried over columns in a M. Braun SPS solvent system before use. Benzene and toluene were distilled under N_2 from purple solutions of sodium dispersion with benzophenone and EtOH was distilled from magnesium turnings and iodine. Deuterated solvents were purchased from Fluorochem and dried over potassium (C_6D_6, $C_6D_5CD_3$, and THF-d_8) or calcium hydride ($CDCl_3$, CD_2Cl_2) and subsequently vacuum-transferred into ampoules fitted with J. Youngs PTFE taps. The gases H_2 (BOC, 99.99 %), D_2 (Isotec, 99.8 %), CO (BOC), ^{13}CO (Promochem, 99 %), NH_3 (Aldrich, 99.99 %), ethene (Aldrich, 99.5 %) and H_2S (Aldrich, 99.5 %) were used as received. $RuCl_3.3H_2O$ was kindly donated by Johnson-Matthey.

5.2 Physical and analytical measurements

NMR spectra were recorded on Bruker Avance 300 or 400 MHz spectrometers and referenced to the chemical shifts of residual protio solvent resonances (C_6D_5H δ 7.15; $C_6D_5CD_2H$ δ 2.09; THF-d_7 δ 3.57; $CHCl_3$ δ 7.26; $CHDCl_2$ δ 5.31). $^{13}C\{^1H\}$ NMR spectra were referenced to C_6D_6 (δ 128.7); $C_6D_5CD_3$ (δ 21.3); THF-d_7 (δ 67.2). $^{31}P\{^1H\}$ and $^{11}B\{^1H\}$ NMR chemical shifts were referenced externally to 85 % H_3PO_4 (δ 0.0) and $BF_3.OEt_2$ (δ 0.0) respectively. ^{19}F NMR chemical shifts were referenced to neat $CFCl_3$ (δ 0.0) and ^{15}N NMR spectra referenced to the IUPAC standard, neat CH_3NO_2 (δ 0.0).

IR spectra were recorded as nujol mulls or in C_6D_6 on a Nicolet Nexus FTIR spectrometer. Elemental analyses were performed by Elemental Microanalysis Ltd., Okehampton, Devon. Mass spectrometry analyses were carried out at the University of Bath on a micrOTOF electrospray time-of-flight (ESI-TOF) mass spectrometer (Bruker Daltonik GmbH) coupled to an Agilent 1200 LC system (Agilent

Technologies) used for autosampling and sample introduction only. 10 μL of sample was injected into a 30:70 flow of H_2O:MeCN at 0.3 mL min^{-1} to the mass spectrometer. The nebulising gas was N_2 (*ca.* 1 atm), as was the drying gas (8 L min^{-1} flow rate, 473 K). Positive ion mode was used with a corresponding capillary voltage of -4000 V. Only full scan data was acquired.

Crystal structures were recorded at the University of Bath on a Nonius KappaCCD diffractometer and at Station 9.8, SRS, Daresbury Laboratory, Daresbury, Cheshire. X-ray data was analysed using the SHELX suite of programs.[1]

5.3 Synthesis of NHC ligands

5.3.1 Preparation of 1,3-bis(2,4,6-trimethylphenylimidazol-2-ylidene (IMes)

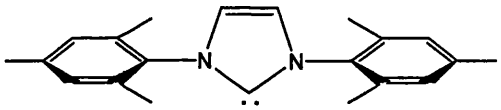

IMes was prepared *via* an adapted literature method.[2]

5.3.1.1 Preparation of glyoxal-bis(2,4,6-trimethylphenyl)diazabutadiene

A 40 % aqueous solution of glyoxal (72.6 g, 0.5 mol), 2,4,6-trimethylphenylamine (135.2 g, 1.0 mol) and degassed EtOH (500 mL) was added to a 1000 mL round-bottomed flask. The mixture was stirred for 12 h at 298 K, during which time a thick yellow precipitate formed. The precipitate was isolated by filtration in air, washed with cold EtOH (3 x 50 mL) and dried *in vacuo*. Yield: 212.0 g (73 %).
FW = 292.42. ^{1}H NMR ($CDCl_3$, 298 K, 300 MHz): δ 8.13 (s, 2H, NC**H**), 6.93 (s, 4H, $C_6H_2Me_3$), 2.32 (s, 6H, *p*-CH_3), 2.19 (s, 12H, *o*-CH_3).

5.3.1.2 Preparation of 1,3-bis(2,4,6-trimethylphenyl)imidazolium chloride

In a 1000 mL round-bottomed flask bis-(2,4,6-trimethylphenyl)-diazabutadiene (20.0 g, 68.5 mmol) was dissolved in undried toluene (500 mL) and paraformaldeyde added (2.0 g, 0.7 mmol). The reaction mixture was heated to 373 K and then cooled

to 313 K, after which time HCl (16.5 mL, 4 M dioxane) was introduced causing a colour change from yellow to dark red. The reaction was maintained at 343 K for 5 h, then allowed to cool to 298 K and stirred for a further 36 h. The product was isolated by filtration in air, washed with THF (3 x 50 mL) and dried extensively *in vacuo* and stored in the glovebox. Yield: 15.6 g (69 %).

FW = 340.89. ^{1}H NMR ($CDCl_3$, 298 K, 300 MHz): δ 10.31 (s, 1H, C**H**), 7.65 (s, 2H, NC**H**), 6.88 (s, 4H, $C_6\mathbf{H}_2Me_3$), 2.22 (s, 6H, *p*-$\mathbf{CH}_3$), 2.04 (s, 12H, *o*-$\mathbf{CH}_3$).

5.3.1.3 Preparation of 1,3-bis(2,4,6-trimethylphenyl)imidazol-2-ylidene (IMes)

A flame-dried Schlenk tube was charged with a stirrer bar, 1,3-bis(2,4,6-trimethylphenyl)imidazolium chloride (10.0 g, 28.0 mmol) and KO^{t}Bu (4.0 g, 36.0 mmol). The dry mixture was stirred and cooled to 195 K in an acetone/dry-ice bath before adding THF (100 mL). The mixture was stirred vigorously and after 20 min the bath was removed and the mixture allowed to warm to 298 K for another 20 min. The solvent was removed *in vacuo* and the residue dried completely. The product was extracted by adding toluene (100 mL) and filtering through celite under inert conditions. The filtrate was dried *in vacuo*. Yield = 6.5 g (73 %).

FW = 304.43. ^{1}H NMR (C_6D_6, 298 K, 300 MHz): δ 6.80 (s, 4H, $C_6\mathbf{H}_2Me_3$), 6.51 (s, 2H, NC**H**), 2.16 (s, 6H, *p*-$\mathbf{CH}_3$), 2.14 (s, 12H, *o*-$\mathbf{CH}_3$).

5.4 Syntheses of ruthenium starting materials

5.4.1 Preparation of $Ru(AsPh_3)_3(CO)H_2$

5.4.1.1 Preparation of $Ru(AsPh_3)_3(CO)Cl_2$

$Ru(AsPh_3)_3(CO)Cl_2$ was prepared using a literature method.[3]

A 500 mL three necked round bottom flask fitted with a magnetic stirrer bar, reflux condenser, argon inlet and outlet bubbler was charged with $AsPh_3$ (7.40 g, 24.2 mmol) and 2-methoxyethanol (*ca.* 200 mL) and heated in the reflux apparatus until boiling. $RuCl_3.H_2O$ (1.18 g, 4.52 mmol) dissolved in 2-methoxyethanol (*ca.* 60 mL) was added quickly to the boiling arsine solution, quickly followed by (previously

degassed) aqueous formaldehyde (88 mL, 40% w/v solution). The mixture was heated under reflux for 2 h, in which time there was a colour change from very dark brown to pale orange. The solution was cooled in an ice bath to precipitate the yellow product and filtered on a Buchner funnel and washed with cold hexane. The powder was dried *in vacuo*. Yield: 4.2 g (66 %).

FW = 1118.69. IR (nujol, cm^{-1}): 1949 (ν_{CO}).

5.4.1.2 Preparation of $Ru(AsPh_3)_3(CO)H_2$

$Ru(AsPh_3)_3(CO)H_2$ was prepared using a literature method.[3]

A 500 mL three necked round bottom flask fitted with a magnetic stirrer bar, reflux condenser, argon inlet and outlet bubbler was charged with $Ru(AsPh_3)_3(CO)Cl_2$ (2.10 g, 17.7 mmol), $NaBH_4$ (4.00 g, 106 mmol) and EtOH (*ca.* 200 mL). The mixture was stirred and refluxed for 1.5 h resulting in a tan slurry. The mixture was subsequently cooled, filtered through a sinter and washed three times with EtOH (3 x 25 mL). The product was extracted from the residue with toluene (*ca.* 80 mL) and the solvent was removed *in vacuo* to leave a brown residue, to which EtOH was added (*ca.* 80 mL) and stirred overnight to precipitate a white powder. The precipitate was washed with cold EtOH (2 x 25 mL) and cold hexane (25 mL) and dried *in vacuo*. Yield: 1.04 g (56 %).

FW = 1049.80. IR (nujol, cm^{-1}): 1928 (ν_{CO}). ^1H NMR (C_6D_6, 298 K, 300 MHz): δ -9.44 (d, 1H, Ru-**H**, J_{HH} = 6.6 Hz), -9.92 (d, 1H, Ru-**H**, J_{HH} = 6.6 Hz).

5.4.2 Preparation of $Ru(PPh_3)_3(CO)(Cl)H$

$Ru(PPh_3)_3(CO)(Cl)H$ was prepared using a scaled-up literature method (x 4).[4]

A 500 mL three necked round bottom flask fitted with a magnetic stirrer bar, reflux condenser, argon inlet and outlet bubbler was charged with PPh_3 (6.32 g, 24 mmol) and 2-methoxyethanol (*ca.* 200 mL) and heated in the reflux apparatus until boiling. $RuCl_3.H_2O$ (1.04 g, 4.0 mmol) dissolved in 2-methoxyethanol (*ca.* 60 mL) was added quickly to the boiling phosphine solution, quickly followed by (previously degassed) aqueous formaldehyde (80 mL, 40% w/v solution). The mixture was heated under reflux for 10 min. The solution was cooled in an ice bath to precipitate the yellow product and filtered on a Buchner funnel and washed with aliquots of cold

EtOH, H_2O, EtOH and hexane. The powder was dried *in vacuo*. Yield = 3.43 g (90 %).

FW = 952.40. IR (nujol, cm^{-1}): 2020 (ν_{CO}), 1922 (ν_{Ru-H}), 1903 (ν_{CO}).

5.4.3 Preparation of $Ru(PPh_3)_3(CO)H_2$

$Ru(PPh_3)_3(CO)H_2$ was prepared using a scaled-up literature method (x 4).[4]

A 1000 mL three necked round bottom flask fitted with a magnetic stirrer bar, reflux condenser, argon inlet and outlet bubbler was charged with PPh_3 (12.56 g, 48 mmol) and EtOH (*ca.* 500 mL) and heated in the reflux apparatus until boiling. $RuCl_3.H_2O$ (2.08 g, 8.0 mmol) dissolved in EtOH (*ca.* 80 mL) was added quickly to the boiling phosphine solution, quickly followed by (previously degassed) aqueous formaldehyde (80 mL, 40% w/v solution) and KOH (2.40 g, 40 mmol) in EtOH (*ca.* 80 mL). The mixture was heated under reflux for 20 min. The solution was cooled in an ice bath to precipitate the yellow product and filtered on a Buchner funnel and washed with aliquots of cold EtOH, H_2O, EtOH and hexane (*ca.* 50 mL each). The powder was dried *in vacuo* and the product extracted with C_6H_6 (*ca.* 50 mL) through neutral alumina. The solution was reduced and stirred in MeOH to precipitate the product, which was subsequently filtered and dried *in vacuo*. Yield = 5.0 g (68 %).

FW = 917.95. IR (nujol, cm^{-1}): 1960 (ν_{CO}). ^1H NMR (C_6D_6, 298 K, 300 MHz): δ -6.53 (ddt, J_{HP} = 30.5, 15.3 Hz, J_{HH} = 6.1 Hz, 1H, Ru-**H**), -8.29 (ddt, J_{HP} = 74.5, 28.1 Hz, J_{HH} = 6.1 Hz, 1H, Ru-**H**). $^{31}P\{^1H\}$: δ 58.2 (d, J_{PP} = 16.8 Hz), 46.1 (t, J_{PP} = 16.8 Hz).

5.4.4 Preparation of $Ru(PPh_3)_3(CO)(F)H$

$Ru(PPh_3)_3(CO)(F)H$ was prepared using a method created by Reade.[5]

An ampoule fitted with a stirrer bar and a J. Youngs' PTFE tap was charged with $Ru(PPh_3)_3(CO)H_2$ (0.45g, 0.49 mmol), $Et_3N.3HF$ (0.24 mL, 1.47 mmol) and THF (*ca.* 20 mL). The reaction mixture was heated at 358 K for 6.5 h and then cooled to 298 K before removing the solvent *in vacuo*. The off-white precipitate was washed with pentane (2 x 20 mL), dried for 16 h *in vacuo* and recrystalised from C_6H_6/hexane twice. Yield: 360 mg (79 %).

FW = 935.94. IR (nujol, cm^{-1}): 1917 (ν_{CO}). ^1H NMR (C_6D_6, 298 K, 400 MHz): δ 7.5-7.2 (m, 17H, P**Ph**$_3$), 6.9-6.6 (m, 28H, P**Ph**$_3$), -5.35 (dt, J_{HP} = 112.5, 25.2 Hz, 1H, Ru-**H**). $^{31}P\{^1H\}$: δ 39.5 (m), 18.7 (m). ^{19}F: δ -380.6 (br s, Ru-**F**)

5.4.5 Preparation of $Ru(IMes)_2(AsPh_3)(CO)H_2$ (1)

A Schlenk tube was charged with $Ru(AsPh_3)_3(CO)H_2$ (0.85 g, 0.81 mmol) and IMes (0.85 g, 2.79 mmol) and the contents dried rigorously *in vacuo* overnight at 298 K. Toluene (*ca.* 10 mL) was added to the Schlenk tube *via* cannula and the reaction mixture stirred at 343 K for 3 days. The solvent was removed *in vacuo* to afford a very reactive oily residue (not isolated).

^1H NMR (C_6D_6, 298 K, 400 MHz): δ -5.71 (d, J_{HH} = 5.9 Hz, 1H, Ru-**H**), -8.93 (d, J_{HH} = 5.9 Hz, 1H, Ru-**H**).

5.5 Syntheses of 16-electron Ru-IMes complexes

5.5.1 Preparation of $Ru(IMes)_2(CO)(OH)H$ (2)

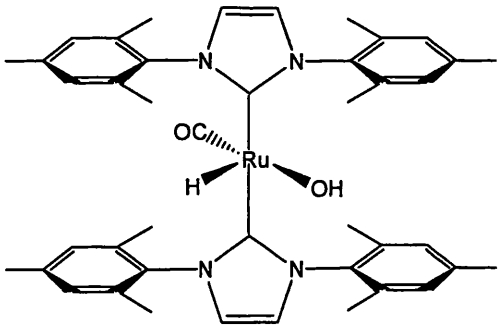

5.5.1.1 Preferred method

$Ru(IMes)_2(CO)(OH)H$ was prepared using a slightly modified literature method.[6] A 50:50 mixture of hexane and H_2O was degassed by bubbling argon through the solvent for 20 min and added *via* cannula to an ampoule fitted with a J. Youngs' PTFE tap, containing a sample of unisolated $Ru(AsPh_3)(IMes)_2(CO)H_2$ (**1**) {prepared *in situ* from $Ru(AsPh_3)_3(CO)H_2$ (0.85 g, 0.81 mmol) and IMes (0.85 g, 2.79 mmol)}. The reaction mixture was stirred overnight and 298 K. The solvent was removed by

filter cannula and the remaining yellow powder washed with dry hexane and dried *in vacuo*. Yield: 496 mg (81 %).

5.5.1.2 Alternative method

An equivalent of KOH (8.7 mg, 0.16 mmol) dissolved in *ca.* 3 mL MeOH was added *via* canula to a sample of $Ru(IMes)_2(CO)(Cl)H$ (**7**) (120 mg, 0.15 mmol) in *ca.* 5 mL THF. The reaction mixture was stirred at 298 K for 10 min and the solvent was subsequently removed *in vacuo*. $Ru(IMes)_2(CO)(OH)H$ (**2**) was extracted from the dry residue with two aliquots of C_6H_6 (*ca.* 3 mL). Yield: 102 mg (87 %).

FW = 755.96. IR (nujol, cm^{-1}): 1861 (ν_{CO}). ^1H NMR (C_6D_6, 298 K, 400 MHz): δ 6.84 (s, 4H, $C_6\mathbf{H}_2Me_3$), 6.78 (s, 4H, $C_6\mathbf{H}_2Me_3$), 6.15 (s, 4H, NC**H**), 2.34 (s, 12H, *p*-$C\mathbf{H}_3$), 2.18 (s, 12H, *o*-$C\mathbf{H}_3$), 2.05 (s, 12H, *o*-$C\mathbf{H}_3$), -23.15 (s, 1H, Ru-**H**).

5.5.2 Preparation of $Ru(IMes)_2(CO)(SH)H$ (4)

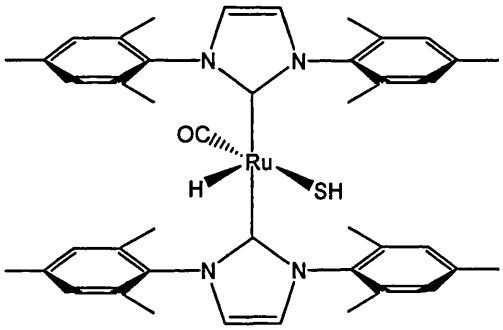

$Ru(IMes)_2(CO)(SH)H$ was prepared using the reported method.[7]

A sample of $Ru(IMes)_2(CO)(OH)H$ (**2**) (75 mg, 0.10 mmol) in a J. Youngs' NMR tube dissolved in *ca.* 0.6 mL C_6D_6 was treated with 1 atm of H_2S. The sample was shaken once and the solvent removed immediately *in vacuo* to afford a yellow solid. The product was washed with hexane (2 x 1 mL) and dried *in vacuo*. Yield: 67 mg (87 %).

NB. Hydrogen sulphide (H_2S) gas is incredibly toxic and this work needs to be carried out in a fume hood with good ventilation.

FW = 772.02. IR (nujol, cm^{-1}): 1879 (ν_{CO}). ^1H NMR (C_6D_6, 298 K, 400 MHz): δ 6.80 (br s, 4H, $C_6\mathbf{H}_2Me_3$), 6.77 (s, 4H, $C_6\mathbf{H}_2Me_3$), 6.20 (s, 4H, NC**H**), 2.32 (s, 12H, $\mathbf{CH}_3$), 2.16 (s, 12H, $\mathbf{CH}_3$), 2.08 (s, 12H, $\mathbf{CH}_3$), -0.58 (s, 1H, S**H**), -24.47 (s, 1H, Ru-**H**).

5.5.3 Preparation of $Ru(IMes)_2(CO)(F)H$ (6)

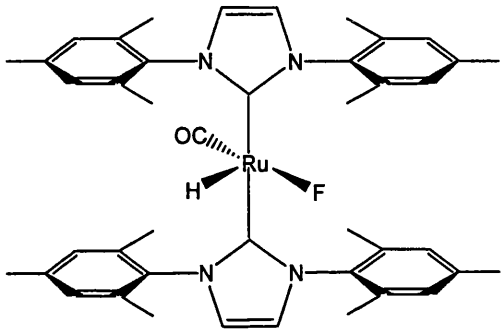

A sample of $Ru(AsPh_3)(IMes)_2(CO)H_2$ (**1**) (30 mg, 0.029 mmol) in a J. Youngs' NMR tube dissolved in *ca.* 0.6 mL C_6D_6 was treated with 5 μL (0.031 mmol) triethylamine trihydrofluoride ($Et_3N.3HF$) in the glovebox. On shaking a yellow precipitate was observed immediately. The precipitate was filtered, washed with hexane and dried in vacuo. Yield: 20 mg (91 %).

FW = 757.94. Anal. found (calcd.) for $C_{43}H_{49}N_4OFRu$: C, 67.9 (68.14); H, 6.40 (6.52); N, 7.33 (7.39). IR (nujol, cm^{-1}): 1873 (ν_{CO}). ^1H NMR (C_6D_6, 298 K, 400 MHz): δ 6.82 (s, 4H, $C_6\mathbf{H}_2Me_3$), 6.80 (s, 4H, $C_6\mathbf{H}_2Me_3$), 6.14 (s, 4H, NC**H**), 2.33 (s, 12H, *p*-$\mathbf{CH}_3$), 2.19 (s, 12H, *o*-$\mathbf{CH}_3$), 2.04 (s, 12H, *o*-$\mathbf{CH}_3$), -24.55 (s, 1H, Ru-**H**). ^{19}F NMR (C_6D_6, 298 K): δ -208.32 (s, Ru-**F**). $^{13}C\{^1H\}$ NMR (C_6D_6, 298 K): δ 206.3 (d, J_{CF} = 14.7 Hz, Ru-**C**O), 197.0 (d, J_{CF} = 4.6 Hz, Ru-**C**), 138.1 (s, N-**C**), 137.7 (s, *o*-$C_6\mathbf{H}_2Me_3$), 137.5 (s, *o*-$C_6\mathbf{H}_2Me_3$), 137.1 (s, *p*-$C_6\mathbf{H}_2Me_3$), 129.5 (s, *m*-$C_6\mathbf{H}_2Me_3$), 129.4 (s, *m*-$C_6\mathbf{H}_2Me_3$), 121.7 (s, NCH), 22.0 (s, *p*-$\mathbf{CH}_3$), 19.0 (s, *o*-$\mathbf{CH}_3$), 18.8 (s, *o*-$\mathbf{CH}_3$).

5.5.4 Preparation of Ru(IMes)$_2$(CO)(Cl)H (7)

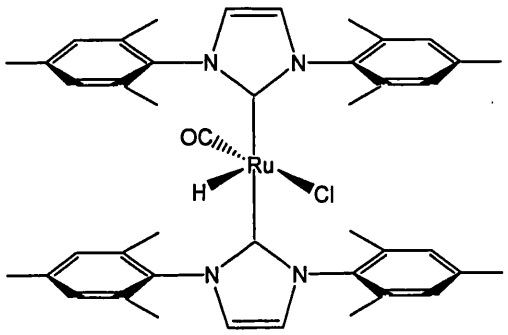

5.5.4.1 Preferred method

A sample of Ru(IMes)$_2$(CO)(OH)H (**2**) (494 mg, 0.65 mmol) was dissolved in *ca.* 10 mL $CHCl_3$ and stirred at 298 K overnight. The solvent was removed *in vacuo* and the residue was washed twice with hexane (*ca.*4 mL). Yield: 496 mg (98 %).

5.5.4.2 Alternative method

An ampoule fitted with a J. Youngs' PTFE tap was charged with Ru(PPh$_3$)$_3$(CO)(Cl)H (1.0 g, 1.05 mmol) and 3 equiv. of IMes (0.96 g, 3.15 mmol). Toluene (*ca.* 10 mL) was added to the ampoule *via* canula and the reaction mixture stirred at 343 K for 1 h. The solvent was removed *in vacuo* and the residue washed twice with *ca.* 4 mL hexane. Yield: 781 mg (96 %).

FW = 774.41. Anal. found (calcd.) for $C_{43}H_{49}N_4OClRu$: C, 66.69 (66.69); H, 6.41 (6.38); N, 7.03 (7.23). IR (nujol, cm^{-1}): 1882 (ν_{CO}). ^1H NMR (C_6D_6, 298 K, 400 MHz): δ 6.82 (s, 4H, *m*-$C_6\mathbf{H}_2Me_3$), 6.78 (s, 4H, *m*-$C_6\mathbf{H}_2Me_3$), 6.18 (s, 4H, NC**H**), 2.32 (s, 12H, $\mathbf{CH}_3$), 2.17 (s, 12H, $\mathbf{CH}_3$), 2.05 (s, 12H, $\mathbf{CH}_3$), -25.39 (s, 1H, Ru-**H**). $^{13}C\{^1H\}$ NMR (C_6D_6, 298 K): δ 202.8 (s, **CO**), 195.9 (s, Ru-**C**), 138.0 (s, *i*, *o* or *p*-$C_6\mathbf{H}_2Me_3$), 137.7 (s, *i*, *o* or *p*-$C_6\mathbf{H}_2Me_3$), 137.1 (s, *i*, *o* or *p*-$C_6\mathbf{H}_2Me_3$), 129.8 (s, *m*-$C_6\mathbf{H}_2Me_3$), 122.3 (s, NCH), 22.0 (s, *p*-$\mathbf{CH}_3$), 19.6 (2s, *o*-$\mathbf{CH}_3$).

5.5.5 Preparation of Ru(PPh$_3$)(IMes)(CO)(Cl)H (8)

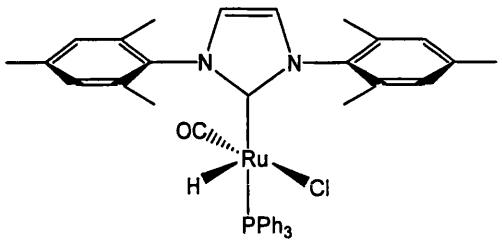

Ru(PPh$_3$)(IMes)(CO)(Cl)H was prepared using a scaled-up literature method.[8]
A Schlenk tube was charged with Ru(PPh$_3$)$_3$(CO)(Cl)H (1.34 mg, 1.41 mmol), 1.4 equiv. IMes (600 mg, 1.97 mmol) and toluene (*ca.* 10 mL). The solution was stirred for 3 h at 298 K and the solvent removed *in vacuo*. The residue was stirred in EtOH (*ca.* 10 mL) to precipitate a microcrystalline yellow solid, which was washed with cold hexane (2 x 5 mL) and dried *in vacuo*. Yield: 0.94 g (91 %).
FW = 732.26. IR (nujol, cm^{-1}): 1913 (ν_{CO}), 1897 (ν_{Ru-H}). ^{1}H NMR (C_6D_6, 298 K, 400 MHz): δ 7.53-7.49 and 7.02-6.94 (m, 15H, PP**h**$_3$), 6.78 (s, 2H, *m*-C$_6$**H**$_2$Me$_3$), 6.73 (s, 2H, *m*-C$_6$**H**$_2$Me$_3$), 6.24 (s, 2H, NC**H**), 2.44 (s, 6H, C**H**$_3$), 2.32 (s, 6H, C**H**$_3$), 2.10 (s, 6H, C**H**$_3$), -25.89 (s, 1H, Ru-**H**). ^{31}P{^{1}H} NMR (C_6D_6, 298 K): δ 42.1 (s).

5.6 Syntheses of 18-electron Ru-IMes complexes

5.6.1 Preparation of Ru(IMes)$_2$(CO)$_2$(F)H (9)

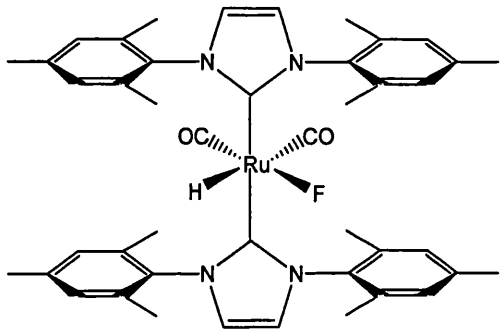

An atmosphere of CO was introduced to a sample of Ru(IMes)$_2$(CO)(F)H (**6**) (20 mg, 0.026 x 10^{-5} mols) dissolved in C_6D_6 (*ca.* 0.6 mL), contained in a J. Youngs' NMR tube. The sample was shaken and there was a colour change from yellow to

colourless. The solvent was removed *in vacuo*, washed with hexane (2 x 1 mL) and dried *in vacuo*. Yield: 19.7 mg, (95 %).

FW = 785.95. Anal. found (calcd.) for $RuC_{44}H_{49}N_4O_2F$: C, 67.35 (67.24); H, 7.30 (6.28); N, 7.45 (7.13). IR (nujol, cm^{-1}): 1991 (ν_{CO}), 1930 (ν_{Ru-H}), 1880 (ν_{CO}). ^1H NMR (C_6D_6, 298 K, 400 MHz): δ 6.80 (s, 4H, $C_6\mathbf{H}_2Me_3$), 6.75 (s, 4H, $C_6\mathbf{H}_2Me_3$), 6.09 (s, 4H, NC**H**), 2.20 (s, 12H, *p*-$\mathbf{CH}_3$), 2.11 (s, 12H, *o*-$\mathbf{CH}_3$), 2.01 (s, 12H, *o*-$\mathbf{CH}_3$), -3.79 (d, J_{HF} = 3.8 Hz, 1H, Ru-**H**). ^{19}F NMR (C_6D_6, 298 K): δ -379.5 (s, Ru-**F**). $^{13}C\{^1H\}$ NMR (C_6D_6, 298 K): δ 205.9 (d, J_{CF} = 68.9 Hz, Ru-**C**O), 193.6 (d, J_{CF} = 9.6 Hz, Ru-**C**O), 187.8 (s, Ru-**C**), 139.5 (s, N-**C**), 138.3 (s, *p*-$\mathbf{C}_6H_2Me_3$), 137.5 (s, *o*-$\mathbf{C}_6H_2Me_3$), 137.1 (s, *o*-$\mathbf{C}_6H_2Me_3$), 129.8 (s, *m*-$\mathbf{C}_6H_2Me_3$), 123.4 (s, NCH), 21.9 (s, *p*-$\mathbf{C}H_3$), 18.9 (s, *o*-$\mathbf{C}H_3$), 18.8 (s, *o*-$\mathbf{C}H_3$).

5.6.2 Preparation of $Ru(IMes)_2(CO)_2(Cl)H$ (10)

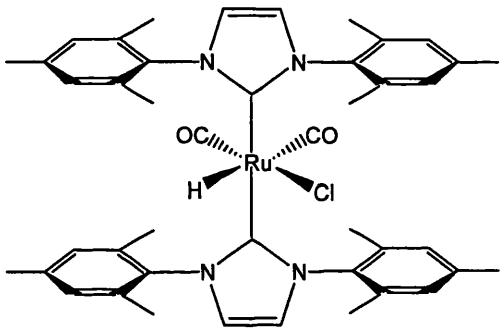

An atmosphere of CO was introduced to a sample of $Ru(IMes)_2(CO)(Cl)H$ (7) (161 mg, 0.21 mmol) dissolved in C_6D_6 (*ca.* 0.6 mL) contained in a J. Youngs' NMR tube. The sample was shaken and an immediate colour change from yellow to pale-straw occurred. Yield: 113 mg (68 %).

FW = 802.41. Anal. found (calcd.) for $C_{44}H_{49}N_4O_2ClRu$: C, 65.45 (65.86); H, 6.03 (6.16); N, 6.75 (6.98). IR (nujol, cm^{-1}): 2037 (ν_{CO}), 1938 (ν_{Ru-H}), 1903 (ν_{CO}). ^1H NMR (C_6D_6, 298 K, 400 MHz): δ 6.72 (s, 4H, *m*-$\mathbf{C}_6H_2Me_3$), 6.71 (s, 4H, *m*-$\mathbf{C}_6H_2Me_3$), 6.09 (s, 4H, NCH), 2.22 (s, 12H, *p*-$\mathbf{CH}_3$), 2.15 (s, 24H, *o*-$\mathbf{CH}_3$), -4.30 (s, 1H, Ru-**H**). $^{13}C\{^1H\}$ NMR (C_6D_6, 298 K): δ 204.4 (s, CO), 194.6 (s, CO), 185.7 (s, Ru-**C**), 139.8 (s, *i*-$\mathbf{C}_6H_2Me_3$), 138.0 (s, *o* or *p*-$\mathbf{C}_6H_2Me_3$), 137.3 (s, *o* or *p*-$\mathbf{C}_6H_2Me_3$), 137.0 (s, *o* or *p*-$\mathbf{C}_6H_2Me_3$), 130.1 (s, *m*-$\mathbf{C}_6H_2Me_3$), 130.0 (s, *m*-$\mathbf{C}_6H_2Me_3$), 123.7 (s, NCH), 21.9 (s, *p*-$\mathbf{C}H_3$), 19.5 (s, *o*-$\mathbf{C}H_3$), 19.4 (s, *o*-$\mathbf{C}H_3$).

5.6.3 Preparation of Ru(PPh$_3$)(IMes)(CO)$_2$(Cl)H (11)

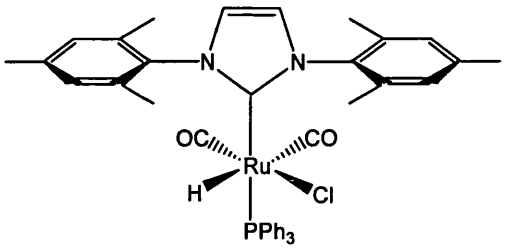

An atmosphere of CO was introduced to a sample of Ru(PPh$_3$)(IMes)(CO)(Cl)H (**8**) (60 mg, 0.082 mmol) dissolved in C_6D_6 (*ca.* 0.6 mL), contained in a J. Youngs' NMR tube. The sample was shaken and an immediate colour change from yellow to pale-brown occurred. X-ray quality crystals were grown from C_6D_6/hexane. Yield: 48 mg, (77 %).

FW = 760.27. ESI-TOF MS $[M\text{-}CO\text{-}Cl+H]^+$ *m/z* = 697.1886 (theoretical *m/z* = 697.1927). IR (nujol, cm^{-1}): 2044 (ν_{CO}), 1945 (ν_{CO}), 1922 ($\nu_{Ru\text{-}H}$). ^1H NMR (C_6D_6, 298 K, 400 MHz): δ 7.73 (m, 6H, *o*-C_6H_5), 6.96 (m, 9H, *m*- and *p*-C_6H_5), 6.92 (s, 2H, $C_6H_2Me_3$), 6.77 (s, 2H, $C_6H_2Me_3$), 6.29 (s, 2H, NCH), 2.33 (s, 6H, *o*-CH_3), 2.26 (s, 6H, *o*-CH_3), 2.20 (s, 6H, *p*-CH_3), -4.25 (d, J_{HP} = 14.7 Hz, 1H, Ru-H). $^{31}P\{^1H\}$ (C_6D_6, 298 K): δ 41.0 (s). $^{13}C\{^1H\}$ NMR (C_6D_6, 298 K): δ 201.8 (d, J_{CP} = 11.6 Hz, Ru-CO), 194.5 (d, J_{CP} = 7.3 Hz, Ru-CO), 184.9 (d, J_{CP} = 96.5 Hz, Ru-C), 139.8 (s, N-C), 139.4 (s, N-C), 137.5 (br s, *i*-C_6H_5), 136.6 (s, *o* or *p*-$C_6H_2Me_3$), 136.1 (s, *o* or *p*-$C_6H_2Me_3$), 135.5 (s, *o*-C_6H_5), 135.4 (s, *o*-C_6H_5), 130.2 (s, *m*-$C_6H_2Me_3$), 130.1 (s, *m*-$C_6H_2Me_3$), 129.9 (s, *p*-C_6H_5), 128.7 (s, *m*-C_6H_5), 128.6 (s, *m*-C_6H_5), 123.5 (2s, NCH), 21.8 (s, *p*-CH_3), 19.5 (s, *o*-CH_3), 19.4 (s, *o*-CH_3).

5.6.4 Preparation of Ru(IMes)$_2$(CO)(Cl)(NH$_3$)H (12)

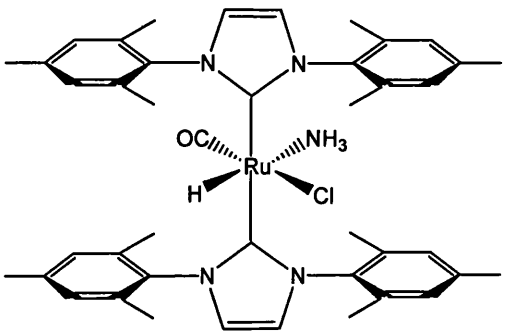

An atmosphere of NH_3 was introduced to a sample of $Ru(IMes)_2(CO)(Cl)H$ (**7**) (30 mg, 0.40 mmol) dissolved in C_6D_6 (*ca.* 0.6 mL), contained in a J. Youngs' NMR tube. The sample was shaken and an immediate colour change from yellow to pale-yellow occurred. X-ray quality crystals were grown from a concentrated solution of **12** layered with NH_3-saturated hexane.

FW = 791.44. IR (C_6D_6, cm^{-1}): 1885 (ν_{CO}). ^1H NMR (C_6D_6, 298 K, 400 MHz): δ 6.77, 6.75, 6.73 (3s, 6H, $C_6\mathbf{H}_2Me_3$), 6.66 (s, 2H, $C_6\mathbf{H}_2Me_3$), 6.15, 5.98 (2s, 1H each, NC**H**), 2.28, 2.20, 2.13, 2.11, 2.10, 1.92 (6s, 3H each, $\mathbf{CH}_3$), 1.60 (s, 3H, Ru-$\mathbf{NH}_3$), -13.94 (s, 1H, Ru-**H**). $^{13}C\{^1H\}$ NMR (C_6D_6, 298 K): δ 208.4 (s, Ru-**C**O), 190.4 (s, Ru-**C**), 138.8, 138.7, 137.7, 137.3, 136.9, 136.4 (6s, *i*-, *o*- or *p*-$C_6\mathbf{H}_2Me_3$), 130.5, 129.1, 129.8, 129.7 (4s, *m*-$C_6\mathbf{H}_2Me_3$), 123.8, 122.6 (2s, N**C**H), 21.9, 21.8, 19.6, 19.5, 19.4, 19.0 (6s, $\mathbf{C}H_3$). $^{15}N\{^1H\}$-^1H HMQC NMR (C_6D_6, 298 K): δ -375.5, -381.4 (2br s, **N**CH), -409.6 (br s, Ru-$\mathbf{N}H_3$).

5.7 Syntheses of 16-electron acetylide complexes

5.7.1 Preparation of $Ru(IMes)_2(CO)(C{\equiv}CPh)H$ (13)

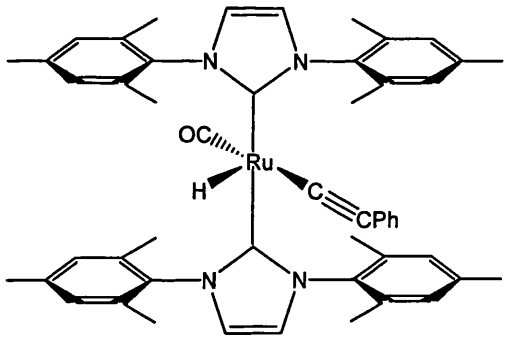

In a J. Youngs' NMR tube, 1 equiv. of phenylacetylene (HC≡CPh) (3.7 μL, 0.034 mmol) was added *via* syringe to a sample of $Ru(IMes)_2(CO)(OH)H$ (**2**) (25.7 mg, 0.034 mmol) dissolved in C_6D_6 (*ca.* 0.6 mL). The sample was shaken, the solvent removed *in vacuo* and the resulting red-brown powder washed twice with (2 x 1 mL) hexane. Yield: 24 mg (84 %).

FW = 840.07. ESI-TOF MS $[M+H]^+$ *m/z* = 841.3376 (theoretical *m/z* = 840.3349). IR (nujol, cm^{-1}): 1887 (ν_{CO}), 2062 ($\nu_{C\equiv C}$). ^1H NMR (C_6D_6, 298 K, 400 MHz): δ 7.30 (d, J_{HH} = 7.3 Hz, 2H, *o*-$C_6\mathbf{H}_5$), 7.22 (t, J_{HH} = 7.3 Hz, 2H, *m*-$C_6\mathbf{H}_5$), 7.02 (t, J_{HH} = 7.3 Hz, 1H, *p*-$C_6\mathbf{H}_5$), 6.80 (s, 4H, $C_6\mathbf{H}_2Me_3$), 6.76 (s, 4H, $C_6\mathbf{H}_2Me_3$), 6.22 (s, 4H, NC**H**), 2.32 (s, 12H, *p*-$\mathbf{CH}_3$),

2.18 (s, 12H, *o*-CH_3), 2.05 (s, 12H, *o*-CH_3), -28.33 (s, 1H, Ru-**H**). $^{13}C\{^1H\}$ NMR (C_6D_6, 298 K): δ 204.0 (s, Ru-**C**O), 197.8 (s, Ru-**C**), 145.9 (s, C_α), 138.2, 137.4, 137.0, 136.8, 132.1 (5s, $C_{quaternary}$), 131.2 (s, *o*-C_6H_5), 129.7 (s, *m*-$C_6H_2Me_3$), 128.6 (s, *m*-C_6H_5), 124.0 (s, *p*-C_6H_5), 122.0 (s, N**C**H), 116.5 (s, C_β), 22.0 (s, *p*-CH_3), 19.4 (2s, *o*-CH_3).

5.7.2 Preparation of Ru(IMes)$_2$(CO)(C≡CPh)$_2$ (14)

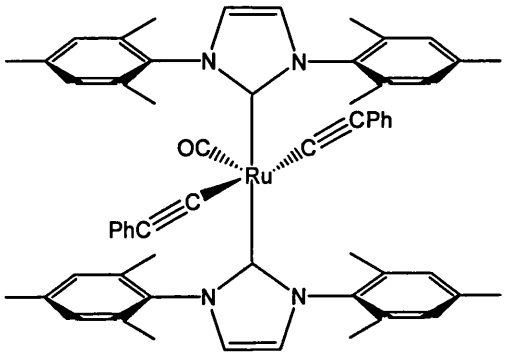

In a J. Youngs' NMR tube, excess phenylacetylene (HC≡CPh) (15.5 μL, 0.15 mmol) was added *via* syringe to a sample of Ru(IMes)$_2$(CO)(OH)H (**2**) (21.4 mg, 0.03 mmol) dissolved in C_6D_6 (*ca.* 0.6 mL) and the reaction mixture left at 298 K for 16 h. The volatiles were removed *in vacuo* and the resulting brown powder washed with hexane (2 x 1 mL). Yield: 19 mg (71 %).

FW = 940.19. Anal. found (calcd.) for $C_{59}H_{58}N_4ORu$: C, 74.51 (75.37); H, 6.31 (6.22); N, 5.95 (5.96). IR (nujol, cm^{-1}): 1954 (ν_{CO}), 2068 ($\nu_{C\equiv C}$). ^1H NMR (C_6D_6, 298 K, 400 MHz): δ 7.54 (d, J_{HH} = 7.7 Hz, 4H, *o*-C_6H_5), 7.29 (t, J_{HH} = 7.7 Hz, 4H, *m*-C_6H_5), 7.07 (t, J_{HH} = 7.7 Hz, 2H, *p*-C_6H_5), 6.55 (s, 8H, $C_6H_2Me_3$), 5.97 (s, 4H, NC**H**), 2.38 (s, 24H, *o*-CH_3), 2.16 (s, 12H, *p*-CH_3). $^{13}C\{^1H\}$ NMR (C_6D_6, 298 K): δ 203.9 (s, Ru-**C**O), 191.3 (s, Ru-**C**), 140.0, 138.4, 137.9, 137.6, 137.1, 136.9 (6s, $C_{quaternary}$), 131.8 (s, *o*-C_6H_5), 130.2 (s, *m*-$C_6H_2Me_3$), 124.8 (s, *m*-C_6H_5), 124.1 (s, *p*-C_6H_5), 123.5 (s, N**C**H), 116.4 (s, **C**≡C), 22.0 (s, *p*-CH_3), 19.5 (s, *o*-CH_3).

5.7.3 Preparation of Ru(IMes)$_2$(CO)(HC=CHPh)Cl (15)

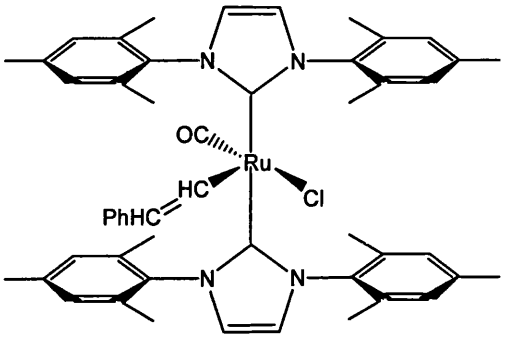

In a J. Youngs' NMR tube, excess phenylacetylene (HC≡CPh) (13.6 μL, 0.12 mmol) was added *via* syringe to a sample of Ru(IMes)$_2$(CO)(Cl)H (**7**) (20 mg, 0.026 mmol) dissolved in C_6D_6 (*ca.* 0.6 mL). The sample was heated at 333 K for 3 days until no starting material remained by ^{1}H NMR spectroscopy, resulting in a colour change from yellow to red. All volatiles were removed *in vacuo* and the tarry residue dissolved in the minimum amount of hexane for crystallisation at low temperature (255 K).

FW = 876.53. ESI-TOF MS $[M\text{-}Cl+H]^+$ *m/z* = 841.3414 (theoretical *m/z* = 841.3427). IR (nujol, cm^{-1}): 1901 (ν_{CO}). ^{1}H NMR (C_6D_6, 298 K, 400 MHz): δ 8.27 (d, J_{HH} = 13.8 Hz, CH_α), 7.4-6.8 (m, PPh_3), 6.72 (s, 4H, $C_6H_2Me_3$), 6.51 (d, J_{PH} = 7.5 Hz, PPh_3) 6.48 (s, 4H, $C_6H_2Me_3$), 5.94 (s, 4H, NCH), 5.82 (d, J_{HH} = 13.8 Hz, CH_β) 2.29 (s, 12H, *o*-CH_3), 2.14 (s, 12H, *p*-CH_3), 2.01 (s, 12H, *o*-CH_3). $^{13}C\{^1H\}$ NMR (C_6D_6, 298 K): δ 205.1 (s, Ru-CO), 187.0 (s, Ru-C), 155.9 (s, Ru-C_α), 140.1, 138.3, 137.7, 136.8, 136.6 (5s, $C_{quaternary}$), 133.4 (s, C_β), 130.2 (s, *m*-$C_6H_2Me_3$), 130.0 (s, *m*-$C_6H_2Me_3$), 129.7-129.2, (C_6H_5), 127.8 (s, C_6H_5), 126.0 (s, C_6H_5), 124.3 (s, NCH), 122.8 (s, C_6H_5), 21.9 (s, *p*-CH_3), 19.7 (s, *o*-CH_3), 19.4 (s, *o*-CH_3).

5.7.4 Preparation of Ru(IMes)$_2$(CO)(C≡CSiMe$_3$)H (16)

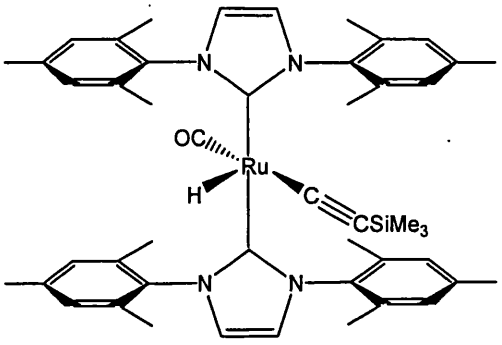

In a J. Youngs' NMR tube, 1 equiv. trimethylsilylacetylene (HC≡CSiMe$_3$) (3.7 μL, 0.026 mmol) was added *via* syringe to a sample of Ru(IMes)$_2$(CO)(OH)H (**2**) (20 mg, 0.026 mmol) dissolved in C_6D_6 (*ca.* 0.6 mL) and the sample shaken. The solvent was removed *in vacuo* and the resulting residue washed with minimal cold hexane (soluble in hexane, pentane, EtOH and Et_2O). Yield (not optimised): 6.1 mg (3 %).

FW = 836.16. IR (nujol, cm^{-1}): 1893 (ν_{CO}), 2042 ($\nu_{C\equiv C}$). ^{1}H NMR (C_6D_6, 298 K, 400 MHz): 6.75 (s, 4H, $C_6\mathbf{H}_2Me_3$), 6.73 (s, 4H, $C_6\mathbf{H}_2Me_3$), 6.21 (s, 4H, NC**H**), 2.48-1.93 (br m, 36H, CH_3), 0.29 (s, Si-CH_3), -28.44 (s, 1H, Ru-**H**). ^{13}C{^{1}H} NMR (C_6D_6, 298 K): δ 203.7 (Ru-**C**O), 197.6 (Ru-**C**), 167.8 (s, C_α), 137.4.0 (s, N-**C**), 129.6 (s, *m*-$C_6\mathbf{H}_2Me_3$), 122.2 (s, N**C**H), 117.9 (C_β), 22.1 (s, $\mathbf{C}H_3$), 2.9 (s, Si-$\mathbf{C}H_3$).

5.8 Syntheses of 18-electron acetylide complexes

5.8.1 Preparation of Ru(IMes)$_2$(CO)$_2$(C≡CPh)H (17)

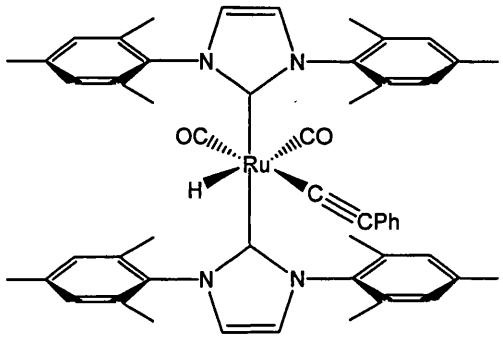

A sample of $Ru(IMes)_2(CO)(C{\equiv}CPh)H$ (**13**) (25 mg, 0.030 mmol) was dissolved in C_6D_6 (*ca.* 0.6 mL) in a J. Youngs' NMR tube. The sample was freeze-pump-thaw degassed and exposed to an atmosphere of CO. The sample was shaken and an immediate colour change from red-brown to very pale yellow. The solvent was removed *in vacuo* and X-ray quality crystals were grown from C_6H_6/hexane. Yield: 24 mg (93 %).

FW = 868.08. Anal. found (calcd.) for $C_{52}H_{54}N_4O_2Ru$ + 1.5 molecules C_6H_6: C, 73.57 (74.36); H, 6.45 (6.45); N, 5.84 (5.69). IR (nujol, cm^{-1}): 1903, 2017 (ν_{CO}), 2094 ($\nu_{C{\equiv}C}$), 1939 ν(Ru-H). ^1H NMR (C_6D_6, 298 K, 400 MHz): δ 7.41 (d, J_{HH} = 7.1 Hz, 2H, *o*-$C_6\mathbf{H}_5$), 7.25 (t, J_{HH} = 7.7 Hz, 2H, *m*-$C_6\mathbf{H}_5$), 7.04 (t, J_{HH} = 7.1 Hz, 1H, *p*-$C_6\mathbf{H}_5$), 6.68 (s, 8H, $C_6\mathbf{H}_2Me_3$), 6.07 (s, 4H, NC**H**), 2.23 (s, 12H, *p*-CH_3), 2.18 (s, 12H, *o*-CH_3), 2.17 (s, 12H, *o*-CH_3), -5.24 (s, 1H, Ru-**H**). $^{13}C\{^1H\}$ NMR (C_6D_6, 298 K): δ 205.2 (s, Ru-**C**O), 196.9 (s, Ru-**C**O), 186.3 (s, Ru-**C**), 140.0, 137.8, 137.1, 136.9, 132.4 (5s, $\mathbf{C}_{quaternary}$), 131.9 (s, *o*-$\mathbf{C}_6H_5$), 130.0 (s, *m*-$\mathbf{C}_6H_2Me_3$), 129.9 (s, *p*-$\mathbf{C}_6H_5$), 124.1 (s, *m*-$\mathbf{C}_6H_5$), 123.4 (s, **N**CH), 111.5 ($\mathbf{C}_\alpha$), 22.0 (s, *p*-$\mathbf{C}H_3$), 19.3 (2s, *o*-$\mathbf{C}H_3$).

5.8.2 Preparation of $Ru(IMes)_2(CO)_2(C{\equiv}CPh)_2$ (18)

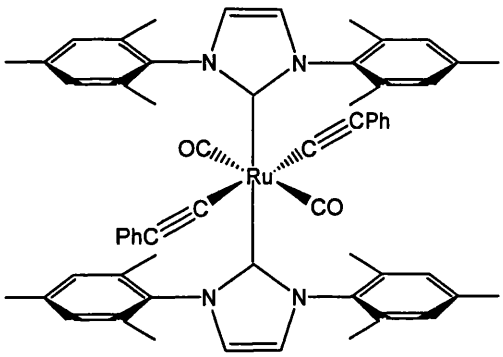

A sample of $Ru(IMes)_2(CO)(C{\equiv}CPh)_2$ (**14**) (25 mg, 0.027 mmol) was dissolved in C_6D_6 (*ca.* 0.6 mL) in a J. Youngs' NMR tube. The sample was freeze-pump-thaw degassed and exposed to an atmosphere of CO followed by shaking at 298 K. The solvent was removed *in vacuo* and X-ray quality crystals were grown from C_6H_6/hexane. Yield: 23 mg (88 %).

FW = 968.20. Anal. found (calcd.) for $C_{60}H_{58}N_4O_2Ru$: C, 73.25 (74.43); H, 6.29 (6.04); N, 5.87 (5.79). IR (nujol, cm^{-1}): 1995 (ν_{CO}), 2086 ($\nu_{C{\equiv}C}$). ^1H NMR (C_6D_6, 298 K, 400 MHz): δ 7.27 (s, 4H, *o*-or *m*-$C_6\mathbf{H}_5$), 7.26 (s, 4H, *o*-or *m*-$C_6\mathbf{H}_5$), 7.00 (m, 2H, *p*-$C_6\mathbf{H}_5$), 6.70 (s, 8H,

$C_6H_2Me_3$), 5.95 (s, 4H, NC**H**), 2.34 (s, 24H, *o*-CH_3), 2.04 (s, 12H, *p*-CH_3). $^{13}C\{^1H\}$ NMR (C_6D_6, 298 K): δ 198.9 (s, Ru-**C**O), 180.2 (s, Ru-**C**), 139.5, 139.3, 137.9, 132.7 (4s, $C_{quaternary}$), 131.8 (s, *o*-or *m*-C_6H_5), 129.8 (s, *m*-$C_6H_2Me_3$), 128.5 (s, *o*-or *m*-C_6H_5), 124.7 (s, N**C**H), 123.5 (s, *p*-C_6H_5), 117.8 (s, **C**≡C), 112.9 (s, C≡**C**), 21.7 (s, *p*-CH_3), 19.6 (s, *o*-CH_3).

5.9 Bis IMes borohydride work

5.9.1 Preparation of Ru(IMes)$_2$(CO)(η^2-BH$_4$)H (19)

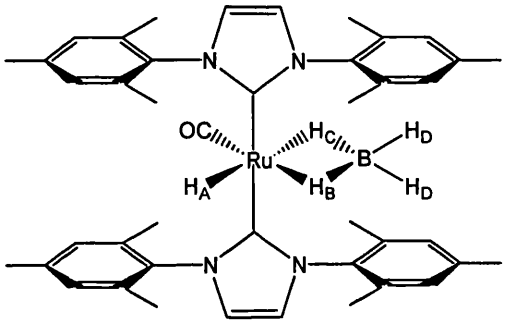

4 equiv. $NaBH_4$ (38 mg, 0.97 mmol) was added to a sample of Ru(IMes)$_2$(CO)(Cl)H (7) (188 mg, 0.24 mmol) in a Schlenk tube equipped with a stirrer bar. EtOH (*ca.* 10 mL) was added to the Schlenk tube *via* a cannula and the reaction mixture stirred for 1 h at 298 K. The solvent was removed *in vacuo* and the product isolated by extraction from the residue with C_6H_6 (2 x 10 mL). The solvent was removed and the product dried *in vacuo*. Crystals were grown from a benzene sample layered with hexane. Yield: 166 mg (91 %).

NB. Hydrogen gas is released throughout the reaction (vigorously when EtOH is initially added) so the reaction vessel was fitted with an outlet needle under a steady flow of argon.

FW = 753.79. Anal. found (calcd.) for $C_{43}H_{53}N_4OBRu$: C, 68.14 (68.52); H, 7.08 (7.09); N, 7.45 (7.43). IR (nujol, cm^{-1}): 1900 (ν_{CO}), 2425, 2400 ($\nu_{term\ B\text{-}H}$), 1156 (B-$H_{deformation}$). ^1H NMR ($C_6D_5CD_3$, 228 K, 400 MHz): δ 6.78 (s, 4H, $C_6H_2Me_3$), 6.75 (s, 4H, $C_6H_2Me_3$), 5.98 (s, 4H, NC**H**), 3.13 (br s, 2H, B-H_D), 2.34 (s, 12H, *p*-CH_3), 2.11 (s, 12H, *o*-CH_3), 2.06 (s, 12H, *o*-CH_3), -5.12 (br s, 1H, B-H_C), -6.98 (br s, 1H, B-H_B), -16.28 (s, 1H, Ru-H_A). $^{13}C\{^1H\}$ NMR ($C_6D_5CD_3$, 228K): δ 205.6 (s, Ru-**C**O), 194.1 (s, Ru-**C**), 138.3 (s, N-**C**), 136.9 (s, *o*-or *p*-$C_6H_2Me_3$), 136.1 (2s, *o*-or *p*-$C_6H_2Me_3$), 128.9 (s, *m*-$C_6H_2Me_3$), 128.8 (s, *m*-

$C_6H_2Me_3$), 121.9 (s, NCH), 121.6 (s, NCH), 21.3 (s, *p*-CH_3), 19.3 (s, *o*-CH_3), 19.1 (s, *o*-CH_3). $^{11}B\{^1H\}$ NMR ($C_6D_5CD_3$, 298 K): δ -2.8.

5.9.2 Preparation of Ru(IMes)$_2$(CO)(η^2-BD$_4$)H (19-d$_4$)

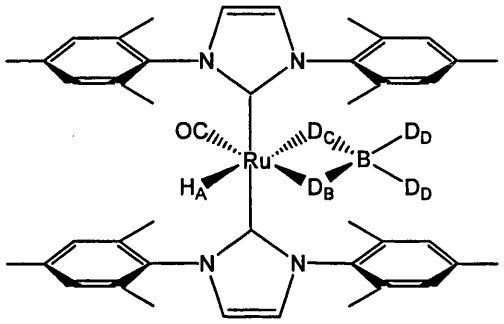

Ru(IMes)$_2$(CO)(η^2-BD$_4$)H (**19-d$_4$**) was formed using the preparation outlined above for the production of **19**, with exception of using $NaBD_4$ rather than $NaBH_4$. ([Ru] 200 mg, 0.26 mmol; $NaBD_4$ 43.2 mg, 1.03 mmol). Yield: 171 mg (87 %).

Selected data for **19-d$_4$**:

FW = 757.81. IR (nujol, cm^{-1}): 1898 (ν_{CO}), 1826, 1765 ($\nu_{term\ B\text{-}D}$), 846 (B-$D_{deformation}$). ^1H NMR ($C_6D_5CD_3$, 230 K, 400 MHz): δ 6.78 (s, 4H, $C_6\mathbf{H}_2Me_3$), 6.75 (s, 4H, $C_6\mathbf{H}_2Me_3$), 5.98 (s, 4H, NC**H**), 2.34 (s, 12H, *p*-CH_3), 2.11 (s, 12H, *o*-CH_3), 2.06 (s, 12H, *o*-CH_3), -16.28 (s, 1H, Ru-$\mathbf{H}_A$). ^2H NMR ($C_6H_5CH_3$, 230K): δ 3.13 (br s, 2H, B-$\mathbf{D}_D$), -5.12 (br s, 1H, B-$\mathbf{D}_C$), -6.98 (br s, 1H, B-$\mathbf{D}_B$).

5.9.3 Preparation of IMes.BH$_3$ (20)

A sample of Ru(IMes)$_2$(CO)(η^2-BH_4)H (**19**) (8 mg, 0.011 mmol) in a J. Youngs' NMR tube was dissolved in C_6D_6 (*ca.* 0.6 mL) and heated at 358 K for a day. The sample was allowed to cool to 298 K, yielding colourless crystals. The solvent was removed by filter canula and the crystals washed with hexane (*ca.* 1 mL).

FW = 318.26. IR (nujol, cm^{-1}): 2362, 2336 ($\nu_{term\ B\text{-}H}$), 1155 (B-$H_{deformation}$). ^1H NMR (THF-d_8, 298 K, 400 MHz): δ 7.17 (s, 2H, NC**H**), 6.97 (s, 4H, $C_6\mathbf{H}_2Me_3$), 2.31 (s, 6H, *p*-CH_3), 2.03 (s, 12H, *o*-CH_3), 0.44 (q, 3H, BH_3, J_{BH} = 85.1 Hz). $^{13}C\{^1H\}$ NMR (THF-d_8, 298 K): δ 178.2 (s, Ru-**C**), 139.1 (s, N-**C**), 136.2 (s, *o*-or *p*-$C_6\mathbf{H}_2Me_3$), 135.8 (s, *o*-or *p*-

$C_6H_2Me_3$), 129.4 (s, *m*-$C_6H_2Me_3$), 121.4 (s, NCH), 21.1 (s, *p*-CH_3), 17.8 (s, *o*-CH_3).
$^{11}B\{^1H\}$ NMR: δ -37.5.

5.9.4. Preparation of $Ru(IMes)_2(CO)_2H_2$ (22)

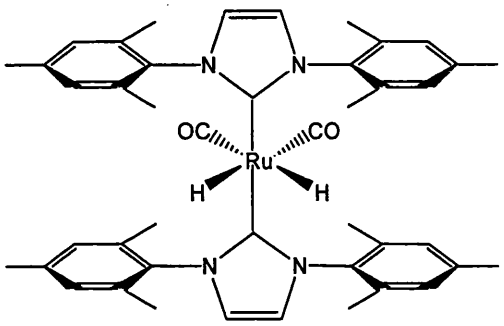

4 equiv. $NaBH_4$ (8.1 mg, 0.21 mmol) was added to a sample of $Ru(IMes)_2(CO)_2(Cl)H$ (**10**) (43.0 mg, 0.054 mmol) in Schlenk tube. EtOH (*ca.* 8 mL) was added and the mixture stirred for 1 h at 298 K. The solvent was removed *in vacuo* and the product isolated by extraction from the residue with C_6H_6 (2 x 5 mL). The solvent was removed and the product dried *in vacuo*. Yield: 34 mg (84 %).

NB. Hydrogen gas is released throughout the reaction (vigorously when EtOH is initially added) so the reaction vessel was fitted with an outlet needle under a steady flow of argon.

Selected data for **22**:

FW = 753.79. IR (nujol, cm^{-1}): 1974, 1938 (ν_{CO}). ^1H NMR (C_6D_6, 293 K, 400 MHz): δ 6.82 (s, 8H, $C_6H_2Me_3$), 6.12 (s, 4H, NC**H**), 2.21 (s, 12H, *p*-CH_3), 2.02 (s, 24H, *o*-CH_3), -6.53 (s, 2H, Ru-**H**). $^{13}C\{^1H\}$ NMR (C_6D_6, 293K): δ 204.3 (s, Ru-CO), 192.5 (s, Ru-**C**), 139.6 (s, N-**C**), 137.3 (s, *o*-or *p*-$C_6H_2Me_3$), 136.3 (s, *o*-or *p*-$C_6H_2Me_3$), 134.1 (s, *o*-or *p*-$C_6H_2Me_3$), 128.9 (s, *m*-$C_6H_2Me_3$), 121.0 (s, NCH), 21.2 (s, *p*-CH_3), 18.6 (s, *o*-CH_3).

5.9.5 Preparation of $Ru(IMes)_2(CO)_3$ (23)

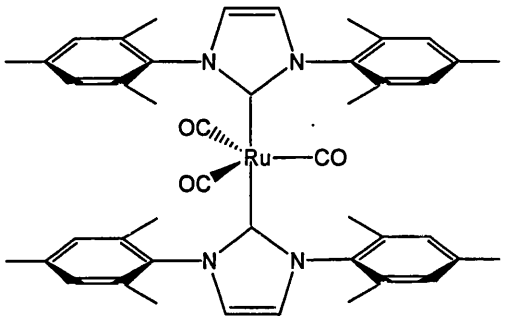

A sample of $Ru(IMes)_2(CO)(\eta^2\text{-}BH_4)H$ (**19**) (10 mg, 0.013 mmol) in a J. Youngs' NMR tube was dissolved in C_6D_6 (*ca.* 0.6 mL), freeze-pump-thaw degassed and exposed to 1 atm CO. Complete conversion to the product was achieved after a day at 298 K. Crystals of X-ray quality were grown from a benzene sample layered with hexane. Yield (not optimised): 3 mg (29 %).

Selected data for **23**:

FW = 793.96. IR (nujol, cm^{-1}): 1950, 1879, 1830 (ν_{CO}). ^1H NMR (C_6D_6, 293 K): δ 6.78 (s, 8H, $C_6\mathbf{H}_2Me_3$), 6.10 (s, 4H, NC**H**), 2.18 (s, 12H, *p*-$\mathbf{CH}_3$), 2.05 (s, 24H, *o*-$\mathbf{CH}_3$). $^{13}C\{^1H\}$ NMR (C_6D_6, 293K): δ 217.6 (s, Ru-**C**O), 186.8 (s, Ru-**C**), 138.9 (s, N-**C**), 137.9 (s, *o*-or *p*-$\mathbf{C}_6H_2Me_3$), 137.1 (s, *o*-or *p*-$\mathbf{C}_6H_2Me_3$), 129.5 (s, *m*-$\mathbf{C}_6H_2Me_3$), 123.4 (s, NCH), 21.6 (s, *p*-$\mathbf{CH}_3$), 19.1 (s, *o*-$\mathbf{CH}_3$).

5.9.6 Preparation of $[Ru(IMes)_2(CO)(^tBuNC)_2H]Cl$ (24)

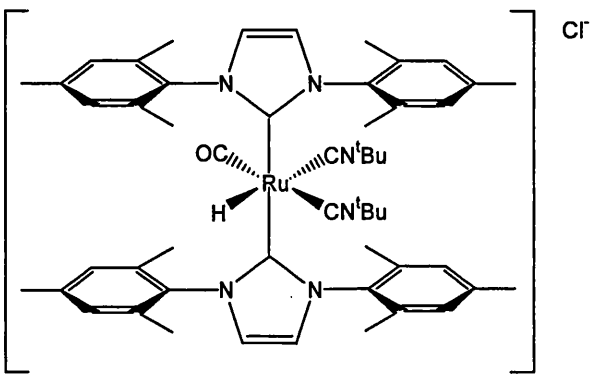

A sample of $Ru(IMes)_2(CO)(\eta^2\text{-}BH_4)H$ (**19**) (18 mg, 0.024 mmol) was dissolved in C_6D_6 in a J. Youngs' NMR tube and 5 equiv. ^{t}BuNC (7.2 μL, 0.12 mmol) added *via* syringe. The sample was shaken and left at 298 K for 5 days. The sample was concentrated to half and layered with hexane to afford crystals of **24**.

Selected data for **24**:

IR (nujol, cm^{-1}): 1965, 1954 (ν_{CO} or $\nu_{Ru\text{-}H}$), 2150, 2123 (ν_{CN}). ^{1}H NMR (C_6D_6, 298 K, 400 MHz): δ 7.14-6.98 (6s, ^{t}**Bu**), 6.79 (s, 4H, $C_6\mathbf{H}_2Me_3$), 6.78 (s, 4H, $C_6\mathbf{H}_2Me_3$), 6.00 (s, 4H, NC**H**), 2.22 (s, 12H, *p*-$\mathbf{CH}_3$), 1.87 (s, 24H, *o*-$\mathbf{CH}_3$), -8.01 (s, 1H, Ru-**H**). ^{1}H-^{13}C HMBC (C_6D_6, 298K): δ 201.6 (s, Ru-**C**O), 182.1 (s, Ru-**C**), 146.9 (s, **C**N^{t}Bu), 143.7 (s, **C**N^{t}Bu).

5.9.7 Preparation of $Ru(IMes)(PMe_2Ph)_2(CO)H$ (25)

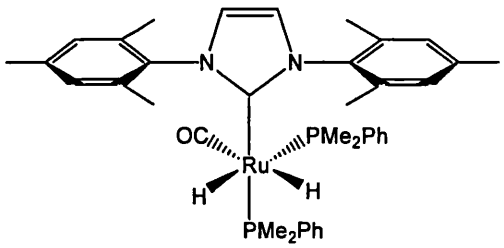

A slight excess (1.2 equiv.) of PMe_2Ph (6.8 μL, 0.047 mmol) was added *via* syringe to a C_6D_6 (*ca.* 0.6 mL) sample of $Ru(IMes)_2(CO)(\eta^2\text{-}BH_4)H$ (**19**) (28.6 mg, 0.038 mmol) in a J. Youngs' NMR tube and the reaction mixture was heated at 343 K for 2 days. **25** was characterised *in situ* due to high solubility (EtOH, hexane, Et_2O).

Selected data for **25**:

^{1}H NMR (C_6D_6, 400 MHz, 298 K): δ 7.39 (m, 2H, $PMe_2\mathbf{Ph}$), 7.03 (m, 8H, $PMe_2\mathbf{Ph}$), 6.94 (s, 2H, $C_6\mathbf{H}_2Me_3$), 6.87 (s, 2H, $C_6\mathbf{H}_2Me_3$), 6.29 (s, 2H, NC**H**), 2.36 (s, 6H, $\mathbf{CH}_3$), 2.27 (s, 6H, $\mathbf{CH}_3$), 2.17 (s, 6H, $\mathbf{CH}_3$), 1.45-1.21 (m, 12H, $\mathbf{PMe}_2$), -6.78 (ddd, J_{HP} = 32.4, J_{HP} = 31.5, J_{HH} = 6.0 Hz, 1H, Ru-**H**), -7.97 (ddd, J_{HP} = 84.5, J_{HP} = 30.7, J_{HH} = 6.0 Hz, 1H, Ru-**H**). ^{13}C{^{1}H} NMR (C_6D_6, 298K): δ 205.9 (t, J_{CP} = 8.3 Hz, Ru-**C**O), 197.8 (dd, J_{CP} = 74.4 Hz, J_{CP} = 9.2 Hz, Ru-**C**), 146.0 (dd, J_{CP} = 33.1 Hz, J_{CP} = 1.8 Hz, P-**Ph**), 146.5 (dd, J_{CP} = 25.7 Hz, J_{CP} = 1.8 Hz, P-**Ph**), 140.8 (s, N-**C**), 138.8, 138.7, 138.4, 137.6, 136.7 (5s, $\mathbf{C}_{quaternary}$), 134.9 (s, **Ph**), 134.7 (s, **Ph**), 129.5 (s, $C_6\mathbf{H}_2Me_3$), 129.4 (s, $\mathbf{C}_6H_2Me_3$), 121.9 (2s, NCH), 28.4 (dd, J_{CP} = 32.2 Hz, J_{CP} = 4.6 Hz, P-$\mathbf{CH}_3$), 25.7 (dd, J_{CP} = 17.5 Hz, J_{CP} = 2.8 Hz, P-$\mathbf{CH}_3$), 24.4 (dd, J_{CP} = 18.4 Hz, J_{CP} = 2.8 Hz, P-$\mathbf{CH}_3$), 23.7 (dd, J_{CP} = 25.7 Hz, J_{CP} = 2.8 Hz, P-$\mathbf{CH}_3$), 21.9 (s,

p-CH_3), 20.6 (s, *o*-CH_3), 20.2 (s, *o*-CH_3). $^{31}P\{^1H\}$ NMR (C_6D_6, 298 K): δ 18.4 (d, J_{PP} = 21.6 Hz), 5.7 (d, J_{PP} = 21.6 Hz).

5.10 Mixed PPh_3/IMes borohydride work

5.10.1 Preparation of Ru(PPh$_3$)(IMes)(CO)(η^2-BH$_4$)H (26)

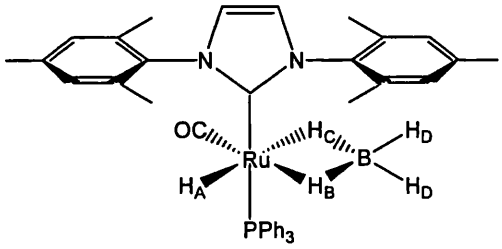

4 equiv. $NaBH_4$ (62 mg, 1.64 mmol) was added to a sample of Ru(PPh_3)(IMes)(CO)(Cl)H (**8**) (0.30 g, 0.41 mmol) in a Schlenk tube equipped with a stirrer bar. EtOH (*ca.* 10 mL) was added to the Schlenk tube *via* a cannula and the reaction mixture stirred for 1 h at 298 K. The solvent was removed *in vacuo* and the product isolated by extraction from the residue with C_6H_6 (2 x *ca.* 10 mL). The solvent was removed and the product dried *in vacuo*. Crystals were grown from a benzene sample layered with hexane. Yield: 274 mg (94 %).

NB. Hydrogen gas is released throughout the reaction (vigorously when EtOH is initially added) so the reaction vessel was fitted with an outlet needle under a steady flow of argon.

FW = 711.65. Anal. found (calcd.) for $C_{40}H_{44}N_2BOPRu$: C, 67.70 (67.51); H, 6.22 (6.23); N, 3.79 (3.94). IR (nujol, cm^{-1}): 1927 (ν_{CO}), 2422, 2399 ($\nu_{term\ B\text{-}H}$), 1163 (B-$H_{deformation}$). ^1H NMR (C_6D_6, 298 K, 400 MHz): δ 7.57-7.48 (m, 6H, **PPh$_3$**) 6.97-6.91 (m, 9H, **PPh$_3$**), 6.83 (br s, 2H, $C_6\mathbf{H}_2Me_3$), 6.74 (br s, 2H, $C_6\mathbf{H}_2Me_3$), 6.24 (s, 2H, NC**H**), 4.16 (v br s, 2H, B-$\mathbf{H}_D$), 2.35 (s, 6H, *o*-CH_3), 2.22 (s, 6H, *o*-CH_3), 2.12 (s, 6H, *p*-CH_3), -4.73 (v br s, 1H, B-$\mathbf{H}_C$), -6.74 (br s, 1H, B-$\mathbf{H}_B$), -13.36 (d, J_{PH} = 23.1 Hz, 1H, Ru-$\mathbf{H}_A$). $^{13}C\{^1H\}$ NMR (C_6D_6, 298K): δ 205.6 (d, J_{CP} = 14.7 Hz, Ru-CO), 190.9 (d, J_{CP} = 90.1 Hz, Ru-**C**), 139.1 (s, N-**C**), 138.4 (s, *o*-or *p*-$C_6\mathbf{H}_2Me_3$), 137.9 (s, *o*-or *p*-$C_6\mathbf{H}_2Me_3$), 137.5 (s, *o*-or *p*-$C_6\mathbf{H}_2Me_3$), 136.9 (d, J_{CP} = 11.0 Hz, **PPh$_3$**), 135.5 (d, J_{CP} = 11.0 Hz, **PPh$_3$**), 130.2 (s, *m*-$C_6\mathbf{H}_2Me_3$), 129.9 (s, *m*-$C_6\mathbf{H}_2Me_3$), 129.7 (d, J_{CP} = 1.8 Hz, **PPh$_3$**), 128.5 (d, J_{CP} = 9.2 Hz, **PPh$_3$**) 123.3 (s, NCH), 123.2 (s, NCH),

21.8 (s, *p*-CH_3), 20.0 (s, *o*-CH_3), 19.7 (s, *o*-CH_3). $^{31}P\{^1H\}$ NMR (C_6D_6, 298 K): δ 52.0 (s). $^{11}B\{^1H\}$ NMR (C_6D_6, 298 K): δ 1.0 (v br).

5.10.2 Preparation of Ru(PPh$_3$)(IMes)(CO)(η^2-BD$_4$)H (26-d$_4$)

Ru(PPh$_3$)(IMes)(CO)(η^2-BD$_4$)H (**26-d$_4$**) was formed using the preparation outlined above for the production of **26**, with exception of using $NaBD_4$ rather than $NaBH_4$. ([Ru] 100 mg, 0.14 mmol; $NaBD_4$ 23 mg, 0.55 mmol). Yield: 75 mg (76 %).

Selected data for **26-d$_4$**:

FW = 715.67. IR (nujol, cm^{-1}): 1924 (ν_{CO}), 1825, 1764, 1715 ($\nu_{term\ B\text{-}D}$), 855 (B-$D_{deformation}$). ^1H NMR (C_6D_6, 280 K, 400 MHz): δ 7.57-7.48 (m, 6H, P**Ph$_3$**) 6.97-6.91 (m, 9H, P**Ph$_3$**), 6.83 (br s, 2H, $C_6\mathbf{H}_2Me_3$), 6.74 (br s, 2H, $C_6\mathbf{H}_2Me_3$), 6.24 (s, 2H, NC**H**), 2.35 (s, 6H, *o*-CH_3), 2.22 (s, 6H, *o*-CH_3), 2.12 (s, 6H, *p*-CH_3), -13.36 (d, J_{PH} = 23.1 Hz, 1H, Ru-**H$_A$**). ^2H NMR (C_6H_6, 280 K): δ 4.56 and 4.09 (2br s, 2H, B-**D$_D$**), -4.62 (br s, 1H, B-**D$_C$**), -6.57 (br s, 1H, B-**D$_B$**).

5.10.3 Preparation of Ru(PPh$_3$)(IMes)(CO)$_2$H$_2$ (28)

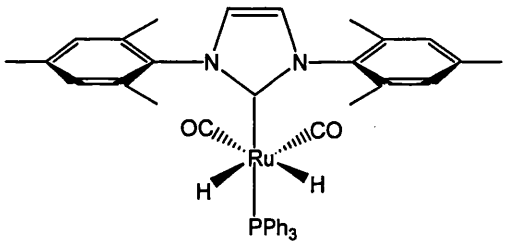

4 equiv. $NaBH_4$ (11.9 mg, 0.32 mmol) was added to a sample of Ru(PPh$_3$)(IMes)(CO)$_2$(Cl)H (**11**) (60 mg, 0.079 mmol) in a Schlenk tube. EtOH (*ca.* 5 mL) was added and the mixture stirred for 1 h at 298 K. The solvent was removed *in vacuo* and the product isolated by extraction from the residue with C_6H_6 (2 x *ca.* 2 mL). The solvent was removed and the product dried *in vacuo*. Crystals of X-ray quality were grown from a benzene sample layered with hexane. Yield (not optimised): 36 mg (63 %).

NB. Hydrogen gas is released throughout the reaction (vigorously when EtOH is initially added) so the reaction vessel was fitted with an outlet needle under a steady flow of argon.

FW = 725.82. ESI-TOF MS $[M\text{-}CO+H]^+$ *m/z* = 713.1809 (theoretical *m/z* = 713.1876). IR (nujol, cm^{-1}): 1995, 1947 (br) (ν_{CO}). ^1H NMR (C_6D_6, 298 K, 400 MHz): δ 7.63 (m, 6H, PPh_3) 7.47 (m, 3H, PPh_3), 6.98 (m, PPh_3 (6H) and $C_6H_2Me_3$ (2H)), 6.85 (s, 2H, $C_6H_2Me_3$), 6.29 (s, 2H, NCH), 2.20 (s, 12H, *o*-CH_3), 2.19 (s, 6H, *p*-CH_3), -6.56 (d, J_{PH} = 26.4 Hz, 2H, Ru-H). $^{13}C\{^1H\}$ NMR (C_6D_6, 298K): δ 203.1 (d, J_{CP} = 8.50 Hz, Ru-CO), 189.9 (d, J_{CP} = 72.5 Hz, Ru-C), 140.2 (t, J_{CP} = 21.3 Hz, *i*-C_6H_5), 138.9 (s, N-C), 136.8 (s, *o*-or *p*-$C_6H_2Me_3$), 135.0 (s, PPh_3), 134.9 (s, PPh_3), 130.0 (s, *m*-$C_6H_2Me_3$), 129.5 (s, PPh_3), 128.4 (s, PPh_3), 128.3 (s, PPh_3), 122.3 (2s, NCH), 21.9 (s, *o*-CH_3), 19.2 (s, *p*-CH_3). $^{31}P\{^1H\}$ NMR (C_6D_6, 298 K): δ 60.5 (s).

5.10.4 Preparation of $Ru(PPh_3)(IMes)(CO)_3$ (29)

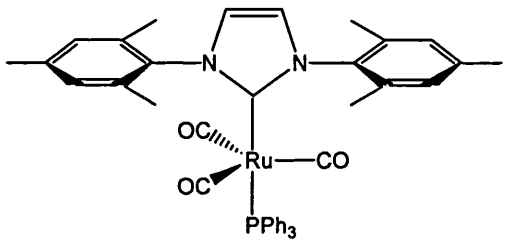

A sample of $Ru(PPh_3)(IMes)(CO)(\eta^2\text{-}BH_4)H$ (**26**) (10 mg, 0.014 mmol) in a J. Youngs' NMR tube was dissolved in C_6D_6 (*ca.* 0.6 mL), freeze-pump-thaw degassed and exposed to 1 atm CO. Complete conversion to the product was achieved after a day at 298 K.

Selected data for **29**:

FW = 793.96. IR (nujol, cm^{-1}): 1878, 1864 (ν_{CO}). ^1H NMR (C_6D_6, 298 K, 400 MHz): δ 7.72-7.65 (m, 9H, PPh_3), 6.96 (m, 6H, PPh_3), 6.26 (br s, 2H, $C_6H_2Me_3$), 6.10 (s, 4H, NCH), 2.22 (s, 12H, *o*-CH_3), 2.16 (s, 6H, *p*-CH_3). $^{31}P\{^1H\}$ NMR (C_6D_6, 298K): δ 60.6 (s).

4.10.5 Preparation of Ru(PPh$_3$)(IMes)(CO)(4-Mepy)H$_2$ (30)

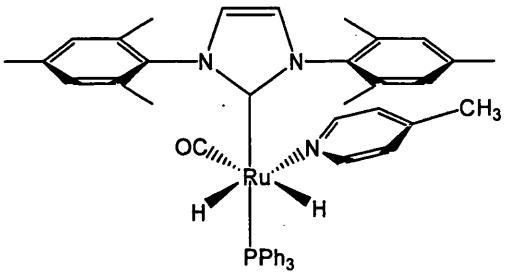

A slight excess (1.2 equiv.) of 4-Mepy (8.3 μL, 0.084 mmol) was added *via* syringe to a C_6D_6 sample (*ca.* 0.6 mL) of Ru(PPh$_3$)(IMes)(CO)(η^2-BH$_4$)H (**26**) (50 mg, 0.070 mmol) in a J. Youngs' NMR tube. The reaction mixture was shaken and **30** characterised *in situ*.

Selected data for **30**:

FW = 790.94. ^{1}H NMR (C_6D_6, 298 K, 400 MHz): δ 8.09 (d, J_{HH} = 6.0 Hz, 1H, 4-Me**py**), 7.99 (br d, J_{HH} = 6.0 Hz, 1H, 4-Me**py**), 7.64 (m, 6H, P**Ph$_3$**), 6.9 (m, 9H, P**Ph$_3$**), 6.86 (s, 1H, C_6**H**$_2$Me$_3$), 6.72 (s, 1H, C_6**H**$_2$Me$_3$), 6.41 (s, 2H, NC**H**), 6.05 (d, J_{HH} = 6.0 Hz, 1H, 4-Me**py**), 5.75 (br d, J_{HH} = 6.0 Hz, 1H, 4-Me**py**), 2.38 (s, 6H, **CH$_3$**), 2.14 (s, 6H, **CH$_3$**), 2.09 (s, 6H, **CH$_3$**), 1.65 (s, 3H, 4-**Me**py), -4.15 (dd, J_{HP} = 31 Hz, J_{HH} = 6.0 Hz, 1H, Ru-**H**), -14.94 (dd, J_{HP} = 26 Hz, J_{HH} = 6.0 Hz, 1H, Ru-H). ^{31}P{^{1}H} NMR (C_6D_6, 298 K): δ 69.3 (s). ^{13}C{^{1}H}-^{1}H NMR (C_6D_6, 298 K): δ 205.3 (Ru-**C**O), 197.5 (Ru-**C**).

5.10.6 Preparation of Ru(PPh$_3$)(IMes)(CO)(4-Mepy)(Cl)H (31)

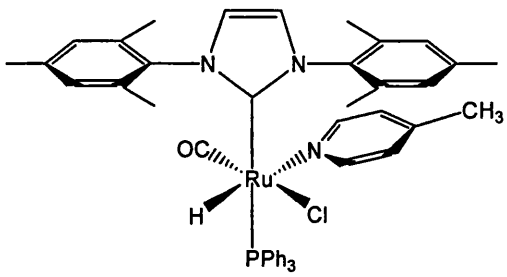

A sample of Ru(PPh$_3$)(IMes)(CO)(Cl)H (**8**) (200 mg, 0.27 mmol) was dissolved in C_6H_6 (*ca.* 8 mL) in a Schlenk tube, into which 1.2 equiv. 4-Mepy (32 μL, 0.33 mmol) was added *via* syringe under argon. Upon stirring at room temperature

quick colour change from yellow to straw occurred. Solvent was removed *in vacuo* and the resultant powder was washed with hexane (2 x *ca.* 8 mL). Pale yellow pyramidal crystals were afforded from a benzene sample layered with hexane. Yield: 210 mg (94 %).

FW = 825.38. Anal. found (calcd.) for $C_{46}H_{47}N_3OClPRu$: C, 66.91 (66.94); H, 5.85 (5.74); N, 5.10 (5.09). IR (nujol, cm^{-1}): 1876 ν(CO). ^1H NMR (C_6D_6, 275 K, 400 MHz): δ 8.76 (br, 1H, 4-Me**py**), 8.17 (br, 1H, 4-Me**py**), 7.65 (m, 6H, **PPh**$_3$), 6.94 (m, 11H, **PPh**$_3$ (9H) and $C_6\mathbf{H}_2Me_3$ (2H)), 6.72 (br, 1H, $C_6\mathbf{H}_2Me_3$), 6.41 (br, 1H, $C_6\mathbf{H}_2Me_3$), 6.23 (s, 2H, N**CH**), 5.92 (br, 2H, 4-Me**py**), 2.54 (s, 6H, *o*-$\mathbf{CH}_3$), 2.30 (s, 6H, *o*-$\mathbf{CH}_3$), 2.04 (s, 6H, *p*-$\mathbf{CH}_3$), 1.68 (s, 3H, 4-**Me**py), -12.67 (d, J_{HP} = 17 Hz, 1H, Ru-**H**). $^{31}P\{^1H\}$ NMR (C_6D_6, 298 K): δ 45.2 (s). $^{13}C\{^1H\}$ NMR (C_6D_6, 298 K): δ 205.3 (d, J_{CP} = 12.9 Hz, Ru-**C**O), 188.6 (d, J_{CP} = 102.0 Hz, Ru-**C**), 144.7 (s, *i*-4-Me**py**), 139.6, 138.5, 137.4, 137.2 (4s, $\mathbf{C}_{quaternary}$), 137.1 (d, J_{CP} = 5.5 Hz, *i*-$\mathbf{C}_6H_5$), 135.6 (s, **PPh**$_3$), 135.5 (s, **PPh**$_3$), 129.4 (s, *m*-$\mathbf{C}_6\mathbf{H}_2Me_3$), 129.0 (s, *m*-$\mathbf{C}_6\mathbf{H}_2Me_3$), 128.1 (s, **PPh**$_3$), 128.0 (s, **PPh**$_3$), 124.4 (br, *m*-4-Me**py**), 123.4 (2s, N**C**H), 21.7 (s, *p*-$\mathbf{C}H_3$), 21.0 (s, 4-**Me**py), 19.8 (s, *o*-$\mathbf{C}H_3$), 19.6 (s, *o*-$\mathbf{C}H_3$).

NB. Any ^1H NMR resonances that change significantly with lowering acquisition temperature are reported here: ^1H NMR ($C_6D_5CD_3$, 250 K, 400 MHz): δ 8.61 (d, J_{HH} = 4.4 Hz, 1H, 4-Me**py**), 8.04 (d, J_{HH} = 4.4 Hz, 1H, 4-Me**py**), 5.84 (d, J_{HH} = 4.4 Hz, 2H 4-Me**py**), -12.72 (d, J_{HP} = 20.3 Hz, 1H, Ru-**H**). $^{13}C\{^1H\}$ NMR ($C_6D_5CD_3$, 250 K): δ 153.1 (s, *o*-4-Me**py**), 151.2 (s, *o*-4-Me**py**), 124.3 (s, *m*-4-Me**py**).

5.11 Aluminohydride and super hydride work

5.11.1 Treatment of Ru(IMes)$_2$(CO)(Cl)H (Cl) with LiAlH$_4$

A sample of Ru(IMes)$_2$(CO)(Cl)H (**7**) (100 mg, 0.13 mmol) and 4 equiv. of $LiAlH_4$ (19.6 mg, 0.52 mmol) were added to a Schlenk tube (in the glovebox). The reaction mixture was dissolved in THF (*ca.* 4 mL) and kept under a flow of Ar. After stirring at 298 K for 1 h there was a colour change from yellow to white. The solvent was removed *in vacuo*, the product (**33**) was dissolved in THF-d_8 (*ca.* 0.6 mL) and characterised *in situ* by ^1H and ^{27}Al spectroscopy.

Selected data for **33**:

IR (nujol, cm^{-1}): 1743, 1609. ^1H NMR (THF-d_8, 298 K, 400 MHz): δ 4.5 (br), -10 (v br). ^{27}Al NMR (THF-d_8, 298 K): δ 69.7 (v br).

5.11.2 Treatment of $Ru(PPh_3)(IMes)(CO)(Cl)H$ (8) with $LiAlH_4$

A sample of $Ru(PPh_3)(IMes)(CO)(Cl)H$ (**8**) (50 mg, 0.068 mmol) and 4 equiv. of $LiAlH_4$ (10.4 mg, 0.27 mmol) were added to a Schlenk tube (in the glovebox). The reaction mixture was dissolved in THF (*ca.* 2 mL) and kept under a flow of Ar. After stirring at 298 K for 15 min there was a colour change from yellow to white. The solvent was removed *in vacuo*, the product dissolved in THF-d_8 (*ca.* 0.6 mL) and characterised *in situ* by ^1H, $^{31}P\{^1H\}$ and ^{27}Al spectroscopy.
Selected data for the product:
^1H NMR (THF-d_8, 298 K, 400 MHz): δ 7.52-7.31 (m, 9H, PPh_3), 7.02 (m, 6H, PPh_3), 6.96 (br s), 6.64 (br s, 2H), 6.25 (s, 2H, NC**H**), 3.70 (v br), 2.42 (s, 6H, CH_3), 2.19 (s, 6H, CH_3), 1.76 (s, 6H, CH_3), -8.03 ppm (s, 1H), -9.24 (br s), -9.59 (d, J_{HP} = 65.7 Hz, 1H), -12.06 (d, J_{HP} = 21.9 Hz, 1H). $^{31}P\{^1H\}$ NMR (THF-d_8, 298 K): δ 51.2 (s). ^{27}Al NMR (THF-d_8, 298 K): δ 99.3 (br).

5.11.3 Treatment of $Ru(IMes)_2(CO)(Cl)H$ (7) with $LiHBEt_3$

A sample of $Ru(IMes)_2(CO)(Cl)H$ (**7**) (10 mg, 0.013 mmol) was dissolved in THF-d_8 (*ca.* 0.6 mL) in a J. Youngs' NMR tube. A slight excess (1.2 equiv.) of 1.0 M $LiHBEt_3$ in THF (15.5 μL, 0.016 mmol) was added to the mixture *via* syringe. At 298 K there was no reaction observed in the ^1H NMR spectrum.

5.11.4 Treatment of $Ru(PPh_3)(IMes)(CO)(Cl)H$ (8) with $LiHBEt_3$

A sample of $Ru(PPh_3)(IMes)(CO)(Cl)H$ (**8**) (10 mg, 0.014 mmol) was dissolved in THF-d_8 (*ca.* 0.6 mL) in a J. Youngs' NMR tube. A slight excess (1.2 equiv.) of 1.0 M $LiHBEt_3$ in THF (13.6 μL, 0.016 mmol) was added to the mixture *via* syringe. A range of hydride containing products including $Ru(PPh_3)_2(IMes)(CO)H_2$.

5.12 Preparation of the dihydrogen dihydride complex $Ru(IMes)_2(CO)(\eta^2\text{-}H_2)H_2$ (34)

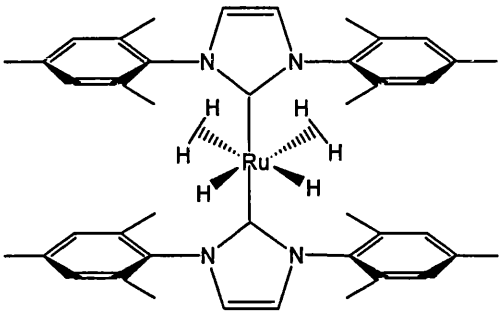

A sample containing $Ru(IMes)_2(CO)(Cl)H$ (7) (54 mg, 0.070 mmol) and $KN(SiMe_3)_2$ (14 mg, 0.070 mmol) in a J. Youngs' NMR tube was dissolved in THF-d_8 *in vacuo*. An atmosphere of H_2 was added and the sample shaken. **34** was characterised *in situ*.

Selected data for **34**:

^{1}H NMR (THF-d_8, 298 K, 400 MHz): δ 6.83-6.77 (m, 8H, $C_6\mathbf{H}_2Me_3$) 6.20-6.15 (m, 4H, NC**H**), 2.34 and 2.32 (2s, 12H, $C\mathbf{H}_3$), 2.16 (s, 6H, $C\mathbf{H}_3$), 2.04 and 2.02 (2s, 18H, $C\mathbf{H}_3$), -6.35 (v br s, 4H, Ru-**H**).

5.13 Silyl transfer work

5.13.1 Preparation of $Ru(PPh_3)_2(IMes)(CO)H_2$ (36)

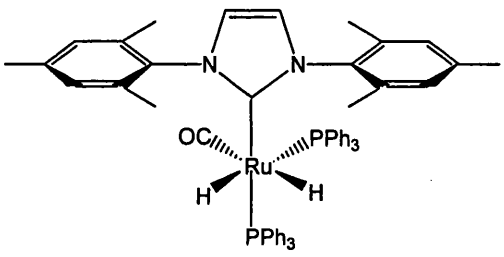

$Ru(PPh_3)_2(IMes)(CO)H_2$ was prepared *via* a published method.[9]

Samples of $Ru(PPh_3)_3(CO)H_2$ (250 mg, 0.27 mmol) and IMes (250 mg, 0.73 mmol) were added to an ampoule fitted with a J. Youngs' PTFE tap and a stirrer bar. The

reaction mixture was dissolved in toluene (*ca.*8 mL), heated at 343 K with stirring for *ca.* 40 h. The reaction was checked regularly by ^{1}H NMR spectroscopy for complete loss of the starting complex. The solvent was removed *in vacuo* to afford a dark oily residue, which was subsequently washed with EtOH (3 x *ca.* 5 mL) and hexane (*ca.* 10 mL) to yield an off-white powder. Yield: 145 mg (56 %).

Selected data for **36**:

FW = 960.10. IR (C_6D_6, cm^{-1}): 1941 (ν_{CO}). ^{1}H NMR (C_6D_6, 298 K, 400 MHz): δ 7.42-7.30 (m, 12H, PPh_3), 6.93 (m, 18H, PPh_3), 6.86 (br s, 2H, $C_6H_2Me_3$), 6.82 (br s, 2H, $C_6H_2Me_3$) 6.25 (br s, 2H, NCH), 2.26 (s, 6H, *p*-CH_3), 2.20 (s, 6H, *o*-CH_3), 1.82 (s, 6H, *o*-CH_3), -6.36 (ddd, J_{HP} = 26.8 and 23.6 Hz, J_{HH} = 6.0 Hz, 1H, Ru-H), -8.08 (ddd, J_{HP} = 81.2 and 33.6 Hz, J_{HH} = 6.0 Hz, 1H, Ru-H). ^{31}P{^{1}H} NMR (C_6D_6, 298K): δ 59.0 (d, J_{PP} = 14.8 Hz), 47.8 (d, J_{PP} = 14.8 Hz).

5.13.2 Preparation of Ru(PPh$_3$)(IMes)(CO)(F)H (35)

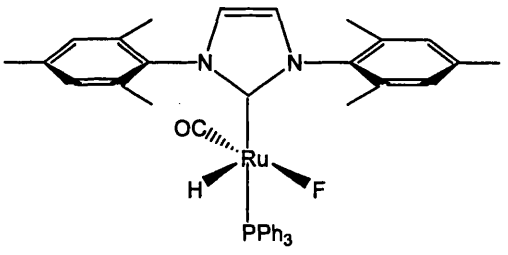

(a) *via* Ru(PPh$_3$)$_3$(CO)(F)H

A J. Youngs' NMR tube was charged with $Ru(PPh_3)_3(CO)(F)H$ (30.0 mg, 0.032 mmol) and 1.2 equiv. IMes (11.7 mg, 0.039 mmol). The reaction mixture was dissolved in C_6D_6 (*ca.* 0.6 mL) and followed by ^{1}H and ^{31}P{^{1}H} NMR spectroscopy. After 1 h at 298 K **35** was observed. Longer reaction times resulted in the formation of $Ru(IMes)_2(CO)(F)H$ (**6**).

(b) *via* Ru(PPh$_3$)$_2$(IMes)(CO)H$_2$

$Ru(PPh_3)_2(IMes)(CO)H_2$ (30 mg, 0.031 mmol) was dissolved in THF-d_8 (*ca.* 0.6 mL) in a Young's NMR tube and 1 equiv. of $Et_3N.3HF$ (5.1 μL, 0.031 mmol) added *via*

syringe. The reaction mixture was shaken and characterised *in situ* by NMR spectroscopy.

Selected data for **35**:

FW = 715.81. ^{1}H NMR (C_6D_6, 298 K, 400 MHz): δ 7.56-7.34 (m, P**Ph**$_3$), 7.09-6.91 (m, P**Ph**$_3$), 6.26 (s, 2H, NC**H**), 2.41 (s, 6H, C**H**$_3$), 2.31 (s, 6H, C**H**$_3$), 2.12 (s, 6H, C**H**$_3$), -21.90 (v br, 1H, Ru-**H**). ^{31}P{^{1}H} NMR (C_6D_6, 298K): δ 40.5 (br).

NB. The aryl region was very messy, hence the aryl protons $C_6H_2Me_3$ could not be assigned confidently.

5.14 Catalytic hydrogenation reactions

Hydrogenation reactions were performed in a Parr 4842 autoclave. The reaction vessel was typically charged with 0.4 mol % catalyst (*ca.* 10 mg) and the substrate (0.3 M) dissolved in *i*-PrOH (degassed) before sealing and charging with 10 atm H_2. The reaction mixture was heated at 343 K and stirred (*ca.* 120 rpm) for 20 h. After this time the vessel and contents were allowed to cool to below 303 K before carefully releasing the pressure. A 1 mL aliquot of the reaction mixture was reduced by half *in vacuo* and the residue dissolved in $CDCl_3$. Conversion from ketone to alcohol was determined by comparison of the methyl peak integrations in the ^{1}H NMR spectrum ($CDCl_3$, 298 K, 300 MHz).

5.15 References

1. Sheldrick, G.M., *Acta. Cryst.*, **1990**, 467.
2. Arduengo, A.J.; Krafczyk, R.; Schmutzler, R.; Craig, H.A.; Goerlich, J.R.; Marshall, W.J.; Unverzagt, M., *Tetrahedron*, **1999**, *55*, 14523.
3. Harris, A.D.; Robinson, S.D., *Inorg. Chim. Acta.*, **1980**, *42*, 25.
4. Ahmad, N.; Levison, J.J.; Robinson, S.D.; Uttley, M.F., *Inorg. Synth.*, **1974**, *15*, 48.
5. Reade, S.P., *unpublished results*, **2007**.
6. Jazzar, R.F.R.; Bhatia, P.H.; Mahon, M.F.; Whittlesey, M.K., *Organometallics*, **2003**, *22*, 670.
7. Chatwin, S.L.; Diggle, R.A.; Jazzar, R.F.R.; Macgregor, S.A.; Mahon, M.F.; Whittlesey, M.K., *Inorg. Chem.*, **2003**, *42*, 7695.
8. Nolan, S.P.; Fogg, D.E.; dos Santos, E.N.; Foucault, H.M.; Dharmasena, U.L., *Organometallics*, **2005**, *24*, 1056.
9. Jazzar, R.F.R.; Macgregor, S.A.; Mahon, M.F.; Richards, S.P.; Whittlesey, M.K., *J. Am. Chem. Soc.*, **2002**, *124*, 4944.

Appendices

Appendices

Appendix 1. crystallographic data, bond lengths and angles for $Ru(IMes)_2(CO)_2(Cl)H$ (10)

Identification code	k06mkw10
Empirical formula	C44 H49 Cl N4 O2 Ru
Formula weight	802.39
Temperature	150(2) K
Wavelength	0.71073 Å
Crystal system	Monoclinic
Space group	$P2_1/a$
Unit cell dimensions	a = 18.5500(1)Å α = 90°
	b = 10.8650(1)Å β = 108.646(1)°
	c = 21.1290(2)Å γ = 90°
Volume	4034.94(6) $Å^3$
Z	4
Density (calculated)	1.321 Mg/m^3
Absorption coefficient	0.495 mm^{-1}
F(000)	1672
Crystal size	0.20 x 0.20 x 0.15 mm
Theta range for data collection	3.54 to 30.50°
Index ranges	-26<=h<=26; -15<=k<=15; -29<=l<=30
Reflections collected	56500
Independent reflections	12272 [R(int) = 0.0469]
Reflections observed (>2σ)	10523
Data Completeness	0.996
Absorption correction	Semi-empirical from equivalents
Max. and min. transmission	0.87 and 0.83
Refinement method	Full-matrix least-squares on F^2
Data / restraints / parameters	12272 / 1 / 511
Goodness-of-fit on F^2	1.086
Final R indices [I>2σ(I)]	R1 = 0.0391 wR2 = 0.0792
R indices (all data)	R1 = 0.0518 wR2 = 0.0829
Largest diff. peak and hole	0.408 and -0.547 $eÅ^{-3}$

Bond lengths (Å) for $Ru(IMes)_2(CO)_2(Cl)H$

Ru(1)-H(1)	1.594(9)	Ru(1)-C(2)	1.864(6)
Ru(1)-C(2A)	1.890(8)	Ru(1)-C(1)	1.9840(19)
Ru(1)-C(24)	2.1064(15)	Ru(1)-C(3)	2.1158(15)
Ru(1)-Cl(1A)	2.384(2)	Ru(1)-Cl(1)	2.4264(15)
O(1)-C(1)	1.136(2)	O(2)-C(2)	1.186(5)
O(2A)-C(2A)	1.200(8)	N(1)-C(3)	1.372(2)
N(1)-C(4)	1.385(2)	N(1)-C(6)	1.438(2)
N(2)-C(3)	1.371(2)	N(2)-C(5)	1.390(2)
N(2)-C(15)	1.445(2)	N(3)-C(24)	1.374(2)
N(3)-C(25)	1.390(2)	N(3)-C(27)	1.448(2)
N(4)-C(24)	1.375(2)	N(4)-C(26)	1.3935(19)
N(4)-C(36)	1.447(2)	C(4)-C(5)	1.336(3)
C(6)-C(7)	1.389(3)	C(6)-C(11)	1.401(3)
C(7)-C(8)	1.392(3)	C(7)-C(12)	1.506(3)
C(8)-C(9)	1.380(3)	C(9)-C(10)	1.396(3)
C(9)-C(13)	1.513(3)	C(10)-C(11)	1.389(3)
C(11)-C(14)	1.509(3)	C(15)-C(20)	1.392(2)
C(15)-C(16)	1.398(2)	C(16)-C(17)	1.394(3)
C(16)-C(21)	1.506(3)	C(17)-C(18)	1.397(3)
C(18)-C(19)	1.385(3)	C(18)-C(22)	1.517(3)
C(19)-C(20)	1.393(3)	C(20)-C(23)	1.504(3)
C(25)-C(26)	1.337(2)	C(27)-C(28)	1.392(3)
C(27)-C(32)	1.401(3)	C(28)-C(29)	1.400(3)
C(28)-C(33)	1.497(3)	C(29)-C(30)	1.389(4)
C(30)-C(31)	1.375(4)	C(30)-C(34)	1.523(3)
C(31)-C(32)	1.399(3)	C(32)-C(35)	1.495(3)
C(36)-C(41)	1.397(3)	C(36)-C(37)	1.398(3)
C(37)-C(38)	1.396(3)	C(37)-C(42)	1.499(3)
C(38)-C(39)	1.383(3)	C(39)-C(40)	1.390(4)
C(39)-C(43)	1.516(3)	C(40)-C(41)	1.396(3)
C(41)-C(44)	1.505(3)		

Bond angles (°) for $Ru(IMes)_2(CO)_2(Cl)H$

H(1)-Ru(1)-C(2)	86.3(9)	H(1)-Ru(1)-C(2A)	83.2(9)
C(2)-Ru(1)-C(2A)	169.6(4)	H(1)-Ru(1)-C(1)	179.1(9)
C(2)-Ru(1)-C(1)	94.4(3)	C(2A)-Ru(1)-C(1)	96.0(3)
H(1)-Ru(1)-C(24)	83.5(8)	C(2)-Ru(1)-C(24)	90.0(2)
C(2A)-Ru(1)-C(24)	88.6(3)	C(1)-Ru(1)-C(24)	96.02(7)
H(1)-Ru(1)-C(3)	85.3(8)	C(2)-Ru(1)-C(3)	88.8(2)
C(2A)-Ru(1)-C(3)	90.5(3)	C(1)-Ru(1)-C(3)	95.17(6)
C(24)-Ru(1)-C(3)	168.81(6)	H(1)-Ru(1)-Cl(1A)	88.9(8)
C(2)-Ru(1)-Cl(1A)	2.5(3)	C(2A)-Ru(1)-Cl(1A)	172.1(3)
C(1)-Ru(1)-Cl(1A)	91.91(9)	C(24)-Ru(1)-Cl(1A)	89.94(7)
C(3)-Ru(1)-Cl(1A)	89.38(7)	H(1)-Ru(1)-Cl(1)	87.8(8)
C(2)-Ru(1)-Cl(1)	174.0(3)	C(2A)-Ru(1)-Cl(1)	4.6(3)
C(1)-Ru(1)-Cl(1)	91.45(7)	C(24)-Ru(1)-Cl(1)	88.33(5)
C(3)-Ru(1)-Cl(1)	91.70(5)	Cl(1A)-Ru(1)-Cl(1)	176.37(8)
C(3)-N(1)-C(4)	112.22(14)	C(3)-N(1)-C(6)	127.44(13)
C(4)-N(1)-C(6)	120.15(14)	C(3)-N(2)-C(5)	111.82(13)
C(3)-N(2)-C(15)	129.33(13)	C(5)-N(2)-C(15)	118.84(13)
C(24)-N(3)-C(25)	112.17(13)	C(24)-N(3)-C(27)	126.55(13)
C(25)-N(3)-C(27)	119.99(13)	C(24)-N(4)-C(26)	111.63(13)
C(24)-N(4)-C(36)	129.30(13)	C(26)-N(4)-C(36)	118.55(13)
O(1)-C(1)-Ru(1)	179.65(16)	O(2)-C(2)-Ru(1)	177.4(8)
N(2)-C(3)-N(1)	102.40(13)	N(2)-C(3)-Ru(1)	127.27(11)
N(1)-C(3)-Ru(1)	130.06(11)	C(5)-C(4)-N(1)	106.64(15)
C(4)-C(5)-N(2)	106.92(15)	C(7)-C(6)-C(11)	122.80(17)
C(7)-C(6)-N(1)	119.42(16)	C(11)-C(6)-N(1)	117.60(16)
C(6)-C(7)-C(8)	117.18(18)	C(6)-C(7)-C(12)	122.43(17)
C(8)-C(7)-C(12)	120.39(18)	C(9)-C(8)-C(7)	122.12(19)
C(8)-C(9)-C(10)	119.06(18)	C(8)-C(9)-C(13)	120.2(2)
C(10)-C(9)-C(13)	120.8(2)	C(11)-C(10)-C(9)	121.2(2)
C(10)-C(11)-C(6)	117.62(18)	C(10)-C(11)-C(14)	121.55(18)
C(6)-C(11)-C(14)	120.80(17)	C(20)-C(15)-C(16)	122.47(16)
C(20)-C(15)-N(2)	118.76(15)	C(16)-C(15)-N(2)	118.21(15)
C(17)-C(16)-C(15)	117.50(17)	C(17)-C(16)-C(21)	120.66(17)
C(15)-C(16)-C(21)	121.83(16)	C(16)-C(17)-C(18)	121.85(18)

C(19)-C(18)-C(17)	118.35(17)	C(19)-C(18)-C(22)	120.7(2)
C(17)-C(18)-C(22)	120.9(2)	C(18)-C(19)-C(20)	122.16(18)
C(15)-C(20)-C(19)	117.66(17)	C(15)-C(20)-C(23)	121.91(16)
C(19)-C(20)-C(23)	120.43(17)	N(3)-C(24)-N(4)	102.49(13)
N(3)-C(24)-Ru(1)	130.33(11)	N(4)-C(24)-Ru(1)	127.08(11)
C(26)-C(25)-N(3)	106.56(14)	C(25)-C(26)-N(4)	107.15(14)
C(28)-C(27)-C(32)	123.15(17)	C(28)-C(27)-N(3)	120.07(17)
C(32)-C(27)-N(3)	116.65(18)	C(27)-C(28)-C(29)	116.7(2)
C(27)-C(28)-C(33)	122.59(17)	C(29)-C(28)-C(33)	120.7(2)
C(30)-C(29)-C(28)	122.0(2)	C(31)-C(30)-C(29)	119.2(2)
C(31)-C(30)-C(34)	121.2(3)	C(29)-C(30)-C(34)	119.5(3)
C(30)-C(31)-C(32)	121.7(2)	C(31)-C(32)-C(27)	117.2(2)
C(31)-C(32)-C(35)	121.1(2)	C(27)-C(32)-C(35)	121.73(18)
C(41)-C(36)-C(37)	122.58(17)	C(41)-C(36)-N(4)	117.42(16)
C(37)-C(36)-N(4)	119.55(16)	C(38)-C(37)-C(36)	117.07(19)
C(38)-C(37)-C(42)	121.05(19)	C(36)-C(37)-C(42)	121.88(16)
C(39)-C(38)-C(37)	122.7(2)	C(38)-C(39)-C(40)	118.13(19)
C(38)-C(39)-C(43)	120.9(2)	C(40)-C(39)-C(43)	121.0(2)
C(39)-C(40)-C(41)	122.2(2)	C(40)-C(41)-C(36)	117.38(19)
C(40)-C(41)-C(44)	120.53(19)	C(36)-C(41)-C(44)	122.07(17)
O(2A)-C(2A)-Ru(1)	176.9(8)		

Appendix 2. crystallographic data, bond lengths and angles for $Ru(PPh_3)(IMes)(CO)_2(Cl)H$ (11)

Identification code	k06mkw11
Empirical formula	C47 H46 Cl N2 O2 P Ru
Formula weight	838.35
Temperature	150(2) K
Wavelength	0.71073 Å
Crystal system	Monoclinic
Space group	$P2_1$
Unit cell dimensions	a = 11.0670(1)Å α = 90°
	b = 13.8480(2)Å β = 104.407(1)°
	c = 14.0060(2)Å γ = 90°
Volume	2079.00(5) $Å^3$
Z	2
Density (calculated)	1.339 Mg/m^3
Absorption coefficient	0.520 mm^{-1}
F(000)	868
Crystal size	0.45 x 0.40 x 0.40 mm
Theta range for data collection	3.62 to 30.00°
Index ranges	-15<=h<=15; -19<=k<=19; -19<=l<=19
Reflections collected	44617
Independent reflections	11963 [R(int) = 0.0443]
Reflections observed (>2σ)	10641
Data Completeness	0.997
Absorption correction	Semi-empirical from equivalents
Max. and min. transmission	0.82 and 0.77
Refinement method	Full-matrix least-squares on F^2
Data / restraints / parameters	11963 / 2 / 498
Goodness-of-fit on F^2	1.034
Final R indices [I>2σ(I)]	$R^1 = 0.0301$ $wR_2 = 0.0593$
R indices (all data)	$R^1 = 0.0396$ $wR_2 = 0.0627$
Absolute structure parameter	-0.027(13)
Largest diff. peak and hole	0.849 and -0.581 $eÅ^{-3}$

Bond lengths (Å) for $Ru(PPh_3)(IMes)(CO)_2(Cl)H$

Ru(1)-H(1)	1.581(15)	Ru(1)-C(2)	1.848(2)
Ru(1)-C(1)	1.973(2)	Ru(1)-C(3)	2.0974(19)
Ru(1)-P(1)	2.3529(5)	Ru(1)-Cl(1)	2.4528(5)
P(1)-C(30)	1.830(2)	P(1)-C(24)	1.834(2)
P(1)-C(36)	1.834(2)	O(1)-C(1)	1.136(3)
O(2)-C(2)	1.136(3)	N(1)-C(3)	1.370(3)
N(1)-C(4)	1.395(3)	N(1)-C(6)	1.443(3)
N(2)-C(3)	1.368(2)	N(2)-C(5)	1.387(3)
N(2)-C(15)	1.446(3)	C(4)-C(5)	1.340(3)
C(6)-C(7)	1.395(3)	C(6)-C(11)	1.397(3)
C(7)-C(8)	1.392(3)	C(7)-C(12)	1.502(3)
C(8)-C(9)	1.390(3)	C(9)-C(10)	1.384(4)
C(9)-C(13)	1.510(3)	C(10)-C(11)	1.397(3)
C(11)-C(14)	1.502(3)	C(15)-C(20)	1.390(3)
C(15)-C(16)	1.392(3)	C(16)-C(17)	1.389(3)
C(16)-C(21)	1.509(3)	C(17)-C(18)	1.386(3)
C(18)-C(19)	1.387(3)	C(18)-C(22)	1.515(3)
C(19)-C(20)	1.396(3)	C(20)-C(23)	1.504(3)
C(24)-C(25)	1.391(3)	C(24)-C(29)	1.393(3)
C(25)-C(26)	1.396(3)	C(26)-C(27)	1.376(3)
C(27)-C(28)	1.384(3)	C(28)-C(29)	1.392(3)
C(30)-C(31)	1.388(3)	C(30)-C(35)	1.390(3)
C(31)-C(32)	1.393(3)	C(32)-C(33)	1.378(3)
C(33)-C(34)	1.395(3)	C(34)-C(35)	1.384(3)
C(36)-C(37)	1.380(3)	C(36)-C(41)	1.393(3)
C(37)-C(38)	1.392(3)	C(38)-C(39)	1.375(4)
C(39)-C(40)	1.371(4)	C(40)-C(41)	1.391(3)
C(42)-C(47)	1.358(4)	C(42)-C(43)	1.380(4)
C(43)-C(44)	1.390(4)	C(44)-C(45)	1.379(4)
C(45)-C(46)	1.362(4)	C(46)-C(47)	1.388(4)

Bond angles (°) for $Ru(PPh_3)(IMes)(CO)_2(Cl)H$

H(1)-Ru(1)-C(2)	80.6(8)	H(1)-Ru(1)-C(1)	174.7(8)
C(2)-Ru(1)-C(1)	98.02(10)	H(1)-Ru(1)-C(3)	86.0(8)
C(2)-Ru(1)-C(3)	91.49(8)	C(1)-Ru(1)-C(3)	99.17(8)
H(1)-Ru(1)-P(1)	80.7(8)	C(2)-Ru(1)-P(1)	92.11(6)
C(1)-Ru(1)-P(1)	94.31(6)	C(3)-Ru(1)-P(1)	165.42(5)
H(1)-Ru(1)-Cl(1)	92.7(8)	C(2)-Ru(1)-Cl(1)	173.18(7)
C(1)-Ru(1)-Cl(1)	88.77(6)	C(3)-Ru(1)-Cl(1)	86.75(6)
P(1)-Ru(1)-Cl(1)	88.014(17)	C(30)-P(1)-C(24)	102.96(9)
C(30)-P(1)-C(36)	104.20(9)	C(24)-P(1)-C(36)	101.71(9)
C(30)-P(1)-Ru(1)	112.74(6)	C(24)-P(1)-Ru(1)	116.09(6)
C(36)-P(1)-Ru(1)	117.35(6)	C(3)-N(1)-C(4)	111.37(17)
C(3)-N(1)-C(6)	126.32(16)	C(4)-N(1)-C(6)	122.09(17)
C(3)-N(2)-C(5)	111.87(17)	C(3)-N(2)-C(15)	125.91(16)
C(5)-N(2)-C(15)	121.94(16)	O(1)-C(1)-Ru(1)	173.19(17)
O(2)-C(2)-Ru(1)	176.2(2)	N(2)-C(3)-N(1)	103.13(16)
N(2)-C(3)-Ru(1)	129.64(14)	N(1)-C(3)-Ru(1)	127.22(13)
C(5)-C(4)-N(1)	106.85(18)	C(4)-C(5)-N(2)	106.78(18)
C(7)-C(6)-C(11)	121.92(19)	C(7)-C(6)-N(1)	118.23(18)
C(11)-C(6)-N(1)	119.78(19)	C(8)-C(7)-C(6)	117.8(2)
C(8)-C(7)-C(12)	120.1(2)	C(6)-C(7)-C(12)	122.1(2)
C(9)-C(8)-C(7)	122.0(2)	C(10)-C(9)-C(8)	118.5(2)
C(10)-C(9)-C(13)	121.4(2)	C(8)-C(9)-C(13)	120.1(2)
C(9)-C(10)-C(11)	121.9(2)	C(6)-C(11)-C(10)	117.7(2)
C(6)-C(11)-C(14)	121.4(2)	C(10)-C(11)-C(14)	120.8(2)
C(20)-C(15)-C(16)	122.32(19)	C(20)-C(15)-N(2)	119.84(18)
C(16)-C(15)-N(2)	117.80(19)	C(17)-C(16)-C(15)	118.1(2)
C(17)-C(16)-C(21)	120.6(2)	C(15)-C(16)-C(21)	121.3(2)
C(18)-C(17)-C(16)	121.7(2)	C(17)-C(18)-C(19)	118.4(2)
C(17)-C(18)-C(22)	121.1(2)	C(19)-C(18)-C(22)	120.5(2)
C(18)-C(19)-C(20)	122.2(2)	C(15)-C(20)-C(19)	117.30(19)
C(15)-C(20)-C(23)	122.1(2)	C(19)-C(20)-C(23)	120.6(2)
C(25)-C(24)-C(29)	119.04(18)	C(25)-C(24)-P(1)	120.95(15)
C(29)-C(24)-P(1)	119.98(15)	C(24)-C(25)-C(26)	119.60(18)

C(27)-C(26)-C(25)	120.9(2)	C(26)-C(27)-C(28)	119.9(2)
C(27)-C(28)-C(29)	119.6(2)	C(28)-C(29)-C(24)	120.9(2)
C(31)-C(30)-C(35)	119.19(18)	C(31)-C(30)-P(1)	122.01(15)
C(35)-C(30)-P(1)	118.53(15)	C(30)-C(31)-C(32)	120.0(2)
C(33)-C(32)-C(31)	120.5(2)	C(32)-C(33)-C(34)	119.9(2)
C(35)-C(34)-C(33)	119.5(2)	C(34)-C(35)-C(30)	120.95(19)
C(37)-C(36)-C(41)	118.40(19)	C(37)-C(36)-P(1)	118.00(16)
C(41)-C(36)-P(1)	123.61(16)	C(36)-C(37)-C(38)	121.0(2)
C(39)-C(38)-C(37)	120.0(2)	C(40)-C(39)-C(38)	119.8(2)
C(39)-C(40)-C(41)	120.5(2)	C(40)-C(41)-C(36)	120.3(2)
C(47)-C(42)-C(43)	120.4(3)	C(42)-C(43)-C(44)	119.4(3)
C(45)-C(44)-C(43)	120.1(3)	C(46)-C(45)-C(44)	119.7(3)
C(45)-C(46)-C(47)	120.5(3)	C(42)-C(47)-C(46)	120.0(3)

Appendix 3. crystallographic data, bond lengths and angles for $Ru(IMes)_2(CO)(NH_3)(Cl)H$ (12)

Identification code	h03mkw6
Empirical formula	$C_{43}H_{51}ClN_5ORu$
Formula weight	790.41
Temperature	150(2) K
Wavelength	0.71073 Å
Crystal system	Monoclinic
Space group	$P2_1/a$
Unit cell dimensions	a = 18.5510(3)Å α = 90°
	b = 10.9490(2)Å β = 108.806(1)°
	c = 20.9330(4)Å γ = 90°
Volume	4024.82(12) $Å^3$
Z	4
Density (calculated)	1.304 Mg/m^3
Absorption coefficient	0.494 mm^{-1}
F(000)	1652
Crystal size	0.15 x 0.15 x 0.15 mm
Theta range for data collection	3.56 to 27.47°
Index ranges	-24<=h<=23; -13<=k<=14; -27<=l<=27
Reflections collected	37172
Independent reflections	9162 [R(int) = 0.0822]
Reflections observed (>2σ)	5696
Data Completeness	0.994
Absorption correction	None
Refinement method	Full-matrix least-squares on F^2
Data / restraints / parameters	9162 / 27 / 504
Goodness-of-fit on F^2	1.005
Final R indices [I>2σ(I)]	$R^1 = 0.0481$ $wR_2 = 0.0944$
R indices (all data)	$R^1 = 0.1045$ $wR_2 = 0.1119$
Largest diff. peak and hole	0.661 and -0.761 $eÅ^{-3}$

Bond lengths (Å) for $Ru(IMes)_2(CO)(NH_3)(Cl)H$

Ru(1)-C(1)	1.822(9)	Ru(1)-C(1A)	1.878(16)
Ru(1)-C(23)	2.102(3)	Ru(1)-C(2)	2.110(3)
Ru(1)-N(5)	2.314(3)	Ru(1)-Cl(1A)	2.387(10)
Ru(1)-Cl(1)	2.488(2)	N(2)-C(2)	1.383(4)
N(2)-C(4)	1.390(4)	N(2)-C(14)	1.435(4)
N(1)-C(2)	1.371(4)	N(1)-C(3)	1.384(4)
N(1)-C(5)	1.439(4)	N(4)-C(23)	1.379(4)
N(4)-C(24)	1.385(4)	N(4)-C(26)	1.451(4)
N(3)-C(23)	1.374(4)	N(3)-C(25)	1.384(4)
N(3)-C(35)	1.455(4)	O(1)-C(1)	1.168(11)
C(10)-C(5)	1.391(4)	C(10)-C(9)	1.392(4)
C(10)-C(13)	1.511(4)	C(24)-C(25)	1.328(4)
C(4)-C(3)	1.324(4)	C(6)-C(7)	1.384(4)
C(6)-C(5)	1.396(4)	C(6)-C(11)	1.507(4)
C(8)-C(9)	1.392(5)	C(8)-C(7)	1.402(5)
C(8)-C(12)	1.516(5)	C(35)-C(40)	1.389(5)
C(35)-C(36)	1.391(4)	C(40)-C(39)	1.395(4)
C(40)-C(43)	1.506(5)	C(26)-C(27)	1.392(5)
C(26)-C(31)	1.393(5)	C(31)-C(30)	1.395(5)
C(31)-C(34)	1.497(5)	C(36)-C(37)	1.397(5)
C(36)-C(41)	1.505(5)	C(22)-C(19)	1.496(5)
C(14)-C(19)	1.383(5)	C(14)-C(15)	1.410(4)
C(20)-C(15)	1.517(5)	C(19)-C(18)	1.384(5)
C(38)-C(39)	1.378(5)	C(38)-C(37)	1.391(5)
C(38)-C(42)	1.519(5)	C(18)-C(17)	1.387(5)
C(15)-C(16)	1.382(5)	C(32)-C(27)	1.502(5)
C(16)-C(17)	1.379(5)	C(17)-C(21)	1.523(5)
C(30)-C(29)	1.374(6)	C(27)-C(28)	1.404(5)
C(28)-C(29)	1.384(6)	C(29)-C(33)	1.527(5)
O(1A)-C(1A)	1.179(18)		

Bond lengths (°) for $Ru(IMes)_2(CO)(NH_3)(Cl)H$

C(1)-Ru(1)-C(1A)	168.0(9)	C(1)-Ru(1)-C(23)	89.7(3)
C(1A)-Ru(1)-C(23)	86.7(8)	C(1)-Ru(1)-C(2)	90.4(3)
C(1A)-Ru(1)-C(2)	91.2(8)	C(23)-Ru(1)-C(2)	170.64(11)
C(1)-Ru(1)-N(5)	97.9(3)	C(1A)-Ru(1)-N(5)	93.8(8)
C(23)-Ru(1)-N(5)	94.89(11)	C(2)-Ru(1)-N(5)	94.36(11)
C(1)-Ru(1)-Cl(1A)	5.6(7)	C(1A)-Ru(1)-Cl(1A)	173.5(9)
C(23)-Ru(1)-Cl(1A)	91.6(3)	C(2)-Ru(1)-Cl(1A)	89.4(3)
N(5)-Ru(1)-Cl(1A)	92.6(4)	C(1)-Ru(1)-Cl(1)	177.5(3)
C(1A)-Ru(1)-Cl(1)	10.5(8)	C(23)-Ru(1)-Cl(1)	88.06(9)
C(2)-Ru(1)-Cl(1)	91.61(9)	N(5)-Ru(1)-Cl(1)	83.33(10)
Cl(1A)-Ru(1)-Cl(1)	175.8(4)	C(2)-N(2)-C(4)	112.1(3)
C(2)-N(2)-C(14)	127.2(3)	C(4)-N(2)-C(14)	120.6(3)
C(2)-N(1)-C(3)	112.3(2)	C(2)-N(1)-C(5)	128.9(2)
C(3)-N(1)-C(5)	118.8(2)	C(23)-N(4)-C(24)	112.4(2)
C(23)-N(4)-C(26)	126.0(3)	C(24)-N(4)-C(26)	120.1(3)
C(23)-N(3)-C(25)	112.5(2)	C(23)-N(3)-C(35)	128.5(2)
C(25)-N(3)-C(35)	118.5(2)	C(5)-C(10)-C(9)	118.5(3)
C(5)-C(10)-C(13)	121.6(3)	C(9)-C(10)-C(13)	119.9(3)
C(25)-C(24)-N(4)	106.8(3)	C(3)-C(4)-N(2)	106.6(3)
C(7)-C(6)-C(5)	117.9(3)	C(7)-C(6)-C(11)	121.0(3)
C(5)-C(6)-C(11)	121.1(3)	C(9)-C(8)-C(7)	118.1(3)
C(9)-C(8)-C(12)	120.5(3)	C(7)-C(8)-C(12)	121.3(3)
C(24)-C(25)-N(3)	106.9(3)	C(40)-C(35)-C(36)	122.2(3)
C(40)-C(35)-N(3)	119.7(3)	C(36)-C(35)-N(3)	117.5(3)
C(35)-C(40)-C(39)	118.1(3)	C(35)-C(40)-C(43)	121.5(3)
C(39)-C(40)-C(43)	120.4(3)	N(1)-C(2)-N(2)	101.6(2)
N(1)-C(2)-Ru(1)	126.5(2)	N(2)-C(2)-Ru(1)	131.6(2)
C(27)-C(26)-C(31)	123.1(3)	C(27)-C(26)-N(4)	119.2(3)
C(31)-C(26)-N(4)	117.7(3)	C(6)-C(7)-C(8)	122.1(3)
C(26)-C(31)-C(30)	117.5(4)	C(26)-C(31)-C(34)	121.7(3)
C(30)-C(31)-C(34)	120.8(4)	C(10)-C(5)-C(6)	121.9(3)
C(10)-C(5)-N(1)	118.9(3)	C(6)-C(5)-N(1)	118.5(3)
C(35)-C(36)-C(37)	117.4(3)	C(35)-C(36)-C(41)	121.9(3)
C(37)-C(36)-C(41)	120.6(3)	C(4)-C(3)-N(1)	107.4(3)

N(3)-C(23)-N(4)	101.4(2)	N(3)-C(23)-Ru(1)	125.9(2)
N(4)-C(23)-Ru(1)	132.5(2)	C(10)-C(9)-C(8)	121.4(3)
C(19)-C(14)-C(15)	122.6(3)	C(19)-C(14)-N(2)	120.1(3)
C(15)-C(14)-N(2)	117.3(3)	C(14)-C(19)-C(18)	117.4(3)
C(14)-C(19)-C(22)	122.2(3)	C(18)-C(19)-C(22)	120.4(3)
C(39)-C(38)-C(37)	118.4(3)	C(39)-C(38)-C(42)	121.1(4)
C(37)-C(38)-C(42)	120.6(4)	C(19)-C(18)-C(17)	122.2(3)
C(38)-C(39)-C(40)	121.8(4)	C(16)-C(15)-C(14)	117.0(3)
C(16)-C(15)-C(20)	122.7(3)	C(14)-C(15)-C(20)	120.2(3)
C(17)-C(16)-C(15)	122.2(3)	C(38)-C(37)-C(36)	122.1(4)
C(16)-C(17)-C(18)	118.5(3)	C(16)-C(17)-C(21)	120.9(3)
C(18)-C(17)-C(21)	120.5(4)	O(1)-C(1)-Ru(1)	174.8(10)
C(29)-C(30)-C(31)	121.6(4)	C(26)-C(27)-C(28)	116.5(3)
C(26)-C(27)-C(32)	122.5(3)	C(28)-C(27)-C(32)	121.0(3)
C(29)-C(28)-C(27)	122.1(4)	C(30)-C(29)-C(28)	119.2(4)
C(30)-C(29)-C(33)	121.1(4)	C(28)-C(29)-C(33)	119.7(4)
O(1A)-C(1A)-Ru(1)	178(3)		

Appendix 4. crystallographic data, bond lengths and angles for $Ru(IMes)_2(CO)(C{\equiv}CPh)H$ (13)

Identification code	bath161
Empirical formula	C51 H54 N4 O Ru
Formula weight	840.05
Temperature	123(2) K
Wavelength	0.84600 Å
Crystal system	?
Space group	?
Unit cell dimensions	a = 11.127(2)Å α = 90°
	b = 26.332(5)Å β = 98.944(5)°
	c = 15.068(3)Å γ = 90°
Volume	4361.3(16) $Å^3$
Z	4
Density (calculated)	1.279 Mg/m^3
Absorption coefficient	0.401 mm^{-1}
F(000)	1760
Crystal size	0.08 x 0.03 x 0.02 mm
Theta range for data collection	4.27 to 33.17°
Index ranges	-14<=h<=13; -32<=k<=33; -14<=l<=19
Reflections collected	22717
Independent reflections	9281 [R(int) = 0.1085]
Reflections observed (>2σ)	4717
Data Completeness	0.939
Max. and min. transmission	0.9920 and 0.9686
Refinement method	Full-matrix least-squares on F^2
Data / restraints / parameters	9281 / 1 / 530
Goodness-of-fit on F^2	0.904
Final R indices [I>2σ(I)]	R1 = 0.0745 wR2 = 0.1490
R indices (all data)	R1 = 0.1512 wR2 = 0.1790
Largest diff. peak and hole	0.618 and -1.239 $eÅ^{-3}$

Bond lengths (Å) for Ru(IMes)$_2$(CO)(C≡CPh)H

Ru(1)-H(1)	1.60(2)	Ru(1)-C(1)	1.847(6)
Ru(1)-C(23)	2.066(5)	Ru(1)-C(2)	2.071(5)
Ru(1)-C(51)	2.084(6)	O(1)-C(1)	1.170(7)
N(1)-C(2)	1.373(6)	N(1)-C(3)	1.379(7)
N(1)-C(5)	1.441(7)	N(2)-C(2)	1.364(7)
N(2)-C(4)	1.394(6)	N(2)-C(14)	1.448(6)
N(3)-C(23)	1.376(7)	N(3)-C(24)	1.404(7)
N(3)-C(26)	1.445(7)	N(4)-C(23)	1.363(6)
N(4)-C(25)	1.387(6)	N(4)-C(35)	1.435(7)
C(3)-C(4)	1.324(8)	C(5)-C(6)	1.382(8)
C(5)-C(10)	1.402(8)	C(6)-C(7)	1.401(8)
C(6)-C(11)	1.501(8)	C(7)-C(8)	1.389(8)
C(8)-C(9)	1.385(8)	C(8)-C(12)	1.515(8)
C(9)-C(10)	1.406(8)	C(10)-C(13)	1.487(8)
C(14)-C(15)	1.388(8)	C(14)-C(19)	1.396(8)
C(15)-C(16)	1.391(8)	C(15)-C(20)	1.514(8)
C(16)-C(17)	1.390(8)	C(17)-C(18)	1.388(8)
C(17)-C(21)	1.517(8)	C(18)-C(19)	1.391(8)
C(19)-C(22)	1.504(7)	C(24)-C(25)	1.343(8)
C(26)-C(27)	1.382(8)	C(26)-C(31)	1.406(8)
C(27)-C(28)	1.384(8)	C(27)-C(32)	1.515(8)
C(28)-C(29)	1.383(9)	C(29)-C(30)	1.377(9)
C(29)-C(33)	1.538(8)	C(30)-C(31)	1.382(8)
C(31)-C(34)	1.496(8)	C(35)-C(36)	1.397(8)
C(35)-C(40)	1.399(8)	C(36)-C(37)	1.396(8)
C(36)-C(41)	1.504(8)	C(37)-C(38)	1.363(8)
C(38)-C(39)	1.374(9)	C(38)-C(42)	1.517(8)
C(39)-C(40)	1.384(8)	C(40)-C(43)	1.515(8)
C(44)-C(49)	1.405(8)	C(44)-C(45)	1.410(8)
C(44)-C(50)	1.434(8)	C(45)-C(46)	1.379(9)
C(46)-C(47)	1.380(9)	C(47)-C(48)	1.395(9)
C(48)-C(49)	1.376(9)	C(50)-C(51)	1.213(8)

Bond angles (°) for $Ru(IMes)_2(CO)(C{\equiv}CPh)H$

H(1)-Ru(1)-C(1)	93(2)	H(1)-Ru(1)-C(23)	104(2)
C(1)-Ru(1)-C(23)	93.0(2)	H(1)-Ru(1)-C(2)	75(2)
C(1)-Ru(1)-C(2)	88.8(2)	C(23)-Ru(1)-C(2)	177.9(2)
H(1)-Ru(1)-C(51)	87(2)	C(1)-Ru(1)-C(51)	179.5(3)
C(23)-Ru(1)-C(51)	87.4(2)	C(2)-Ru(1)-C(51)	90.8(2)
C(2)-N(1)-C(3)	112.2(5)	C(2)-N(1)-C(5)	125.9(4)
C(3)-N(1)-C(5)	121.5(4)	C(2)-N(2)-C(4)	111.6(5)
C(2)-N(2)-C(14)	124.6(4)	C(4)-N(2)-C(14)	123.7(5)
C(23)-N(3)-C(24)	112.0(5)	C(23)-N(3)-C(26)	125.1(4)
C(24)-N(3)-C(26)	122.6(5)	C(23)-N(4)-C(25)	112.7(5)
C(23)-N(4)-C(35)	124.4(4)	C(25)-N(4)-C(35)	122.9(4)
O(1)-C(1)-Ru(1)	179.1(5)	N(2)-C(2)-N(1)	102.3(4)
N(2)-C(2)-Ru(1)	129.1(4)	N(1)-C(2)-Ru(1)	128.4(4)
C(4)-C(3)-N(1)	106.9(5)	C(3)-C(4)-N(2)	107.0(5)
C(6)-C(5)-C(10)	122.5(6)	C(6)-C(5)-N(1)	118.1(5)
C(10)-C(5)-N(1)	119.4(5)	C(5)-C(6)-C(7)	118.5(6)
C(5)-C(6)-C(11)	121.6(6)	C(7)-C(6)-C(11)	120.0(6)
C(8)-C(7)-C(6)	121.3(6)	C(9)-C(8)-C(7)	118.5(6)
C(9)-C(8)-C(12)	120.6(6)	C(7)-C(8)-C(12)	120.9(6)
C(8)-C(9)-C(10)	122.5(6)	C(5)-C(10)-C(9)	116.8(6)
C(5)-C(10)-C(13)	123.1(5)	C(9)-C(10)-C(13)	120.2(6)
C(15)-C(14)-C(19)	122.4(5)	C(15)-C(14)-N(2)	118.5(6)
C(19)-C(14)-N(2)	119.1(5)	C(14)-C(15)-C(16)	117.3(6)
C(14)-C(15)-C(20)	121.6(6)	C(16)-C(15)-C(20)	121.1(6)
C(17)-C(16)-C(15)	122.6(6)	C(18)-C(17)-C(16)	117.9(6)
C(18)-C(17)-C(21)	121.3(6)	C(16)-C(17)-C(21)	120.8(6)
C(17)-C(18)-C(19)	121.9(6)	C(18)-C(19)-C(14)	117.8(6)
C(18)-C(19)-C(22)	120.9(6)	C(14)-C(19)-C(22)	121.2(5)
N(4)-C(23)-N(3)	102.4(4)	N(4)-C(23)-Ru(1)	130.6(4)
N(3)-C(23)-Ru(1)	127.0(4)	C(25)-C(24)-N(3)	106.0(5)
C(24)-C(25)-N(4)	106.9(5)	C(27)-C(26)-C(31)	122.2(5)
C(27)-C(26)-N(3)	119.8(5)	C(31)-C(26)-N(3)	118.0(5)
C(26)-C(27)-C(28)	118.2(6)	C(26)-C(27)-C(32)	120.9(5)
C(28)-C(27)-C(32)	121.0(6)	C(29)-C(28)-C(27)	121.6(6)

C(30)-C(29)-C(28)	118.5(6)	C(30)-C(29)-C(33)	120.4(7)
C(28)-C(29)-C(33)	121.1(7)	C(29)-C(30)-C(31)	122.7(6)
C(30)-C(31)-C(26)	116.8(6)	C(30)-C(31)-C(34)	121.8(6)
C(26)-C(31)-C(34)	121.3(5)	C(36)-C(35)-C(40)	121.6(6)
C(36)-C(35)-N(4)	119.9(5)	C(40)-C(35)-N(4)	118.3(5)
C(37)-C(36)-C(35)	117.0(6)	C(37)-C(36)-C(41)	120.6(6)
C(35)-C(36)-C(41)	122.3(6)	C(38)-C(37)-C(36)	122.8(6)
C(37)-C(38)-C(39)	118.6(6)	C(37)-C(38)-C(42)	121.3(6)
C(39)-C(38)-C(42)	120.1(6)	C(38)-C(39)-C(40)	122.2(6)
C(39)-C(40)-C(35)	117.8(6)	C(39)-C(40)-C(43)	121.7(6)
C(35)-C(40)-C(43)	120.5(6)	C(49)-C(44)-C(45)	117.0(6)
C(49)-C(44)-C(50)	123.4(6)	C(45)-C(44)-C(50)	119.6(6)
C(46)-C(45)-C(44)	120.7(6)	C(45)-C(46)-C(47)	121.0(7)
C(46)-C(47)-C(48)	119.8(7)	C(49)-C(48)-C(47)	119.2(7)
C(48)-C(49)-C(44)	122.4(7)	C(51)-C(50)-C(44)	176.9(7)
C(50)-C(51)-Ru(1)	178.1(5)		

Appendix 5. crystallographic data, bond lengths and angles for $Ru(IMes)_2(CO)(C{\equiv}CPh)_2$ (14)

Identification code	k04mkw12
Empirical formula	$C_{59}H_{58}N_4ORu$
Formula weight	940.16
Temperature	150(2) K
Wavelength	0.71073 Å
Crystal system	Monoclinic
Space group	C2/c
Unit cell dimensions	a = 12.8750(4)Å α = 90°
	b = 20.1040(6)Å β = 106.111(1)°
	c = 19.8520(7)Å γ = 90°
Volume	4936.7(3) $Å^3$
Z	4
Density (calculated)	1.265 Mg/m^3
Absorption coefficient	0.362 mm^{-1}
F(000)	1968
Crystal size	0.20 x 0.12 x 0.12 mm
Theta range for data collection	3.75 to 27.45°
Index ranges	-16<=h<=16; -25<=k<=25; -25<=l<=25
Reflections collected	34711
Independent reflections	5555 [R(int) = 0.0491]
Reflections observed (>2σ)	4872
Data Completeness	0.981
Absorption correction	Semi-empirical from equivalents
Max. and min. transmission	0.95 and 0.84
Refinement method	Full-matrix least-squares on F^2
Data / restraints / parameters	5555 / 0 / 302
Goodness-of-fit on F^2	1.148
Final R indices [I>2σ(I)]	$R^1 = 0.0508$ $wR_2 = 0.1154$
R indices (all data)	$R^1 = 0.0615$ $wR_2 = 0.1211$
Largest diff. peak and hole	1.953 and -1.210 $eÅ^{-3}$

Bond lengths (Å) for $Ru(IMes)_2(CO)(C{\equiv}CPh)_2$

Ru(1)-C(1)	1.803(5)	Ru(1)-C(23)#1	2.047(3)
Ru(1)-C(23)	2.047(3)	Ru(1)-C(2)	2.094(3)
Ru(1)-C(2)#1	2.094(3)	O(1)-C(1)	1.163(6)
N(1)-C(2)	1.363(3)	N(1)-C(3)	1.385(4)
N(1)-C(5)	1.447(4)	N(2)-C(2)	1.373(3)
N(2)-C(4)	1.393(4)	N(2)-C(14)	1.442(4)
C(3)-C(4)	1.337(5)	C(5)-C(10)	1.396(4)
C(5)-C(6)	1.398(4)	C(6)-C(7)	1.392(5)
C(6)-C(11)	1.499(5)	C(7)-C(8)	1.385(6)
C(8)-C(9)	1.374(6)	C(8)-C(12)	1.521(5)
C(9)-C(10)	1.397(5)	C(10)-C(13)	1.503(5)
C(14)-C(15)	1.390(4)	C(14)-C(19)	1.395(4)
C(15)-C(16)	1.391(4)	C(15)-C(20)	1.509(5)
C(16)-C(17)	1.388(5)	C(17)-C(18)	1.387(5)
C(17)-C(21)	1.511(4)	C(18)-C(19)	1.390(4)
C(19)-C(22)	1.508(4)	C(23)-C(24)	1.219(4)
C(24)-C(25)	1.446(4)	C(25)-C(30)	1.385(5)
C(25)-C(26)	1.392(4)	C(26)-C(27)	1.396(4)
C(27)-C(28)	1.364(6)	C(28)-C(29)	1.404(6)
C(29)-C(30)	1.379(5)		

Bond angles (°) for Ru(IMes)$_2$(CO)(C≡CPh)$_2$

C(1)-Ru(1)-C(23)#1	92.47(8)	C(1)-Ru(1)-C(23)	92.47(8)
C(23)#1-Ru(1)-C(23)	175.06(17)	C(1)-Ru(1)-C(2)	93.95(7)
C(23)#1-Ru(1)-C(2)	86.12(11)	C(23)-Ru(1)-C(2)	93.54(11)
C(1)-Ru(1)-C(2)#1	93.95(7)	C(23)#1-Ru(1)-C(2)#1	93.54(11)
C(23)-Ru(1)-C(2)#1	86.12(11)	C(2)-Ru(1)-C(2)#1	172.10(14)
C(2)-N(1)-C(3)	112.5(2)	C(2)-N(1)-C(5)	127.1(2)
C(3)-N(1)-C(5)	120.1(2)	C(2)-N(2)-C(4)	111.9(2)
C(2)-N(2)-C(14)	127.1(2)	C(4)-N(2)-C(14)	120.6(2)
O(1)-C(1)-Ru(1)	180.0	N(1)-C(2)-N(2)	102.4(2)
N(1)-C(2)-Ru(1)	126.62(19)	N(2)-C(2)-Ru(1)	130.65(19)
C(4)-C(3)-N(1)	106.7(3)	C(3)-C(4)-N(2)	106.5(3)
C(10)-C(5)-C(6)	122.1(3)	C(10)-C(5)-N(1)	119.3(3)
C(6)-C(5)-N(1)	117.8(3)	C(7)-C(6)-C(5)	117.6(3)
C(7)-C(6)-C(11)	121.1(3)	C(5)-C(6)-C(11)	121.1(3)
C(8)-C(7)-C(6)	122.0(4)	C(9)-C(8)-C(7)	118.5(3)
C(9)-C(8)-C(12)	120.8(4)	C(7)-C(8)-C(12)	120.6(4)
C(8)-C(9)-C(10)	122.5(4)	C(5)-C(10)-C(9)	117.3(3)
C(5)-C(10)-C(13)	122.1(3)	C(9)-C(10)-C(13)	120.6(3)
C(15)-C(14)-C(19)	122.5(3)	C(15)-C(14)-N(2)	119.7(3)
C(19)-C(14)-N(2)	117.8(3)	C(14)-C(15)-C(16)	117.2(3)
C(14)-C(15)-C(20)	121.5(3)	C(16)-C(15)-C(20)	121.3(3)
C(17)-C(16)-C(15)	122.3(3)	C(18)-C(17)-C(16)	118.4(3)
C(18)-C(17)-C(21)	120.4(3)	C(16)-C(17)-C(21)	121.1(3)
C(17)-C(18)-C(19)	121.6(3)	C(18)-C(19)-C(14)	117.8(3)
C(18)-C(19)-C(22)	121.8(3)	C(14)-C(19)-C(22)	120.4(3)
C(24)-C(23)-Ru(1)	175.0(3)	C(23)-C(24)-C(25)	177.6(3)
C(30)-C(25)-C(26)	117.4(3)	C(30)-C(25)-C(24)	122.3(3)
C(26)-C(25)-C(24)	120.2(3)	C(25)-C(26)-C(27)	120.8(3)
C(28)-C(27)-C(26)	120.7(3)	C(27)-C(28)-C(29)	119.6(3)
C(30)-C(29)-C(28)	118.9(3)	C(29)-C(30)-C(25)	122.6(3)

Appendix 6. crystallographic data, bond lengths and angles for $Ru(IMes)_2(CO)(Cl)(HC{=}CHPh)$ (15)

Identification code	k07mkw16
Empirical formula	C60 H76 Cl N4 O Ru
Formula weight	1005.77
Temperature	150(2) K
Wavelength	0. 71073 Å
Crystal system	Triclinic
Space group	P-1
Unit cell dimensions	a = 11.2760(2)Å α = 87.782(1)°
	b = 12.4440(2)Å β = 88.450(1)°
	c = 19.4100(3)Å γ = 89.476(1)°
Volume	2720.46(8) $Å^3$
Z	2
Density (calculated)	1.228 Mg/m^3
Absorption coefficient	0.380 mm^{-1}
F(000)	1066
Crystal size	0.12 x 0.10 x 0.10 mm
Theta range for data collection	3.62 to 27.47°
Index ranges	-14<=h<=14; -15<=k<=16; -25<=l<=25
Reflections collected	38604
Independent reflections	12354 [R(int) = 0.0382]
Reflections observed (>2σ)	10679
Data Completeness	0.989
Absorption correction	Semi-empirical from equivalents
Max. and min. transmission	0.96 and 0.91
Refinement method	Full-matrix least-squares on F^2
Data / restraints / parameters	12354 / 0 / 632
Goodness-of-fit on F^2	1.064
Final R indices [I>2σ(I)]	R1 = 0.0408 wR2 = 0.1011
R indices (all data)	R1 = 0.0506 wR2 = 0.1086
Largest diff. peak and hole	1.135 and -0.709 $eÅ^{-3}$

Bond lengths (Å) for $Ru(IMes)_2(CO)(Cl)(HC{=}CHPh)$

Ru(1)-C(1)	1.864(3)	C(26)-C(27)	1.389(3)
Ru(1)-C(8)	2.011(2)	C(26)-C(31)	1.504(3)
Ru(1)-C(34)	2.117(2)	C(27)-C(28)	1.391(4)
Ru(1)-C(2)	2.119(2)	C(28)-C(29)	1.392(4)
Ru(1)-Cl(1)	2.4128(6)	C(28)-C(32)	1.508(4)
O(1)-C(1)	1.096(3)	C(29)-C(30)	1.395(4)
N(1)-C(2)	1.366(3)	C(30)-C(33)	1.506(4)
N(1)-C(3)	1.381(3)	C(35)-C(36)	1.334(4)
N(1)-C(16)	1.444(3)	C(37)-C(42)	1.390(3)
N(2)-C(2)	1.364(3)	C(37)-C(38)	1.396(3)
N(2)-C(4)	1.387(3)	C(38)-C(39)	1.393(4)
N(2)-C(25)	1.448(3)	C(38)-C(43)	1.505(4)
N(3)-C(34)	1.365(3)	C(39)-C(40)	1.397(4)
N(3)-C(35)	1.396(3)	C(40)-C(41)	1.383(4)
N(3)-C(37)	1.450(3)	C(40)-C(44)	1.508(4)
N(4)-C(34)	1.372(3)	C(41)-C(42)	1.401(3)
N(4)-C(36)	1.391(3)	C(42)-C(45)	1.503(4)
N(4)-C(46)	1.439(3)	C(46)-C(51)	1.394(3)
C(3)-C(4)	1.345(4)	C(46)-C(47)	1.396(3)
C(8)-C(9)	1.333(3)	C(47)-C(48)	1.396(3)
C(9)-C(10)	1.474(3)	C(47)-C(52)	1.503(4)
C(10)-C(15)	1.377(4)	C(48)-C(49)	1.385(4)
C(10)-C(11)	1.388(4)	C(49)-C(50)	1.387(4)
C(11)-C(12)	1.379(4)	C(49)-C(53)	1.514(4)
C(12)-C(13)	1.379(5)	C(50)-C(51)	1.392(4)
C(13)-C(14)	1.389(5)	C(51)-C(54)	1.510(4)
C(14)-C(15)	1.391(4)	C(55)-C(56)	1.593(14)
C(16)-C(21)	1.394(4)	C(56)-C(57)	1.467(13)
C(16)-C(17)	1.405(4)	C(57)-C(58)	1.445(13)
C(17)-C(18)	1.402(5)	C(58)-C(59)	1.563(13)
C(17)-C(22)	1.500(5)	C(59)-C(60)	1.433(15)
C(18)-C(19)	1.373(6)	C(61)-C(62)#1	1.200(14)
C(19)-C(20)	1.386(6)	C(61)-C(62)	1.200(14)
C(19)-C(23)	1.521(5)	C(61)-C(62A)	1.561(13)

C(20)-C(21)	1.400(4)	C(61)-C(62A)#1	1.561(13)
C(21)-C(24)	1.498(5)	C(62)-C(63)	1.575(15)
C(25)-C(30)	1.391(4)	C(63)-C(62A)	1.250(15)
C(25)-C(26)	1.393(3)	C(63)-C(64)	1.553(15)

Bond angles (°) for $Ru(IMes)_2(CO)(Cl)(HC{=}CHPh)$

C(1)-Ru(1)-C(8)	87.11(10)	C(25)-C(26)-C(31)	121.5(2)
C(1)-Ru(1)-C(34)	93.80(9)	C(26)-C(27)-C(28)	121.8(2)
C(8)-Ru(1)-C(34)	92.02(9)	C(27)-C(28)-C(29)	118.4(2)
C(1)-Ru(1)-C(2)	90.37(9)	C(27)-C(28)-C(32)	120.1(3)
C(8)-Ru(1)-C(2)	96.40(9)	C(29)-C(28)-C(32)	121.5(3)
C(34)-Ru(1)-C(2)	170.78(9)	C(28)-C(29)-C(30)	122.0(3)
C(1)-Ru(1)-Cl(1)	169.98(7)	C(25)-C(30)-C(29)	117.3(2)
C(8)-Ru(1)-Cl(1)	102.81(7)	C(25)-C(30)-C(33)	121.5(3)
C(34)-Ru(1)-Cl(1)	87.27(6)	C(29)-C(30)-C(33)	121.2(3)
C(2)-Ru(1)-Cl(1)	87.22(6)	N(3)-C(34)-N(4)	102.85(17)
C(2)-N(1)-C(3)	112.5(2)	N(3)-C(34)-Ru(1)	133.50(16)
C(2)-N(1)-C(16)	129.90(19)	N(4)-C(34)-Ru(1)	123.04(15)
C(3)-N(1)-C(16)	117.6(2)	C(36)-C(35)-N(3)	107.0(2)
C(2)-N(2)-C(4)	112.0(2)	C(35)-C(36)-N(4)	106.6(2)
C(2)-N(2)-C(25)	129.71(18)	C(42)-C(37)-C(38)	122.7(2)
C(4)-N(2)-C(25)	117.8(2)	C(42)-C(37)-N(3)	119.7(2)
C(34)-N(3)-C(35)	111.62(19)	C(38)-C(37)-N(3)	117.1(2)
C(34)-N(3)-C(37)	129.23(18)	C(39)-C(38)-C(37)	117.6(2)
C(35)-N(3)-C(37)	118.70(18)	C(39)-C(38)-C(43)	120.2(2)
C(34)-N(4)-C(36)	111.90(19)	C(37)-C(38)-C(43)	122.2(2)
C(34)-N(4)-C(46)	126.87(18)	C(38)-C(39)-C(40)	121.6(3)
C(36)-N(4)-C(46)	120.76(19)	C(41)-C(40)-C(39)	118.6(2)
O(1)-C(1)-Ru(1)	176.9(2)	C(41)-C(40)-C(44)	121.6(3)
N(2)-C(2)-N(1)	102.54(18)	C(39)-C(40)-C(44)	119.8(3)
N(2)-C(2)-Ru(1)	133.12(16)	C(40)-C(41)-C(42)	122.1(2)

N(1)-C(2)-Ru(1)	124.31(16)	C(37)-C(42)-C(41)	117.2(2)
C(4)-C(3)-N(1)	106.2(2)	C(37)-C(42)-C(45)	123.0(2)
C(3)-C(4)-N(2)	106.7(2)	C(41)-C(42)-C(45)	119.6(2)
C(9)-C(8)-Ru(1)	133.90(18)	C(51)-C(46)-C(47)	122.6(2)
C(8)-C(9)-C(10)	126.6(2)	C(51)-C(46)-N(4)	117.5(2)
C(15)-C(10)-C(11)	116.4(2)	C(47)-C(46)-N(4)	119.6(2)
C(15)-C(10)-C(9)	120.1(2)	C(46)-C(47)-C(48)	117.0(2)
C(11)-C(10)-C(9)	123.5(2)	C(46)-C(47)-C(52)	121.6(2)
C(12)-C(11)-C(10)	121.9(3)	C(48)-C(47)-C(52)	121.4(2)
C(13)-C(12)-C(11)	120.6(3)	C(49)-C(48)-C(47)	122.2(3)
C(12)-C(13)-C(14)	119.0(3)	C(48)-C(49)-C(50)	118.6(2)
C(13)-C(14)-C(15)	118.9(3)	C(48)-C(49)-C(53)	121.0(3)
C(10)-C(15)-C(14)	123.1(3)	C(50)-C(49)-C(53)	120.4(3)
C(21)-C(16)-C(17)	122.7(3)	C(49)-C(50)-C(51)	121.7(3)
C(21)-C(16)-N(1)	118.9(2)	C(50)-C(51)-C(46)	117.8(2)
C(17)-C(16)-N(1)	117.6(2)	C(50)-C(51)-C(54)	120.9(2)
C(18)-C(17)-C(16)	116.7(3)	C(46)-C(51)-C(54)	121.3(2)
C(18)-C(17)-C(22)	120.7(3)	C(57)-C(56)-C(55)	108.7(8)
C(16)-C(17)-C(22)	122.5(3)	C(58)-C(57)-C(56)	108.0(8)
C(19)-C(18)-C(17)	122.6(3)	C(57)-C(58)-C(59)	110.7(7)
C(18)-C(19)-C(20)	118.7(3)	C(60)-C(59)-C(58)	119.9(8)
C(18)-C(19)-C(23)	121.2(4)	C(62)#1-C(61)-C(62)	180.0(11)
C(20)-C(19)-C(23)	120.0(4)	C(62)#1-C(61)-C(62A)	137.6(6)
C(19)-C(20)-C(21)	122.1(3)	C(62)-C(61)-C(62A)	42.4(6)
C(16)-C(21)-C(20)	117.2(3)	C(62A)-C(63)-C(64)	121.9(8)
C(16)-C(21)-C(24)	122.4(3)	C(62A)-C(63)-C(62)	41.8(6)
C(20)-C(21)-C(24)	120.4(3)	C(64)-C(63)-C(62)	89.0(7)
C(30)-C(25)-C(26)	122.7(2)	C(63)-C(62A)-C(61)	135.9(9)
C(30)-C(25)-N(2)	118.8(2)	C(62)#1-C(61)-C(62A)#1	42.4(6)
C(26)-C(25)-N(2)	117.9(2)	C(62)-C(61)-C(62A)#1	137.6(6)
C(27)-C(26)-C(25)	117.8(2)	C(62A)-C(61)-C(62A)#1	180.000(3)
C(27)-C(26)-C(31)	120.7(2)	C(61)-C(62)-C(63)	139.8(10)

Appendix 7. crystallographic data, bond lengths and angles for $Ru(IMes)_2(CO)(C{\equiv}CSiMe_3)H$ (16)

Identification code	k05mkw19
Empirical formula	C60 H70 N4 O Ru Si
Formula weight	992.36
Temperature	150(2) K
Wavelength	0.71073 Å
Crystal system	Triclinic
Space group	P-1
Unit cell dimensions	a = 11.1550(1)Å α = 75.184(1)°
	b = 13.5620(1)Å β = 87.834(1)°
	c = 18.6520(2)Å γ = 83.729(1)°
Volume	2711.47(4) $Å^3$
Z	2
Density (calculated)	1.215 Mg/m^3
Absorption coefficient	0.354 mm^{-1}
F(000)	1048
Crystal size	0.30 x 0.25 x 0.20 mm
Theta range for data collection	3.58 to 29.96°
Index ranges	-15<=h<=15; -19<=k<=19; -26<=l<=26
Reflections collected	51275
Independent reflections	15607 [R(int) = 0.0357]
Reflections observed (>2σ)	14007
Data Completeness	0.991
Absorption correction	Semi-empirical from equivalents
Max. and min. transmission	0.93 and 0.90
Refinement method	Full-matrix least-squares on F^2
Data / restraints / parameters	15607 / 1 / 620
Goodness-of-fit on F^2	1.036
Final R indices [I>2σ(I)]	$R^1 = 0.0321$ $wR_2 = 0.0766$
R indices (all data)	$R^1 = 0.0401$ $wR_2 = 0.0804$
Largest diff. peak and hole	0.560 and -0.542 $eÅ^{-3}$

Bond lengths (Å) for $Ru(IMes)_2(CO)(C{\equiv}CSiMe_3)H$

Ru(1)-C(1)	1.8612(16)	Ru(1)-C(23)	2.0725(13)
Ru(1)-C(2)	2.0740(13)	Ru(1)-C(44)	2.0874(15)
Si(1)-C(45)	1.8204(16)	Si(1)-C(46)	1.8718(17)
Si(1)-C(48)	1.8750(18)	Si(1)-C(47)	1.8762(18)
O(1)-C(1)	1.1585(19)	N(1)-C(2)	1.3701(17)
N(1)-C(3)	1.3873(17)	N(1)-C(5)	1.4407(17)
N(2)-C(2)	1.3669(17)	N(2)-C(4)	1.3910(18)
N(2)-C(14)	1.4417(17)	N(3)-C(23)	1.3659(17)
N(3)-C(24)	1.3918(18)	N(3)-C(26)	1.4430(17)
N(4)-C(23)	1.3681(17)	N(4)-C(25)	1.3916(18)
N(4)-C(35)	1.4366(17)	C(3)-C(4)	1.344(2)
C(5)-C(10)	1.394(2)	C(5)-C(6)	1.399(2)
C(6)-C(7)	1.397(2)	C(6)-C(11)	1.507(2)
C(7)-C(8)	1.388(3)	C(8)-C(9)	1.387(2)
C(8)-C(12)	1.514(2)	C(9)-C(10)	1.395(2)
C(10)-C(13)	1.502(2)	C(14)-C(19)	1.394(2)
C(14)-C(15)	1.396(2)	C(15)-C(16)	1.393(2)
C(15)-C(20)	1.505(2)	C(16)-C(17)	1.391(2)
C(17)-C(18)	1.387(2)	C(17)-C(21)	1.511(2)
C(18)-C(19)	1.397(2)	C(19)-C(22)	1.504(2)
C(24)-C(25)	1.344(2)	C(26)-C(27)	1.396(2)
C(26)-C(31)	1.396(2)	C(27)-C(28)	1.397(2)
C(27)-C(32)	1.501(2)	C(28)-C(29)	1.386(2)
C(29)-C(30)	1.388(2)	C(29)-C(33)	1.511(2)
C(30)-C(31)	1.391(2)	C(31)-C(34)	1.507(2)
C(35)-C(40)	1.398(2)	C(35)-C(36)	1.398(2)
C(36)-C(37)	1.394(2)	C(36)-C(41)	1.507(2)
C(37)-C(38)	1.384(2)	C(38)-C(39)	1.393(2)
C(38)-C(42)	1.507(2)	C(39)-C(40)	1.394(2)
C(40)-C(43)	1.507(2)	C(44)-C(45)	1.221(2)
C(49)-C(54)	1.369(3)	C(49)-C(50)	1.382(3)
C(50)-C(51)	1.382(3)	C(51)-C(52)	1.372(3)
C(52)-C(53)	1.380(3)	C(53)-C(54)	1.367(3)
C(55)-C(59)	1.362(3)	C(55)-C(60)	1.366(3)

C(56)-C(60)	1.372(4)	C(56)-C(57)	1.372(4)
C(57)-C(58)	1.372(4)	C(58)-C(59)	1.380(4)

Bond angles (°) for $Ru(IMes)_2(CO)(C{\equiv}CSiMe_3)H$

C(1)-Ru(1)-C(23)	91.92(6)	C(1)-Ru(1)-C(2)	92.05(6)
C(23)-Ru(1)-C(2)	175.99(5)	C(1)-Ru(1)-C(44)	178.59(6)
C(23)-Ru(1)-C(44)	87.32(5)	C(2)-Ru(1)-C(44)	88.70(5)
C(45)-Si(1)-C(46)	108.81(8)	C(45)-Si(1)-C(48)	112.27(8)
C(46)-Si(1)-C(48)	107.47(8)	C(45)-Si(1)-C(47)	109.67(8)
C(46)-Si(1)-C(47)	109.83(9)	C(48)-Si(1)-C(47)	108.75(9)
C(2)-N(1)-C(3)	111.87(12)	C(2)-N(1)-C(5)	125.07(11)
C(3)-N(1)-C(5)	123.06(11)	C(2)-N(2)-C(4)	111.90(11)
C(2)-N(2)-C(14)	123.89(11)	C(4)-N(2)-C(14)	123.87(12)
C(23)-N(3)-C(24)	112.04(12)	C(23)-N(3)-C(26)	125.40(11)
C(24)-N(3)-C(26)	122.26(12)	C(23)-N(4)-C(25)	111.91(11)
C(23)-N(4)-C(35)	125.59(11)	C(25)-N(4)-C(35)	122.48(11)
O(1)-C(1)-Ru(1)	179.58(14)	N(2)-C(2)-N(1)	102.90(11)
N(2)-C(2)-Ru(1)	128.43(9)	N(1)-C(2)-Ru(1)	128.67(10)
C(4)-C(3)-N(1)	106.75(12)	C(3)-C(4)-N(2)	106.57(12)
C(10)-C(5)-C(6)	122.13(13)	C(10)-C(5)-N(1)	119.61(13)
C(6)-C(5)-N(1)	118.19(13)	C(7)-C(6)-C(5)	117.62(15)
C(7)-C(6)-C(11)	121.64(14)	C(5)-C(6)-C(11)	120.74(14)
C(8)-C(7)-C(6)	121.91(15)	C(9)-C(8)-C(7)	118.50(14)
C(9)-C(8)-C(12)	120.18(17)	C(7)-C(8)-C(12)	121.30(16)
C(8)-C(9)-C(10)	122.00(15)	C(5)-C(10)-C(9)	117.77(14)
C(5)-C(10)-C(13)	122.55(14)	C(9)-C(10)-C(13)	119.68(15)
C(19)-C(14)-C(15)	122.26(13)	C(19)-C(14)-N(2)	119.71(13)
C(15)-C(14)-N(2)	118.02(13)	C(16)-C(15)-C(14)	117.98(14)
C(16)-C(15)-C(20)	120.71(14)	C(14)-C(15)-C(20)	121.30(14)
C(17)-C(16)-C(15)	121.76(15)	C(18)-C(17)-C(16)	118.25(14)
C(18)-C(17)-C(21)	121.93(17)	C(16)-C(17)-C(21)	119.82(16)
C(17)-C(18)-C(19)	122.39(15)	C(14)-C(19)-C(18)	117.31(14)

C(14)-C(19)-C(22)	121.02(14)	C(18)-C(19)-C(22)	121.66(14)
N(3)-C(23)-N(4)	102.88(11)	N(3)-C(23)-Ru(1)	127.64(10)
N(4)-C(23)-Ru(1)	129.48(10)	C(25)-C(24)-N(3)	106.53(13)
C(24)-C(25)-N(4)	106.64(12)	C(27)-C(26)-C(31)	122.18(13)
C(27)-C(26)-N(3)	119.57(13)	C(31)-C(26)-N(3)	118.17(13)
C(26)-C(27)-C(28)	117.47(13)	C(26)-C(27)-C(32)	122.63(13)
C(28)-C(27)-C(32)	119.90(14)	C(29)-C(28)-C(27)	122.08(14)
C(28)-C(29)-C(30)	118.45(14)	C(28)-C(29)-C(33)	120.75(16)
C(30)-C(29)-C(33)	120.80(16)	C(29)-C(30)-C(31)	121.96(15)
C(30)-C(31)-C(26)	117.84(14)	C(30)-C(31)-C(34)	120.60(15)
C(26)-C(31)-C(34)	121.56(14)	C(40)-C(35)-C(36)	122.00(13)
C(40)-C(35)-N(4)	118.58(13)	C(36)-C(35)-N(4)	119.34(13)
C(37)-C(36)-C(35)	117.73(14)	C(37)-C(36)-C(41)	119.54(14)
C(35)-C(36)-C(41)	122.70(14)	C(38)-C(37)-C(36)	122.07(14)
C(37)-C(38)-C(39)	118.59(14)	C(37)-C(38)-C(42)	120.14(15)
C(39)-C(38)-C(42)	121.25(16)	C(38)-C(39)-C(40)	121.68(14)
C(39)-C(40)-C(35)	117.92(14)	C(39)-C(40)-C(43)	120.78(14)
C(35)-C(40)-C(43)	121.30(13)	C(45)-C(44)-Ru(1)	174.97(13)
C(44)-C(45)-Si(1)	170.96(14)	C(54)-C(49)-C(50)	120.2(2)
C(49)-C(50)-C(51)	119.73(19)	C(52)-C(51)-C(50)	119.58(19)
C(51)-C(52)-C(53)	120.3(2)	C(54)-C(53)-C(52)	120.0(2)
C(53)-C(54)-C(49)	120.20(19)	C(59)-C(55)-C(60)	119.8(2)
C(60)-C(56)-C(57)	120.2(2)	C(56)-C(57)-C(58)	119.6(3)
C(57)-C(58)-C(59)	119.7(2)	C(55)-C(59)-C(58)	120.4(2)
C(55)-C(60)-C(56)	120.3(2)		

Appendix 8. crystallographic data, bond lengths and angles for $Ru(IMes)_2(CO)_2(C{\equiv}CPh)H$ (17)

Identification code	k05mkw20
Empirical formula	C61 H63 N4 O2 Ru
Formula weight	985.22
Temperature	150(2) K
Wavelength	0.71073 Å
Crystal system	Triclinic
Space group	P-1
Unit cell dimensions	a = 13.7940(1)Å α = 93.500(1)°
	b = 18.6470(2)Å β = 106.902(1)°
	c = 21.5710(2)Å γ = 96.427(1)°
Volume	5249.76(8) $Å^3$
Z	4
Density (calculated)	1.247 Mg/m^3
Absorption coefficient	0.345 mm^{-1}
F(000)	2068
Crystal size	0.35 x 0.30 x 0.30 mm
Theta range for data collection	3.53 to 30.10°
Index ranges	-19<=h<=19; -26<=k<=26; -30<=l<=30
Reflections collected	101358
Independent reflections	30580 [R(int) = 0.0558]
Reflections observed (>2σ)	21132
Data Completeness	0.990
Absorption correction	Semi-empirical from equivalents
Max. and min. transmission	0.91 and 0.86
Refinement method	Full-matrix least-squares on F^2
Data / restraints / parameters	30580 / 0 / 1257
Goodness-of-fit on F^2	1.019
Final R indices [I>2σ(I)]	$R^1 = 0.0481$ $wR_2 = 0.1060$
R indices (all data)	$R^1 = 0.0855$ $wR_2 = 0.1233$
Largest diff. peak and hole	1.119 and -0.785 $eÅ^{-3}$

bond lengths (Å) for $Ru(IMes)_2(CO)_2(C{\equiv}CPh)H$

Ru(1)-C(2)	1.883(2)	Ru(1)-C(1)	1.961(2)
Ru(1)-C(47)	2.085(2)	Ru(1)-C(26)	2.109(2)
Ru(1)-C(5)	2.109(2)	Ru(2)-C(3)	1.870(3)
Ru(2)-C(4)	1.962(3)	Ru(2)-C(97)	2.083(3)
Ru(2)-C(76)	2.100(2)	Ru(2)-C(55)	2.117(2)
O(1)-C(1)	1.138(3)	O(2)-C(2)	1.150(3)
O(3)-C(3)	1.139(3)	O(4)-C(4)	1.131(3)
N(1)-C(5)	1.371(3)	N(1)-C(6)	1.390(3)
N(1)-C(8)	1.444(3)	N(2)-C(5)	1.369(3)
N(2)-C(7)	1.391(3)	N(2)-C(17)	1.439(3)
N(3)-C(26)	1.370(3)	N(3)-C(27)	1.386(3)
N(3)-C(29)	1.443(3)	N(4)-C(26)	1.371(3)
N(4)-C(28)	1.390(3)	N(4)-C(38)	1.445(3)
N(5)-C(55)	1.374(3)	N(5)-C(56)	1.389(3)
N(5)-C(58)	1.442(3)	N(6)-C(55)	1.371(3)
N(6)-C(57)	1.392(3)	N(6)-C(67)	1.445(3)
N(7)-C(76)	1.374(3)	N(7)-C(77)	1.383(3)
N(7)-C(79)	1.449(3)	N(8)-C(76)	1.372(3)
N(8)-C(78)	1.378(3)	N(8)-C(88)	1.444(3)
C(6)-C(7)	1.332(3)	C(8)-C(9)	1.390(4)
C(8)-C(13)	1.395(3)	C(9)-C(10)	1.390(4)
C(9)-C(14)	1.508(4)	C(10)-C(11)	1.395(4)
C(11)-C(12)	1.378(4)	C(11)-C(15)	1.519(4)
C(12)-C(13)	1.393(3)	C(13)-C(16)	1.500(4)
C(17)-C(18)	1.393(3)	C(17)-C(22)	1.399(3)
C(18)-C(19)	1.389(3)	C(18)-C(23)	1.504(3)
C(19)-C(20)	1.388(4)	C(20)-C(21)	1.390(4)
C(20)-C(24)	1.506(3)	C(21)-C(22)	1.390(3)
C(22)-C(25)	1.505(3)	C(27)-C(28)	1.334(3)
C(29)-C(30)	1.388(4)	C(29)-C(34)	1.392(4)
C(30)-C(31)	1.414(4)	C(30)-C(35)	1.491(5)
C(31)-C(32)	1.381(5)	C(32)-C(33)	1.368(5)
C(32)-C(36)	1.524(4)	C(33)-C(34)	1.393(4)
C(34)-C(37)	1.504(4)	C(38)-C(39)	1.390(3)

C(38)-C(43)	1.400(3)	C(39)-C(40)	1.396(3)
C(39)-C(44)	1.499(4)	C(40)-C(41)	1.385(4)
C(41)-C(42)	1.388(4)	C(41)-C(45)	1.514(4)
C(42)-C(43)	1.387(3)	C(43)-C(46)	1.504(4)
C(47)-C(48)	1.220(3)	C(48)-C(49)	1.447(3)
C(49)-C(54)	1.392(4)	C(49)-C(50)	1.397(3)
C(50)-C(51)	1.383(4)	C(51)-C(52)	1.387(4)
C(52)-C(53)	1.390(5)	C(53)-C(54)	1.385(4)
C(56)-C(57)	1.333(4)	C(58)-C(59)	1.389(4)
C(58)-C(63)	1.399(4)	C(59)-C(60)	1.388(4)
C(59)-C(64)	1.505(4)	C(60)-C(61)	1.382(4)
C(61)-C(62)	1.388(4)	C(61)-C(65)	1.514(4)
C(62)-C(63)	1.392(3)	C(63)-C(66)	1.504(4)
C(67)-C(72)	1.378(3)	C(67)-C(68)	1.407(4)
C(68)-C(69)	1.388(4)	C(68)-C(73)	1.513(4)
C(69)-C(70)	1.374(4)	C(70)-C(71)	1.374(4)
C(70)-C(74)	1.529(4)	C(71)-C(72)	1.428(4)
C(72)-C(75)	1.486(4)	C(77)-C(78)	1.334(4)
C(79)-C(80)	1.378(4)	C(79)-C(84)	1.401(4)
C(80)-C(81)	1.415(4)	C(80)-C(85)	1.506(5)
C(81)-C(82)	1.374(5)	C(82)-C(83)	1.364(5)
C(82)-C(86)	1.528(4)	C(83)-C(84)	1.397(4)
C(84)-C(87)	1.489(4)	C(88)-C(93)	1.385(4)
C(88)-C(89)	1.399(4)	C(89)-C(90)	1.395(4)
C(89)-C(94)	1.505(4)	C(90)-C(91)	1.393(4)
C(91)-C(92)	1.376(4)	C(91)-C(95)	1.519(4)
C(92)-C(93)	1.398(3)	C(93)-C(96)	1.503(4)
C(97)-C(98)	1.218(3)	C(98)-C(99)	1.435(3)
C(99)-C(100)	1.394(3)	C(99)-C(104)	1.405(3)
C(100)-C(101)	1.380(4)	C(101)-C(102)	1.383(4)
C(102)-C(103)	1.392(4)	C(103)-C(104)	1.376(4)
C(1S)-C(2S)	1.314(9)	C(1S)-C(6S)	1.326(8)
C(2S)-C(3S)	1.366(11)	C(3S)-C(4S)	1.332(11)
C(4S)-C(5S)	1.307(10)	C(5S)-C(6S)	1.345(9)
C(7S)-C(8S)	1.306(6)	C(7S)-C(12S)	1.367(7)

C(8S)-C(9S)	1.307(5)	C(9S)-C(10S)	1.321(5)
C(10S)-C(11S)	1.370(6)	C(11S)-C(12S)	1.446(8)
C(13S)-C(14S)	1.355(5)	C(13S)-C(18S)	1.378(5)
C(14S)-C(15S)	1.368(5)	C(15S)-C(16S)	1.358(5)
C(16S)-C(17S)	1.392(6)	C(17S)-C(18S)	1.368(6)

bond angles (°) for $Ru(IMes)_2(CO)_2(C{\equiv}CPh)H$

C(2)-Ru(1)-C(1)	97.31(10)	C(2)-Ru(1)-C(47)	174.11(10)
C(1)-Ru(1)-C(47)	88.49(9)	C(2)-Ru(1)-C(26)	90.97(10)
C(1)-Ru(1)-C(26)	95.42(9)	C(47)-Ru(1)-C(26)	89.52(9)
C(2)-Ru(1)-C(5)	92.05(10)	C(1)-Ru(1)-C(5)	96.81(8)
C(47)-Ru(1)-C(5)	86.20(9)	C(26)-Ru(1)-C(5)	166.93(8)
C(3)-Ru(2)-C(4)	95.46(13)	C(3)-Ru(2)-C(97)	172.82(12)
C(4)-Ru(2)-C(97)	91.71(10)	C(3)-Ru(2)-C(76)	93.25(11)
C(4)-Ru(2)-C(76)	95.90(9)	C(97)-Ru(2)-C(76)	85.76(9)
C(3)-Ru(2)-C(55)	92.26(11)	C(4)-Ru(2)-C(55)	95.89(9)
C(97)-Ru(2)-C(55)	87.23(9)	C(76)-Ru(2)-C(55)	166.45(9)
C(5)-N(1)-C(6)	111.93(19)	C(5)-N(1)-C(8)	129.60(19)
C(6)-N(1)-C(8)	118.33(19)	C(5)-N(2)-C(7)	112.06(18)
C(5)-N(2)-C(17)	127.00(18)	C(7)-N(2)-C(17)	120.55(18)
C(26)-N(3)-C(27)	112.30(19)	C(26)-N(3)-C(29)	128.11(19)
C(27)-N(3)-C(29)	119.51(19)	C(26)-N(4)-C(28)	112.22(19)
C(26)-N(4)-C(38)	129.01(18)	C(28)-N(4)-C(38)	118.63(18)
C(55)-N(5)-C(56)	112.2(2)	C(55)-N(5)-C(58)	126.9(2)
C(56)-N(5)-C(58)	120.3(2)	C(55)-N(6)-C(57)	111.9(2)
C(55)-N(6)-C(67)	128.3(2)	C(57)-N(6)-C(67)	119.43(19)
C(76)-N(7)-C(77)	112.1(2)	C(76)-N(7)-C(79)	129.6(2)
C(77)-N(7)-C(79)	118.3(2)	C(76)-N(8)-C(78)	112.2(2)
C(76)-N(8)-C(88)	127.7(2)	C(78)-N(8)-C(88)	120.0(2)
O(1)-C(1)-Ru(1)	178.0(2)	O(2)-C(2)-Ru(1)	176.1(2)
O(3)-C(3)-Ru(2)	179.6(3)	O(4)-C(4)-Ru(2)	177.9(3)
N(2)-C(5)-N(1)	102.41(18)	N(2)-C(5)-Ru(1)	129.80(15)

N(1)-C(5)-Ru(1)	127.50(15)	C(7)-C(6)-N(1)	106.9(2)
C(6)-C(7)-N(2)	106.7(2)	C(9)-C(8)-C(13)	122.7(2)
C(9)-C(8)-N(1)	118.0(2)	C(13)-C(8)-N(1)	118.5(2)
C(10)-C(9)-C(8)	117.4(3)	C(10)-C(9)-C(14)	120.8(3)
C(8)-C(9)-C(14)	121.7(2)	C(9)-C(10)-C(11)	122.3(3)
C(12)-C(11)-C(10)	117.8(2)	C(12)-C(11)-C(15)	121.2(3)
C(10)-C(11)-C(15)	121.0(3)	C(11)-C(12)-C(13)	122.8(3)
C(12)-C(13)-C(8)	117.0(3)	C(12)-C(13)-C(16)	122.0(2)
C(8)-C(13)-C(16)	121.0(2)	C(18)-C(17)-C(22)	122.4(2)
C(18)-C(17)-N(2)	118.8(2)	C(22)-C(17)-N(2)	118.7(2)
C(19)-C(18)-C(17)	117.9(2)	C(19)-C(18)-C(23)	121.2(2)
C(17)-C(18)-C(23)	120.9(2)	C(20)-C(19)-C(18)	121.8(2)
C(19)-C(20)-C(21)	118.3(2)	C(19)-C(20)-C(24)	121.1(2)
C(21)-C(20)-C(24)	120.6(2)	C(20)-C(21)-C(22)	122.5(2)
C(21)-C(22)-C(17)	117.0(2)	C(21)-C(22)-C(25)	120.9(2)
C(17)-C(22)-C(25)	122.1(2)	N(3)-C(26)-N(4)	102.09(18)
N(3)-C(26)-Ru(1)	130.57(16)	N(4)-C(26)-Ru(1)	127.21(15)
C(28)-C(27)-N(3)	106.9(2)	C(27)-C(28)-N(4)	106.5(2)
C(30)-C(29)-C(34)	122.5(2)	C(30)-C(29)-N(3)	118.3(3)
C(34)-C(29)-N(3)	119.0(2)	C(29)-C(30)-C(31)	117.2(3)
C(29)-C(30)-C(35)	120.8(3)	C(31)-C(30)-C(35)	122.0(3)
C(32)-C(31)-C(30)	121.5(3)	C(33)-C(32)-C(31)	118.9(3)
C(33)-C(32)-C(36)	121.2(4)	C(31)-C(32)-C(36)	119.8(4)
C(32)-C(33)-C(34)	122.4(3)	C(29)-C(34)-C(33)	117.5(3)
C(29)-C(34)-C(37)	122.1(2)	C(33)-C(34)-C(37)	120.3(3)
C(39)-C(38)-C(43)	122.4(2)	C(39)-C(38)-N(4)	119.4(2)
C(43)-C(38)-N(4)	117.9(2)	C(38)-C(39)-C(40)	117.5(2)
C(38)-C(39)-C(44)	121.2(2)	C(40)-C(39)-C(44)	121.3(2)
C(41)-C(40)-C(39)	122.2(2)	C(40)-C(41)-C(42)	118.1(2)
C(40)-C(41)-C(45)	121.4(3)	C(42)-C(41)-C(45)	120.5(3)
C(43)-C(42)-C(41)	122.4(3)	C(42)-C(43)-C(38)	117.4(2)
C(42)-C(43)-C(46)	121.3(2)	C(38)-C(43)-C(46)	121.3(2)
C(48)-C(47)-Ru(1)	177.5(2)	C(47)-C(48)-C(49)	178.8(3)
C(54)-C(49)-C(50)	117.8(2)	C(54)-C(49)-C(48)	121.6(2)
C(50)-C(49)-C(48)	120.5(2)	C(51)-C(50)-C(49)	121.3(3)

C(50)-C(51)-C(52)	120.3(3)	C(51)-C(52)-C(53)	119.0(3)
C(54)-C(53)-C(52)	120.5(3)	C(53)-C(54)-C(49)	121.0(3)
N(6)-C(55)-N(5)	102.30(19)	N(6)-C(55)-Ru(2)	127.52(16)
N(5)-C(55)-Ru(2)	130.08(16)	C(57)-C(56)-N(5)	106.6(2)
C(56)-C(57)-N(6)	107.0(2)	C(59)-C(58)-C(63)	122.7(2)
C(59)-C(58)-N(5)	119.7(2)	C(63)-C(58)-N(5)	117.5(2)
C(60)-C(59)-C(58)	117.4(2)	C(60)-C(59)-C(64)	121.4(3)
C(58)-C(59)-C(64)	121.1(2)	C(61)-C(60)-C(59)	122.0(3)
C(60)-C(61)-C(62)	118.8(2)	C(60)-C(61)-C(65)	121.3(3)
C(62)-C(61)-C(65)	119.8(3)	C(61)-C(62)-C(63)	121.7(3)
C(62)-C(63)-C(58)	117.2(2)	C(62)-C(63)-C(66)	121.5(2)
C(58)-C(63)-C(66)	121.3(2)	C(72)-C(67)-C(68)	123.6(2)
C(72)-C(67)-N(6)	119.9(2)	C(68)-C(67)-N(6)	115.9(2)
C(69)-C(68)-C(67)	116.9(3)	C(69)-C(68)-C(73)	120.7(3)
C(67)-C(68)-C(73)	122.3(3)	C(70)-C(69)-C(68)	121.9(3)
C(71)-C(70)-C(69)	120.0(3)	C(71)-C(70)-C(74)	120.0(3)
C(69)-C(70)-C(74)	120.0(3)	C(70)-C(71)-C(72)	121.2(3)
C(67)-C(72)-C(71)	116.3(3)	C(67)-C(72)-C(75)	121.4(2)
C(71)-C(72)-C(75)	122.3(2)	N(8)-C(76)-N(7)	102.05(19)
N(8)-C(76)-Ru(2)	130.35(17)	N(7)-C(76)-Ru(2)	127.54(16)
C(78)-C(77)-N(7)	106.7(2)	C(77)-C(78)-N(8)	107.0(2)
C(80)-C(79)-C(84)	122.5(2)	C(80)-C(79)-N(7)	118.3(2)
C(84)-C(79)-N(7)	118.5(2)	C(79)-C(80)-C(81)	117.2(3)
C(79)-C(80)-C(85)	121.6(3)	C(81)-C(80)-C(85)	121.1(3)
C(82)-C(81)-C(80)	121.5(3)	C(83)-C(82)-C(81)	119.3(3)
C(83)-C(82)-C(86)	120.4(3)	C(81)-C(82)-C(86)	120.3(3)
C(82)-C(83)-C(84)	122.1(3)	C(83)-C(84)-C(79)	117.3(3)
C(83)-C(84)-C(87)	120.1(3)	C(79)-C(84)-C(87)	122.6(2)
C(93)-C(88)-C(89)	122.5(2)	C(93)-C(88)-N(8)	118.6(2)
C(89)-C(88)-N(8)	118.8(2)	C(90)-C(89)-C(88)	117.1(3)
C(90)-C(89)-C(94)	121.4(3)	C(88)-C(89)-C(94)	121.5(2)
C(91)-C(90)-C(89)	121.8(3)	C(92)-C(91)-C(90)	118.9(2)
C(92)-C(91)-C(95)	120.7(3)	C(90)-C(91)-C(95)	120.3(3)
C(91)-C(92)-C(93)	121.5(3)	C(88)-C(93)-C(92)	118.0(2)
C(88)-C(93)-C(96)	121.6(2)	C(92)-C(93)-C(96)	120.4(2)

C(98)-C(97)-Ru(2)	178.9(2)	C(97)-C(98)-C(99)	178.0(3)
C(100)-C(99)-C(104)	117.7(2)	C(100)-C(99)-C(98)	121.2(2)
C(104)-C(99)-C(98)	121.1(2)	C(101)-C(100)-C(99)	121.5(2)
C(100)-C(101)-C(102)	120.2(3)	C(101)-C(102)-C(103)	119.1(3)
C(104)-C(103)-C(102)	120.8(2)	C(103)-C(104)-C(99)	120.6(2)
C(2S)-C(1S)-C(6S)	120.8(6)	C(1S)-C(2S)-C(3S)	120.3(7)
C(4S)-C(3S)-C(2S)	117.2(7)	C(5S)-C(4S)-C(3S)	122.9(7)
C(4S)-C(5S)-C(6S)	118.9(7)	C(1S)-C(6S)-C(5S)	119.8(6)
C(8S)-C(7S)-C(12S)	120.2(5)	C(9S)-C(8S)-C(7S)	122.5(4)
C(8S)-C(9S)-C(10S)	122.5(4)	C(9S)-C(10S)-C(11S)	119.3(4)
C(10S)-C(11S)-C(12S)	117.9(4)	C(7S)-C(12S)-C(11S)	117.5(4)
C(14S)-C(13S)-C(18S)	120.3(3)	C(13S)-C(14S)-C(15S)	121.0(3)
C(16S)-C(15S)-C(14S)	119.1(4)	C(15S)-C(16S)-C(17S)	120.7(4)
C(18S)-C(17S)-C(16S)	119.3(4)	C(17S)-C(18S)-C(13S)	119.5(4)

Appendix 9. crystallographic data, bond lengths and angles for $Ru(IMes)_2(CO)_2(C{\equiv}CPh)_2$ (18)

Identification code	bath159
Empirical formula	C60 H58 N4 O2 Ru
Formula weight	968.17
Temperature	150(2) K
Wavelength	0.84600 Å
Crystal system	Monoclinic
Space group	C2/c
Unit cell dimensions	a = 12.846(2)Å α = 90°
	b = 20.091(4)Å β = 105.843(3)°
	c = 20.065(5)Å γ = 90°
Volume	4981.9(17) $Å^3$
Z	4
Density (calculated)	1.291 Mg/m^3
Absorption coefficient	0.362 mm^{-1}
F(000)	2024
Crystal size	0.08 x 0.05 x 0.03 mm
Theta range for data collection	4.48 to 34.69°
Index ranges	-16<=h<=16; -25<=k<=25; -26<=l<=25
Reflections collected	18326
Independent reflections	5347 [R(int) = 0.0763]
Reflections observed (>2σ)	4077
Data Completeness	0.843
Absorption correction	Semi-empirical from equivalents
Max. and min. transmission	0.98 and 0.97
Refinement method	Full-matrix least-squares on F^2
Data / restraints / parameters	5347 / 65 / 370
Goodness-of-fit on F^2	1.030
Final R indices [I>2σ(I)]	R1 = 0.0685 wR2 = 0.1614
R indices (all data)	R1 = 0.0900 wR2 = 0.1767
Largest diff. peak and hole	1.227 and -1.013 $eÅ^{-3}$

bond lengths (Å) for $Ru(IMes)_2(CO)_2(C{\equiv}CPh)_2$

Ru(1)-C(2)	1.876(7)	Ru(1)-C(1)#1	2.008(14)
Ru(1)-C(1)	2.008(14)	Ru(1)-C(3A)#1	2.05(5)
Ru(1)-C(3A)	2.05(5)	Ru(1)-C(3)#1	2.081(17)
Ru(1)-C(3)	2.081(17)	Ru(1)-C(24)	2.135(5)
Ru(1)-C(24)#1	2.135(5)	O(1)-C(1)	1.200(15)
O(1)-C(1)#1	1.839(18)	O(1)-C(20A)	1.848(19)
O(2)-C(2)	1.144(8)	N(1)-C(4)	1.358(8)
N(1)-C(3)	1.362(18)	N(1)-C(6)	1.450(7)
N(2)-C(3)	1.344(19)	N(2)-C(5)	1.361(8)
N(2)-C(15)	1.486(13)	N(1A)-C(3A)	1.34(5)
N(1A)-C(4A)	1.39(3)	N(1A)-C(6)	1.472(18)
N(2A)-C(5A)	1.16(2)	N(2A)-C(3A)	1.34(5)
N(2A)-C(15A)	1.38(3)	C(1)-C(1)#1	1.01(3)
C(1)-O(1)#1	1.839(18)	C(4)-C(5)	1.350(8)
C(6)-C(11)	1.428(7)	C(6)-C(7)	1.433(7)
C(7)-C(8)	1.392(6)	C(7)-C(12)	1.534(7)
C(8)-C(9)	1.410(8)	C(9)-C(10)	1.408(8)
C(9)-C(13)	1.518(7)	C(10)-C(11)	1.384(7)
C(11)-C(14)	1.548(8)	C(15)-C(16)	1.416(12)
C(15)-C(20)	1.430(12)	C(16)-C(17)	1.404(12)
C(16)-C(21)	1.574(15)	C(17)-C(18)	1.392(15)
C(18)-C(19)	1.443(15)	C(18)-C(22)	1.526(11)
C(20)-C(19)	1.339(10)	C(20)-C(23)	1.582(14)
C(24)-C(25)	1.266(7)	C(25)-C(26)	1.492(7)
C(26)-C(31)	1.340(6)	C(26)-C(27)	1.407(7)
C(27)-C(28)	1.449(8)	C(28)-C(29)	1.313(8)
C(29)-C(30)	1.391(8)	C(30)-C(31)	1.440(7)
C(4A)-C(5A)	1.455(17)	C(15A)-C(16A)	1.395(5)
C(15A)-C(20A)	1.395(5)	C(16A)-C(17A)	1.392(5)
C(16A)-C(21A)	1.47(3)	C(17A)-C(18A)	1.398(5)
C(17A)-C(21A)	2.00(3)	C(18A)-C(19A)	1.402(5)
C(18A)-C(22A)	1.62(3)	C(19A)-C(20A)	1.397(5)
C(20A)-C(23A)	1.54(2)		

bond angles (°) for Ru(IMes)$_2$(CO)$_2$(C≡CPh)$_2$

C(2)-Ru(1)-C(1)#1	165.5(5)	C(2)-Ru(1)-C(1)	165.5(5)
C(1)#1-Ru(1)-C(1)	29.1(9)	C(2)-Ru(1)-C(3A)#1	92.5(14)
C(1)#1-Ru(1)-C(3A)#1	86.5(15)	C(1)-Ru(1)-C(3A)#1	88.7(15)
C(2)-Ru(1)-C(3A)	92.5(14)	C(1)#1-Ru(1)-C(3A)	88.7(15)
C(1)-Ru(1)-C(3A)	86.5(15)	C(3A)#1-Ru(1)-C(3A)	175(3)
C(2)-Ru(1)-C(3)#1	92.2(5)	C(1)#1-Ru(1)-C(3)#1	84.9(7)
C(1)-Ru(1)-C(3)#1	90.9(7)	C(3A)#1-Ru(1)-C(3)#1	7.7(9)
C(3A)-Ru(1)-C(3)#1	171.0(10)	C(2)-Ru(1)-C(3)	92.2(5)
C(1)#1-Ru(1)-C(3)	90.9(7)	C(1)-Ru(1)-C(3)	84.9(7)
C(3A)#1-Ru(1)-C(3)	171.0(10)	C(3A)-Ru(1)-C(3)	7.7(9)
C(3)#1-Ru(1)-C(3)	175.7(10)	C(2)-Ru(1)-C(24)	91.00(12)
C(1)#1-Ru(1)-C(24)	103.5(5)	C(1)-Ru(1)-C(24)	74.5(5)
C(3A)#1-Ru(1)-C(24)	91.9(7)	C(3A)-Ru(1)-C(24)	88.0(7)
C(3)#1-Ru(1)-C(24)	99.6(4)	C(3)-Ru(1)-C(24)	80.3(4)
C(2)-Ru(1)-C(24)#1	91.00(12)	C(1)#1-Ru(1)-C(24)#1	74.5(5)
C(1)-Ru(1)-C(24)#1	103.5(5)	C(3A)#1-Ru(1)-C(24)#1	88.0(7)
C(3A)-Ru(1)-C(24)#1	91.9(7)	C(3)#1-Ru(1)-C(24)#1	80.3(4)
C(3)-Ru(1)-C(24)#1	99.6(4)	C(24)-Ru(1)-C(24)#1	178.0(2)
C(1)-O(1)-C(1)#1	30.4(11)	C(1)-O(1)-C(20A)	100.8(13)
C(1)#1-O(1)-C(20A)	99.9(10)	C(4)-N(1)-C(3)	110.6(9)
C(4)-N(1)-C(6)	120.1(5)	C(3)-N(1)-C(6)	127.6(9)
C(3)-N(2)-C(5)	110.4(9)	C(3)-N(2)-C(15)	133.2(10)
C(5)-N(2)-C(15)	114.4(6)	C(3A)-N(1A)-C(4A)	107(2)
C(3A)-N(1A)-C(6)	131(2)	C(4A)-N(1A)-C(6)	121.3(14)
C(5A)-N(2A)-C(3A)	116(3)	C(5A)-N(2A)-C(15A)	117.9(17)
C(3A)-N(2A)-C(15A)	126(3)	C(1)#1-C(1)-O(1)	112.5(11)
C(1)#1-C(1)-O(1)#1	37.1(6)	O(1)-C(1)-O(1)#1	75.5(14)
C(1)#1-C(1)-Ru(1)	75.5(5)	O(1)-C(1)-Ru(1)	171.9(15)
O(1)#1-C(1)-Ru(1)	112.5(8)	O(2)-C(2)-Ru(1)	180.000(1)
N(2)-C(3)-N(1)	104.8(12)	N(2)-C(3)-Ru(1)	125.2(11)
N(1)-C(3)-Ru(1)	129.3(12)	C(5)-C(4)-N(1)	106.5(5)
C(4)-C(5)-N(2)	107.5(5)	C(11)-C(6)-C(7)	123.9(4)
C(11)-C(6)-N(1)	112.7(5)	C(7)-C(6)-N(1)	123.3(5)
C(11)-C(6)-N(1A)	132.7(7)	C(7)-C(6)-N(1A)	103.4(6)

N(1)-C(6)-N(1A)	20.0(5)	C(8)-C(7)-C(6)	117.2(5)
C(8)-C(7)-C(12)	121.4(5)	C(6)-C(7)-C(12)	121.4(5)
C(7)-C(8)-C(9)	120.4(5)	C(10)-C(9)-C(8)	120.2(4)
C(10)-C(9)-C(13)	121.3(5)	C(8)-C(9)-C(13)	118.4(6)
C(11)-C(10)-C(9)	122.7(5)	C(10)-C(11)-C(6)	115.4(5)
C(10)-C(11)-C(14)	121.5(5)	C(6)-C(11)-C(14)	123.1(5)
C(16)-C(15)-C(20)	124.3(10)	C(16)-C(15)-N(2)	127.0(9)
C(20)-C(15)-N(2)	108.6(9)	C(17)-C(16)-C(15)	115.1(11)
C(17)-C(16)-C(21)	131.5(10)	C(15)-C(16)-C(21)	112.9(9)
C(18)-C(17)-C(16)	122.3(11)	C(17)-C(18)-C(19)	119.5(8)
C(17)-C(18)-C(22)	120.9(10)	C(19)-C(18)-C(22)	119.6(9)
C(19)-C(20)-C(15)	117.9(10)	C(19)-C(20)-C(23)	118.6(9)
C(15)-C(20)-C(23)	123.5(8)	C(25)-C(24)-Ru(1)	176.9(4)
C(24)-C(25)-C(26)	178.2(5)	C(31)-C(26)-C(27)	112.6(5)
C(31)-C(26)-C(25)	121.5(5)	C(27)-C(26)-C(25)	126.0(4)
C(26)-C(27)-C(28)	125.3(5)	C(29)-C(28)-C(27)	120.9(6)
C(28)-C(29)-C(30)	115.0(5)	C(29)-C(30)-C(31)	124.4(5)
C(26)-C(31)-C(30)	122.0(5)	N(2A)-C(3A)-N(1A)	105(3)
N(2A)-C(3A)-Ru(1)	126(3)	N(1A)-C(3A)-Ru(1)	129(3)
N(1A)-C(4A)-C(5A)	102.8(17)	N(2A)-C(5A)-C(4A)	106.7(15)
C(20)-C(19)-C(18)	120.9(8)	N(2A)-C(15A)-C(16A)	98.5(14)
N(2A)-C(15A)-C(20A)	141.6(16)	C(16A)-C(15A)-C(20A)	119.8(19)
C(17A)-C(16A)-C(15A)	125(2)	C(17A)-C(16A)-C(21A)	88.2(14)
C(15A)-C(16A)-C(21A)	145.8(19)	C(16A)-C(17A)-C(18A)	115(2)
C(16A)-C(17A)-C(21A)	47.6(11)	C(18A)-C(17A)-C(21A)	160.8(17)
C(17A)-C(18A)-C(19A)	120.4(18)	C(17A)-C(18A)-C(22A)	115.3(15)
C(19A)-C(18A)-C(22A)	124.1(15)	C(20A)-C(19A)-C(18A)	123.9(16)
C(15A)-C(20A)-C(19A)	115.6(16)	C(15A)-C(20A)-C(23A)	121.1(13)
C(19A)-C(20A)-C(23A)	123.2(13)	C(15A)-C(20A)-O(1)	100.7(11)
C(19A)-C(20A)-O(1)	91.6(11)	C(23A)-C(20A)-O(1)	81.8(10)
C(16A)-C(21A)-C(17A)	44.2(7)		

Appendix 10. crystallographic data, bond lengths and angles for $Ru(IMes)_2(CO)_3$ (23)

Identification code	h05mkw21
Empirical formula	C45 H48 N4 O3 Ru
Formula weight	793.94
Temperature	150(2) K
Wavelength	0.71073 Å
Crystal system	Monoclinic
Space group	$P2_1/a$
Unit cell dimensions	a = 18.7240(1)Å α = 90°
	b = 10.8140(1)Å β = 108.651(1)°
	c = 20.9130(2)Å γ = 90°
Volume	4012.11(6) $Å^3$
Z	4
Density (calculated)	1.314 Mg/m^3
Absorption coefficient	0.435 mm^{-1}
F(000)	1656
Crystal size	0.25 x 0.25 x 0.25 mm
Theta range for data collection	3.77 to 30.03 °.
Index ranges	-25<=h<=26; -13<=k<=15; -29<=l<=29
Reflections collected	84494
Independent reflections	11676 [R(int) = 0.0479]
Reflections observed (>2σ)	9160
Data Completeness	0.994
Absorption correction	Semi-empirical from equivalents
Max. and min. transmission	0.90 and 0.87
Refinement method	Full-matrix least-squares on F^2
Data / restraints / parameters	11676 / 0 / 490
Goodness-of-fit on F^2	1.041
Final R indices [I>2σ(I)]	R^1 = 0.0399 wR_2 = 0.0981
R indices (all data)	R^1 = 0.0580 wR_2 = 0.1075
Largest diff. peak and hole	1.943 and -0.814 $eÅ^{-3}$

bond lengths (Å) for $Ru(IMes)_2(CO)_3$

Ru(1)-C(3)	1.900(3)	Ru(1)-C(2)	1.927(2)
Ru(1)-C(1)	1.944(3)	Ru(1)-C(4)	2.1093(19)
Ru(1)-C(25)	2.1125(19)	O(1)-C(1)	1.141(3)
O(2)-C(2)	1.147(3)	O(3)-C(3)	1.157(3)
N(1)-C(4)	1.372(2)	N(1)-C(5)	1.388(2)
N(1)-C(7)	1.446(2)	N(2)-C(4)	1.369(2)
N(2)-C(6)	1.394(2)	N(2)-C(16)	1.445(3)
N(3)-C(25)	1.368(3)	N(3)-C(26)	1.391(3)
N(3)-C(28)	1.438(3)	N(4)-C(25)	1.374(3)
N(4)-C(27)	1.389(3)	N(4)-C(37)	1.441(3)
C(5)-C(6)	1.341(3)	C(7)-C(8)	1.395(3)
C(7)-C(12)	1.405(3)	C(8)-C(9)	1.400(3)
C(8)-C(13)	1.494(4)	C(9)-C(10)	1.376(4)
C(10)-C(11)	1.384(4)	C(10)-C(14)	1.518(4)
C(11)-C(12)	1.395(3)	C(12)-C(15)	1.500(3)
C(16)-C(21)	1.392(3)	C(16)-C(17)	1.393(3)
C(17)-C(18)	1.401(3)	C(17)-C(22)	1.498(4)
C(18)-C(19)	1.377(5)	C(19)-C(20)	1.372(5)
C(19)-C(23)	1.512(4)	C(20)-C(21)	1.400(3)
C(21)-C(24)	1.493(4)	C(26)-C(27)	1.339(3)
C(28)-C(33)	1.391(3)	C(28)-C(29)	1.393(3)
C(29)-C(30)	1.400(3)	C(29)-C(34)	1.501(4)
C(30)-C(31)	1.379(5)	C(31)-C(32)	1.380(5)
C(31)-C(35)	1.515(4)	C(32)-C(33)	1.394(4)
C(33)-C(36)	1.501(4)	C(37)-C(38)	1.395(3)
C(37)-C(42)	1.398(3)	C(38)-C(39)	1.391(4)
C(38)-C(43)	1.488(4)	C(39)-C(40)	1.373(5)
C(40)-C(41)	1.383(5)	C(40)-C(44)	1.528(4)
C(41)-C(42)	1.397(4)	C(42)-C(45)	1.504(4)

bond angles (°) for $Ru(IMes)_2(CO)_3$

C(3)-Ru(1)-C(2)	111.32(12)	C(3)-Ru(1)-C(1)	139.56(14)
C(2)-Ru(1)-C(1)	109.12(13)	C(3)-Ru(1)-C(4)	90.21(9)
C(2)-Ru(1)-C(4)	95.74(8)	C(1)-Ru(1)-C(4)	85.97(9)
C(3)-Ru(1)-C(25)	83.67(9)	C(2)-Ru(1)-C(25)	94.82(8)
C(1)-Ru(1)-C(25)	92.87(9)	C(4)-Ru(1)-C(25)	169.16(7)
C(4)-N(1)-C(5)	111.79(16)	C(4)-N(1)-C(7)	128.49(16)
C(5)-N(1)-C(7)	119.11(16)	C(4)-N(2)-C(6)	112.06(16)
C(4)-N(2)-C(16)	126.94(16)	C(6)-N(2)-C(16)	120.01(16)
C(25)-N(3)-C(26)	112.25(17)	C(25)-N(3)-C(28)	127.34(17)
C(26)-N(3)-C(28)	119.97(17)	C(25)-N(4)-C(27)	111.87(17)
C(25)-N(4)-C(37)	128.32(16)	C(27)-N(4)-C(37)	119.65(17)
O(1)-C(1)-Ru(1)	174.9(3)	O(2)-C(2)-Ru(1)	179.7(3)
O(3)-C(3)-Ru(1)	175.1(3)	N(2)-C(4)-N(1)	102.70(15)
N(2)-C(4)-Ru(1)	130.63(14)	N(1)-C(4)-Ru(1)	126.50(13)
C(6)-C(5)-N(1)	107.10(17)	C(5)-C(6)-N(2)	106.34(17)
C(8)-C(7)-C(12)	122.2(2)	C(8)-C(7)-N(1)	119.86(19)
C(12)-C(7)-N(1)	117.35(18)	C(7)-C(8)-C(9)	117.1(2)
C(7)-C(8)-C(13)	122.4(2)	C(9)-C(8)-C(13)	120.4(2)
C(10)-C(9)-C(8)	122.5(2)	C(9)-C(10)-C(11)	118.8(2)
C(9)-C(10)-C(14)	120.8(3)	C(11)-C(10)-C(14)	120.4(3)
C(10)-C(11)-C(12)	121.8(2)	C(11)-C(12)-C(7)	117.5(2)
C(11)-C(12)-C(15)	120.1(2)	C(7)-C(12)-C(15)	122.3(2)
C(21)-C(16)-C(17)	122.9(2)	C(21)-C(16)-N(2)	117.2(2)
C(17)-C(16)-N(2)	119.9(2)	C(16)-C(17)-C(18)	116.6(3)
C(16)-C(17)-C(22)	122.2(2)	C(18)-C(17)-C(22)	121.2(3)
C(19)-C(18)-C(17)	122.5(3)	C(20)-C(19)-C(18)	118.9(2)
C(20)-C(19)-C(23)	120.4(4)	C(18)-C(19)-C(23)	120.7(4)
C(19)-C(20)-C(21)	121.9(3)	C(16)-C(21)-C(20)	117.3(3)
C(16)-C(21)-C(24)	121.3(2)	C(20)-C(21)-C(24)	121.4(3)
N(3)-C(25)-N(4)	102.45(16)	N(3)-C(25)-Ru(1)	130.19(14)
N(4)-C(25)-Ru(1)	126.64(14)	C(27)-C(26)-N(3)	106.46(19)
C(26)-C(27)-N(4)	106.96(19)	C(33)-C(28)-C(29)	122.9(2)
C(33)-C(28)-N(3)	119.5(2)	C(29)-C(28)-N(3)	117.49(19)

C(28)-C(29)-C(30)	117.7(2)	C(28)-C(29)-C(34)	121.1(2)
C(30)-C(29)-C(34)	121.2(2)	C(31)-C(30)-C(29)	121.2(3)
C(30)-C(31)-C(32)	119.0(3)	C(30)-C(31)-C(35)	120.5(4)
C(32)-C(31)-C(35)	120.4(3)	C(31)-C(32)-C(33)	122.6(3)
C(28)-C(33)-C(32)	116.6(3)	C(28)-C(33)-C(36)	121.3(2)
C(32)-C(33)-C(36)	122.1(3)	C(38)-C(37)-C(42)	122.1(2)
C(38)-C(37)-N(4)	119.7(2)	C(42)-C(37)-N(4)	117.8(2)
C(39)-C(38)-C(37)	117.3(3)	C(39)-C(38)-C(43)	120.1(2)
C(37)-C(38)-C(43)	122.5(2)	C(40)-C(39)-C(38)	122.5(3)
C(39)-C(40)-C(41)	118.8(2)	C(39)-C(40)-C(44)	120.4(3)
C(41)-C(40)-C(44)	120.8(3)	C(40)-C(41)-C(42)	121.7(3)
C(41)-C(42)-C(37)	117.6(3)	C(41)-C(42)-C(45)	120.7(3)
C(37)-C(42)-C(45)	121.7(2)		

Appendix 11. crystallographic data, bond lengths and angles for $[Ru(IMes)_2(CO)(^tBuNC)_2H]^+Cl^-$ (24)

Identification code	bath231a
Empirical formula	C74 H91 Cl N6 O Ru
Formula weight	1217.05
Temperature	150(2) K
Wavelength	0.69040 Å
Crystal system	Monoclinic
Space group	$P2_1/n$
Unit cell dimensions	a = 14.8945(9)Å α = 90°
	b = 20.9811(12)Å β = 108.680(1)°
	c = 22.8039(13)Å γ = 90°
Volume	6750.9(7) $Å^3$
Z	4
Density (calculated)	1.197 Mg/m^3
Absorption coefficient	0.319 mm^{-1}
F(000)	2584
Crystal size	0.05 x 0.03 x 0.02 mm
Theta range for data collection	3.42 to 22.55°
Index ranges	-14<=h<=16; -23<=k<=22; -25<=l<=24
Reflections collected	31454
Independent reflections	9665 [R(int) = 0.1137]
Reflections observed (>2σ)	6343
Data Completeness	0.996
Absorption correction	Semi-empirical from equivalents
Max. and min. transmission	1.00 and 0.98
Refinement method	Full-matrix least-squares on F^2
Data / restraints / parameters	9665 / 1 / 716
Goodness-of-fit on F^2	0.931
Final R indices [I>2σ(I)]	$R^1 = 0.0597$ $wR_2 = 0.1510$
R indices (all data)	$R^1 = 0.0890$ $wR_2 = 0.1659$
Largest diff. peak and hole	0.802 and -0.934 $eÅ^{-3}$

bond lengths (Å) for [Ru(IMes)$_2$(CO)(^{t}BuNC)$_2$H]$^+$Cl$^-$

Ru(1)-C(1)	1.872(6)	Ru(1)-C(44)	2.034(6)
Ru(1)-C(49)	2.071(6)	Ru(1)-C(2)	2.100(5)
Ru(1)-C(23)	2.126(5)	O(2)-C(1)	1.153(6)
N(1)-C(2)	1.371(6)	N(1)-C(3)	1.384(6)
N(1)-C(5)	1.458(6)	N(2)-C(4)	1.382(6)
N(2)-C(2)	1.382(6)	N(2)-C(14)	1.452(6)
N(3)-C(24)	1.374(7)	N(3)-C(23)	1.378(6)
N(3)-C(26)	1.448(7)	N(4)-C(23)	1.366(6)
N(4)-C(25)	1.393(6)	N(4)-C(35)	1.443(6)
C(44)-N(44)	1.160(6)	C(49)-N(49)	1.141(6)
C(3)-C(4)	1.317(7)	C(5)-C(10)	1.379(7)
C(5)-C(6)	1.384(7)	C(6)-C(7)	1.386(7)
C(6)-C(11)	1.506(7)	C(7)-C(8)	1.366(8)
C(8)-C(9)	1.380(8)	C(8)-C(12)	1.512(7)
C(9)-C(10)	1.402(7)	C(10)-C(13)	1.505(7)
C(14)-C(15)	1.389(7)	C(14)-C(19)	1.389(7)
C(15)-C(16)	1.392(7)	C(15)-C(20)	1.511(7)
C(16)-C(17)	1.389(7)	C(17)-C(18)	1.388(7)
C(17)-C(21)	1.505(7)	C(18)-C(19)	1.377(7)
C(19)-C(22)	1.515(7)	C(24)-C(25)	1.326(8)
C(26)-C(27)	1.378(8)	C(26)-C(31)	1.393(7)
C(27)-C(28)	1.397(8)	C(27)-C(32)	1.515(8)
C(28)-C(29)	1.382(8)	C(29)-C(30)	1.370(8)
C(29)-C(33)	1.522(8)	C(30)-C(31)	1.376(8)
C(31)-C(34)	1.502(8)	C(35)-C(40)	1.392(7)
C(35)-C(36)	1.407(7)	C(36)-C(37)	1.396(8)
C(36)-C(41)	1.517(8)	C(37)-C(38)	1.363(8)
C(38)-C(39)	1.389(8)	C(38)-C(42)	1.518(8)
C(39)-C(40)	1.377(7)	C(40)-C(43)	1.501(7)
N(44)-C(45)	1.479(7)	C(45)-C(46)	1.513(8)
C(45)-C(47)	1.514(8)	C(45)-C(48)	1.518(8)
N(49)-C(50)	1.484(7)	C(50)-C(53)	1.510(8)
C(50)-C(51)	1.520(7)	C(50)-C(52)	1.535(8)
C(54)-C(59)	1.364(9)	C(54)-C(55)	1.386(9)

C(54)-C(60)	1.504(9)	C(55)-C(56)	1.385(10)
C(56)-C(57)	1.372(11)	C(57)-C(58)	1.346(11)
C(58)-C(59)	1.365(10)	C(61)-C(66)	1.330(10)
C(61)-C(62)	1.439(11)	C(61)-C(67)	1.443(12)
C(62)-C(63)	1.337(10)	C(63)-C(64)	1.408(11)
C(64)-C(65)	1.353(11)	C(65)-C(66)	1.400(10)
C(68)-C(69)	1.333(14)	C(68)-C(73)	1.392(15)
C(68)-C(74)	1.510(16)	C(69)-C(70)	1.417(19)
C(70)-C(71)	1.378(15)	C(71)-C(72)	1.429(18)
C(72)-C(73)	1.161(17)	C(76)-C(68A)	1.62(3)
C(68A)-C(69A)	1.3900	C(68A)-C(73A)	1.3900
C(69A)-C(70A)	1.3900	C(70A)-C(71A)	1.3900
C(71A)-C(72A)	1.3900	C(72A)-C(73A)	1.3900

bond angles (°) for [Ru(IMes)$_2$(CO)(^{t}BuNC)$_2$H]$^+$Cl$^-$

C(1)-Ru(1)-C(44)	95.1(2)	C(1)-Ru(1)-C(49)	168.2(2)
C(44)-Ru(1)-C(49)	84.1(2)	C(1)-Ru(1)-C(2)	95.6(2)
C(44)-Ru(1)-C(2)	90.37(19)	C(49)-Ru(1)-C(2)	96.2(2)
C(1)-Ru(1)-C(23)	82.0(2)	C(44)-Ru(1)-C(23)	104.15(19)
C(49)-Ru(1)-C(23)	86.83(19)	C(2)-Ru(1)-C(23)	165.42(18)
C(2)-N(1)-C(3)	112.8(4)	C(2)-N(1)-C(5)	130.2(4)
C(3)-N(1)-C(5)	116.6(4)	C(4)-N(2)-C(2)	112.6(4)
C(4)-N(2)-C(14)	119.4(4)	C(2)-N(2)-C(14)	127.1(4)
C(24)-N(3)-C(23)	111.6(4)	C(24)-N(3)-C(26)	121.4(4)
C(23)-N(3)-C(26)	127.1(4)	C(23)-N(4)-C(25)	111.8(4)
C(23)-N(4)-C(35)	128.7(4)	C(25)-N(4)-C(35)	119.5(4)
N(44)-C(44)-Ru(1)	171.3(4)	N(49)-C(49)-Ru(1)	167.4(5)
O(2)-C(1)-Ru(1)	171.7(4)	N(1)-C(2)-N(2)	100.8(4)
N(1)-C(2)-Ru(1)	131.6(4)	N(2)-C(2)-Ru(1)	127.6(4)
C(4)-C(3)-N(1)	106.9(5)	C(3)-C(4)-N(2)	106.9(5)
C(10)-C(5)-C(6)	123.3(5)	C(10)-C(5)-N(1)	117.1(4)
C(6)-C(5)-N(1)	118.7(5)	C(5)-C(6)-C(7)	117.3(5)

C(5)-C(6)-C(11)	123.1(5)	C(7)-C(6)-C(11)	119.6(5)
C(8)-C(7)-C(6)	121.8(5)	C(7)-C(8)-C(9)	119.2(5)
C(7)-C(8)-C(12)	120.0(6)	C(9)-C(8)-C(12)	120.7(6)
C(8)-C(9)-C(10)	121.5(5)	C(5)-C(10)-C(9)	116.7(5)
C(5)-C(10)-C(13)	121.7(5)	C(9)-C(10)-C(13)	121.5(5)
C(15)-C(14)-C(19)	122.3(5)	C(15)-C(14)-N(2)	119.6(5)
C(19)-C(14)-N(2)	117.8(5)	C(14)-C(15)-C(16)	117.9(5)
C(14)-C(15)-C(20)	120.6(5)	C(16)-C(15)-C(20)	121.5(5)
C(17)-C(16)-C(15)	121.4(5)	C(18)-C(17)-C(16)	118.3(5)
C(18)-C(17)-C(21)	120.0(5)	C(16)-C(17)-C(21)	121.7(5)
C(19)-C(18)-C(17)	122.3(5)	C(18)-C(19)-C(14)	117.7(5)
C(18)-C(19)-C(22)	121.2(5)	C(14)-C(19)-C(22)	121.1(5)
N(4)-C(23)-N(3)	102.5(4)	N(4)-C(23)-Ru(1)	132.0(3)
N(3)-C(23)-Ru(1)	125.0(4)	C(25)-C(24)-N(3)	107.7(5)
C(24)-C(25)-N(4)	106.5(5)	C(27)-C(26)-C(31)	122.5(5)
C(27)-C(26)-N(3)	119.1(5)	C(31)-C(26)-N(3)	118.2(5)
C(26)-C(27)-C(28)	116.9(5)	C(26)-C(27)-C(32)	122.5(5)
C(28)-C(27)-C(32)	120.6(5)	C(29)-C(28)-C(27)	122.2(6)
C(30)-C(29)-C(28)	118.2(6)	C(30)-C(29)-C(33)	120.7(5)
C(28)-C(29)-C(33)	121.1(5)	C(29)-C(30)-C(31)	122.5(6)
C(30)-C(31)-C(26)	117.5(5)	C(30)-C(31)-C(34)	121.0(5)
C(26)-C(31)-C(34)	121.4(5)	C(40)-C(35)-C(36)	121.2(5)
C(40)-C(35)-N(4)	120.1(5)	C(36)-C(35)-N(4)	118.0(5)
C(37)-C(36)-C(35)	116.8(5)	C(37)-C(36)-C(41)	120.7(5)
C(35)-C(36)-C(41)	122.5(5)	C(38)-C(37)-C(36)	123.0(6)
C(37)-C(38)-C(39)	118.6(6)	C(37)-C(38)-C(42)	120.9(6)
C(39)-C(38)-C(42)	120.5(6)	C(40)-C(39)-C(38)	121.3(6)
C(39)-C(40)-C(35)	119.0(5)	C(39)-C(40)-C(43)	120.5(5)
C(35)-C(40)-C(43)	120.4(5)	C(44)-N(44)-C(45)	177.3(5)
N(44)-C(45)-C(46)	107.6(4)	N(44)-C(45)-C(47)	107.3(4)
C(46)-C(45)-C(47)	112.0(5)	N(44)-C(45)-C(48)	107.5(4)
C(46)-C(45)-C(48)	111.6(5)	C(47)-C(45)-C(48)	110.6(5)
C(49)-N(49)-C(50)	173.0(5)	N(49)-C(50)-C(53)	106.9(4)
N(49)-C(50)-C(51)	107.8(4)	C(53)-C(50)-C(51)	112.3(5)
N(49)-C(50)-C(52)	109.3(4)	C(53)-C(50)-C(52)	110.4(5)

C(51)-C(50)-C(52)	110.1(5)	C(59)-C(54)-C(55)	118.1(7)
C(59)-C(54)-C(60)	121.3(7)	C(55)-C(54)-C(60)	120.5(7)
C(56)-C(55)-C(54)	120.3(8)	C(57)-C(56)-C(55)	119.7(8)
C(58)-C(57)-C(56)	119.5(8)	C(57)-C(58)-C(59)	121.3(9)
C(54)-C(59)-C(58)	121.0(8)	C(66)-C(61)-C(62)	120.7(8)
C(66)-C(61)-C(67)	119.8(9)	C(62)-C(61)-C(67)	119.5(9)
C(63)-C(62)-C(61)	117.7(8)	C(62)-C(63)-C(64)	123.9(9)
C(65)-C(64)-C(63)	115.1(9)	C(64)-C(65)-C(66)	124.2(9)
C(61)-C(66)-C(65)	118.4(8)	C(69)-C(68)-C(73)	118.2(12)
C(69)-C(68)-C(74)	119.3(11)	C(73)-C(68)-C(74)	122.5(11)
C(68)-C(69)-C(70)	121.4(12)	C(71)-C(70)-C(69)	117.9(14)
C(70)-C(71)-C(72)	113.4(13)	C(73)-C(72)-C(71)	128.9(15)
C(72)-C(73)-C(68)	120.1(14)	C(69A)-C(68A)-C(73A)	120.0
C(69A)-C(68A)-C(76)	120.9(13)	C(73A)-C(68A)-C(76)	119.0(13)
C(68A)-C(69A)-C(70A)	120.0	C(71A)-C(70A)-C(69A)	120.0
C(70A)-C(71A)-C(72A)	120.0	C(73A)-C(72A)-C(71A)	120.0
C(72A)-C(73A)-C(68A)	120.0		

Appendix 12. crystallographic data, bond lengths and angles for $Ru(PPh_3)(IMes)(CO)_2H_2$ (28)

Identification code	k07mkw10
Empirical formula	C41 H40.90 Cl0.10 N2 O2 P Ru
Formula weight	729.24
Temperature	150(2) K
Wavelength	0.71073 Å
Crystal system	Monoclinic
Space group	P21/a
Unit cell dimensions	a = 15.1750(2)Å α = 90°
	b = 14.0430(2)Å β = 100.837(1)°
	c = 17.2770(2)Å γ = 90°
Volume	3616.11(8) $Å^3$
Z	4
Density (calculated)	1.339 Mg/m^3
Absorption coefficient	0.522 mm^{-1}
F(000)	1510
Crystal size	0.30 x 0.25 x 0.25 mm
Theta range for data collection	3.51 to 30.00°
Index ranges	-21<=h<=21; -19<=k<=19; -24<=l<=24
Reflections collected	68346
Independent reflections	10509 [R(int) = 0.0445]
Reflections observed (>2σ)	8530
Data Completeness	0.997
Absorption correction	Semi-empirical from equivalents
Max. and min. transmission	0.90 and 0.86
Refinement method	Full-matrix least-squares on F^2
Data / restraints / parameters	10509 / 3 / 438
Goodness-of-fit on F^2	1.053
Final R indices [I>2σ(I)]	$R^1 = 0.0326$ $wR_2 = 0.0742$
R indices (all data)	$R^1 = 0.0466$ $wR_2 = 0.0814$
Largest diff. peak and hole	1.007 and -0.641 $eÅ^{-3}$

bond lengths (Å) for $Ru(PPh_3)(IMes)(CO)_2H_2$

Ru(1)-H(2)	1.580(10)	Ru(1)-H(1)	1.604(9)
Ru(1)-C(1)	1.9202(18)	Ru(1)-C(2)	1.9315(19)
Ru(1)-C(3)	2.0874(17)	Ru(1)-P(1)	2.3228(4)
Ru(1)-Cl(1)	2.460(3)	P(1)-C(30)	1.8317(17)
P(1)-C(36)	1.8387(18)	P(1)-C(24)	1.8413(18)
O(1)-C(1)	1.145(2)	O(2)-C(2)	1.126(2)
N(1)-C(3)	1.368(2)	N(1)-C(4)	1.390(2)
N(1)-C(6)	1.440(2)	N(2)-C(3)	1.373(2)
N(2)-C(5)	1.390(2)	N(2)-C(15)	1.442(2)
C(4)-C(5)	1.336(3)	C(6)-C(7)	1.392(3)
C(6)-C(11)	1.397(3)	C(7)-C(8)	1.398(3)
C(7)-C(12)	1.507(3)	C(8)-C(9)	1.388(4)
C(9)-C(10)	1.375(4)	C(9)-C(13)	1.519(3)
C(10)-C(11)	1.389(3)	C(11)-C(14)	1.497(3)
C(15)-C(16)	1.391(3)	C(15)-C(20)	1.395(3)
C(16)-C(17)	1.395(3)	C(16)-C(21)	1.504(3)
C(17)-C(18)	1.387(3)	C(18)-C(19)	1.389(3)
C(18)-C(22)	1.513(3)	C(19)-C(20)	1.395(3)
C(20)-C(23)	1.501(3)	C(24)-C(29)	1.386(3)
C(24)-C(25)	1.393(3)	C(25)-C(26)	1.392(3)
C(26)-C(27)	1.379(3)	C(27)-C(28)	1.375(3)
C(28)-C(29)	1.394(3)	C(30)-C(35)	1.390(2)
C(30)-C(31)	1.396(3)	C(31)-C(32)	1.385(3)
C(32)-C(33)	1.383(3)	C(33)-C(34)	1.376(3)
C(34)-C(35)	1.390(3)	C(36)-C(37)	1.390(2)
C(36)-C(41)	1.395(3)	C(37)-C(38)	1.388(3)
C(38)-C(39)	1.386(3)	C(39)-C(40)	1.374(3)
C(40)-C(41)	1.393(3)		

bond angles (°) for $Ru(PPh_3)(IMes)(CO)_2H_2$

H(2)-Ru(1)-H(1)	80.8(13)	H(2)-Ru(1)-C(1)	96.4(11)
H(1)-Ru(1)-C(1)	173.7(8)	H(2)-Ru(1)-C(2)	170.0(11)
H(1)-Ru(1)-C(2)	89.2(8)	C(1)-Ru(1)-C(2)	93.58(7)
H(2)-Ru(1)-C(3)	83.5(11)	H(1)-Ru(1)-C(3)	85.6(8)
C(1)-Ru(1)-C(3)	99.70(7)	C(2)-Ru(1)-C(3)	95.52(7)
H(2)-Ru(1)-P(1)	78.6(11)	H(1)-Ru(1)-P(1)	79.7(8)
C(1)-Ru(1)-P(1)	94.22(5)	C(2)-Ru(1)-P(1)	100.02(5)
C(3)-Ru(1)-P(1)	158.42(5)	H(2)-Ru(1)-Cl(1)	5.2(11)
H(1)-Ru(1)-Cl(1)	86.0(8)	C(1)-Ru(1)-Cl(1)	91.2(2)
C(2)-Ru(1)-Cl(1)	175.2(2)	C(3)-Ru(1)-Cl(1)	83.8(2)
P(1)-Ru(1)-Cl(1)	79.5(2)	C(30)-P(1)-C(36)	100.97(8)
C(30)-P(1)-C(24)	102.50(8)	C(36)-P(1)-C(24)	101.75(8)
C(30)-P(1)-Ru(1)	116.63(6)	C(36)-P(1)-Ru(1)	117.02(6)
C(24)-P(1)-Ru(1)	115.56(6)	C(3)-N(1)-C(4)	111.97(15)
C(3)-N(1)-C(6)	125.86(14)	C(4)-N(1)-C(6)	122.11(15)
C(3)-N(2)-C(5)	111.42(15)	C(3)-N(2)-C(15)	126.43(14)
C(5)-N(2)-C(15)	121.97(15)	O(1)-C(1)-Ru(1)	173.11(15)
O(2)-C(2)-Ru(1)	178.68(16)	N(1)-C(3)-N(2)	102.86(14)
N(1)-C(3)-Ru(1)	129.58(12)	N(2)-C(3)-Ru(1)	127.42(12)
C(5)-C(4)-N(1)	106.55(16)	C(4)-C(5)-N(2)	107.20(16)
C(7)-C(6)-C(11)	122.36(18)	C(7)-C(6)-N(1)	118.75(18)
C(11)-C(6)-N(1)	118.85(18)	C(6)-C(7)-C(8)	116.9(2)
C(6)-C(7)-C(12)	121.56(19)	C(8)-C(7)-C(12)	121.5(2)
C(9)-C(8)-C(7)	122.1(2)	C(10)-C(9)-C(8)	118.9(2)
C(10)-C(9)-C(13)	119.7(3)	C(8)-C(9)-C(13)	121.4(3)
C(9)-C(10)-C(11)	121.6(2)	C(10)-C(11)-C(6)	118.0(2)
C(10)-C(11)-C(14)	120.3(2)	C(6)-C(11)-C(14)	121.7(2)
C(16)-C(15)-C(20)	122.06(17)	C(16)-C(15)-N(2)	118.23(16)
C(20)-C(15)-N(2)	119.68(17)	C(15)-C(16)-C(17)	118.11(18)
C(15)-C(16)-C(21)	120.96(18)	C(17)-C(16)-C(21)	120.92(19)
C(18)-C(17)-C(16)	121.8(2)	C(17)-C(18)-C(19)	118.27(18)
C(17)-C(18)-C(22)	120.7(2)	C(19)-C(18)-C(22)	121.1(2)
C(18)-C(19)-C(20)	122.20(19)	C(19)-C(20)-C(15)	117.55(18)

C(19)-C(20)-C(23)	120.75(19)	C(15)-C(20)-C(23)	121.61(18)
C(29)-C(24)-C(25)	118.24(17)	C(29)-C(24)-P(1)	121.47(14)
C(25)-C(24)-P(1)	120.24(14)	C(26)-C(25)-C(24)	120.62(19)
C(27)-C(26)-C(25)	120.4(2)	C(28)-C(27)-C(26)	119.42(19)
C(27)-C(28)-C(29)	120.5(2)	C(24)-C(29)-C(28)	120.8(2)
C(35)-C(30)-C(31)	118.40(17)	C(35)-C(30)-P(1)	123.25(14)
C(31)-C(30)-P(1)	118.34(13)	C(32)-C(31)-C(30)	120.83(18)
C(33)-C(32)-C(31)	120.3(2)	C(34)-C(33)-C(32)	119.14(19)
C(33)-C(34)-C(35)	121.1(2)	C(34)-C(35)-C(30)	120.18(19)
C(37)-C(36)-C(41)	118.71(17)	C(37)-C(36)-P(1)	119.30(13)
C(41)-C(36)-P(1)	121.98(14)	C(38)-C(37)-C(36)	120.53(18)
C(39)-C(38)-C(37)	120.32(19)	C(40)-C(39)-C(38)	119.7(2)
C(39)-C(40)-C(41)	120.4(2)	C(40)-C(41)-C(36)	120.36(19)

Appendix 13. crystallographic data, bond lengths and angles for $Ru(PPh_3)(IMes)(CO)(Cl)(4\text{-}Mepy)H$ (31)

Identification code	h06mkw8
Empirical formula	C46 H47 Cl N3 O P Ru
Formula weight	825.36
Temperature	150(2) K
Wavelength	0.71073 Å
Crystal system	Monoclinic
Space group	$P2_1/a$
Unit cell dimensions	a = 15.4150(1)Å α = 90°
	b = 14.5050(1)Å β = 108.625(1)°
	c = 18.9280(2)Å γ = 90°
Volume	4010.55(6) $Å^3$
Z	4
Density (calculated)	1.367 Mg/m^3
Absorption coefficient	0.536 mm^{-1}
F(000)	1712
Crystal size	0.40 x 0.30 x 0.30 mm
Theta range for data collection	4.10 to 30.02°
Index ranges	-21<=h<=21; -20<=k<=20; -26<=l<=26
Reflections collected	71528
Independent reflections	11683 [R(int) = 0.0353]
Reflections observed (>2σ)	9765
Data Completeness	0.997
Absorption correction	Semi-empirical from equivalents
Max. and min. transmission	0.86 and 0.81
Refinement method	Full-matrix least-squares on F^2
Data / restraints / parameters	11683 / 1 / 539
Goodness-of-fit on F^2	1.059
Final R indices [I>2σ(I)]	$R^1 = 0.0283$ $wR_2 = 0.0706$
R indices (all data)	$R^1 = 0.0392$ $wR_2 = 0.0754$
Largest diff. peak and hole	0.563 and -0.538 $eÅ^{-3}$

bond lengths (Å) for Ru(PPh$_3$)(IMes)(CO)(Cl)(4-Mepy)H

Ru(1)-H(1)	1.5993	Ru(1)-C(1A)	1.776(7)
Ru(1)-C(1)	1.812(4)	Ru(1)-C(2)	2.1049(15)
Ru(1)-N(3)	2.2901(13)	Ru(1)-P(1)	2.3395(4)
Ru(1)-Cl(1A)	2.483(2)	Ru(1)-Cl(1)	2.4842(12)
P(1)-C(23)	1.800(3)	P(1)-C(35)	1.8323(18)
P(1)-C(29)	1.8372(14)	P(1)-C(23A)	1.911(4)
O(1)-C(1)	1.146(4)	O(1A)-C(1A)	1.196(6)
N(1)-C(2)	1.3653(19)	N(1)-C(3)	1.390(2)
N(1)-C(5)	1.440(2)	N(2)-C(2)	1.373(2)
N(2)-C(4)	1.381(2)	N(2)-C(14)	1.447(2)
N(3)-C(45)	1.3426(19)	N(3)-C(41)	1.344(2)
C(3)-C(4)	1.341(2)	C(5)-C(10)	1.392(2)
C(5)-C(6)	1.395(2)	C(6)-C(7)	1.393(2)
C(6)-C(11)	1.504(2)	C(7)-C(8)	1.392(2)
C(8)-C(9)	1.395(2)	C(8)-C(12)	1.507(2)
C(9)-C(10)	1.394(2)	C(10)-C(13)	1.505(2)
C(14)-C(19)	1.393(2)	C(14)-C(15)	1.399(2)
C(15)-C(16)	1.391(2)	C(15)-C(20)	1.506(3)
C(16)-C(17)	1.383(3)	C(17)-C(18)	1.391(3)
C(17)-C(21)	1.511(2)	C(18)-C(19)	1.394(2)
C(19)-C(22)	1.505(3)	C(23)-C(24)	1.3900
C(23)-C(28)	1.3900	C(24)-C(25)	1.3900
C(25)-C(26)	1.3900	C(26)-C(27)	1.3900
C(27)-C(28)	1.3900	C(29)-C(30)	1.3906
C(29)-C(34)	1.400(2)	C(30)-C(31)	1.386(2)
C(31)-C(32)	1.386(3)	C(32)-C(33)	1.374(3)
C(33)-C(34)	1.390(3)	C(35)-C(36)	1.390(3)
C(35)-C(40)	1.398(2)	C(36)-C(37)	1.396(3)
C(37)-C(38)	1.369(4)	C(38)-C(39)	1.378(4)
C(39)-C(40)	1.401(3)	C(41)-C(42)	1.382(2)
C(42)-C(43)	1.386(2)	C(43)-C(44)	1.385(2)
C(43)-C(46)	1.500(2)	C(44)-C(45)	1.384(2)
C(23A)-C(24A)	1.3900	C(23A)-C(28A)	1.3900
C(24A)-C(25A)	1.3900	C(25A)-C(26A)	1.3900

C(26A)-C(27A)	1.3900	C(27A)-C(28A)	1.3900

bond angles (°) for $Ru(PPh_3)(IMes)(CO)(Cl)(4\text{-}Mepy)H$

H(1)-Ru(1)-C(1A)	88.0	H(1)-Ru(1)-C(1)	87.7
C(1A)-Ru(1)-C(1)	174.77(19)	H(1)-Ru(1)-C(2)	83.2
C(1A)-Ru(1)-C(2)	86.72(17)	C(1)-Ru(1)-C(2)	89.80(10)
H(1)-Ru(1)-N(3)	175.5	C(1A)-Ru(1)-N(3)	92.27(17)
C(1)-Ru(1)-N(3)	92.23(9)	C(2)-Ru(1)-N(3)	101.26(5)
H(1)-Ru(1)-P(1)	82.6	C(1A)-Ru(1)-P(1)	87.22(16)
C(1)-Ru(1)-P(1)	95.20(9)	C(2)-Ru(1)-P(1)	164.70(4)
N(3)-Ru(1)-P(1)	93.00(3)	H(1)-Ru(1)-Cl(1A)	91.1
C(1A)-Ru(1)-Cl(1A)	175.53(17)	C(1)-Ru(1)-Cl(1A)	3.69(10)
C(2)-Ru(1)-Cl(1A)	88.83(6)	N(3)-Ru(1)-Cl(1A)	88.93(6)
P(1)-Ru(1)-Cl(1A)	97.02(5)	H(1)-Ru(1)-Cl(1)	92.6
C(1A)-Ru(1)-Cl(1)	4.68(17)	C(1)-Ru(1)-Cl(1)	178.06(9)
C(2)-Ru(1)-Cl(1)	88.33(5)	N(3)-Ru(1)-Cl(1)	87.65(4)
P(1)-Ru(1)-Cl(1)	86.74(3)	Cl(1A)-Ru(1)-Cl(1)	175.05(5)
C(23)-P(1)-C(35)	100.48(11)	C(23)-P(1)-C(29)	97.08(11)
C(35)-P(1)-C(29)	103.94(7)	C(23)-P(1)-C(23A)	8.52(18)
C(35)-P(1)-C(23A)	106.66(12)	C(29)-P(1)-C(23A)	100.90(12)
C(23)-P(1)-Ru(1)	120.28(10)	C(35)-P(1)-Ru(1)	112.75(5)
C(29)-P(1)-Ru(1)	119.29(4)	C(23A)-P(1)-Ru(1)	111.96(12)
C(2)-N(1)-C(3)	112.14(13)	C(2)-N(1)-C(5)	126.47(13)
C(3)-N(1)-C(5)	121.39(13)	C(2)-N(2)-C(4)	111.74(13)
C(2)-N(2)-C(14)	126.77(13)	C(4)-N(2)-C(14)	121.49(14)
C(45)-N(3)-C(41)	115.93(14)	C(45)-N(3)-Ru(1)	121.54(10)
C(41)-N(3)-Ru(1)	121.99(10)	O(1)-C(1)-Ru(1)	177.6(4)
N(1)-C(2)-N(2)	102.66(13)	N(1)-C(2)-Ru(1)	132.50(11)
N(2)-C(2)-Ru(1)	124.83(11)	C(4)-C(3)-N(1)	106.27(15)
C(3)-C(4)-N(2)	107.19(15)	C(10)-C(5)-C(6)	122.20(14)
C(10)-C(5)-N(1)	118.75(14)	C(6)-C(5)-N(1)	118.93(15)
C(7)-C(6)-C(5)	117.82(15)	C(7)-C(6)-C(11)	120.68(15)

C(5)-C(6)-C(11)	121.49(15)	C(8)-C(7)-C(6)	122.03(15)
C(7)-C(8)-C(9)	118.08(15)	C(7)-C(8)-C(12)	120.99(15)
C(9)-C(8)-C(12)	120.93(16)	C(10)-C(9)-C(8)	121.95(16)
C(5)-C(10)-C(9)	117.88(15)	C(5)-C(10)-C(13)	121.01(15)
C(9)-C(10)-C(13)	121.11(16)	C(19)-C(14)-C(15)	122.24(15)
C(19)-C(14)-N(2)	118.82(15)	C(15)-C(14)-N(2)	118.92(15)
C(16)-C(15)-C(14)	117.62(16)	C(16)-C(15)-C(20)	120.23(17)
C(14)-C(15)-C(20)	122.15(15)	C(17)-C(16)-C(15)	122.03(17)
C(16)-C(17)-C(18)	118.52(16)	C(16)-C(17)-C(21)	121.11(19)
C(18)-C(17)-C(21)	120.36(18)	C(17)-C(18)-C(19)	121.90(17)
C(14)-C(19)-C(18)	117.58(17)	C(14)-C(19)-C(22)	122.36(15)
C(18)-C(19)-C(22)	120.07(17)	C(24)-C(23)-C(28)	120.0
C(24)-C(23)-P(1)	117.93(10)	C(28)-C(23)-P(1)	122.07(10)
C(23)-C(24)-C(25)	120.0	C(26)-C(25)-C(24)	120.0
C(25)-C(26)-C(27)	120.0	C(28)-C(27)-C(26)	120.0
C(27)-C(28)-C(23)	120.0	C(30)-C(29)-C(34)	118.60(13)
C(30)-C(29)-P(1)	118.61(9)	C(34)-C(29)-P(1)	122.65(11)
C(31)-C(30)-C(29)	120.69(14)	C(30)-C(31)-C(32)	120.13(17)
C(33)-C(32)-C(31)	119.83(17)	C(32)-C(33)-C(34)	120.48(17)
C(33)-C(34)-C(29)	120.22(16)	C(36)-C(35)-C(40)	118.53(18)
C(36)-C(35)-P(1)	119.63(13)	C(40)-C(35)-P(1)	120.95(16)
C(35)-C(36)-C(37)	121.0(2)	C(38)-C(37)-C(36)	120.2(2)
C(37)-C(38)-C(39)	119.7(2)	C(38)-C(39)-C(40)	121.0(2)
C(35)-C(40)-C(39)	119.6(2)	N(3)-C(41)-C(42)	123.77(15)
C(41)-C(42)-C(43)	120.05(15)	C(44)-C(43)-C(42)	116.48(15)
C(44)-C(43)-C(46)	121.78(16)	C(42)-C(43)-C(46)	121.74(16)
C(45)-C(44)-C(43)	120.19(15)	N(3)-C(45)-C(44)	123.57(14)
O(1A)-C(1A)-Ru(1)	176.1(6)	C(24A)-C(23A)-C(28A)	120.0
C(24A)-C(23A)-P(1)	122.22(17)	C(28A)-C(23A)-P(1)	117.74(17)
C(25A)-C(24A)-C(23A)	120.0	C(24A)-C(25A)-C(26A)	120.0
C(27A)-C(26A)-C(25A)	120.0	C(26A)-C(27A)-C(28A)	120.0
C(27A)-C(28A)-C(23A)	120.0		